DESIGNING RESILIENT INTERDEPENDENT INFRASTRUCTURES ACROSS SPATIAL AND TEMPORAL SCALES

by

Charalampos C. Avraam

A dissertation submitted to The Johns Hopkins University in conformity with the requirements for the degree of Doctor of Philosophy.

Baltimore, Maryland

July 2021

Abstract

Modern infrastructures are comprised of networked, interdependent systems that deliver critical services. A failure in an infrastructure's component can propagate through the network and affect interconnected assets. Addressing the challenges faced by modern infrastructures requires understanding disruptions across regional and temporal scales, and how disruptions propagate to other infrastructures through their interdependencies. This dissertation contributes to the design of resilient electricity, natural gas, and food infrastructures across spatial and temporal scales.

In the electricity sector, we develop a controller of flexible loads that enhances power systems resilience by preventing voltage collapse. Voltage collapse is a blackout-inducing dynamic instability that occurs when power demand exceeds the maximum transferable power through a network. We formulate the dynamic voltage stability problem for a star direct current network and introduce a voltage collapse stabilization controller that stabilizes power supply at the maximum transferable power under extreme loading conditions, for given potential of flexible loads. The controller allocates total load shedding proportionally among flexible loads.

ABSTRACT

In the natural gas sector, we assess the resilience of North American natural gas infrastructure to long-term changes in resource availability, global crude oil prices, and technological progress, and identify vulnerable regional assets in the integrated Canada-U.S.-Mexico markets. Natural gas demand in North America depends on gas-fired power generation that can change due to policy shifts. We study the resilience of North American natural gas infrastructure to more stringent Renewable Portfolio Standards and greater inter-regional coordination of renewable policies through 2050. We distinguish between three levels of regional renewable policies coordination–regional, national, and international–and establish the relationship between renewable policy coordination and regional natural gas prices.

In the food sector, we assess the resilience of international livestock infrastructures to global coordination policies that aim to curb antimicrobial use. We propose an integrated framework that is an advancement over existing statistical methods by endogenously accounting for competing agents in global meat markets, antimicrobial use in livestock production, and inter-country trade. We formulate three global coordination scenarios in order to understand the tradeoff between national antimicrobial use and international trade. We identify vulnerabilities of Low-and-Middle-Income-Countries and derive policy insights.

ABSTRACT

Readers:

Sauleh Siddiqui (doctoral advisor)
Associate Professor
Department of Environmental Science
American University

Assistant Research Professor
Department of Civil and Systems Engineering
Johns Hopkins University

Enrique Mallada (doctoral advisor)
Assistant Professor
Department of Electrical and Computer Engineering
Johns Hopkins University

Kimia Ghobadi
John C. Malone Assistant Professor
Department of Civil amd Systems Engineering
Johns Hopkins University

Acknowledgments

First and foremost, I would like to express my deepest gratitude to my advisers Dr. Sauleh Siddiqui and Dr. Enrique Mallada. Their enduring support, endless patience, and comprehensive guidance have been vital in my academic and personal growth. Looking back, I am honored for the opportunity to work and learn from them. This work would not have been possible without them.

Next, I would like to thank Dr. Kimia Ghobadi for her keen advice and mentorship and for agreeing to serve in my dissertation committee. I would also like to thank Dr. Benjamin Hobbs for his generous academic and professional advice and for agreeing to head my graduate board oral exam committee. I am also thankful to my graduate board oral exam committee members, Dr. Takeru Igusa and Dr. Stavros Gaitanaros, and my degree qualification exam committee member, Dr. Benjamin Schafer, for their valuable feedback.

I am grateful to Dr. Felipe Feijoo and Dr. Stavros Gaitanaros for their mentorship and for helping me navigate the process of doctoral research. I would also like to thank Dr. Ali Khan for graciously sharing his deeply insightful perspective on research, teaching, and pedagogy.

CHAPTER 0. ACKNOWLEDGMENT

I am thankful to all members of MODL, NetDLab, CSSE, and the Hobbs group at Johns Hopkins University for providing valuable feedback on my research. I am also grateful to the graduate and undergraduate members and collaborators of the research groups that helped me grow as a mentor.

I would like to thank my parents and siblings, Paraskevi Giantsi, Christos Avraam, Evripides Avraam, Alexandros Avraam, and Myrto Avraam, for their unconditional love and support that allows me to persevere. I am deeply grateful to my dear friends, Dr. Elina Spyrou and Georgios Baltas for the countless hours they have spent discussing, brainstorming, and supporting me.

I also want to acknowledge all funding sources. The work in this dissertation was supported in part by the National Science Foundation (NSF Grant #1745375), the United States Department of Energy (U.S. DoE award DE-EE0008006), and the Johns Hopkins University (Johns Hopkins Discovery Award 2016). Such support does not constitute an endorsement by the funding agency of the opinions expressed in this dissertation. I would also like to thank the A.G. Leventis Foundation for its generous support between the years 2017 and 2020.

Dedicated to the Academic who inspired me and urged me to pursue a PhD, Nikos Kotzias.

Contents

List of Tables

LIST OF TABLES

List of Figures

Chapter 1

Introduction

1.1 Motivation

Modern infrastructures are comprised of networked, interdependent systems that deliver critical services. The networked structure implies that for a single infrastructure, a localized failure of a subset of the network's components can propagate through the network and affect interconnected assets. For example, during the Northeastern Blackout in August 14, 2003, a failure of FirstEnergy[1] to accurately measure the voltage and respond in Akron, Ohio resulted in outages in New York, Connecticut, Massachusetts, Rhode Island, northern Pennsylvania, northeastern New Jersey, and Ontario, Canada (U.S.-Canada-Power-System-Outage-Task-Force, 2003). The interdependent structure of national infrastructures implies that a localized failure in one

[1]FirstEnergy is an electric utility that operates in the Midwest and Mid-Atlantic regions of the United States.

infrastructure can disrupt the functioning of another. In the same blackout, water, communication, and transportation infrastructure systems were also compromised. Close to a million people lost their water in Akron, Ohio on August 14 (CNN, 2003), while the operator of the Detroit-Windsor Tunnel at the U.S.-Canada border had to shut down the tunnel and evacuate it following the blackout (DeBlasio et al., 2004).

A failure in energy and food supply chains can have significant resilience implications, leading to food shortages, inability to cover basic human needs, and high economic losses. The 2003 Northeastern Blackout highlights the critical role of energy infrastructure in the workings of a society. The estimated costs were between $4 and $10 billion U.S. dollars (U.S.-Canada-Power-System-Outage-Task-Force, 2006). An extreme ice storm initiated the 2021 Texas Blackout that left most of Texas without power for extended periods of time between February 13 and February 18 and resulted in millions of people facing near-freezing, life-threatening conditions (Gilbert and Bazilian, 2021). The Texas Department of State Health Services reports 151 winter-storm related deaths (TDSHS, 2021), rendering the incident a public health threat. The COVID-19 outbreak led to labor shortages, transportation disruptions, restrictions on the movement of goods, and affected the availability of fresh foods, particularly for vulnerable populations (Hobbs, 2020). Given their critical role, the U.S. Cybersecurity and Infrastructure Agency ranks the electricity, natural gas, and food infrastructures among the 16 critical infrastructure systems *"whose assets, systems, and networks, whether physical or virtual, are considered so vital to the United*

States that their incapacitation or destruction would have a debilitating effect on security, national economic security, national public health or safety, or any combination thereof" (CISA, 2021).

The impact of blackouts varies in spatial and temporal scale compared to human-induced climate change and other disruptions. Human-induced climate change is an ongoing international disruption that has not been contained decades after the United Nations Framework Convention on Climate Change in 1992 (UN, 2015). On the other hand, it took only a few hours for the combined failures to evolve into the 2003 Northeastern Blackout and the 2021 Texas Blackout, with the first one affecting a collection of states and the second one affecting mostly Texas. In addition, the scale of a disruptive event can be decoupled from the scale of its implications. For example, in the 2021 Texas Blackout, a series of storms stressed the power system between February 11 and February 20 (NWS, 2021). Apart from the short-term impact, *i.e.,* the power outages during the storms, the long-term impact was also significant, with farmers losing in some cases a year's worth of crop and the estimated losses of farmers amounting to $600 million U.S. dollars (Reiley, 2021). Nevertheless, in all the above cases, we can isolate a combination of incidents that disrupt energy and food supply chains, and consequently the functioning of societies.

However, energy and food infrastructures are disrupted also by events that evolve slower, and whose increasing stress is aggregated through time. This is the case with climate change and antimicrobial resistance. Climate change is also the result of

decades-long human activity and is mainly attributed to increasing carbon emissions. Antimicrobial resistance describes a pathogen that is resistant to existing antimicrobials, complicating the recovery of vulnerable patients and limiting treatment options. Both challenges arise from the design and operation of energy and food supply chains and the incentives for the individual agents within the supply chains. Moving toward non-emitting energy-producing technologies and less antimicrobial-intensive meat production can curb carbon emissions and antimicrobial resistance respectively.

1.2 Objective

Addressing the challenges faced by modern infrastructures requires understanding their implications across regional and temporal scales, and also how disruptions can propagate to other infrastructures through their interdependencies. This dissertation aims to contribute to the design of electricity, natural gas, and food infrastructures that are resilient to a range of disruptions across spatial and temporal scales. By resilience, we mean *"the joint ability of infrastructure systems to resist (prevent and withstand) any possible hazards, absorb the initial damage, and recover to normal operation"* (Ouyang et al., 2012). Resilient interdependent infrastructures need to ensure robust, secure operation, and rapid recovery at the event of a disruption. We inform infrastructures design by identifying vulnerabilities in the electricity, natural gas, and food infrastructures under technological progress, market shocks, and changing food

and renewable policies.

1.3 Contributions

In this dissertation, we focus on the electricity, natural gas, and food sectors. In each sector we face a different problem, at a different time scale, which requires the use and development of the appropriate mathematical tool. Figure 1.1 illustrates the specific topics and their time scale, regional coverage, and sector of interest.

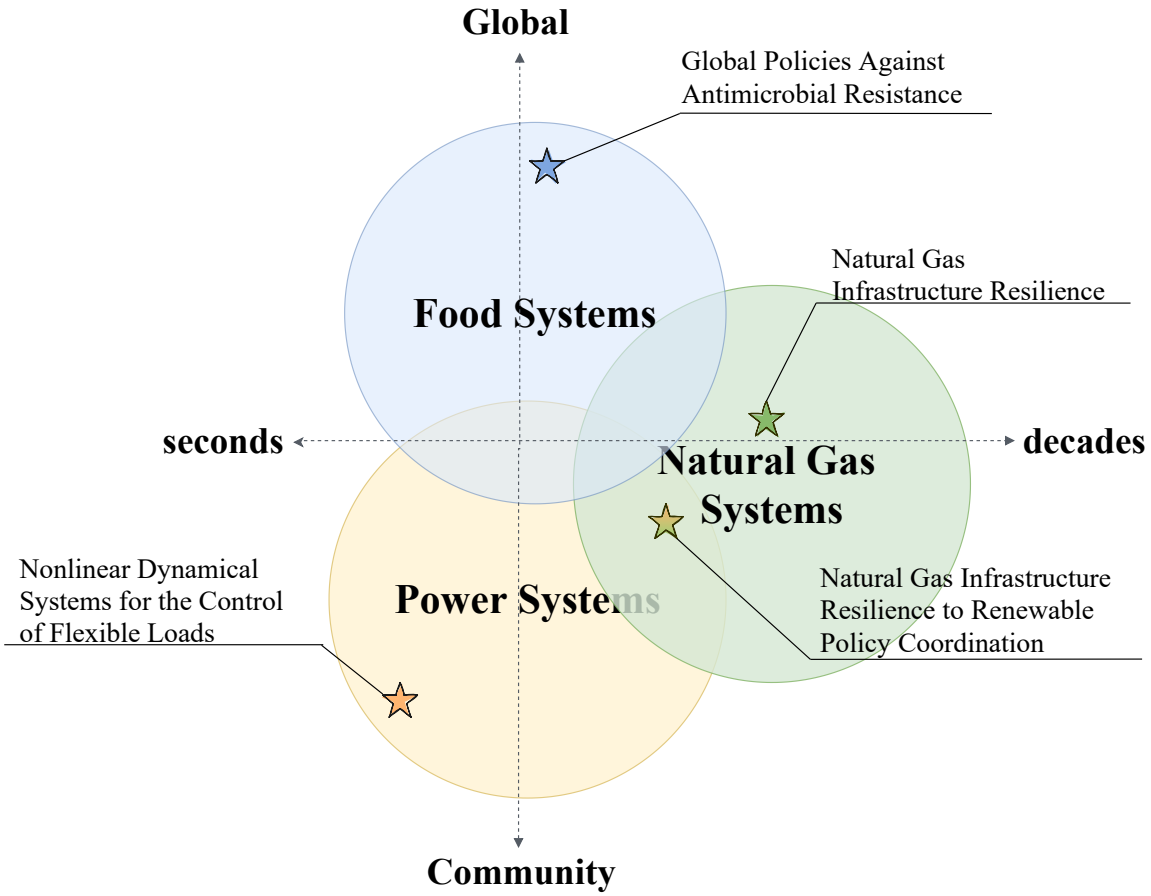

Figure 1.1: Research Overview: Resilience topics on electricity, natural gas, and food infrastructures across spatial and temporal scales.

In the electricity sector, we investigate how we can enhance the resilience of a power system by preventing voltage collapse under extreme loading. Voltage collapse is a type of blackout-inducing dynamic instability that occurs when power demand exceeds the maximum power that can be transferred through a network. The traditional approach to avoid voltage collapse is based on preventing the network from reaching its maximum capacity. However, such an approach leads to inefficient use of network resources and does not account for unforeseen events. We seek to design load controllers against voltage collapse. We formulate the problem of voltage stability for a star direct current network as a dynamic problem where each load seeks to achieve a constant power consumption by updating its conductance as the voltage changes. We contribute to power systems resilience by introducing a voltage collapse stabilization controller, and showing that the high-voltage equilibrium is stabilized. We also prove that our controller achieves proportional load shedding among flexible loads under extreme loading conditions. Our analysis has been submitted for publication to an academic journal and can be cited as: C. Avraam and E. Mallada. Voltage collapse stabilization in star DC networks, 2021.

In the natural gas sector, we investigate the resilience of North American natural gas markets and infrastructure to future market and policy trends. The exploitation of low-cost shale gas in the Marcellus Formation, the deregulation initiatives in the U.S. and Mexico, and the emergence of natural gas as a bridging fuel to a low-carbon economy has fueled the growth of North American natural gas production. Greater

introduction of renewables and deeper electrification can suppress both supply and demand for natural gas in the long-term. The long lead times of pipeline operation and field exploitation render the timing of phasing out natural gas use critical to natural gas infrastructure stakeholders. Full integration of the natural gas markets of the U.S., Canada, and Mexico implies that the phase-out trajectories of the three countries are tightly linked. We study the development of the integrated North American natural gas markets and infrastructure under different assumptions on resource availability, technological progress, and global crude oil prices. We quantify the impact of each scenario by using the North American Natural Gas Model. Our analysis contributes to the assessment of resilience of cross-border natural gas trade in North America. We also identify regions whose natural gas production and trade are more vulnerable to the three shocks and the tradeoff between growing natural gas production of Mexico and U.S.-Mexico cross-border trade. Our analysis has been published in an academic journal and the publication can be cited as: C. Avraam, D. Chu, and S. Siddiqui. Natural gas infrastructure development in North America under integrated markets. *Energy Policy*, 147:111757, 2020.

At the interdependence between the natural gas and electricity sectors, we investigate the resilience of North American natural gas markets to renewable policy coordination in the electricity sector. Renewable Portfolio Standards (RPS) are policies that accelerate renewables deployment but their impact on gas-fired plants remains ambiguous. We study the implications for the natural gas sector of more stringent

RPS under different coordination schemes in an integrated North American natural gas market. The scenarios assume that Renewable Energy Certificates generated in each region are traded 1) among all countries, 2) only within each country, and 3) only within model regions. We implement the three policies in four different energy and electricity models to generate projections of future natural gas consumption. Subsequently, we feed regional or country-level consumption changes of each model in each scenario to the North American Natural Gas Model. Our analysis establishes the impact of RPS on regional natural gas infrastructure investment and natural gas prices and trade. Our analysis has been published in an academic journal and the publication can be cited as: C. Avraam, J. E. Bistline, M. Brown, K. Vaillancourt, and S. Siddiqui. North American natural gas market and infrastructure developments under different mechanisms of renewable policy coordination. *Energy Policy*, 148:111855, 2021a.

In the food sector, we investigate the resilience of national food supply chains to international policies aiming to curb antimicrobial use in livestock production. Antimicrobial Resistance (AMR) is a threat to global health, aggravated by the use of antimicrobials in animal husbandry. Mitigating the growing economic costs related to AMR requires strong global coordination, and to that end policy makers can leverage global and national food animal trade policies, such as bans and user fees. Evaluation of such policies requires representing the interactions between competing producers in the global meat market, which is usually out of the scope of statistical models. For

that, we developed a game-theoretic food system model of global livestock production and trade between 18 countries and aggregate world regions. The model comprises the largest producing and consuming countries, the explicit interconnections between countries, and the use of antimicrobials in food animal production. Our study fills two critical knowledge gaps regarding antimicrobial use in the livestock sector. First, we endogenously account both for inter-country trade and antimicrobial use in meat production by proposing a game-theoretic framework. Second, we formulate global policy coordination scenarios based on the published literature and contemporary policy recommendations to derive policy insights on the impact of such policies to Low and Middle Income Countries (LMICs). Our work is an advancement over existing statistical models that cannot consider endogenous trade between countries and policy coordination scenarios. Our analysis has been published in an academic journal and the publication can be cited as: C. Avraam, A. S. Lambrou, W. Jiang, and S. Siddiqui. Antimicrobial resistance and livestock trade for low and middle income countries: Regional analysis of global coordination policies. *Frontiers in Sustainable Food Systems*, 5:79, 2021b.

1.4 Organization of Dissertation

The rest of the dissertation is organized as follows. In Chapter 2 we describe the mathematical theory underpinning the study of disruptions across spatial and tem-

poral scales. Section 2.1 is an introduction to nonlinear dynamical systems theory and stability, and Section 2.2 is an introduction to equilibrium methods for modeling interacting agents within infrastructures. Section 2.3 describes a bilevel optimization framework that can leverage the market interactions between agents as an additional source of information to generate data at the interdependencies of critical infrastructures. In Chapter 3 we build on nonlinear dynamical systems theory to develop a controller of flexible loads in the power system which can prevent voltage collapse in a star Direct Current network. Chapters 4 and 5 employ large-scale optimization-based tools to study the development and response of North American natural gas markets and infrastructure to market disruptions and shifts in renewable policy. In Chapter 6 we develop an equilibrium model of international meat production, consumption, and trade to assess global policies against antimicrobial resistance. Chapter 7 summarizes the main findings and identifies future research topics. Figure 1.2 displays the organization of this dissertation. All submitted and published papers have been edited for clarity and consistency with the rest of the dissertation.

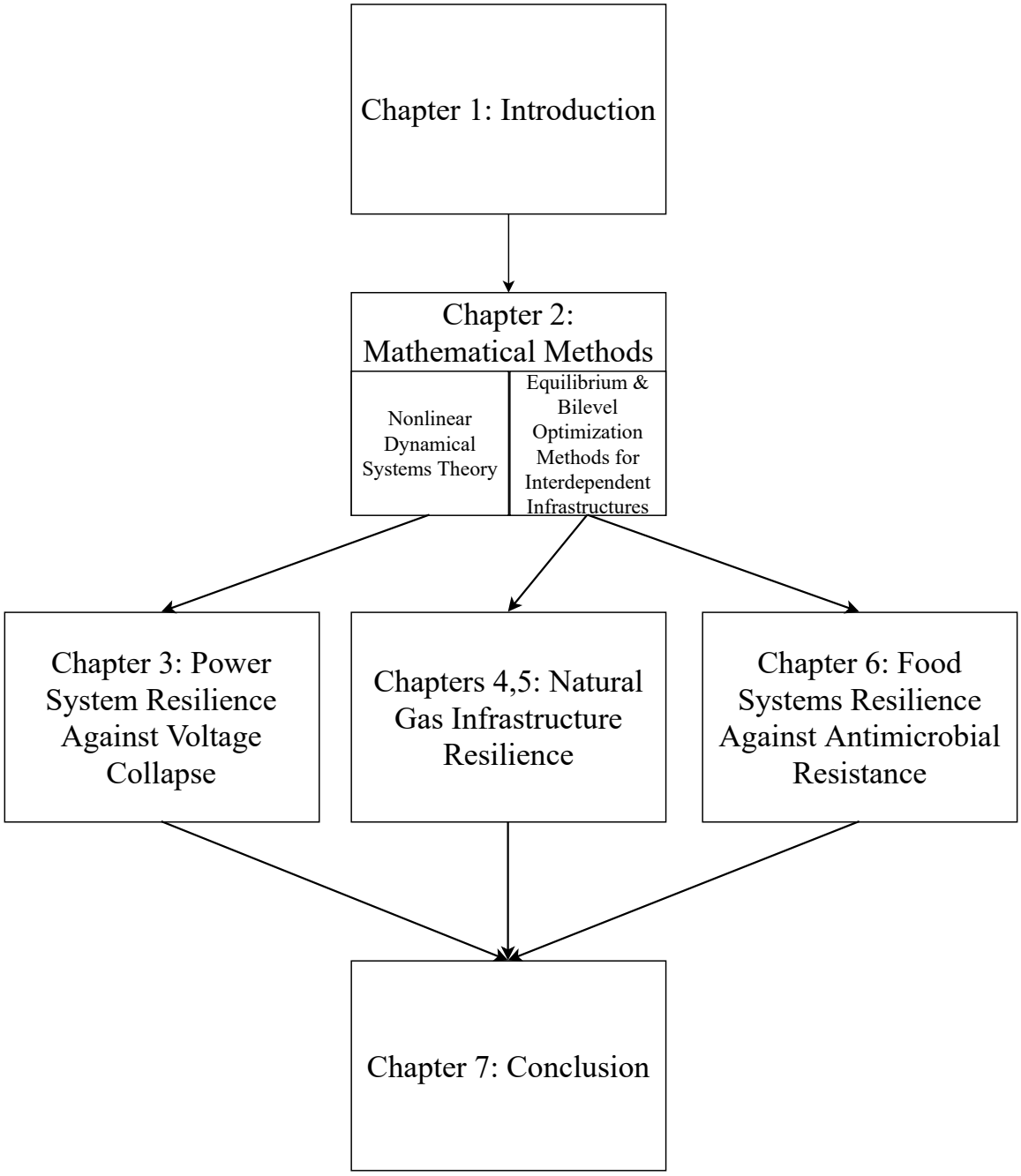

Figure 1.2: Organization of Dissertation.

Chapter 2

Mathematical Methods for Interdependent Infrastructures

2.1 Nonlinear Dynamical Systems Theory

2.1.1 Definitions

An *autonomous* or *time invariant* dynamical system comprises a finite number of first-order differential equations (Khalil, 2002), *i.e.,*

$$\begin{aligned} \dot{x}_1 &= f_1(x_1(t), x_2(t), \ldots, x_n(t)) \\ \dot{x}_2 &= f_2(x_1(t), x_2(t), \ldots, x_n(t)) \\ &\vdots \\ \dot{x}_n &= f_n(x_1(t), x_2(t), \ldots, x_n(t)) \end{aligned} \tag{2.1}$$

Variables $x_1, x_2, \ldots, x_n$ are the *state variables* of the system. We denote the derivative of each state with respect to time by $\dot{x}_i = \frac{dx_i}{dt}(t)$, for all $i = 1, 2, \ldots, n$. Vector $x = \begin{bmatrix} x_1 & x_2 & \ldots & x_n \end{bmatrix}^T \in V \subseteq \mathbb{R}^n$ is called the *state* of the system. Function $f = \begin{bmatrix} f_1 & f_2 & \ldots & f_n \end{bmatrix}^T : V \to \mathbb{R}^n$ is the state transition function and describes the underlying laws that govern the evolution of the system through time. The system (2.1) can also be written as

$$\dot{x} = f(x).$$

When f is nonlinear, the system (2.1) is called *nonlinear time invariant*, whereas when f is linear, the system (2.1) is called *linear time invariant* and can be written compactly in matrix form as

$$\dot{x} = Ax, \qquad A \in \mathbb{R}^n \times \mathbb{R}^n. \tag{2.2}$$

An *equilibrium* or *fixed point* of (2.1) is a vector x^* such that

$$\dot{x} = 0 \Rightarrow f(x^*) = 0. \tag{2.3}$$

Definition 1 (Definition 4.1 in Khalil (2002))**.** *The equilibrium point x^* of (2.1) is*

- *stable, if for each $\epsilon > 0$, there is $\delta = \delta(\epsilon) > 0$ such that*

$$||x(0) - x^*|| < \delta \Rightarrow ||x(t) - x^*|| < \epsilon, \quad \forall t \geq 0$$

- *unstable, if it is not stable*

- *asymptotically stable, if it stable and δ can be chosen such that*

$$||x(0) - x^*|| < \delta \Rightarrow \lim_{t\to\infty} x(t) = x^*.$$

2.1.2 Linearization

We can extract useful information on the behavior of a nonlinear dynamical system locally by studying the linearization of the system around a fixed point x^*. Let $v = x - x^*$, then the linearization of system (2.1) around x^* (Strogatz, 2015) is

$$\dot{v} = f(x^*) + \left[\frac{\partial f}{\partial x}(x)\right]_{x^*} v + O\left(v^2\right). \tag{2.4}$$

We call matrix $A = \left[\frac{\partial f}{\partial x}(x)\right]_{x^*} \in \mathbb{R}^n \times \mathbb{R}^n$ the *Jacobian* of (2.1). When x^* is an equilibrium point, then $f(x^*) = 0$. If we discard the quadratic terms we can rewrite equation (2.4) as a linear time invariant system

$$\dot{v} = Av. \tag{2.5}$$

The *characteristic polynomial* $p(s)$ of matrix A in (2.5) is given by

$$p(s) = \det(A - s\mathbb{I}_n) = a_n + a_{n-1} \cdot s + a_2 \cdot s^2 + \cdots + a_1 \cdot s^{n-1} + a_0 \cdot s^n \tag{2.6}$$

The roots of $p(s)$ are the eigenvales of matrix A.

2.1.3 Stability Theory

Assessing stability of complex nonlinear dynamical systems can be cumbersome. Theorem 1 establishes that, under certain assumptions, we can assess the stability of an equilibrium point of a nonlinear dynamical system by studying the stability of the linearized system around the equilibrium point.

Theorem 1 (Khalil (2002), Theorem 4.7)**.** *Let x^* be an equilibrium point of* (2.1)*, where $f : D \to \mathbb{R}^n$ is continuously differentiable and D is a neighborhood of x^*. Let*

$$A = \frac{\partial f}{\partial x}(x)\Big|_{x=x^*}.$$

Then,

1. *The point x^* is asymptotically stable if $Re(s_i) < 0$ for all eigenvalues of A.*

2. *The point x^* is unstable if $Re(s_i) > 0$ for one or more of the eigenvalues of A.*

Note that Theorem 1 is inconclusive if the linearized system has a zero eigenvalue or if the linearization fails. We can compute the eigenvalues of the Jacobian of a linearized system by finding the roots of the characteristic polynomial (2.6). The Routh-Hurwitz criterion establishes a method to assess the number of roots of a characteristic polynomial, thus eigenvalues of the Jacobian of the linearized system, that have positive real part.

Theorem 2 (Routh-Hurwitz Criterion, adjusted from Anagnost and Desoer (1991))**.**

Consider a n^{th}-order polynomial in s:

$$p(s) = a_n + a_{n-1} \cdot s + a_2 \cdot s^2 + \cdots + a_1 \cdot s^{n-1} + a_0 \cdot s^n,$$

where $a_i \in \mathbb{R}$, $a_n > 0$, and $a_0 \neq 0$. Construct the Routh table, written as in Table 2.1.

Table 2.1: Routh table for a real characteristic polynomial $p(s)$.

s^n	a_0	a_2	a_4	a_6	$\ldots$
s^{n-1}	a_1	a_3	a_5	a_7	$\ldots$
s^{n-2}	b_1	b_2	b_3	b_4	$\ldots$
s^{n-3}	c_1	c_2	c_3	c_4	$\ldots$
s^{n-4}	d_1	d_2	d_3	d_4	$\ldots$
$\vdots$	$\vdots$	$\vdots$	$\vdots$		
s^2	e_1	e_2			
s^1	f_1				
s^0	g_0				

The unknown coefficients are

$$b_1 = \frac{a_1 a_2 - a_0 a_3}{a_1}, \qquad b_2 = \frac{a_1 a_4 - a_0 a_5}{a_1}, \qquad b_1 = \frac{a_1 a_6 - a_0 a_7}{a_1}, \ldots$$

$$c_1 = \frac{b_1 a_3 - a_1 b_2}{b_1}, \qquad c_2 = \frac{b_1 a_5 - a_1 b_3}{b_1}, \qquad c_3 = \frac{b_1 a_7 - a_1 b_4}{b_1}, \ldots$$

$$d_1 = \frac{c_1 b_2 - b_1 c_2}{c_1}, \qquad d_2 = \frac{c_1 b_3 - b_1 c_3}{c_1}, \ldots$$

$$\vdots$$

and all entries of the first column are nonzero. Then, the roots of $p(s)$ have

$Re(s_i) < 0$ if and only if each element of the first column of the Routh Table is positive.

Equilibria of system (2.1) can change if we vary the parameters of the system. We can rewrite system (2.1) as

$$\dot{x} = f(x; r),$$

where $r \in \mathbb{R}$ is a parameter. The roots $s(r)$ of the characteristic polynomial of A in (2.5) also change for different values of r. When matrix A in (2.5) has a zero eigenvalue, the linearization fails. At an equilibrium point where the Jacobian of the system has a zero eigenvalue, two or more equilibria of the system collide into one. The change in the quantity, from two to one, or the quality of equilibria, from stable to unstable and vice versa, is called *bifurcation* (Strogatz, 2015). When the Jacobian of a nonlinear system has a zero eigenvalue, the bifurcation that occurs is called a *zero-eigenvalue bifurcation*. In this dissertation we encounter two zero-eigenvalue bifurcations.

- A *saddle-node* bifurcation, that occurs when an asymptotically stable and an unstable equilibrium collide and mutually annihilate (Strogatz, 2015).

- A *supercritical pitchfork* bifurcation, that occurs when two asymptotically stable equilibria and an unstable equilibrium collide and the stable equilibria annihilate, while the unstable equilibrium becomes asymptotically stable (Strogatz, 2015).

Figure 2.1 shows the qualitative and quantitave changes in equilibria of a system in a saddle-node and a supercritical pitchfork bifurcation.

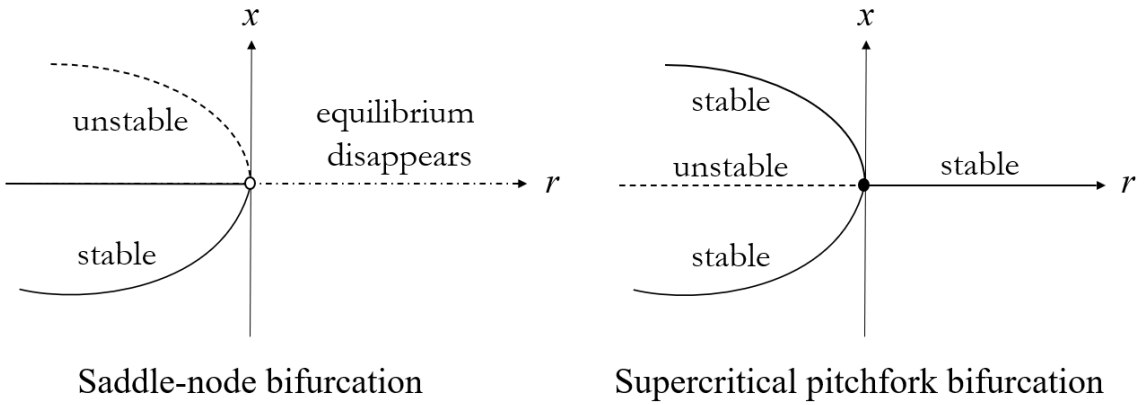

Figure 2.1: Types of zero-eigenvalue bifurcations in this dissertation. The equilibria of the system x^* change as we vary a system parameter $r \in \mathbb{R}$. In a saddle-node bifurcation (left), an asymptotically stable and an unstable equilibrium collide at $r = 0$ and disappear for $r > 0$. In a supercritical pitchfork bifurcation, three equilibria, one unstable and two asymptotically stable, collide for $r = 0$. The two stable equilibria disappear, and the unstable equilibrium becomes asymptotically stable for $r > 0$.

We can transform the type of bifurcation happening at $r = 0$ of a system (2.1) by introducing an input signal $u \in \mathbb{R}^m$. The new control system is

$$\begin{aligned} \dot{x} &= f(x, u; r) \\ y &= g(x, u) \\ \dot{\zeta} &= h(\zeta, y) \\ u &= l(\zeta, y) \end{aligned} \tag{2.7}$$

where $y \in \mathbb{R}^p$ is the vector of outputs of the system, and $\zeta \in \mathbb{R}^q$ are intermediate states that inform the input vector u. Functions $g : \mathbb{R}^n \times \mathbb{R}^m \to \mathbb{R}^p$, $l : \mathbb{R}^q \times \mathbb{R}^p \to \mathbb{R}^m$ compute the output and input vectors respectively, and function $h : \mathbb{R}^q \times \mathbb{R}^p \to \mathbb{R}^q$ is

the transition function of intermediate states ζ.

2.2 Equilibrium Methods for Interdependent Infrastructures

2.2.1 Mathematical Optimization Problems

An optimization problem computes a vector $x \in X \subseteq \mathbb{R}^n$ that minimizes an objective function $f : \mathbb{R}^n \to \mathbb{R}$, where $X = \{x \in \mathbb{R}^n : g(x) \leq 0 \text{ and } h(x) = 0\}$ is the *feasible set* of the optimization problem with $g : \mathbb{R}^n \to \mathbb{R}^m$ and $h : \mathbb{R}^n \to \mathbb{R}^o$.

$$\begin{aligned} &\min_{x \in \mathbb{R}^n} f(x; p) \\ &\text{subject to} \\ &\qquad g_\sigma(x; p) \leq 0, \qquad \sigma = 1, \ldots, m \quad (\lambda_\sigma) \\ &\qquad h_\tau(x; p) = 0, \qquad \tau = 1, \ldots, o \quad (\mu_\tau) \end{aligned} \tag{2.8}$$

We denote by $p \in \mathbb{R}^r$ the parameters of the optimization problem. Function f is called the *objective function*, $g_\sigma : \mathbb{R}^n \to \mathbb{R}$ are the *inequality constraints*, and $h_\tau : \mathbb{R}^n \to \mathbb{R}$ are the *equality constraints*. Variables λ_σ, μ_τ are the *dual variables* or *Lagrange multipliers* of the inequality and equality constraints respectively. A solution to problem (2.8) is called a *minimizer*.

Definition 2 (Global minimizer, Rockafellar (2015))**.** *The vector x^* is a global min-*

imizer of the optimization problem (2.8) *if*

$$f(x^*; p) \leq f(x; p) \qquad \forall x \in X.$$

Definition 3 (Local minimizer, Rockafellar (2015))**.** *The vector x^* is a local minimizer of the optimization problem* (2.8) *if*

$$f(x^*; p) \leq f(x; p) \qquad \forall x \in X \; satisfying \; ||x - x^*|| \leq \epsilon, \; for \; some \; \epsilon > 0.$$

Depending on the properties of functions f, g, h we can distinguish between *linear* and *nonlinear* optimization problems.

Definition 4 (Linear optimization problem, Boyd and Vandenberghe (2004))**.** *An optimization problem* (2.8) *is called a linear optimization problem or linear program when f, g, h are affine functions.*

When either f or any g_σ, h_τ are nonlinear functions, problem (2.8) is called a *nonlinear optimization problem* or *nonlinear program* (NLP) (Boyd and Vandenberghe, 2004). We can also distinguish between *convex* and *nonconvex* optimization problems.

Definition 5 (Convex optimization problem, Boyd and Vandenberghe (2004))**.** *An optimization problem* (2.8) *is called a convex optimization problem or convex program when f, g are convex and h is affine.*

When any condition of Definition 5 is violated, the optimization problem is a *nonconvex optimization problem* or *nonconvex program.* The *Lagrangian* function of

(2.8) is defined as

$$L(x, \lambda, \mu) = f(x; p) + \sum_{\sigma=1}^{m} g_\sigma(x; p)\lambda_\sigma + \sum_{\tau=1}^{o} h_\tau(x; p)\mu_\tau$$

From the Lagrangian, we can derive the *Karush-Kuhn-Tucker* (KKT) conditions of problem (2.8) as

$$\begin{aligned} \frac{\partial L}{\partial x_i}(x, \lambda, \mu) = \frac{\partial f}{\partial x_i}(x; p) + \sum_{\sigma=1}^{m} \frac{\partial g_\sigma}{\partial x_i}(x; p)\lambda_\sigma + \sum_{\tau=1}^{o} \frac{\partial h_\tau}{\partial x_i}(x; p)\mu_\tau = 0, \qquad & i = 1, \ldots, n \\ -g_\sigma(x; p) \geq 0, \qquad \lambda_\sigma \geq 0, \qquad \lambda_\sigma \cdot g_\sigma(x; p) = 0, \qquad & \sigma = 1, \ldots, m \\ h_\tau(x; p) = 0, \qquad \mu_\tau : \text{free}, \qquad & \tau = 1, \ldots, o \end{aligned} \tag{2.9}$$

Theorem 3 (Rockafellar (2015))**.** *For the optimization problem* (2.8)*, if* f, g_σ *are convex,* h_τ *are affine, and* (x^*, λ^*, μ^*) *satisfy* (2.9)*, then* x^* *is a global minimizer of* (2.8)*.*

In an optimization problem, the point x^* is called the *primal solution*, and (λ^*, μ^*) is called the *dual solution.*

2.2.2 Mixed Complementarity Problems

A Mixed Complementarity Problem (MCP) computes a vector $z \in \mathbb{R}^n$, for some finite $n \in \mathbb{N}$, function $F : \mathbb{R}^n \to \mathbb{R}^n$ and parameter vector $p \in \mathbb{R}^r$, that solves

$$\begin{aligned} z_\rho \geq 0, \qquad F_\rho(z;p) \geq 0, \qquad z_\rho F_\rho(z;p) = 0, \qquad \forall \rho \in \mathcal{I} \\ z_\rho : \text{free}, \qquad F_\rho(z;p) = 0, \qquad \forall \rho \in \mathcal{J} \end{aligned} \tag{2.10}$$

where $\mathcal{I} \subseteq \{1, \ldots, n\}$ is the subset of indices of functions $F_\rho \geq 0$ and $\mathcal{J} = \{1, \ldots, n\} \setminus \mathcal{I}$ is the subset of indices of functions $F_\rho = 0$. We can rewrite (2.10) more compactly (Facchinei and S. Pang, 2003) as

$$\begin{aligned} 0 \leq z_\rho \perp F_\rho(z;p) \geq 0, \qquad \rho \in \mathcal{I} \\ \text{free} : z_\rho \perp F_\rho(z;p) = 0, \qquad \rho \in \mathcal{J} \end{aligned} \tag{2.11}$$

Therefore, the KKT conditions (2.9) of an optmization problem can be viewed as a MCP

$$\begin{aligned} 0 \leq \quad & \lambda_\sigma \quad \perp \quad -g_\sigma(x;p) \geq 0, && \sigma = 1, \ldots, m \\ \text{free} : \quad & x_i \quad \perp \quad \tfrac{\partial L}{\partial x_i}(x, \lambda, \mu) = 0, && i = 1, \ldots, n \\ \text{free} : \quad & \mu_\tau \quad \perp \quad h_\tau(x;p) = 0, && \tau = 1, \ldots, o \end{aligned}$$

with

$$z = \begin{bmatrix} \lambda \\ x \\ \mu \end{bmatrix}, \qquad F(z;p) = \begin{bmatrix} -g(x;p) \\ \nabla_x f(x;p) + (\nabla_x g(x;p))^T \lambda + (\nabla_x h(x;p))^T \mu \\ h(x;p) \end{bmatrix}$$

Using MCPs, we can represent engineering systems or the decision making process of a single agent within a supply chain. We can also use MCPs to model interacting agents across interdependent infrastructures in a single framework. In this dissertation we will asume that interdependent infrastructures comprise interacting agents.

In our framework, *agents* describe decision-makers that decide on a variable of the interdependent system. For that, an agent could be a producer or a consumer in a supply chain, but could also be an entity, *e.g.,* a System Operator, or a device that decides control signals that ensure the operation of a component of the interdependent system. By *interacting* agents we imply that a decision of an agent affects the decisions of another. Agents can interact within a single infrastructure, across infrastructures, or both within and across infrastructures.

We denote by N the number of all interacting agents, and by $I = \{1, \ldots, N\}$ the set of all interacting agents, each deciding a set of variables $x^{(i)} \in \mathbb{R}^{n_i}$, where n_i is a finite number in $\mathbb{N}$. Each agent decides their action based on their individual objective and capabilities either using an optimization problem or a MCP. We denote by $I_C \subseteq I$ the set of agents who decide based on a MCP,

$$\begin{aligned} 0 \leq \quad & x_{\rho_i}^{(i)} \perp F_{\rho_i}^{(i)}\left(x;, p^{(i)}\right) \geq 0, && \rho_i \in \mathcal{I}^{(i)} \\ \text{free}: \quad & x_{\rho_i}^{(i)} \perp F_{\rho_i}^{(i)}\left(x; p^{(i)}\right) = 0, && \rho_i \in \mathcal{J}^{(i)} \end{aligned} \tag{2.12}$$

We denote by $\mathcal{I}^{(i)}$ the subset of indices of equations $F_{\rho_i}^{(i)} \geq 0$, and by $\mathcal{J}^{(i)}$ the subset of indices of equations $F_{\rho_i}^{(i)} = 0$.

We denote by $I_O = I \backslash I_C$ the set of agents who decide based on an optimization problem,

$$\min_{x^{(i)} \in \mathbb{R}^{n_i}} f^{(i)}\left(x; p^{(i)}\right)$$

subject to

$$\begin{aligned} g_{\sigma_i}^{(i)}\left(x; p^{(i)}\right) \leq 0, \qquad & \sigma_i = 1, \ldots, m_i \qquad && \left(\lambda_{\sigma_i}^{(i)}\right) \\ h_{\tau_i}^{(i)}\left(x; p^{(i)}\right) = 0, \qquad & \tau_i = 1, \ldots, o_i \qquad && \left(\mu_{\tau_i}^{(i)}\right) \end{aligned} \tag{2.13}$$

We denote by m_i, o_i the number of inequality and equality constraints of the optimization problem i respectively.

If $f^{(i)}, g_{\sigma_i}^{(i)}$ are convex, and $h_{\tau_i}^{(i)}$ are affine for each $i \in I_O$, by Theorem 3 we are guaranteed that a point that satisfies the KKT conditions of optimization problem i is also a minimizer of the optimization problem i. The KKT conditions of optimization problem i can be rewritten as complementarity conditions,

$$\begin{aligned} \text{free} : x_j^{(i)} \perp \quad & \frac{\partial f^{(i)}}{\partial x_j^{(i)}}\left(x; p^{(i)}\right) + \sum_{\sigma_i=1}^{m_i} \frac{\partial g_{\sigma_i}^{(i)}}{\partial x_j^{(i)}}\left(x; p^{(i)}\right) \lambda_{\sigma_i}^{(i)} + \sum_{\tau_i=1}^{o_i} \frac{\partial h_{\tau_i}^{(i)}}{\partial x_j^{(i)}}\left(x; p^{(i)}\right) \mu_{\tau_i}^{(i)} = 0, \\ & \qquad\qquad\qquad\qquad\qquad\qquad\qquad\qquad\qquad\qquad\qquad\qquad j \in \{1, \ldots, n_i\} \\ 0 \leq \lambda_{\sigma_i}^{(i)} \perp \quad & -g_{\sigma_i}^{(i)}\left(x; p^{(i)}\right) \geq 0, \qquad\qquad\qquad\qquad\qquad\qquad\qquad\qquad \sigma_i \in \{1, \ldots, m_i\} \\ \text{free} : \mu_{\tau_i}^{(i)} \perp \quad & h_{\tau_i}^{(i)}\left(x; p^{(i)}\right) = 0, \qquad\qquad\qquad\qquad\qquad\qquad\qquad\qquad \tau_i \in \{1, \ldots, o_i\} \end{aligned}$$

By grouping the complementarity conditions of all interacting agents, we can pose the problem of finding a vector z that is a minimizer of all optimization problems and a solution to all complementarity problems as a single MCP

$$
\begin{array}{lllll}
0 \leq & x_{\rho_i}^{(i)} & \perp & F_{\rho_i}^{(i)}\left(x; p^{(i)}\right) \geq 0, & \rho_i \in \mathcal{I}^{(i)}, \quad i \in I_C \\
\text{free}: & x_{\rho_i}^{(i)} & \perp & F_{\rho_i}^{(i)}\left(x; p^{(i)}\right) = 0, & \rho_i \in \mathcal{J}^{(i)}, \quad i \in I_C \\
\text{free}: & x_j^{(i)} & \perp & \frac{\partial f^{(i)}}{\partial x_j^{(i)}}\left(x; p^{(i)}\right) & \\
 & & & + \sum_{\sigma_i=1}^{m_i} \frac{\partial g_{\sigma_i}^{(i)}}{\partial x_j^{(i)}}\left(x; p^{(i)}\right) \lambda_{\sigma_i}^{(i)} & \\
 & & & + \sum_{\tau_i=1}^{o_i} \frac{\partial h_{\tau_i}^{(i)}}{\partial x_j^{(i)}}\left(x; p^{(i)}\right) \mu_{\tau_i}^{(i)} = 0, & j \in \{1, \ldots, n_i\}, \quad i \in I_O \\
0 \leq & \lambda_{\sigma_i}^{(i)} & \perp & -g_{\sigma_i}^{(i)}\left(x; p^{(i)}\right) \geq 0, & \sigma_i \in \{1, \ldots, m_i\}, \quad i \in I_O \\
\text{free}: & \mu_{\tau_i}^{(i)} & \perp & h_{\tau_i}^{(i)}\left(x; p^{(i)}\right) = 0, & \tau_i \in \{1, \ldots, o_i\}, \quad i \in I_O
\end{array}
\tag{2.14}
$$

A solution of (2.14) needs to satisfy the complementarity conditions of every agent i of the interdependent system. By Theorem 3, we are guaranteed that the solution $x^{(i)*}$ of (2.14) is also a minimizer of the optimization problem of each agent $i \in I_O$. In other words, no agent has the incentive to deviate from $x^{(i)*}$. To better understand the implications of this result, we introduce some basic notions of game theory.

Definition 6 (Normal Form Game, Fudenberg and Tirole (1991))**.** *A Normal Form Game is given by the triple* $\langle I, X, f \rangle$ *where:*

1. $I = \{1, ..., N\}$*, is the set of agents.*

2. $X := X^{(1)} \times ... \times X^{(N)}$*, with* $X^{(i)}$ *being the strategy set of agents* $i \in N$*, is the set of strategies.*

3. $f = \left\{f^{(i)}, i \in N\right\}$*, where* $f^{(i)} : X := X^{(1)} \times ... \times X^{(N)} \to \mathbb{R}$ $\forall i \in N$*, is the set of payoff functions.*

Definition 7 (Nash Equilibrium, Fudenberg and Tirole (1991))**.** *A strategy* $x^* = \left(x^{(1)*}, .., x^{(N)*}\right) \in X$ *is a Nash Equilibrium (NE) of a Normal Form Game if and only if for each* $i \in I$

$$f^{(i)}\left(x^*\right) \leq f^{(i)}\left(x\right), \qquad \forall x^{(i)} \in X^{(i)}. \tag{2.15}$$

In our setting,

$$\begin{aligned} X^{(i)} = \big\{ x^{(i)} \in \mathbb{R}^{n_i} \mid 0 \leq \;\; & x^{(i)}_{\rho_i} \perp F^{(i)}_{\rho_i}\left(x; p^{(i)}\right) \geq 0 \quad \forall \rho_i \in \mathcal{I}^{(i)}, \\ & \text{free} : x^{(i)}_{\rho_i} \perp F^{(i)}_{\rho_i}\left(x; p^{(i)}\right) = 0 \quad \forall \rho_i \in \mathcal{J}^{(i)} \,\big\}, \qquad i \in I_C \\ X^{(i)} = \big\{ x^{(i)} \in \mathbb{R}^{n_i} \mid & \; g^{(i)}\left(x; p^{(i)}\right) \leq 0 \text{ and } h^{(i)}\left(x; p^{(i)}\right) = 0 \,\big\}, \qquad i \in I_O \end{aligned}$$

The point x^* is a *Nash Equilibrium* of the game between the agents of interdependent infrastructures. For that, the MCP (2.14) is also called an *Equilibrium Problem* (EP) (Ferris and Munson, 2000). Equilibrium problems often comprise both types of agents,*i.e.,* $I_C \neq \emptyset$ and $I_O \neq \emptyset$. For example, we can pose the competition of profit-maximizing agents i in a single market under perfect competition as an equilibrium problem Mathiesen (1985). The price of the product needs to ensure that supply and demand are met at equilibrium, and so it is complementary to the market clearing constraint.

$$\begin{aligned} & x^{(i)} \in \arg\min_{x^{(i)}} \left\{ \pi - c^{(i)} \cdot x^{(i)} \;\; : \;\; x^{(i)} \in X^{(i)} \right\}, \qquad \forall i \in I_O \\ & \text{free} : \pi \perp \sum_{i=1}^{N} x^{(i)} - d = 0 \end{aligned} \tag{2.16}$$

where $x^{(i)} \in \mathbb{R}$ is the production of every agent, $c^{(i)} > 0$ is the marginal cost of

production of agent i, π is the market price, and d is the demand. The equilibrium problem (2.16) comprises interacting agents and a complementarity condition. We can think of the complementarity condition as the agent who ensures that production clears consumption and decides the price in the market.

Figure 2.2 depicts how we arrive at the MCP formulation for all agents across all interdependent infrastructures. At the top we find all agents within interdependent infrastructures that decide based on a MCP (top left) or an optimization problem (top right). For the set of agents $i \in I_O$, we derive the KKT conditions and pose them as a MCP (bottom right). We retrieve the model of interdependent infrastructures by collecting and jointly solving the complementarity conditions of all agents, which is also a MCP.

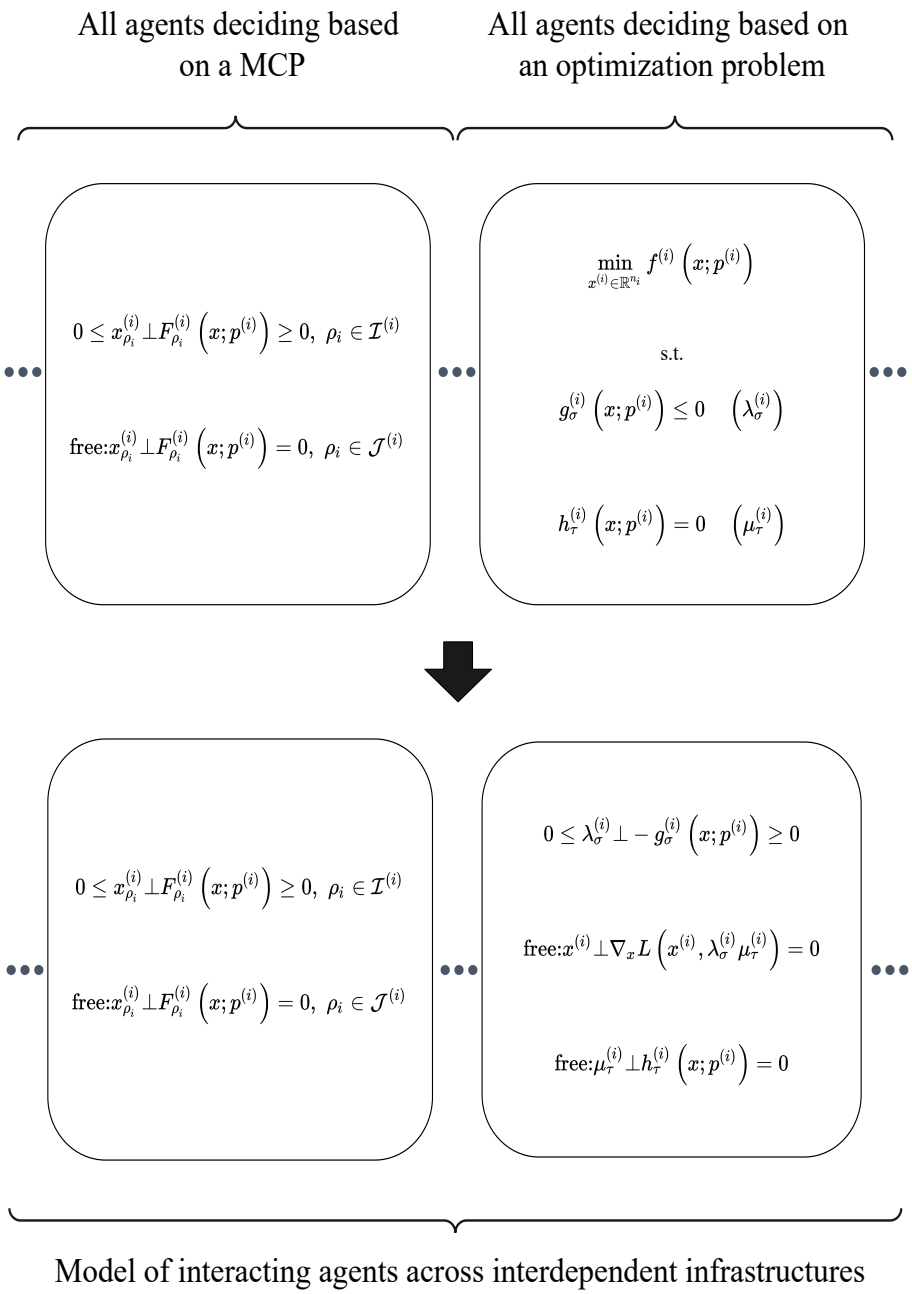

Figure 2.2: Model of interacting agents across interdependent infrastructures. The model is a single Mixed Complementarity Problem comprising the Mixed Complementarity Problems of all interacting agents across infrastructures.

2.3 Bilevel Optimization for Interdependent Infrastructures

2.3.1 Bilevel Optimization Problems

A *bilevel optimization problem* or *bilevel program* computes a vector that minimizes an objective function and is constrained by equality and inequality constraints, optimization problems, and complementarity conditions. The optimization problems that are constraints of the bilevel optimization problem are called *lower-level problems*. We assume that they are convex optimization problems. When the lower-level problems and complementarity conditions compose an equilibrium problem, we call the bilevel program a *Mathematical Program with Equilibrium Constraints* (MPEC) (Ralph, 2008). We focus on lower-level problems and complementarity conditions that describe the decisions $x^{(i)}$ of a finite set of interacting agents $i \in I$ within interdependent infrastructures, who we also refer to as *followers*.

$$\min_{(x,y)} V(x,y)$$

subject to

$$\begin{aligned} & x^{(i)} \in \arg\min_{x^{(i)}} \left\{ f^{(i)}\left(x; y, \bar{p}^{(i)}\right) \ : \ x^{(i)} \in X^{(i)} \right\}, && \forall i \in I_O \\ 0 \leq \quad & x_{\rho_i}^{(i)} \ \perp \ F_{\rho_i}^{(i)}\left(x; y, \bar{p}^{(i)}\right) \geq 0, && \forall \rho_i \in \mathcal{I}^{(i)},\ i \in I_C \\ \text{free}: \quad & x_{\rho_i}^{(i)} \ \perp \ F_{\rho_i}^{(i)}\left(x; y, \bar{p}^{(i)}\right) = 0, && \forall \rho_i \in \mathcal{J}^{(i)},\ i \in I_C \end{aligned} \tag{2.17}$$

We denote by $y \in \mathbb{R}^q$ the set of *upper-level variables*, who we also refer to as *leader* or *design* vector. Note that variable y of the bilevel optimization problem is considered a parameter of the lower-level problems and so is vector $\bar{p} \in \mathbb{R}^r$. Function $V : \prod_{i=1}^{N} \mathbb{R}^{n_i} \times \mathbb{R}^q \to \mathbb{R}$ is the objective function of the upper-level problem. Assuming that functions $f^{(i)}, g_\sigma^{(i)}, h_\tau^{(i)}$ are differentiable, finding a local minimizer of the bilevel optimization problem (2.17) is equivalent to finding a local minimizer of the following bilevel optimization problem

$$\min_{(x,y)} V(x,y)$$

subject to

$$\begin{aligned}
0 \leq \;& x_{\rho_i}^{(i)} \perp F_{\rho_i}^{(i)}\left(x; y, \bar{p}^{(i)}\right) \geq 0, && \rho_i \in \mathcal{I}^{(i)}, && i \in I_C \\
\text{free} : \;& x_{\rho_i}^{(i)} \perp F_{\rho_i}^{(i)}\left(x; y, \bar{p}^{(i)}\right) = 0, && \rho_i \in \mathcal{J}^{(i)}, && i \in I_C \\
\text{free} : \;& x_j^{(i)} \perp \frac{\partial f^{(i)}}{\partial x_j^{(i)}}\left(x; y, \bar{p}^{(i)}\right) \\
& \qquad + \sum_{\sigma_i=1}^{m_i} \frac{\partial g_{\sigma_i}^{(i)}}{\partial x_j^{(i)}}\left(x; y, \bar{p}^{(i)}\right) \lambda_{\sigma_i}^{(i)} \\
& \qquad + \sum_{\tau_i=1}^{o_i} \frac{\partial h_{\tau_i}^{(i)}}{\partial x_j^{(i)}}\left(x; y, \bar{p}^{(i)}\right) \mu_{\tau_i}^{(i)} = 0, && j \in \{1, \ldots, n_i\}, && i \in I_O \\
0 \leq \;& \lambda_{\sigma_i}^{(i)} \perp -g_{\sigma_i}^{(i)}\left(x; y, \bar{p}^{(i)}\right) \geq 0, && \sigma_i \in \{1, \ldots, m_i\}, && i \in I_O \\
\text{free} : \;& \mu_{\tau_i}^{(i)} \perp h_{\tau_i}^{(i)}\left(x; y, \bar{p}^{(i)}\right) = 0, && \tau_i \in \{1, \ldots, o_i\}, && i \in I_O
\end{aligned} \tag{2.18}$$

The bilevel program (2.18) comprises only complementarity constraints and for that it is called a *Mathematical Program with Complementarity Constraints* (MPCC). Ralph (2008) shows how we can use MPCCs to generate data within an infrastructure and studies problems in traffic networks. MPCCs are nonconvex programs and finding a global minimizer of a MPCC is a combinatorial problem, even when all lower-level functions are linear (Luo et al., 1996). The vast majority of MPCC algorithms are able to retrieve a solution to MPCCs by reformulating the bilevel optimization problem either into a mixed-integer program, *i.e.,* an optimization problem with some of the decision variables being integers, or into a NLP (Ferris and Munson, 2000). A MPCC can have multiple solutions (Gabriel et al., 2013).

2.3.2 Data Generation Framework for Critical Interdependent Infrastructures

In this section, we describe the bilevel optimization framework for data generation at the interdependencies of critical infrastructures. Following the assumptions and notation of Section 2.3.1, we distinguish between the subset of *unknown* parameters U_i and the subset of *known* parameters K_i of every agent $i \in N$, so $p^{(i)} = \left(y^{(i)}, \bar{p}^{(i)}\right) \in \mathbb{R}^{|U_i|} \times \mathbb{R}^{|K_i|}$ and

$$y = \left(y^{(1)}, y^{(2)}, \ldots, y^{(N)}\right) \in \prod_{i=1}^{N} \mathbb{R}^{|U_i|}, \qquad \bar{p} = \left(\bar{p}^{(1)}, \bar{p}^{(2)}, \ldots, \bar{p}^{(N)}\right) \prod_{i=1}^{N} \in \mathbb{R}^{|K_i|},$$

$$p = (y, \bar{p}) \in \prod_{i=1}^{N} \mathbb{R}^{|U_i|} \times \prod_{i=1}^{N} \mathbb{R}^{|K_i|}, \quad \text{with } \sum_{i=1}^{N} |U_i| + |K_i| = r.$$

Our goal is to compute the unknown parameters using bilevel optimization. Figure 2.3 shows the structure of the problem with interacting agents in two interdependent infrastructures.

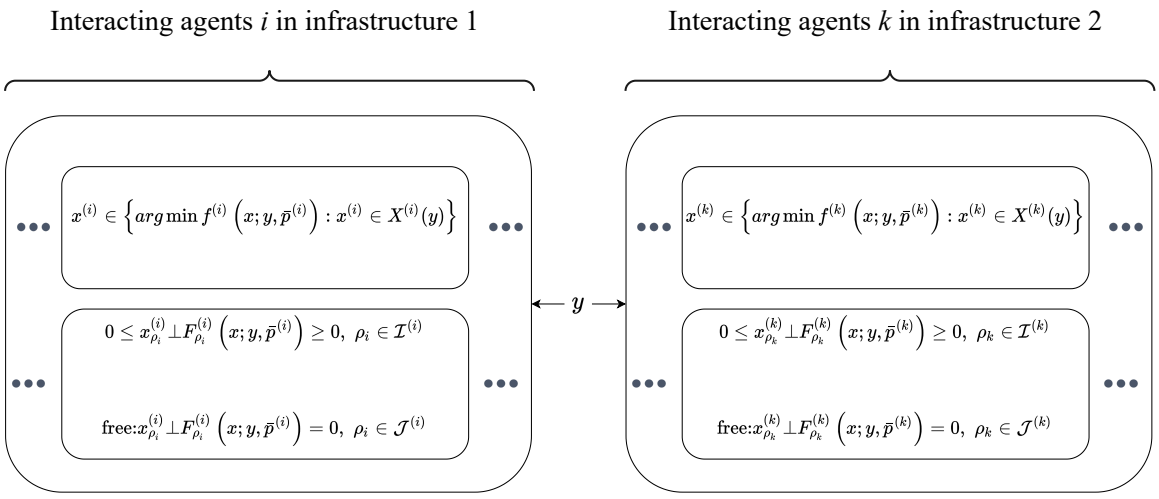

Figure 2.3: Two interdependent infrastructures, comprising multiple interacting agents in each infrastructure. The infrastructures are linked through a vector of parameters y.

We assume that we are provided with vector x^0, which includes either an observed equilibrium value of a variable or an estimation of the equilibrium value. We also have a preliminary estimate of our unknown parameters y^0. Our goal is to compute a vector y of the system (2.18), given $\bar{p}$ and x^0, that is informed by initial estimates y^0, but also from the decision-making process and the interactions between all agents across all interdependent infrastructures. The *Generalized Inverse Complementarity Problem* (GICP) is posed as a MPCC

$$\min_{(x,y)} \sum_{i=1}^{N} \sum_{j=1}^{n_i} w_{x,j}^{(i)} \left(x_j^{(i)} - x_j^{(i)0} \right)^2 + \sum_{i=1}^{N} \sum_{j=1}^{|U_i|} w_{y,j}^{(i)} \left(y_j^{(i)} - y_j^{(i)0} \right)^2$$

subject to

$$\begin{aligned}
0 \leq \;& x_{\rho_i}^{(i)} \perp F_{\rho_i}^{(i)} \left(x; y, \bar{p}^{(i)} \right) \geq 0, && \rho_i \in \mathcal{I}^{(i)}, && i \in I_C \\
\text{free} : \;& x_{\rho_i}^{(i)} \perp F_{\rho_i}^{(i)} \left(x; y, \bar{p}^{(i)} \right) = 0, && \rho_i \in \mathcal{J}^{(i)}, && i \in I_C \\
\text{free} : \;& x_j^{(i)} \perp \frac{\partial f^{(i)}}{\partial x_j^{(i)}} \left(x; y, \bar{p}^{(i)} \right) \\
& \qquad + \sum_{\sigma_i=1}^{m_i} \frac{\partial g_{\sigma_i}^{(i)}}{\partial x_j^{(i)}} \left(x; y, \bar{p}^{(i)} \right) \lambda_{\sigma_i}^{(i)} \\
& \qquad + \sum_{\tau_i=1}^{o_i} \frac{\partial h_{\tau_i}^{(i)}}{\partial x_j^{(i)}} \left(x; y, \bar{p}^{(i)} \right) \mu_{\tau_i}^{(i)} = 0, j \in \{1, \ldots, n_i\}, && && i \in I_O \\
0 \leq \;& \lambda_{\sigma_i}^{(i)} \perp -g_{\sigma_i}^{(i)} \left(x; y, \bar{p}^{(i)} \right) \geq 0, && \sigma_i \in \{1, \ldots, m_i\}, && i \in I_O \\
\text{free} : \;& \mu_{\tau_i}^{(i)} \perp h_{\tau_i}^{(i)} \left(x; y, \bar{p}^{(i)} \right) = 0, && \tau_i \in \{1, \ldots, o_i\}, && i \in I_O \\
0 \leq \;& G_\alpha \left(x, y, p \right) && && \alpha \in A_I \\
0 = \;& H_\alpha \left(x, y, p \right) && && \alpha \in A_E
\end{aligned} \tag{2.19}$$

We denote by A_I the set of all additional *inequality* constraints and by A_E the set of all additional *equality* constraints of the data-generation bilevel optimization problem (2.19). The additional constraints can incorporate additional information on certain variables of the GICP. For example, we can introduce upper and lower limits on natural gas production costs, which are additional inequality constraint. Another example involves finding regional retail livestock prices when we know the retail price of livestock products in a collection of regions. In this case we need to introduce an equality constraint that links the regional retail prices with the observed retail price

of the collection of regions. The MPCC reformulation allows us to incorporate more knowledge into the original MPEC (2.17) through additional constraints and arrive to a more informed approximation of the unknown parameters. Following the notation in Section 2.3.1, the objective function is

$$V(x,y) = \sum_{i=1}^{N}\sum_{j=1}^{n_i} w_{x,j}^{(i)}\left(x_j^{(i)} - x_j^{(i)0}\right)^2 + \sum_{i=1}^{N}\sum_{j=1}^{|U_i|} w_{y,j}^{(i)}\left(y_j^{(i)} - y_j^{(i)0}\right)^2.$$

The choice of the objective can affect the results of the framework. Choosing another objective function can lead to another feasible point (x, y) being the minimizer of (2.19). In our setting, vector y is unknown. For that, we choose to minimize the sum of squared differences because a quadratic objective function does not penalize large deviations of x, y from the observed or estimated values x^0, y^0. Moreover, the chosen objective function is twice differentiable, which allows us to use more efficient MPCC algorithms compared to the case where V is a weighted L-1 norm.

Although the goal is to compute y, in the general case we also include in the objective function a subset of variables x. Our framework is used to compute parameters, but also to reconcile inconsistencies between agents' variables when they track the same variable. For example, for a gas-fired power plant, natural gas purchasing reported at a selling point may differ from the reported natural gas consumption by the power plant. Substituting the data reported at the point of purchasing into the complementarity conditions of the power generator will likely violate a constraint related to the combustion process. A data-generating MPCC (2.19) can compute variable

"natural gas consumption for power generation" at the interdependence of the natural gas and electricity sectors that satisfies the KKT conditions of *all* interacting agents in the two systems. The same can happen between interacting agents within the same infrastructure. The weights $w_{x,j}^{(i)}, w_{y,j}^{(i)} \geq 0$ grasp our confidence on x^0, y^0 respectively. Greater confidence in x^0, y^0 translates to larger value of $w_{x,j}^{(i)}, w_{y,j}^{(i)}$. When we require a solution of MPCC (2.19) to be $x_l^{(i)0}$, then we can simply substitute $x_l^{(i)} := x_l^{(i)0}$ to MPCC (2.19).

Finally, the data-generation bilevel program offers a unifying framework for parameter estimation. When the constraints of (2.19) arise from a single optimization problem, then estimating a subset of unknown parameters y given an observed value for the variables x^0 is called a *(Generalized) Inverse Optimization Problem* (Chan et al., 2018). Statistical models that are expressed as a set of equalities, *e.g.,* linear regression models (Stock and Watson, 2011), are the special case where $I_C, I_O, A_I = \emptyset$. The bilevel optimization framework accommodates also jointly estimating parameters and variables of any combination of optimization problems and statistical models.

2.3.3 Data Generation at the Interdependencies of Critical Infrastructures

In this section we focus on problems that have a particular structure. First, all agents decide a *production* variable $\tilde{x}^{(i)} \geq 0$, demand variables $s^{(i)} \in \mathbb{R}^N_{\geq 0}$, and additional

agent-specific variables $\hat{x}^{(i)} \in \mathbb{R}^{n_i - N - 1}$, *i.e.*,

$$x^{(i)} = \left(\tilde{x}^{(i)}, s^{(i)}, \hat{x}^{(i)}\right).$$

Agents $i \in I_O$ decide $x^{(i)}$ based on the following optimization problem

$$\begin{aligned} &\min_{x^{(i)} \in \mathbb{R}^n} \pi^{(i)} \cdot \tilde{x}^{(i)} - c^{(i)}\left(x; y, \bar{p}^{(i)}\right) \\ &\text{subject to} \\ &\quad A_\sigma^{(i)}\left(y, \bar{p}^{(i)}\right) x^{(i)} \leq b_\sigma^{(i)}\left(y, \bar{p}^{(i)}\right), \qquad \left(\lambda_\sigma^{(i)}\right) \\ &\quad A_\tau^{(i)}\left(y, \bar{p}^{(i)}\right) x^{(i)} = b_\tau^{(i)}\left(y, \bar{p}^{(i)}\right), \qquad \left(\mu_\tau^{(i)}\right) \end{aligned} \tag{2.20}$$

where $f^{(i)}\left(x; y, \bar{p}^{(i)}\right) = \pi^{(i)} \cdot \tilde{x}^{(i)} - c^{(i)}\left(x; y, \bar{p}^{(i)}\right)$ is assumed to be convex on $x^{(i)}$. Matrices $A_\sigma^{(i)} \in \mathbb{R}^{m_i \times n_i}$, $A_\tau^{(i)} \in \mathbb{R}^{o_i \times n_i}$, and vectors $b_\sigma \in \mathbb{R}^{m_i}$, $b_\tau \in \mathbb{R}^{o_i}$ can comprise both known and unknown parameters of the respective constraints. We denote the price of product i by $\pi^{(i)}$. Function $\pi^{(i)} \cdot \tilde{x}^{(i)}$ is the *revenue function* and $c^{(i)}\left(x; y, \bar{p}^{(i)}\right)$ is the *cost function* of agent i. For agents $i \in I_C$ we assume linear complementarity conditions, which is also the case for market clearing conditions in economic equilibrium problems (Mathiesen, 1985), *i.e.*,

$$\begin{aligned} 0 \leq \quad & x_j^{(i)} \quad \perp \quad \textstyle\sum_{l=1}^{N} \sum_{k=1}^{n_i} m_k^{(l)}\left(y, \bar{p}^{(l)}\right) \cdot x_k^{(l)} + v^{(i)}\left(y, \bar{p}^{(i)}\right) \geq 0, \quad j \in \mathcal{I}^{(i)} \\ \text{free}: \quad & x_j^{(i)} \quad \perp \quad \textstyle\sum_{l=1}^{N} \sum_{k=1}^{n_i} m_k^{(l)}\left(y, \bar{p}^{(i)}\right) \cdot x_k^{(l)} + v^{(i)}\left(y, \bar{p}^{(l)}\right) = 0, \quad j \in \mathcal{J}^{(i)} \end{aligned} \tag{2.21}$$

We assume that $m_k^{(l)}, v^{(i)} \in \mathbb{R}$ can comprise both known or unknown parameters. Therefore, in (2.19), the only nonlinear function can be the cost function $c^{(i)}\left(x; y, \bar{p}^{(i)}\right)$. Substituting $c^{(i)}\left(x^{(i)}; y, \bar{p}^{(i)}\right)$ into MPCC (2.19) can introduce nonlinearities in the computation of unknown cost function parameters. For example, We

can think of an agent $i \in I_O$ of the system with the convex cost function

$$c^{(i)} = a_0^{(i)} + a_1^{(i)} \cdot \tilde{x}^{(i)} + \frac{1}{2} \cdot a_2^{(i)} \cdot \left(\tilde{x}^{(i)}\right)^2 + a_3^{(i)} \cdot e^{\delta^{(i)} \cdot \tilde{x}^{(i)}}. \tag{2.22}$$

A conventional MPCC algorithm will require additional time for operations related to the exponential term. The optimization problem (2.20) with a convex cost function (2.22) is still a convex optimization problem, since it has a convex objective function, convex inequality constraints, and affine equality constraints, but introduces nonlinearities that are harder to solve than an optimization problem with a quadratic cost function.

We assume that agents buy and sell products in markets under perfect competition. The market clearing constraint of each product i, which is a lower-level complementarity condition, ensures that the price $\pi^{(i)}$ is such that supply of product i satisfies demand, *i.e.,*

$$0 \leq \ \pi^{(i)} \ \perp \tilde{x}^{(i)} - \sum_{j=1}^{N} s_i^{(j)} - \bar{d}^{(i)} \ \geq 0. \tag{2.23}$$

The demand variable $s_i^{(j)}$ denotes the demand for product i from agent j, while parameter $\bar{d}^{(i)}$ is some fixed exogenous demand for product i. At the interdependencies, the interaction between agents j and i is driven by the demand of an agent in one infrastructure for the product of an agent in another. We assume that demand $s_i^{(j)}$ of agent j for input i is proportional to the level of output $\tilde{x}^{(j)}$, *i.e.,*

$$s_i^{(j)} = \alpha_i^{(j)} \cdot \tilde{x}^{(j)} \tag{2.24}$$

Therefore, generating data at the interdependencies of critical infrastructures translates into computing parameters $\alpha_i^{(j)}$.

Moreover, we assume that we know the *value share* $\beta_i^{(j)} \geq 0$ of input i for the production of j, which is the value of revenues divided by the cost of input i, *i.e.*,

$$\beta_i^{(j)} = \frac{\pi^{(i)} \cdot s_i^{(j)}}{\pi^{(j)} \cdot \tilde{x}^{(j)}} \tag{2.25}$$

By substituting equation (2.24) into the definition of value share (2.25), we retrieve

$$\beta_i^{(j)} = \alpha_i^{(j)} \cdot \frac{\pi^{(i)}}{\pi^{(j)}} \Rightarrow \alpha_i^{(i)} = \beta_i^{(j)} \cdot \frac{\pi^{(j)}}{\pi^{(i)}}. \tag{2.26}$$

Equation (2.26) says that in order to compute $\alpha_i^{(j)}$, we need the value share parameter and equilibrium prices of products i, j.

Based on the structure of the problem, we design a two-stage decomposition process to compute parameters $\alpha_i^{(j)}$. In the first stage we aim to compute prices $\pi^{(i)}$. For that, instead of solving a data-generating MPCC (2.19) for all interdependent infrastructures, we formulate a MPCC for interacting agents only within the same infrastructure. Hence, in the first stage we need to solve one MPCC for each infrastructure. In order to address potential nonlinearities in the cost function, we do not substitute $c^{(i)}\left(x; y, \bar{p}^{(i)}\right)$ into the MPCC, but assume that $c^{(i)}$ are parameters in the bilevel framework and can be known or unknown. In order to address the interdependence arising from $s_i^{(j)}$, we substitute

$$\bar{s}_j := \sum_{i=1}^{N} s_j^{(i)},$$

and assume that $\bar{s}_j$ is a parameter in (2.23).

In this way, we achieve two goals at the first stage of the process. First, we avoid solving a single MPCC with hundreds of thousands of variables by solving smaller MPCCs that are parallelizable. Second, each MPCC comprises linear functions, since all functions in the constraints are linear. The solution of the individual MPCCs provides prices $\pi^{(i)*}$ for all agents i in the interdependent system. In the second stage, for given value shares $\beta_i^{(j)}$, we compute parameters $\alpha_i^{(j)}$ by substituting $\pi^{(i)*}$ from the first stage to equation (2.26).

In conclusion, generating data at the interdependencies of critical infrastructures in our framework translates into computing parameters $\alpha_i^{(j)}$ in equation (2.26). If we know the value share of input i in the production of product j and assuming that inputs are used in fixed proportions, then finding $\alpha_i^{(j)}$ requires computing the prices $\pi^{(j)}, \pi^{(i)}$. Based on this observation, we design a two-stage decomposition process which in the first stage decomposes the original data-generation MPCC into smaller, parallelizable MPCCs, one for each infrastructure. The second stage receives equilibrium prices as inputs and finds $\alpha_i^{(j)}$ through equation (2.26). The ability to decompose the problem into smaller, parallelizable problems, can speed up the MPCC solution-finding process. Especially for problems with hunderds of thousands of variables.

We identify three limitations of the methodology. The first arises from data availability. Using bilevel optimization we are able to leverage additional knowledge from the market interactions between agents. For example, if we know that trade happens

between two regions then, assuming profit-maximizing traders and in the absence of other incentives, the purchasing price of the traded good in the start region needs to be smaller than the selling price of the good at the end region. This is knowledge that arises from the decision-making problem of the trader. Therefore, knowing that trade happens, even without knowing the exact quantity, bounds the purchasing or selling price. However, this additional knowledge may still not be enough to generate robust parameter and variable estimates if we lack other reliable data. Second, the data at the interdependencies are generated by assuming that production of j requires a fixed amount of product i. This may not be the case and the relationship of the two products can be nonlinear. The fixed inputs assumption is applicable for data-generation purposes where we are trying to generate input-output data. However, when attempting to integrate models of critical interdependent infrastructures to study resilience scenarios, this assumption may constrain model integration, or drive the scenario results. Finally, large-scale implementations of MPCCs are usually easier to handle via a NLP compared to a mixed interger reformulation. For a NLP reformulation, we are not guaranteed that a solution to the NLP is a minimizer and can instead be a stationary point that is not a minimizer (Ralph, 2008). Moreover, finding a global minimizer of MPCCs is computationally hard and there can exist many local minimizers (Gabriel et al., 2013). Hence, we can view the MPCC solution as a more informed estimate compared to y^0. The flexibility of adding additional constraints to the data-generating MPCC can ensure that the generated data are

"reasonable", if we constrain the feasible space to "reasonable" values. Nontheless, the methodology allows us to identify data gaps and better understand the interactions between critical infrastructures.

Chapter 3

Enhancing Power Systems Resilience Against Voltage Collapse

3.1 Introduction

Loads with constant power consumption tend to dynamically reduce their effective impedance as a means to compensate for a reduction on the power supplied by the network (Van Cutsem and Vournas, 1998). However, when the network power transfer capacity is met, further reduction on the effective impedance results in a greater gap between the power supplied to the load and the power demanded by it. This continuous update on the effective impedance results in an abrupt voltage drop that leads to voltage collapse (VC) (Kundur et al., 1994, 2004). From a dynamical systems perspective, VC is the manifestation of a saddle node bifurcation where a stable and

an unstable equilibrium coalesce, and disappear. As a result, VC is by definition a dynamic phenomenon that naturally depends on the load dynamics.

Despite its dynamic nature, voltage stability studies have traditionally focused on static analyses, based on load flow equations (Dobson, 1992), ensuring enough generation and transmission capacity to avoid VC (Irisarri et al., 1997). The vast majority of work focuses on the quantification of generation- and network-side voltage stability margins. Demand-side management tools are limited (Strbac et al., 1998). Operating within the stability margins ensures the system never reaches its limits. Classical system stability metrics include (Obadina and Berg, 1988; Cutsem, 1991; Alvarado et al., 1994; Bompard et al., 1996), and more recently (Vournas et al., 2016; John W. Simpson-Porco, 2016). However, existing stability margins implicitly enforce a trade-off between reliability against VC and efficient use of resources (Strbac, 2008).

Fortunately, the rapid development of power electronics and information technology (Bayoumi, 2015) has the potential to provide enough demand-side controllability that could allow us to consider more alternatives for preventing VC. Here, we introduce one such alternative with the study of *voltage collapse stabilization*. Specifically, we aim to investigate how to use (flexible) demand response to reduce consumption and match network capacity, when total demand exceeds it. In this way we prevent inflexible demand from driving the system to VC. To the best of our knowledge, this work is the first effort to design dynamic, demand-side controllers aimed at preventing VC. Such a control scheme needs to overcome several challenges that arise from the

dynamic nature of VC.

First, the controller needs to stabilize an operating point that is unstable under normal operating conditions[1]. Further, the stabilization procedure should be robust to the presence of conventional loads that are not willing to reduce their consumption, referred here as inflexible loads. Thus, in the presence of both flexible and inflexible loads in a system, we ask the following questions:

- Is voltage collapse stabilization feasible?
- Can a stabilizing controller distribute efficiently the necessary demand reduction among flexible loads?

In this chapter, we provide an initial answer to the research questions for a star direct current network. We consider a resistive star network where each load seeks to consume a constant amount of power by dynamically updating its conductance using a first order voltage droop. Despite its simplicity, this model captures the fundamental drivers of VC[2].

Indeed, when all loads are inflexible (nominal conditions), we show that if the total demand is smaller than the network capacity, the system has a stable and an unstable equilibrium. Further, when demand exceeds capacity, we analytically show that the voltage $v(t) \to 0$ as $t \to \infty$, *i.e.,* the voltage collapses. Once the setup has been analytically validated, we introduce the voltage collapse stabilization controller

[1]At a saddle node bifurcation a stable and an unstable equilibrium coalesce, which leads to an unstable equilibrium (Khalil, 2002).

[2]The model and our results also extend to a fully reactive alternating current star networks.

that stabilizes voltage collapse, even in the presence of inflexible loads, as long as flexible demand is not depleted. Further, we show that stabilization can be achieved with a proportionally fair allocation of load shedding.

The rest of the chapter is organized as follows. Section 3.2.1 introduces our DC network model of constant power loads. Section 3.2.2 investigates the properties of a system that comprises only inflexible loads and characterizes the region of stable equilibria. Section 3.2.3 describes our voltage collapse stabilization controller and characterizes the equilibria of the new system. Section 3.2.4 studies the stability of each equilibrium point at different operating conditions. We illustrate several features of our controller using numerical simulations in Section 3.3 and conclude in Section 3.4.

3.2 Methods

3.2.1 Problem Setup

We consider the star DC network model shown in Figure 3.1**,** where E denotes the source voltage, g_l the conductance of a transmission line that transfers power to n loads, and g_i denotes the ith load conductance, $i \in N := \{1, \ldots, n\}$. We consider two sets of loads, with $F = \{1, ..., n_F\}$ being the set of *flexible* loads ($n_{\mathrm{F}} = |F|$), and $I = \{n_F + 1, ..., n\}$ being the set of *inflexible* loads ($n_I = |I|$). The set of all loads is

$N = I \cup F = \{1, \ldots, n\}$. For any subset $S \subseteq N$, we denote the vector of conductances of loads in S by $g_S \in \mathbb{R}^{|S|}_{\geq 0}$ and

$$\bar{g}_{\mathrm{S}}(g) = \sum_{i \in S} g_i. \tag{3.1}$$

Throughout the chapter it is important to keep track of the dependence of several quantities, *e.g.,* voltages, powers, and their derivatives. This explicit dependence $(\cdot)$ (*e.g.,* $\bar{g}_{\mathrm{S}}(g)$) is highlighted when quantities are introduced, but dropped later on (*e.g.,* $\bar{g}_{\mathrm{S}}$) to improve readability of the formulae.

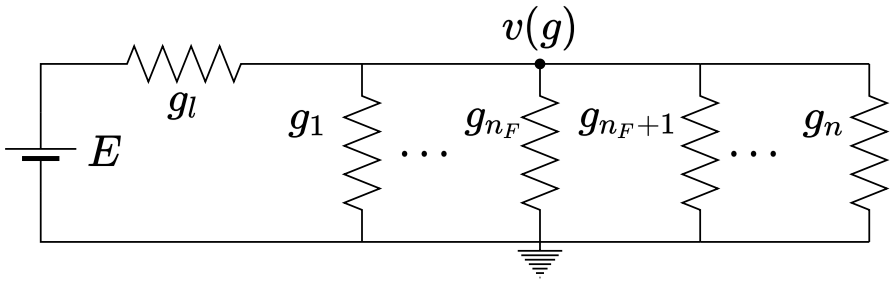

Figure 3.1: Star DC network with n dynamic loads.

Using this notation, we can use Kirchoff's Voltage and Current Laws (KVL and KCL) to compute the voltage applied to each load

$$v\left(\bar{g}_{\mathrm{N}}\right) = \frac{E \cdot g_l}{\bar{g}_{\mathrm{N}} + g_l}. \tag{3.2}$$

where, from (3.1), $\bar{g}_{\mathrm{N}} = \sum_{i \in N} g_i$.

Then, the total power consumed by each load $i \in N$ becomes

$$P_i(g) = v^2 g_i = \left(\frac{E \cdot g_l}{\bar{g}_{\mathrm{N}} + g_l}\right)^2 g_i. \tag{3.3}$$

The difference between the power consumed by each load $i \in N$ and its nominal demand $P_{0,i} \geq 0$ is

$$\Delta P_i(g) = P_i - P_{0,i}. \tag{3.4}$$

The total power consumed by all loads in the system is

$$\bar{P}_{\mathrm{N}}(\bar{g}_{\mathrm{N}}) = \sum_{i=1}^{n} P_i = \frac{(E \cdot g_l)^2}{(\bar{g}_{\mathrm{N}} + g_l)^2} \bar{g}_{\mathrm{N}}. \tag{3.5}$$

Similarly, total demand is defined as

$$\bar{P}_{0,\mathrm{N}} = \sum_{i=1}^{n} P_{0,i}, \tag{3.6}$$

and the difference between total power supply and power demand is

$$\overline{\Delta P}_{\mathrm{N}}(\bar{g}_{\mathrm{N}}) = \sum_{i=1}^{n} (P_i - P_{0,i}) = \bar{P}_{\mathrm{N}} - \bar{P}_{0,\mathrm{N}}, \tag{3.7}$$

where the dependence on $\bar{g}_{\mathrm{N}}$ follows from (3.5).

Network Capacity ($P_{\max}$): Voltage collapse in a DC network can result from the network reaching its maximum capacity (Van Cutsem and Vournas, 1998). Therefore, it is of interest to compute the maximum value of $\bar{P}_{\mathrm{N}}(\bar{g}_{\mathrm{N}})$ in (3.5). A straightforward calculation leads to

$$\frac{\partial}{\partial \bar{g}_{\mathrm{N}}} \bar{P}_{\mathrm{N}}(\bar{g}_{\mathrm{N}}) = \frac{(E g_l)^2}{(\bar{g}_{\mathrm{N}} + g_l)^3} (g_l - \bar{g}_{\mathrm{N}}). \tag{3.8}$$

From (3.8), we can see that $\bar{P}_{\mathrm{N}}(\bar{g}_{\mathrm{N}})$ is an increasing function of $\bar{g}_{\mathrm{N}}$ whenever $\bar{g}_{\mathrm{N}} < g_l$, and decreasing when $\bar{g}_{\mathrm{N}} > g_l$. Therefore, when $\bar{g}_{\mathrm{N}} := g_l$, the maximum

power that can be supplied through the line is

$$P_{\max} = \frac{E^2 g_l}{4}. \tag{3.9}$$

Dynamic Load Model: We assume that each load $i \in N$ has a constant power demand $P_{0,i}$. For an *inflexible load* $i \in I$, this demand $P_{0,i}$ must always be (approximately) satisfied. This is achieved by dynamically changing the conductance g_i in order to change the power supply $P_i(g)$. Following Vournas and Sakellaridis (2008), we use the following dynamic model

$$\dot{g}_i = -\left(v^2 g_i - P_{0,i}\right) = -\Delta P_i, \qquad i \in I. \tag{3.10}$$

We track demand at the seconds scale. Notice that $\mathbb{R}^n_{\geq 0}$ is invariant, since whenever $g_i = 0$ then (3.10) implies that $\dot{g}_i > 0$.

For the *flexible loads*, we assume that they are willing to consume less than $P_{0,i}$ whenever $\bar{P}_{0,\mathrm{N}} := \sum_{i \in N} P_{0,i} > P_{\max}$. Thus, our goal is to design a control law

$$\dot{g}_i = u_i, \quad i \in F, \tag{3.11}$$

where the input u_i is such that in equilibrium $\Delta P_i(g) = 0$ whenever $\bar{P}_{0,\mathrm{N}} < P_{\max}$.

Power Flow Solutions: Given an equilibrium g^* of (3.10)-(3.11), there exists a unique voltage v^* and power consumption $P(g^*) = (P_i(g^*),\, i \in N)$. The pair (v, P) is referred as *power flow solution*. Thus, given the one-to-one relationship between g and the pair (v, P), we refer to g^* as a power flow solution.

Loads of modern power systems are predominantly inflexible. For that, in the

following subsection we will study the case where all loads are inflexible and are controlled via (3.10). The case where $N = I$ serves also as the baseline for our study. In Section 3.2.3 we will revisit this assumption in order to enhance the resilience of a star DC network.

3.2.2 System Analysis with Inflexible Loads

Throughout this section we validate our inflexible load model by showing that, when $N = I$ (all loads are inflexible), if the demand $\bar{P}_{0,\mathrm{N}}$ exceeds the maximum deliverable power $P_{\max}$ ($\bar{P}_{0,\mathrm{N}} > P_{\max}$), the system undergoes VC. We further characterize the region of stable equilibria of (3.10) when $\bar{P}_{0,\mathrm{N}} < P_{\max}$ and motivate the need for coordination to prevent voltage collapse. For the purpose of our analysis, we assume that demand of each load $P_{0,i}$ is constant and varies slowly. Therefore, the dynamics (3.10) are able to track the changes in demand and the system converges to a new equilibrium when $\bar{P}_{0,\mathrm{N}} < P_{\max}$.

3.2.2.1 Voltage Collapse

We first show that (3.10) undergoes VC in the overload regime ($\bar{P}_{0,\mathrm{N}} > P_{\max}$). To this aim, we provide a formal definition to VC.

Definition 8 (Voltage Collapse)**.** *The system* (3.10) *undergoes voltage collapse whenever* $v(g(t)) \to 0$ *as* $t \to +\infty$.

We can show that voltage collapse occurs from the response of loads to overloading.

Theorem 4 (Voltage Collapse)**.** *The dynamic load model* (3.10) *with* $I = N$ *undergoes voltage collapse whenever* $\varepsilon := \bar{P}_{0,\mathrm{N}} - P_{max} > 0$.

Proof. We have already pointed out that $\mathbb{R}^n_{\geq 0}$ is invariant. Also, it is easy to check that (3.10) is globally Lipschitz on $\mathbb{R}^n_{\geq 0}$ since $g_l > 0$. Thus, by (Khalil, 2002, Theorem 3.2) there is a unique solution to (3.10), $g(t)$, that is defined $\forall t \geq 0$. Now, consider the function $V(g) = \sum_{i \in N} g_i$, and let $S_V^+(a) = \{g \in \mathbb{R}^n_{\geq 0} : V(g) \leq a\}$. By taking the time derivative of V we get

$$\begin{aligned}\dot{V}(g) &= \sum_{i=1}^{n} \dot{g}_i = -\sum_{i=1}^{n} P_i(g) - P_{0,i} \\ &\geq \bar{P}_{0,\mathrm{N}} - P_{\max} = \varepsilon > 0.\end{aligned}$$

Therefore, $\forall a \geq 0$, if $g(0) \in S_V^+(a)$, the solution $g(t)$ escapes $S_V^+(a)$ in finite time. It follows then that $\|g(t)\| \to \infty$ as $t \to \infty$, *i.e.,* $\bar{g}_{\mathrm{N}}(t)$ grows unbounded. Therefore, by (3.2) $v(\bar{g}_{\mathrm{N}}(t)) \to 0$ and the system's voltage collapses. □

3.2.2.2 Equilibrium Analysis with Inflexible Loads

Since (3.10) undergoes VC when $\bar{P}_{0,\mathrm{N}} > P_{\max}$, in this section we will study the properties of the equilibria of (3.10) when $\bar{P}_{0,\mathrm{N}} < P_{\max}$. The following lemma will allow us to characterize these equilibria.

Lemma 1 (Intermediate Value Theorem (Rudin, 1976))**.** *Let* $f : \mathbb{R} \to [a, b] \subset \mathbb{R}$,

continuous function. For any $\psi \in (f(a), f(b))$ *there exists* $\xi \in [a, b]$ *such that* $f(\xi) = \psi$.

Theorem 5 (Equilibrium Characterization of (3.10))**.** *Let* $I = N$*. Then, the equilibria of system* (3.12) *have the following properties*

a) When $0 < \bar{P}_{0,\mathrm{N}} < P_{\max}$*, the system* (3.12) *has two equilibria* $g_1^*, g_2^* \in \mathbb{R}^n$ *such that*

$$\bar{g}_{\mathrm{N}}(g_1^*) < g_l < \bar{g}_{\mathrm{N}}(g_2^*). \tag{3.12}$$

b) When $\bar{P}_{0,\mathrm{N}} = 0$*, the system* (3.12) *has one equilibrium* $g_1^* = 0$.

c) When $\bar{P}_{0,\mathrm{N}} = P_{\max}$*, the system* (3.12) *has one equilibrium* g^* *such that* $\bar{g}_{\mathrm{N}}(g^*) = g_l$.

Proof. Let g^* an equilibrium of (3.10). Summing (3.10) for all $i \in N$ together with (3.7) and (3.5) gives

$$\overline{\Delta P}_{\mathrm{N}}(\bar{g}_{\mathrm{N}}^*) = \frac{(Eg_l)^2 \bar{g}_{\mathrm{N}}^*}{(\bar{g}_{\mathrm{N}}^* + g_l)^2} - \bar{P}_{0,\mathrm{N}} = 0. \tag{3.13}$$

a) Since $\bar{P}_{0,\mathrm{N}} > 0$, we multiply both sides of (3.13) by $-\frac{(\bar{g}_{\mathrm{N}}^* + g_l)^2}{\bar{P}_{0,\mathrm{N}}}$ to get

$$(\bar{g}_{\mathrm{N}}^*)^2 + \left(2g_l - \frac{(Eg_l)^2}{\bar{P}_{0,\mathrm{N}}}\right)\bar{g}_{\mathrm{N}}^* + g_l^2 = 0. \tag{3.14}$$

This is a second order polynomial in $\bar{g}_{\mathrm{N}}^*$ and has at most two real roots $\bar{g}_{\mathrm{N}}^{(1)}, \bar{g}_{\mathrm{N}}^{(2)}$.

Equation (3.14) has 2 distinct real roots if and only if

$$\left(2g_l - \frac{(Eg_l)^2}{\bar{P}_{0,\mathrm{N}}}\right)^2 - 4g_l^2 > 0 \iff$$

$$\bar{P}_{0,\mathrm{N}} < \frac{\left(Eg_l\right)^2}{4g_l} = \frac{E^2 g_l}{4} \overset{(3.9)}{=} P_{\max}. \tag{3.15}$$

Thus, when $\bar{P}_{0,\mathrm{N}} < P_{\max}$ then (3.14) has two equilibria g_1^* and g_2^* whose sum, $\bar{g}_{\mathrm{N}}^{(1)}$ and $\bar{g}_{\mathrm{N}}^{(2)}$, are distinct. We assume, without loss of generality, $\bar{g}_{\mathrm{N}}^{(1)} < \bar{g}_{\mathrm{N}}^{(2)}$. Consider the function $\overline{\Delta P}_{\mathrm{N}}(\bar{g}_{\mathrm{N}})$ given in (3.13). It follows from (3.7) that

$$\frac{\partial \overline{\Delta P}_{\mathrm{N}}(\bar{g}_{\mathrm{N}})}{\partial \bar{g}_{\mathrm{N}}} = \frac{\partial \bar{P}_{\mathrm{N}}(\bar{g}_{\mathrm{N}})}{\partial \bar{g}_{\mathrm{N}}} \overset{(3.8)}{=} \begin{cases} > 0, & \bar{g}_{\mathrm{N}} < g_l \\ \\ < 0, & \bar{g}_{\mathrm{N}} > g_l \end{cases}$$

We can prove by contradiction that the two roots of $\overline{\Delta P}_{\mathrm{N}}(\bar{g}_{\mathrm{N}})$ satisfy (3.12). If (3.12) is not met, then both equilibria $\bar{g}_{\mathrm{N}}^{(1)}, \bar{g}_{\mathrm{N}}^{(2)}$ are either in $(0, g_l)$ or in $(g_l, +\infty)$. In the first interval $\overline{\Delta P}_{\mathrm{N}}$ is strictly increasing, whereas in the second $\overline{\Delta P}_{\mathrm{N}}$ is strictly decreasing. In this case,

$$0 = \Delta \bar{P}_{\mathrm{N}}\left(\bar{g}_{\mathrm{N}}^{(1)}\right) \neq \Delta \bar{P}_{\mathrm{N}}\left(\bar{g}_{\mathrm{N}}^{(2)}\right) = 0,$$

contradiction. Therefore, (3.12) holds.

Finally, we show that (3.10) has exactly two equilibria by computing all possible equilibria. Substituting $\bar{g}_{\mathrm{N}}^{(i)}$, $i = 1, 2$, into (3.2) results in

$$v\left(\bar{g}_{\mathrm{N}}^{(i)}\right) = \frac{Eg_l}{\bar{g}_{\mathrm{N}}^{(i)} + g_l} \overset{(3.10)}{\Rightarrow} g_j^{(i)} = \frac{P_{0,i}}{v^2\left(\bar{g}_{\mathrm{N}}^{(i)}\right)},\ i = 1, 2,$$

for all $j \in N$.

b) Since $P_{0,i} \geq 0\ \forall i \in N$, then the trivial case where $\bar{P}_{0,\mathrm{N}} = 0$ arises only when $P_{0,i} = 0\ \forall i \in N$. In that case (3.10) immediately leads to $g_i^* = 0\ \forall i \in N$. We can also

check that when $g_2^* \geq 0$ and $\bar{g}_{\mathrm{N}}(g_2^*) = +\infty$, then g_2^* also satisfies (3.13). However, g_2^* is not finite.

c) In the non-trivial case where $\bar{P}_{0,\mathrm{N}} = P_{\max} \overset{(3.9)}{=} \frac{E^2 g_l}{4}$, the discriminant of (3.14) becomes

$$\Delta = \left(2g_l - \frac{(Eg_l)^2}{P_{\max}}\right) - 4g_l^2 \overset{(3.9)}{=} \left(2g_l - \frac{(Eg_l)^2}{\frac{E^2 g_l}{4}}\right) - 4g_l^2 = 0.$$

Then, (3.14) becomes

$$(\bar{g}_{\mathrm{N}}^*)^2 + \left(2g_l - \frac{(Eg_l)^2}{\frac{E^2 g_l}{4}}\right)\bar{g}_{\mathrm{N}}^* + g_l^2 = (\bar{g}_{\mathrm{N}}^* - g_l)^2 = 0,$$

which has the unique solution $\bar{g}_{\mathrm{N}}^* = g_l$. Substituting $\bar{g}_{\mathrm{N}}^* = g_l$ into (3.2) leads to $v^* = \frac{E}{2}$. Plugging v^* into (3.10) and solving for g_i^* gives the unique solution $g_i^* = \frac{4P_{0,i}}{E^2}$ $\forall i \in N$.

□

Theorem 5 offers an exhaustive characterization of the number of equilibria in the system. We deduce that that for any number of loads, system (3.10) with $N = I$ can have at most two equilibria, depending on the level of demand. In the following section we will assess the stability of the different equilibria.

3.2.2.3 Stable Region Characterization

We end this section by characterizing the region of the state space that admits locally asymptotically stable equilibrium points of (3.10). The following lemma will be

instrumental for this task.

Lemma 2 (Rank-1 plus scaled identity matrix)**.** *For $w \in \mathbb{C}^{n\times 1}$, $\mathbf{1}_n \in \mathbb{R}^n$ a column vector of all ones, $\mathbb{I}_n \in \mathbb{C}^{n\times n}$ the $n \times n$ identity matrix, and $q \in \mathbb{C}$, the eigenvalue-eigenvector pairs $(\rho, x) \in \mathbb{C} \times \mathbb{C}^n$ of the Rank-1 Plus Scaled Identity (RPSI) matrix $B = w\mathbf{1}_n^T + q\mathbb{I}_n$ are*

$$(\rho, x) = \begin{cases} (q, e_1 - e_i)\,, & i \in \{1, .., n-1\}\,; \\ \left(\sum_{i=1}^n w_i + q, w\right), & i = n. \end{cases} \tag{3.16}$$

We are now ready to characterize the stable region of (3.10). For that, we consider the set

$$M := \left\{ g \in \mathbb{R}^n_{\geq 0} : \sum_{i\in N} g_i < g_l \right\}. \tag{3.17}$$

Theorem 6 (Stable Region Characterization)**.** *A hyperbolic equilibrium[3] g^* of (3.10) is stable if and only if $g^* \in M$.*

Proof. Let g^* be an equilibrium of (3.10), *i.e.,* $\Delta P_i(g^*) = 0$ for all $i \in N$, $v^* := v(g^*)$ and $\bar{g}^*_{\mathrm{N}} := \bar{g}_{\mathrm{N}}(g^*)$. The Jacobian of the system (3.10) evaluated at g^* is given by

$$J\left(g^*\right) = \frac{2v^{*2}}{\bar{g}^*_{\mathrm{N}} + g_l} g^* \mathbf{1}_n^T - v^{*2}\mathbb{I}_n. \tag{3.18}$$

Moreover, $J\left(g^*\right)$ is a RPSI matrix. Therefore, we can compute its eigenvalues by

[3] An equilibrium is hyperbolic if the Jacobian of the system at the equilibrium point is nonsingular.

substituting $q = -v^{*2}$ and $w = \frac{2v^{*2}}{\bar{g}_{\mathrm{N}}^* + g_l} g^*$ in Lemma 2:

$$\lambda_i(J) = \begin{cases} -v^{*2}, & i = 1, .., n-1; \\ \\ \frac{2v^{*2}}{\bar{g}_{\mathrm{N}}^* + g_l} \bar{g}_{\mathrm{N}}^* - v^{*2}, & i = n. \end{cases}$$

We can now prove the statement of the theorem.

($\Rightarrow$) If g^* is an asymptotically stable hyperbolic equilibrium, then $J(g^*)$ is Hurwitz and thus: $\lambda_n(J) < 0 \Rightarrow v^{*2} \left(\frac{2\bar{g}_{\mathrm{N}}^*}{\bar{g}_{\mathrm{N}}^* + g_l} - 1 \right) < 0 \Rightarrow \bar{g}_{\mathrm{N}}^* < g_l$.

($\Leftarrow$) If $g^* \in M$, then: $\lambda_n(J) < 0$. Since all eigenvalues of $J(g^*)$ are negative, by Lyapunov's Indirect Method (Khalil, 2002, Theorem 3.5) g^* is asymptotically stable. $\square$

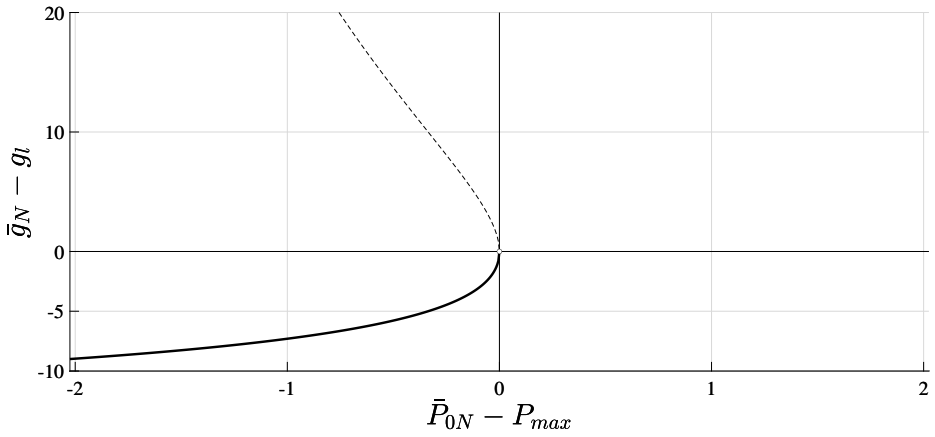

Figure 3.2: Bifurcation Diagram of (3.10). As total demand approaches the capacity of the line ($\bar{P}_{0,\mathrm{N}} = P_{\max}$), the two equilibria of (3.10) converge to $\bar{g}_{\mathrm{N}}(g_1^*) = \bar{g}_{\mathrm{N}}(g_2^*) = g_l$, coallesce at $\bar{P}_{0,\mathrm{N}} = P_{\max}$, and disappear for $\bar{P}_{0,\mathrm{N}} > P_{\max}$. Therefore, the system (3.10) undergoes a saddle-node bifurcation at $\bar{P}_{0,\mathrm{N}} = P_{\max}$.

3.2.2.4 Voltage Collapse as Lack of Load Coordination

The above analysis shows how the load model (3.10) captures the underlying principles of voltage collapse. More precisely, whenever $\bar{P}_{0,\mathrm{N}} < P_{\max}$, the system has two equilibria, one of which allows each load to stably meet its own demand (provided that $\bar{g}_{\mathrm{N}}^{*} < g_l$) by updating its own conductance (Theorem 6). Figure 3.2 shows that the system undergoes a saddle-node bifurcation at $\bar{P}_{0,\mathrm{N}} = P_{\max}$ and the equilibria disappear for $\bar{P}_{0,\mathrm{N}} > P_{\max}$. At any operating point $\bar{P}_{0,\mathrm{N}} > P_{\max}$, the network is unable to provide sufficient power to all loads. As a result, every load seeks to increase its conductance, leading to voltage collapse (Theorem 4). Notably, it is this individual (selfish) action of each loads that leads to the overall system collapse, a behavior akin to the game-theoretic notion of the Tragedy of the Commons (Faysse, 2005). This observation motivates investigating coordination strategies that address the selfish behavior. In this way, we seek to transform the type of bifurcation happening at $\bar{P}_{0,\mathrm{N}} = P_{\max}$ such that a locally asymptotically stable equilibrium exists, at the bifurcation point, and for operating points $\bar{P}_{0,\mathrm{N}} > P_{\max}$.

3.2.3 Voltage Collapse Stabilization

In this section we illustrate that it is possible to prevent voltage collapse by allowing a certain level of coordination among a subset of *flexible* loads that are willing to coordinate their actions. We study the general case where both flexible and inflexible

loads are present, since it is more likely to arise in a power system. In this way, our analysis also includes the trivial case $N = F$ where we can control all loads to avoid VC.

3.2.3.1 VCS Controller

We now consider the system (3.10)-(3.11), with $F \neq \emptyset$. For each flexible load $i \in F$, we seek to control its consumption using

$$u_i = -\Delta P_i(g) - \kappa_i \cdot \phi + b\left(\hat{g}_i - g_i\right), \forall i \in F \tag{3.19a}$$

$$\dot{\hat{g}}_i = -a\left(\hat{g}_i - g_i\right), \qquad \forall i \in F \tag{3.19b}$$

where the shared state ϕ evolves according to

$$\dot{\phi} = \overline{\Delta P}_{\mathrm{N}}(\bar{g}_{\mathrm{N}}) \cdot \frac{\partial}{\partial \bar{g}_{\mathrm{N}}} \overline{\Delta P}_{\mathrm{N}}\left(\bar{g}_{\mathrm{N}}\right). \tag{3.19c}$$

A few explanations are in order. The parameters $\kappa_i > 0$, $i \in F$, in (3.19a) are called load shedding parameters, and will be used to control the fraction of excess consumption that is shed by load $i \in F$. We will further define $\bar{\kappa} := \sum_{i \in F} \kappa_i$, and $a, b > 0$. We will see in the following section that a and b affect the stability of the equilibria of the full system (c.f. (3.20)). The second term in (3.19a) ensures proportional load shedding. Finally, the third term in (3.19a) together with (3.19b) introduces dynamic damping, and is akin to regularization techniques present in saddle-point dynamics (You and Mallada, 2020). If the demand of an inflexible load is zero then

we omit it. Therefore, the above dynamics implicitly assume that $P_{0,j} > 0$ for all $j \in I$.

For the vector $(\ g, \ \ \phi, \ \ \hat{g} \ ) \in \mathbb{R}^n_{\geq 0} \times \mathbb{R} \times \mathbb{R}^{n_F}$ of state variables, we obtain the following closed-loop dynamics:

$$\dot{g}_i = -\Delta P_i(g) - \kappa_i \cdot \phi + b\,(\hat{g}_i - g_i)\,, \forall i \in F \tag{3.20a}$$

$$\dot{g}_i = -\Delta P_i(g), \qquad \forall i \in I \tag{3.20b}$$

$$\dot{\phi} = \overline{\Delta P}_{\mathrm{N}}(\bar{g}_{\mathrm{N}}) \cdot \frac{\partial}{\partial \bar{g}_{\mathrm{N}}} \overline{\Delta P}_{\mathrm{N}}\,(\bar{g}_{\mathrm{N}})\,, \tag{3.20c}$$

$$\dot{\hat{g}}_i = -\,a\,(\hat{g}_i - g_i)\,, \qquad \forall i \in F \tag{3.20d}$$

3.2.3.2 Equilibrium Characterization

We end this section by providing a characterization of the equilibria of (3.20).

Theorem 7 (Equilibrium Characterization of (3.20))**.** *The system* (3.20) *has two sets of equilibria, the load satisfaction set*

$$\mathcal{E}_s = \left\{ \left(\ g^*, \phi^*, \hat{g}^* \ \right) \in \mathbb{R}^n_{\geq 0} \times \mathbb{R} \times \mathbb{R}^{n_F} : \Delta P_i(g^*) = 0 \quad \forall i \in N,\ \phi^* = 0, \quad \hat{g}^* = g^* \right\}, \tag{3.21}$$

where the demand of all loads is satisfied, and the proportional allocation set

$$\mathcal{E}_p = \Big\{ \left(\ g^*, \phi^*, \hat{g}^* \ \right) \in \mathbb{R}^n_{\geq 0} \times \mathbb{R} \times \mathbb{R}^{n_F} : \Delta P_i(g^*) = \frac{\kappa_i}{\bar{\kappa}} \left(P_{\max} - \bar{P}_{0,\mathrm{N}} \right) \forall i \in F,$$
$$\Delta P_i(g^*) = 0 \ \forall i \in I,\ \phi^* = \frac{\bar{P}_{0,\mathrm{N}} - P_{\max}}{\bar{\kappa}}, \hat{g}^* = g^* \Big\}, \tag{3.22}$$

where the difference $\bar{P}_{0,\mathrm{N}} - P_{\max}$ *is proportionally allocated among flexible loads.*

Proof. If $(g^*, \phi^*, \hat{g}^*)$ is an equilibrium of (3.20), then (3.20d) implies that $\hat{g}_i^* = g_i^*$ for all $i \in F$. Moreover, (3.20a), (3.20b) lead to

$$\Delta P_i(g^*) = -\kappa_i \phi^* \ \forall i \in F, \quad \Delta P_i(g^*) = 0 \ \forall i \in I. \tag{3.23}$$

Last, by (3.20c) either $\overline{\Delta P}_{\mathrm{N}}(\bar{g}_{\mathrm{N}}^*) = 0$ or $\frac{\partial \overline{\Delta P}_{\mathrm{N}}(\bar{g}_{\mathrm{N}})}{\partial \bar{g}_{\mathrm{N}}}\Big|_{\bar{g}_{\mathrm{N}}^*} = 0$.

- If $\overline{\Delta P}_{\mathrm{N}}(\bar{g}_{\mathrm{N}}^*) = 0$, then by (3.23)

$$0 = \overline{\Delta P}_{\mathrm{N}}(\bar{g}_{\mathrm{N}}^*) = \sum_{i \in N} \Delta P_i(g^*) \overset{(3.23)}{=} -\bar{\kappa}\phi^* \Rightarrow \phi^* = 0.$$

  Substituting $\phi^* = 0$ back into (3.23) gives $\Delta P_i(g^*) = 0$ for all $i \in N$. Hence, the first set of equilibria is

$$\mathcal{E}_s = \left\{ \begin{pmatrix} g^*, & \phi^*, & \hat{g}^* \end{pmatrix} \in \mathbb{R}^n_{\geq 0} \times \mathbb{R} \times \mathbb{R}^{n_F} : \Delta P_i(g^*) = 0 \ \forall i \in N, \ \phi^* = 0, \ \hat{g}^* = g^* \right\} \tag{3.24}$$

  When $\bar{P}_{0,\mathrm{N}} < P_{\max}$, by Theorem 5 there exist two equilibrium vectors of conductances g^* such that $\Delta P_i(g^*) = 0 \ \forall i \in N$. Therefore, the load satisfaction set $\mathcal{E}_s$ comprises two equilibria $\begin{pmatrix} g_1^*, & \phi^*, & \hat{g}_1^* \end{pmatrix}$, $\begin{pmatrix} g_2^*, & \phi^*, & \hat{g}_2^* \end{pmatrix}$ such that $\bar{g}_{\mathrm{N}}(g_1^*) < g_l < \bar{g}_{\mathrm{N}}(g_2^*)$.

- If $\frac{\partial \overline{\Delta P}_{\mathrm{N}}(\bar{g}_{\mathrm{N}})}{\partial \bar{g}_{\mathrm{N}}}\Big|_{\bar{g}_{\mathrm{N}}^*} = 0$, then by (3.9) $\bar{g}_{\mathrm{N}}^* = g_l$ and $\bar{P}_{\mathrm{N}}^* = P_{\max}$, *i.e.*,

$$\sum_{i \in N} \left(P_i(g^*) - P_{0,i} \right) = P_{\max} - \sum_{i \in N} P_{0,i}$$

$$\overset{(3.4)}{\Rightarrow} \sum_{i\in F} \Delta P_i\left(g^*\right) + \sum_{i\in I} \Delta P_i\left(g^*\right) = P_{\max} - \bar{P}_{0,\mathrm{N}}$$

$$\overset{(3.23)}{\Rightarrow} -\sum_{i\in F} \kappa_i \phi^* = P_{\max} - \bar{P}_{0,\mathrm{N}} \Rightarrow \phi^* = \frac{\bar{P}_{0,\mathrm{N}} - P_{\max}}{\bar{\kappa}}.$$

Substituting $\phi^* = \frac{\bar{P}_{0,\mathrm{N}} - P_{\max}}{\bar{\kappa}}$ back into (3.23) gives $\Delta P_i(g^*) = \frac{\kappa_i}{\bar{\kappa}}\left(P_{\max} - \bar{P}_{0,\mathrm{N}}\right)$ $\forall i \in F$. Hence, the second set of equilibria is

$$\mathcal{E}_p = \Big\{ \Big(\ g^*, \phi^*, \hat{g}^* \ \Big) \in \mathbb{R}^n_{\geq 0} \times \mathbb{R} \times \mathbb{R}^{n_F} : \Delta P_i(g^*) = \frac{\kappa_i}{\bar{\kappa}}\left(P_{\max} - \bar{P}_{0,\mathrm{N}}\right) \ \forall i \in F,$$
$$\Delta P_i(g^*) = 0 \ \forall i \in I, \ \phi^* = \frac{\bar{P}_{0,\mathrm{N}} - P_{\max}}{\bar{\kappa}}, \hat{g}^* = g^* \Big\}. \tag{3.25}$$

Since $\bar{g}^*_{\mathrm{N}} = g_l$ when $(g^*,\ \phi^*,\ \hat{g}^*) \in \mathcal{E}_p$, then (3.2) defines a unique voltage $v^* = \frac{E}{2}$, which in turn leads to the unique vector of conductances

$$\Delta P_i(g^*) = \begin{cases} \frac{\kappa_i}{\bar{\kappa}}\left(P_{\max} - \bar{P}_{0,\mathrm{N}}\right), & \forall i \in F \\ 0, & \forall i \in I \end{cases}$$
$$\Rightarrow g^*_i = \begin{cases} \frac{1}{\left(\frac{E}{2}\right)^2}\left(P_{0,i} + \frac{\kappa_i}{\bar{\kappa}}\left(P_{\max} - \bar{P}_{0,\mathrm{N}}\right)\right), & \forall i \in F \\ \frac{1}{\left(\frac{E}{2}\right)^2} P_{0,i}, & \forall i \in I \end{cases} \tag{3.26}$$

Therefore, for any demand $\bar{P}_{0,\mathrm{N}} \geq 0$, the proportional allocation set $\mathcal{E}_p$ is a singleton $\mathcal{E}_p = \{(g^*,\ \phi^*,\ \hat{g}^*)\}$.

□

An equilibrium of the *load satisfaction* set $g^* \in \mathcal{E}_s$ ensures that all loads $i \in N$ satisfy their individual demand $P_i(g^*) = P_{0,i}$. Similarly, the equilibrium of the

proportional allocation set $g^* \in \mathcal{E}_p$ ensures that the amount $\bar{P}_{0,\mathrm{N}} - P_{\max}$ is distributed among flexible loads proportional to the load-shedding parameter κ_i, $i \in F$.

3.2.4 Stability Analysis of VCS Controller

In this section we evaluate the stability of the equilibria of (3.20) under different loading conditions. To assess stability of each equilibrium we study the linearised model at that point.

3.2.4.1 Stability Analysis of Efficient Operating Points

The Jacobian of (3.20) is

$$J_{SC}(g) = \begin{bmatrix} J(g) - \left[\begin{array}{c|c} b\mathbb{I}_F & \mathbf{0}_{n_F}\mathbf{0}_{n_I}^T \\ \hline \mathbf{0}_{n_I}\mathbf{0}_{n_F}^T & \mathbf{0}_{n_I}\mathbf{0}_{n_I}^T \end{array}\right] & \left[\begin{array}{c} -\kappa \\ \hline \mathbf{0}_{n_I} \end{array}\right] & \left[\begin{array}{c} b\mathbb{I}_{n_F} \\ \hline \mathbf{0}_{n_I} \end{array}\right] \\ c\mathbf{1}_n^T & 0 & \mathbf{0}_{n_I}^T \\ \left[\begin{array}{c|c} a\mathbb{I}_{n_F} & \mathbf{0}_{n_F}\mathbf{0}_{n_I}^T \end{array}\right] & \mathbf{0}_{n_F} & -a\mathbb{I}_{n_F} \end{bmatrix} \tag{3.27}$$

with $\mathbf{0}_n \in \mathbb{R}^n$ column vector of all zeros.

Lemma 3 (Eigenvalue Characterization of (3.27))**.** *Let* $0 < m < M < +\infty$*, and consider* $b > 0$ *in* (3.20a) *and* $a > 0$ *in* (3.20d) *such that*

$$a \in (0, v_{\min}^2), \quad v_{\min} := \min_{g: m \le g_i \le M,\ \forall i \in I} \quad v \tag{3.28}$$

Matrix $J_{SC}(g)$ *as in* (3.27) *has* $2n_F - 2$ *eigenvalues that are roots of*

$$\lambda^2 + \left(a + b + v^2\right)\lambda + av^2 = 0, \tag{3.29}$$

$n_I - 1$ *eigenvalues that are* $-v^2$ *and four eigenvalues that are roots of*

$$\lambda^4 + \alpha_3(g)\,\lambda^3 + \alpha_2(g)\,\lambda^2 + \alpha_1(g)\,\lambda + \alpha_0(g) = 0, \tag{3.30a}$$

$$\alpha_0(g) = \bar{\kappa}acv^2 \tag{3.30b}$$

$$\alpha_1(g) = av^2\tilde{\lambda} + \bar{\kappa}c\left(a + v^2\right) \tag{3.30c}$$

$$\alpha_2(g) = \bar{\kappa}c + v^2(a + b) - \frac{2bv^2\bar{g}_{\mathrm{I}}}{\bar{g}_{\mathrm{N}} + g_l} + \tilde{\lambda}\left(a + v^2\right) \tag{3.30d}$$

$$\alpha_3(g) = b + a + v^2 + \tilde{\lambda} \tag{3.30e}$$

where

$$\tilde{\lambda}(\bar{g}_{\mathrm{N}}) = v^2 - \frac{2v^2\bar{g}_{\mathrm{N}}}{\bar{g}_{\mathrm{N}} + g_l} \tag{3.31}$$

$$c(\bar{g}_{\mathrm{N}}) = \left(\frac{v^2(g_l - \bar{g}_{\mathrm{N}})}{\bar{g}_{\mathrm{N}} + g_l}\right)^2 + \overline{\Delta P}_{\mathrm{N}}\frac{2v^2(\bar{g}_{\mathrm{N}} - 2g_l)}{(\bar{g}_{\mathrm{N}} + g_l)^2} \tag{3.32}$$

Proof. We provide a complete proof in Appendix A. □

Theorem 8 (Stability of VCS Controller)**.** *Consider the system* (3.20) *with* $a > 0$ *satisfying* (3.28)*. For* a *in* (3.20d) *sufficiently small and* $b > 0$ *in* (3.20a)*, the following hold:*

1. When $\bar{P}_{0,\mathrm{N}} > P_{max}$*, the unique equilibrium* $(g^*,\ \phi^*,\ \hat{g}^*) \in \mathcal{E}_p$ *is locally asymptoti-*

cally stable.

2. *When* $\bar{P}_{0,\mathrm{N}} < P_{max}$*, the equilibrium* $(g^*,\ \phi^*,\ \hat{g}^*) \in \mathcal{E}_s \cap \mathrm{cl}(M) = \{(g^*,\ \phi^*,\ \hat{g}^*)\}$ *is locally asymptotically stable.*

Proof. To assess stability of (3.20) we will study the linearized system. The Jacobian of the system is (3.27). By Theorem 3, $J_{SC}(g)$ has $n_I - 1$ eigenvalues that are $-v^2 < 0$ and $2n_F - 2$ eigenvalues that are roots of (3.29). When $v^2 > 0$, by the Routh-Hurwitz criterion, (3.29) has two roots λ_1, λ_2 with negative real parts. Therefore, the stability of the system depends on the last four eigenvalues that are roots of (3.30). The Routh-Hurwitz table of (3.30) is

$$\begin{array}{c|cccc} s^4 & 1 & \alpha_2(g) & \alpha_0(g) & 0 \\ s^3 & \alpha_3(g) & \alpha_1(g) & 0 & 0 \\ s^2 & b_1(g) & b_2(g) & 0 & 0 \\ s^1 & c_1(g) & 0 & 0 & 0 \\ s^0 & d_1(g) & 0 & 0 & 0 \end{array} \tag{3.33a}$$

$$b_1(g) = \frac{\alpha_3(g)\alpha_2(g) - 1 \cdot \alpha_1(g)}{\alpha_3(g)} \tag{3.33b}$$

$$b_2(g) = \frac{\alpha_3(g)\alpha_0(g) - 1 \cdot 0}{\alpha_3(g)} = \alpha_0(g) \tag{3.33c}$$

$$c_1(g) = \frac{b_1(g)\alpha_1(g) - \alpha_3(g)b_2\,(g)}{b_1(g)} \tag{3.33d}$$

$$d_1(g) = \frac{c_1(g)b_2(g)}{c_1(g)} = b_2(g) = \alpha_0(g) \tag{3.33e}$$

We can immediately check that

$$\alpha_3(g) = -\frac{2v^2\bar{g}_{\mathrm{N}}}{\bar{g}_{\mathrm{N}}+g_l} + 2v^2 + a + b > 0;$$
$$d_1(g) \overset{(3.32)}{=} \bar{\kappa}av^2\left[\left(\frac{v^2}{\bar{g}_{\mathrm{N}}+g_l}\left(g_l-\bar{g}_{\mathrm{N}}\right)\right)^2 + \overline{\Delta P}_{\mathrm{N}}\frac{2v^2}{\left(\bar{g}_{\mathrm{N}}+g_l\right)^2}\left(\bar{g}_{\mathrm{N}}-2g_l\right)\right]$$

Moreover, we can rewrite (3.33b) and (3.33d) respectively as

$$b_1(g) = \bar{\kappa}c\frac{b+\tilde{\lambda}}{b+a+v^2+\tilde{\lambda}} + v^2(a+b) - \frac{2bv^2\bar{g}_{\mathrm{I}}}{\bar{g}_{\mathrm{N}}+g_l} + \tilde{\lambda}\left(v^2 + \frac{a\left(b+a+\tilde{\lambda}\right)}{b+a+v^2+\tilde{\lambda}}\right) \tag{3.34}$$

$$c_1(g) = \bar{\kappa}c\frac{\left(a+v^2\right)b_1(g) - \left(b+a+v^2\right)av^2}{b_1(g)} + \tilde{\lambda}av^2\left(1-\frac{\bar{\kappa}c^2}{b_1(g)}\right) \tag{3.35}$$

1. When $\bar{P}_{0,\mathrm{N}} > P_{\max}$, then the *load satisfaction* set is empty, *i.e.*, $\mathcal{E}_s = \emptyset$, and the *proportional allocation* set is a singleton, $\mathcal{E}_p = \{(g^*,\ \phi^*,\ \hat{g}^*)\}$. Moreover,

$$(3.9) \Rightarrow \bar{g}_{\mathrm{N}}^* = g_l, \quad (3.31) \Rightarrow \tilde{\lambda}^* = \tilde{\lambda}(g_l) = 0,$$

$$(3.32) \Rightarrow c^* = \left(\bar{P}_{0,\mathrm{N}} - P_{\max}\right)\frac{v^{*2}}{2g_l} > 0 \overset{(3.33\mathrm{e})}{\Rightarrow} d_1(g^*) > 0.$$

Notice that

$$\bar{g}_{\mathrm{I}}^* \le \bar{g}_{\mathrm{N}}^* = g_l \Rightarrow v^{*2}(a+b) - \frac{bv^{*2}\bar{g}_{\mathrm{I}}^*}{g_l} > 0.$$

Substituting $c^*, \tilde{\lambda}^*$ into (3.34) and (3.35) and assuming $a \to 0^+$ gives

$$\lim_{a\to 0^+} b_1(g^*) = \frac{b\bar{\kappa}c^*}{b+v^{*2}} + bv^{*2}\left(1-\frac{\bar{g}_{\mathrm{I}}^*}{g_l}\right) > 0;$$

$$\lim_{a\to 0^+} c_1(g^*) = \bar{\kappa}c^*v^{*2} > 0.$$

Hence, all terms in the first column of (3.33a) are strictly positive. By the Routh-Hurwitz criterion $(g^*,\ \phi^*,\ \hat{g}^*)$ is a locally asymptotically stable equilibrium of (3.20).

2. When $\bar{P}_{0,\mathrm{N}} < P_{\max}$, by Theorem 7 there exist two equilibria $(g^*,\ \phi^*,\ \hat{g}^*)$ in the load satisfaction set $\mathcal{E}_s$ such that $\Delta P_i(g^*) = 0$ for all $i \in N$. We need to show that $\{(g^*,\ \phi^*,\ \hat{g}^*) \in \mathcal{E}_s : \bar{g}^*_{\mathrm{N}} < g_l\}$ is asymptotically stable. When $(g^*,\ \phi^*,\ \hat{g}^*) \in \mathcal{E}_s$ and $\bar{g}^*_{\mathrm{N}} < g_l$, then by (3.32)

$$c^* = \left(\frac{v^{*2}}{\bar{g}_{\mathrm{N}} + g_l}\left(g_l - \bar{g}^*_{\mathrm{N}}\right)\right)^2 > 0 \Rightarrow d_1\left(g^*\right) > 0.$$

Notice that

$$\bar{g}^*_{\mathrm{I}} \leq \bar{g}^*_{\mathrm{N}} < g_l \overset{(3.31)}{\Rightarrow} \tilde{\lambda}^* > 0,\ v^{*2}b - \frac{2bv^{*2}\bar{g}^*_{\mathrm{I}}}{\bar{g}^*_{\mathrm{N}} + g_l} > 0.$$

Substituting $c^*, \tilde{\lambda}^*$ into (3.34) and (3.35) and assuming $a \to 0^+$ gives

$$\lim_{a\to 0^+} b_1(g^*) = \frac{b\bar{\kappa}c^*}{b + v^{*2}} + bv^{*2}\left(1 - \frac{\bar{g}^*_{\mathrm{I}}}{g_l}\right) > 0;$$

$$\lim_{a\to 0^+} c_1(g^*) = \bar{\kappa}c^*v^{*2} > 0.$$

Hence, all terms in the first column of (3.33a) are strictly positive. By the Routh-Hurwitz criterion $(g^*,\ \phi^*,\ \hat{g}^*)$ is a locally asymptotically stable equilibrium of (3.20).

□

3.2.4.2 Bifurcation Analysis

In the proof of Theorem 7 we showed that when $\bar{P}_{0,\mathrm{N}} < P_{\max}$ the system (3.20) has two equilibria in the load satisfaction set $\mathcal{E}_s$ and one in the proportional allocation set $\mathcal{E}_p$, thus a total of three equilibria. When $\bar{P}_{0,\mathrm{N}} > P_{\max}$, the set $\mathcal{E}_s$ is empty and the system (3.20) has a unique equilibrium in $\mathcal{E}_p$. In this section, we aim to understand the type of bifurcation our VCS controller undergoes at $\bar{P}_{0,\mathrm{N}} = P_{\max}$.

To that end, we need to evaluate the stability of all equilibria of (3.20) around $\bar{P}_{0,\mathrm{N}} = P_{\max}$. The load satisfaction equilibrium $\{(g^*,\ \phi^*,\ \hat{g}^*) \in \mathcal{E}_s : \bar{g}^*_{\mathrm{N}} > g_l\}$ results in lower voltage compared to $\{(g^*,\ \phi^*,\ \hat{g}^*) \in \mathcal{E}_s : \bar{g}^*_{\mathrm{N}} < g_l\}$ studied in Section 3.2.4.1. Moreover, when $\bar{P}_{0,\mathrm{N}} < P_{\max}$, the unique proportional allocation equilibrium $(g^*,\ \phi^*,\ \hat{g}^*)$ results in inefficient supply of flexible loads:

$$P_i(g^*) = P_{0,i} + \frac{\kappa_i}{\bar{\kappa}} \left(P_{\max} - \bar{P}_{0,\mathrm{N}}\right) > P_{0,i}.$$

Hence, understanding the type of bifurcation at $\bar{P}_{0,\mathrm{N}} = P_{\max}$ requires understanding the stability of the *undesired* equilibria $\{(g^*,\ \phi^*,\ \hat{g}^*) \in \mathcal{E}_s : \bar{g}^*_{\mathrm{N}} > g_l\}$ and $(g^*,\ \phi^*,\ \hat{g}^*) \in \mathcal{E}_p$, when $\bar{P}_{0,\mathrm{N}} < P_{\max}$. The next Lemma shows that parameter b affects the stability of the undesired load satisfaction equilibrium around $\bar{g}^*_{\mathrm{N}} = g_l$.

Lemma 4 (Stabilization property of b in (3.20))**.** *Let $b > 0$ as in* (3.20a)*. Then,*

(1) For $b \in \left(0, \frac{E^2}{27}\right)$, there exist $0 < m_b \leq M_b < +\infty$ such that all equilibria

$$\{(g^*,\ \phi^*,\ \hat{g}^*) \in \mathcal{E}_s : \bar{g}_{\mathrm{N}}^* \leq g_l + m_b\}$$

are locally asymptotically stable, and all equilibria

$$\{(g^*,\ \phi^*,\ \hat{g}^*) \in \mathcal{E}_s : g_l + m_b \leq \bar{g}_{\mathrm{N}}^* \leq g_l + M_b\}$$

are unstable.

(2) For any $b_1, b_2 \in \left(0, \frac{E^2}{27}\right)$, $b_1 < b_2$, *then*

$$m_{b_1} < m_{b_2} \qquad \textit{and} \qquad M_{b_2} < M_{b_1}.$$

We can now characterize the stability of all equilibria close to the bifurcation point $\bar{P}_{0,\mathrm{N}} = P_{\max}$.

Theorem 9 (Bifurcation Analysis of (3.20))**.** *Consider the system* (3.20) *with* $a > 0$ *satisfying* (3.28)*. When* $b \in \left(0, \frac{E^2}{27}\right)$ *and for a sufficiently small, the system* (3.20) *undergoes a super-critical pitchfork bifurcation at* $\bar{P}_{0,\mathrm{N}} = P_{\max}$.

Proof. When $\bar{P}_{0,\mathrm{N}} < P_{\max}$, we have shown in the proof of Theorem 7 that the system (3.20) has a total of three equilibria. When $\bar{P}_{0,\mathrm{N}} > P_{\max}$, the two equilibria in $\mathcal{E}_s$ disappear. Therefore, the system undergoes a pitchfork bifurcation. In Theorem 8 we show that $\{(g^*,\ \phi^*,\ \hat{g}^*) \in \mathcal{E}_s : \bar{g}_{\mathrm{N}}^* \leq g_l\}$ when $\bar{P}_{0,\mathrm{N}} < P_{\max}$, and $(g^*,\ \phi^*,\ \hat{g}^*) \in \mathcal{E}_p$ when $\bar{P}_{0,\mathrm{N}} > P_{\max}$, are locally asymptotically stable. Moreover, Lemma 4 states that for $b \in \left(0, \frac{E^2}{27}\right)$, there exists $m_b > 0$ such that any *"undesired"* equilibrium

$\{(g^*,\ \phi^*,\ \hat{g}^*) \in \mathcal{E}_s : g_l \leq \bar{g}_{\mathrm{N}}^* \leq g_l + m_b\}$ is locally asymptotically stable. Therefore, the system (3.20) undergoes a super-critical pitchfork bifurcation if for $\bar{P}_{0,\mathrm{N}} < P_{\max}$, the remaining *"undesired"* equilibrium $(g^*,\ \phi^*,\ \hat{g}^*) \in \mathcal{E}_p$ is unstable close to $P_{\max}$.

When $(g^*,\ \phi^*,\ \hat{g}^*) \in \mathcal{E}_p$, then $\bar{g}_{\mathrm{N}}^* = g_l$ and by (3.32)

$$c^* = \left(\bar{P}_{0,\mathrm{N}} - P_{\max}\right) \frac{v^{*2}}{2g_l} < 0.$$

Then, by (3.33e) $d_1(g^*) = \alpha_0(g^*) = \bar{\kappa} a c^* v^{*2} < 0$. Therefore, there exists at least one sign change between the terms in the first column of (3.33a). By the Routh-Hurwitz criterion g^* is an unstable equilibrium and the system (3.20) undergoes a super-critical pitchfork bifurcation at $\bar{P}_{0,\mathrm{N}} = P_{\max}$. □

Theorem 9 implies that the VCS controller succeeds in transforming the type of bifurcation at $\bar{P}_{0,\mathrm{N}} = P_{\max}$. The transformation of the bifurcation comes at the cost of stabilizing the undesired equilibrium $\{(g^*,\ \phi^*,\ \hat{g}^*) \in \mathcal{E}_s : \bar{g}_{\mathrm{N}}^* \geq g_l\}$ in some region $\{(g^*, \phi^*, \hat{g}^*) \in \mathcal{E}_s : g_l \leq \bar{g}_{\mathrm{N}}^* < g_l + m_b\}$.

Remark 1. *Theorem 8 shows that parameter $a > 0$ in* (3.20d) *affects the stability of the efficient equilibria, while Theorem 4 shows that parameter $b > 0$ in* (3.20a) *affects the stability of the undesired equilibrium $\{(g^*,\ \phi^*,\ \hat{g}^*) \in \mathcal{E}_s : \bar{g}_{\mathrm{N}}^* \geq g_l\}$. Choosing $a \to 0^+$ stabilizes the efficient equilibria, but there is not a single desired value for $b \in \left(0, \frac{E^2}{27}\right)$. Smaller values of $b \in \left(0, \frac{E^2}{27}\right)$ lead to a smaller $m_b > 0$ in Theorem 4 and thus a smaller region around $\bar{g}_{\mathrm{N}}^* = g_l$ where the undesired equilibrium is locally asymptotically stable. However, $b = 0$ would result in $b_1 = 0$ in* (3.33b). *In that case,*

the linearization would fail and our analysis would be inconclusive.

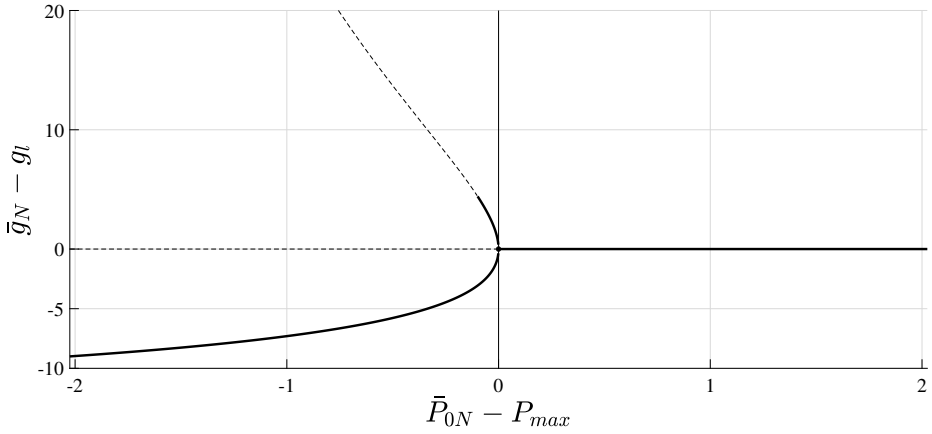

Figure 3.3: Bifurcation Diagram of (3.20). As total demand approaches the capacity of the line ($\bar{P}_{0,\mathrm{N}} = P_{\max}$), an unstable equilibrium becomes locally asymptotically stable. At the bifurcation point, the two locally asymptotically stable equilibria and the unstable equilibrium coalesce, resulting in a single locally asymptotically stable equilibrium for $\bar{P}_{0,\mathrm{N}} > P_{\max}$.

3.3 Results

In this section, we validate our theoretical results using numerical illustrations. In all the experiments we start the simulations with initial set-points such that $\bar{P}_{0,\mathrm{N}} < P_{\max}$ and with conductances close to the equilibrium g^* where all demands are met, *i.e.,* $g^* \in \mathcal{E}_s \cap M$. We explore the parameter space by *slowly* varying the demand (P_0) with time and observing the changes in the equilibria.

The load-shedding property of the VCS controller is better understood using more than one loads. For that, we will study a system where loads 1 and 2 are flexible and load 3 is inflexible. First, we look at the behavior of the system when the conventional

controller (3.10) is applied to all three loads. Figure 3.4 shows that when total demand exceeds the maximum transferable power through the line, voltage collapses.

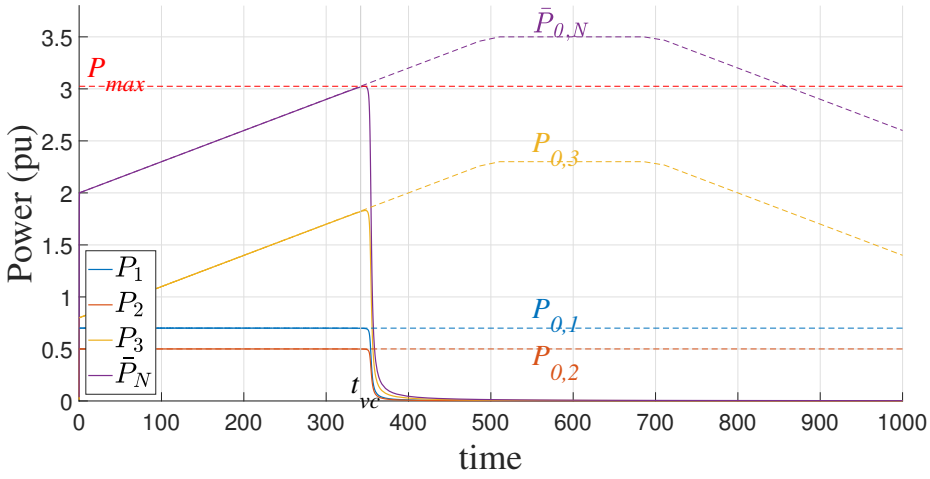

Figure 3.4: Power supply when all three loads are controlled with the traditional control strategy. When $\bar{P}_{0,\mathrm{N}} > P_{\max}$ voltage collapses.

On the other hand, Figure 3.5 shows how flexible loads adjust in the overloading regime, when the flexible loads are controlled using the VCS controller. The adjustment is proportional to the parameter κ_i, consistent with the definition of $\mathcal{E}_p$ in Section 3.2.3. Finally, Figure 3.6 illustrates how voltage inevitably collapses when the demand of inflexible loads exceed the capabilities of the line.

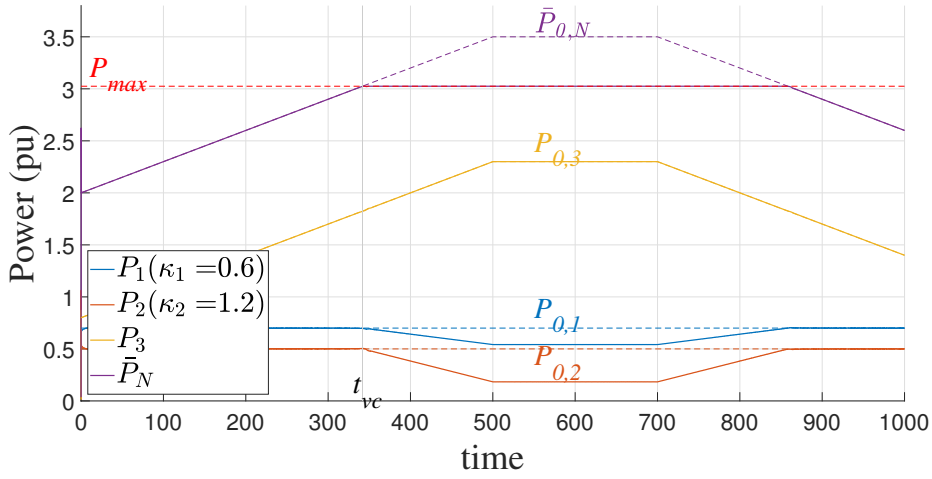

Figure 3.5: Power supply for $a = 0.1$, $b = 0.1$ when loads $1, 2$ are flexible and load 3 is inflexible. When total demand exceeds the maximum, the adjustment of power supply to the flexible loads is proportional to the parameters κ_i $\forall i = 1, 2$.

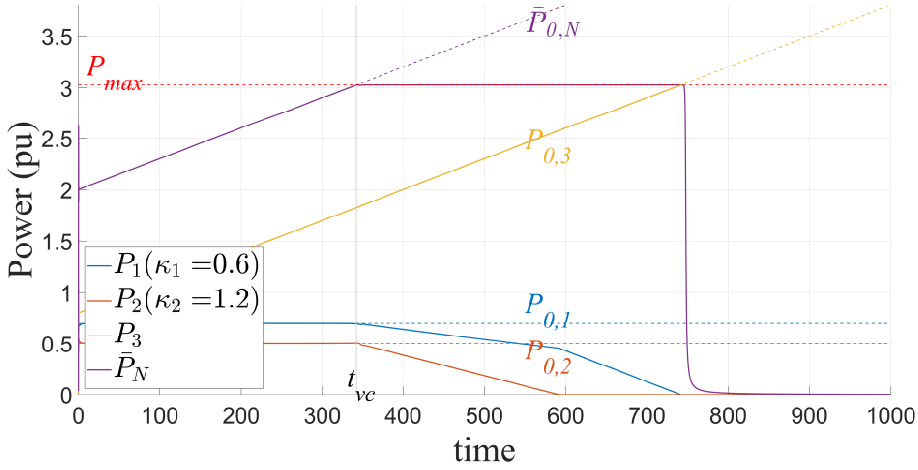

Figure 3.6: Power supply for $a = 0.1$, $b = 0.1$ when loads $1, 2$ are flexible and load 3 is inflexible. Voltage collapses when the demand of the inflexible load exceeds the capabilities of the line.

Remark 1 highlights the impact of parameters a, b on the stability of the equilibria of (3.20). To better understand the impact of a and b, we will consider a simple version of the DC network in Figure 3.1 with one flexible and one inflexible load. Figure 3.7 verifies that small, non-zero values of both a and b result in stable power

supply. On the other hand, when a is bigger and $\bar{P}_{0,\mathrm{N}} > P_{\max}$, the equilibrium that ensures proportional shedding becomes unstable. Moreover, when total demand is smaller than $P_{\max}$ but very close, larger values of b result in the undesired equilibrium $g^* \in \mathcal{E}_s \cap M^c$ being stable. Finally, Figure 3.8 reveals that for small values of a and total demand close to $P_{\max}$, we always track the desired equilibrium $g^* \in \mathcal{E}_s \cap M$.

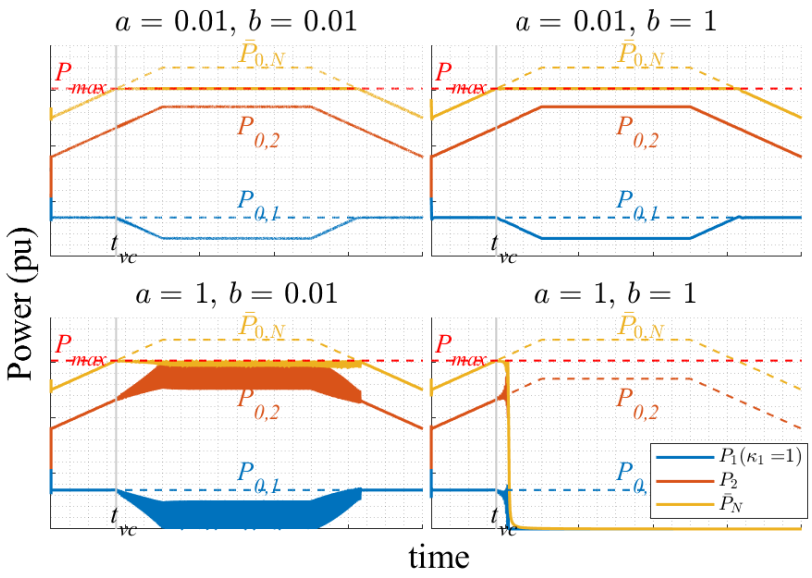

Figure 3.7: Power supply for different values of a, b when load 1 is flexible and load 2 is inflexible. For a small –upper two plots– and $\bar{P}_{0,\mathrm{N}} > P_{\max}$, power supply to load 1 adjusts accordingly. For higher a –lower two plots– and $\bar{P}_{0,\mathrm{N}} > P_{\max}$, voltage collapses.

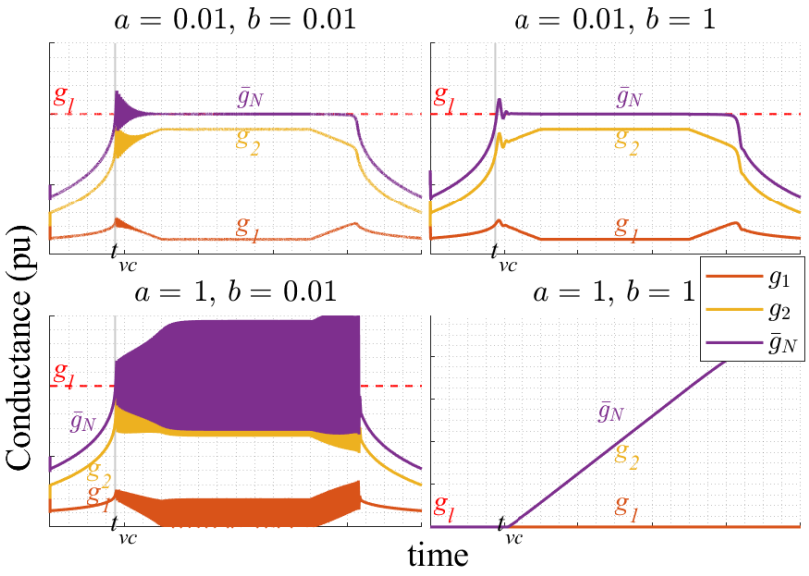

Figure 3.8: Response of conductances for different values of a, b when load 1 is flexible and load 2 is inflexible. For small a, when $\bar{P}_{0,\mathrm{N}} < P_{\max}$, the VCS controller tracks $g^* \in \mathcal{E}_s \cap M$. When $\bar{P}_{0,\mathrm{N}} > P_{\max}$ then $\bar{g}_{\mathrm{N}}^* = g_l$. For higher values of a, conductances diverge when $\bar{P}_{0,\mathrm{N}} > P_{\max}$.

3.4 Conclusion

This chapter seeks to initiate the study of voltage collapse stabilization as a mechanism to enhance power system resilience against voltage collapse and allow for more efficient and reliable operation of electric power grids. We develop a Voltage Collapse Stabilization controller that is able to not only prevent voltage collapse, but also proportionally distribute the curtailment among all flexible loads in a star DC network. The methodology can be readily applied to a fully reactive alternating current star network, where the controller changes the suscenptance instead of the conductance. Further research needs to be conducted to fully characterize the behavior of our so-

lution at the bifurcation point. The point where $\bar{P}_{0,\mathrm{N}} = P_{\max}$ is a non-trivial point, where the Jacobian of the system is identically zero and thus requires the treatment of higher order dynamics.

Acknowledgements

The author thanks Dr. Enrique Mallada, who contributed to the work in this chapter. An older version of the work in this chapter was previously published in the conference proceedings of the 2019 American Control Conference (Avraam et al., 2019). The author thanks Jesse Rines, Aurik Sarker, and Dr. Fernando Paganini who contributed to the work in the earlier version of this chapter.

Chapter 4

Natural Gas Infrastructure Resilience in North America Under Integrated Markets

4.1 Introduction

The North American natural gas sector has been growing the last decade and Natural gas in the U.S. surpassed coal for the first time in 2016 as the primary fuel used for electricity generation[1]. Moreover, U.S. exports of liquified natural gas continue to grow and are projected to constitute more than 55% of total U.S. exports by 2030 per the "Annual Energy Outlook 2019" (EIA, 2019c). Mexico's domestic natural gas demand grew by 47.5% between 2005 and 2015 (EIA, 2017). Finally, Canada's production is projected to grow by 11.23% by 2040 compared to 2016 (NEB, 2017).

[1]See "Electricity explained. Electricity in the United States." Available at: https://www.eia.gov/energyexplained.

Growth of North American natural gas production between 2011−2020 was mainly the result of the rapid expansion of U.S. natural gas production. The latter is mainly attributed to the discovery of low-cost, technologically recoverable shale gas in the Marcellus Formation in 2008, rendering the U.S. the largest producer of natural gas since 2012 (EIA, 2019d). Consequently, new pipeline projects were planned and completed (EIA, 2019b) in order to facilitate the distribution of the newfound resources in mainland U.S. In addition, the decreasing cost of transforming and shipping (Maxwell and Zhu, 2011) Liquified Natural Gas (LNG) provides U.S. producers with the opportunity to expand their reach beyond Canada and Mexico, who have been the major natural gas trade partners of the U.S. Moreover, U.S. demand is projected to grow modestly (EIA, 2017) in the short-term.

The boost of North American natural gas production between 2011 − 2021 has come not only as a result of unforeseen events, but also as a result of (de)regulatory initiatives. On the supply-side, the ongoing deregulation of the natural gas market, starting from the Natural Gas Policy Act (NGPA) of 1978 (EIA, 1978), is a policy-induced attempt to increase the penetration of natural gas into the U.S. energy mix. Starting in 1978, the U.S. has gradually removed stringent wellhead price ceilings set by the Natural Gas Act in 1938. The new price ceilings enforced by the NGPA were designed to account also for the geology, location, and other characteristics of each well. The new wellhead prices incentivized producers to increase their production and expand their search for new sites. All wellhead price ceilings were removed under

the Natural Gas Wellhead Decontrol Act of 1989 (FERC, 1989). Canada started dismantling protections for domestic crude oil and natural gas producers with the introduction of the "Western Accord on Energy" in 1985 (Fertel et al., 2013). The legislation aimed to address the increasing surplus of supply in Canada during the 1980s.

In addition, Mexican policy-makers introduced in 2013 the Energy Reform (Alemán-Nava et al., 2014) in order to promote Mexican production and exploit domestic resources. In an attempt to curb the decline of Mexican natural gas production and increase investment on existing sites, in 2019 the Mexican government called for restrictions on invitations for oil block bids that were previously allowed under the 2013 Energy Reform (Graham, 2018). The government has also proposed stricter regulations on pipeline contracts between the Mexican government and pipeline operators as a way to decrease the cost for the public sector. This has led to the renegotiation of contracts for new pipelines that subsequently delayed their connection to the system (Stilman, 2019). However, restrictions on natural gas infrastructure need to be the same for both domestic investors, *i.e.,* state owned companies, and U.S. investors under the United States-Mexico-Canada (USMCA) Agreement (Gantz, 2019).

On the demand-side, excise tax and infrastructure tax credits have contributed to the adoption of natural gas in the commercial and residential sectors. Finally, state-level policies aiming to mitigate climate change, such as cap-and-trade (Tsao et al., 2011), has led to the substitution of coal-fired plants with natural-gas fired plants.

Gas-fired generation contributes to the resilience of the power system. First, fuel-fired power plants contribute to the stability of the power grid's frequency (Ulbig et al., 2014). Second, the operation of renewables requires a certain amount of active fuel-fired power plants at all times (Bruninx et al., 2016). However, the transition to a low-carbon economy (EC, 2018), as a result of climate change, necessitates the decrease of emissions in the power sector and the increase of energy efficiency of all sectors of the economy. The policies to reduce emissions include the creation of a market for emissions allowances (Goulder et al., 2010), carbon taxes (Karp and Livernois, 1994), as well as updated buildings insulation standards (Li and Colombier, 2009). The first two policies favor natural gas-fired plants over other conventional fuel-fired plants due to the low emissions rate of natural gas consumption. For that, natural gas has emerged as a bridging fuel during the transition to a low-carbon economy. Hence, in North America natural gas is both an economically competitive and a "cleaner" option for power production compared to coal and oil due to the low emissions rate of natural gas consumption, the availability of natural gas resources, and the power system's reserves and grid frequency stability requirements.

Still, natural gas-fired power plants remain CO_2 emitters. Consequently, deeper penetration of renewables results in greater displacement of natural gas-fired plants in the long-term. A complete treatment of the change in natural gas consumption would need to rely on an integrated framework that would grasp the interactions between the natural gas sector and the rest of the economy. However, some trends

are prevalent. Natural gas is being displaced in fuel-intensive sectors, such as the transportation sector (Williams et al., 2012), due to increasing electrification.

Therefore, the timing of natural gas abatement, which is critical for the maintenance and development of natural gas production and pipeline infrastructure, depends on multiple factors. At the same time, moving to a low-carbon economy implies the abatement of natural gas in the long-term. Hence, the challenge of studying the development of the natural gas sector in North America lies in the complexity of the interactions of the natural gas sector with all other sectors of the economy, the political nature of fossil fuels exploitation, and the uncertainty of resource availability. In the current chapter we isolate potential sources of disruption for the natural gas sector and look to understand their impact. Specifically, we ask:

- How resilient is North American natural gas production and pipeline infrastructure, given uncertainty in future resource availability and technological progress?

- Which North American producers and pipeline operators are the most vulnerable and should be accounted for in policy design?

- How does the growing exposure of the U.S. to international markets affect Canada and Mexico?

4.1.1 Literature Review

We can divide the studies of the natural gas market into two categories: global and regional. While global studies aim to analyze the drivers of increasing LNG trade, regional analyses focus on arbitraging between regions and pipeline infrastructure development. Egging et al. (2010) study international LNG trade using the World Gas Model (WGM), which includes 80 countries and assumes Nash-Cournot competition between representative producers. In WGM, Mexico is represented by one node, Canada is divided into two, and the U.S. into six. Avetisyan et al. (2011) use WGM to study the impact of CO_2 emissions policies and availability of resources in the U.S. to the international natural gas market. To do so, they updated WGM to include environmental regulations. Siddiqui and Gabriel (2013), enhanced WGM by assuming that the census region that contains the two largest shale plays, the Barnett and Haynesville shale plays, is a leader in the market in a "Leader-Follower" setting. Egging (2013) enhanced WGM by introducing a Benders Decomposition scheme for stochastic mixed complementarity problems. Apart from the US, neither Canada nor Mexico are included in the latter version. Finally, Aune et al. (2009) highlight the role of decreasing LNG costs on integrating global markets. The authors develop FRISBEE, a recursive-dynamic, partial-equilibrium model of the global natural gas market with 13 regions where the U.S. is represented as its own region, whereas Canada and Mexico are part of other regions.

Focusing on Europe, the Price-Induced Market Equilibrium System (PRIMES) includes a detailed natural gas submodule with regional detail of Europe, Russia, Middle Africa, North Sea, China, and India, and has been used to produce the "EU Reference Scenario 2016" (EC, 2016). Golombek et al. (1995) focus on the liberalization of Western European natural gas markets. Modeling-wise, they are the first to introduce a nonlinear marginal cost of production. Holz et al. (2008) highlight the importance of liberalizing the downstream market using GASMOD. In their analysis they only represent the European natural gas market with added detail on the regions that import and export natural gas from and to the European Union. Abada et al. (2013) study the impact of long-term contracts using GaMMES. GaMMES is formulated as a Generalized Nash Equilibrium problem.

Beltramo et al. (1986) were among the first to study the outlook of the natural gas sector of North American countries. For this, they developed the North American Gas Trade Model (GTM) which was one of the first models of North America with regional detail regarding the U.S. and Canada that explicitly took into account pipeline interconnections between the two countries. Gabriel et al. (2005) introduced a model with 12 regions for the U.S. and two regions for Canada to study market power in North America. Finally, the Natural Gas Market Module (NGMM) (EIA, 2018), a submodule of the National Energy Modeling System (NEMS) developed by the U.S. Energy Information Administration (EIA) has been used to produce Annual Energy Outlooks for the U.S. NGMM incorporates the nine census regions, one region for

Canada and another for Mexico. In NGMM, capacity expansion is not endogenous, but extra capacity is allocated exogenously based on the increase in national demand. On the other hand, the North American Natural Gas Model (NANGAM), developed by Feijoo et al. (2016), accounts for endogenous capacity expansion both in production and in pipeline infrastructure. Moreover, it includes all nine census regions for the U.S. but breaks down Canada into two regions and Mexico into five. NANGAM has been used to study the impact of the Mexican Energy Reform to cross-border Mexico-U.S. infrastructure.

Although the models in all the above studies implicitly assume some level of market interaction between regions, only few of them explicitly deal with market integration. Evidence on the lack of market integration in the 1990's can be found in De Vany and Walls (1995). On the other hand, Serletis (1997) argues that there is no split between Eastern and Western U.S. prices. Serletis and Herbert (1999) suggest that greater integration between North American regions, as a result of the liberalization of the natural gas market, leads to more effective arbitraging mechanisms. Siliverstovs et al. (2005) also try to empirically assess market integration, but focus on the global market. Feijoo et al. (2016) and Sankaranarayanan et al. (2018) treat a fully integrated North American natural gas market and aim to study the development of cross-border infrastructure. They find that higher Mexican demand leads to higher pipeline exports from the West South-Central region to Mexico. Feijoo et al. (2018) focus on the impact of socioeconomic factors that influence natural gas infras-

tructure. The study concludes that the resulting heterogeneity in demand can lead to investment in certain pipeline interconnections while other pipeline interconnections are underutilized.

The low international natural gas prices, the recent discovery of low-cost shale gas in the Middle-Atlantic region of the U.S., the Energy Reform in Mexico, and the recent discovery of the largest hydrocarbon reserves deposit in the last 30 years in Mexico (Ore et al., 2019) constitute major changes that can affect the North American natural gas market in the long-term. In lieu of these developments, this chapter provides the most up to date assessment of the impact of resource availability, international trade, and low oil prices on natural gas infrastructure development in North America.

4.1.2 Objectives and Scenarios

Our objective is to analyze the implications for the natural gas production and pipeline infrastructure of a range of scenarios under integrated North American natural gas markets. For that, we formulate a comprehensive list of scenarios that are designed to explore the uncertainty of future resource availability, technological progress, and potential policy changes:

a) **Reference:** A scenario that serves as benchmark against which all other scenarios will be compared to. Reference production and consumption projections are consistent with AEO2017 for the U.S. (EIA, 2017), "Canada's Energy Fu-

ture 2017" for Canada (NEB, 2017), and the "Natural Gas Outlook 2016–2030" of the Mexican Secretary of Energy (Secretaría de Energía) SENER (SENER, 2017) for Mexico. The process of attaining the Reference scenario is detailed in Section 4.2.

b) **Low_Oil_Price:** Following the low natural gas prices after 2014 (Linn and Muehlenbachs, 2018), we assume a shock in the international market that consequently affects regional demand. This scenario aims to quantify the resilience of the North American natural gas system to decreased oil prices which consequently lead to decreased demand for natural gas. We implement this scenario by computing the change in regional natural gas demand with respect to reference demand in the "Low Oil Price" scenario of the "Annual Energy Outlook 2017" (EIA, 2017). We then impose the same percentage change to NANGAM's reference regional demand (variable Q^D_{yhnde} in Feijoo et al. (2016)), starting from 2020.

c) **High_Gas_Supply:** We assume that due to technological improvements, the cost of production of natural gas decreases by 20% in 2020, 30% by 2030, and by 30% for the remainder of the time horizon. We decrease all terms of the marginal cost function, namely the linear, quadratic, and Golombek terms (parameters lin^P_{ysne}, qud^P_{ysne}, gol^P_{ysne} in Feijoo et al. (2016)) by the respective percentages of each time period.

d) **Natural Gas Resources:** We assume that our medium-term projections regarding the availability of natural gas are correct and introduce a shock to the availability of resources in 2030 through 2050. By simulating two different variations, these scenarios aim to explore the ability of natural gas infrastructure to adjust to the (un)availability of resources.

i. **High Natural Gas Resources (High_NG_Res)**: We constrain natural gas infrastructure (variables z^P_{ysne}, z^A_{ya} in Feijoo et al. (2016)) to be the same as in the Reference scenario up until 2030, and allow endogenous change in infrastructure for the remainder of the time horizon. Beyond 2030, the greater availability of resources translates into our model to a lower operational cost of natural gas production in the US. The linear, quadratic, and Golombek terms of the marginal cost function (parameters lin^P_{ysne}, qud^P_{ysne}, gol^P_{ysne} in Feijoo et al. (2016)) are changed according to the percentage change in the operational cost of each region in the U.S. The percentage change in the operational cost is calculated using the "High Oil and Gas Resources" scenario of AEO2017.

ii. **Low Natural Gas Resources (Low_NG_Res):** The implementation is identical to the "High Natural Gas Resources" scenario, with the exception that the applied percentage changes are calculated using data from the "Low Oil and Gas Resources" of AEO2017.

In both High_Gas_Supply and High_NG_Res we change the parameters of the marginal cost function. Nonetheless, the High_NG_Res aims to study the response of the system in a scenario of abundant U.S. resources, whereas the High_Gas_Supply studies the effect of higher productivity in all of North America. Therefore, the implementation differs. In the High_Gas_Supply, the parameters of the marginal cost function of all producers are decreased by 20% in 2020, whereas in the High_NG_Res scenario the decrease in 2020 is 15%. The change in marginal cost parameters is different between the two scenarios for all subsequent years as well.

4.2 Methods

4.2.1 North American Natural Gas Model

The North American Natural Gas Model (NANGAM) is an intertemporal, bottom-up, partial-equilibrium model of the interconnected natural gas sectors of the U.S., Canada, and Mexico (EIA, 2018). NANGAM is built with a focus on North America. It comprises nine census regions of the U.S. (Figure 4.1), a region for Alaska and Hawaii, five regions for Mexico (Northwest, Northeast, Interior, Interior-West, South-Southwest), two regions for Canada (East, West), amounting to seventeen regions in total. There exist 13 producing regions, based on regional historical capacity data, namely census regions 2–9, both regions in Canada, Northeast Mexico, and

South-Southwest Mexico. In addition, the seventeen regions are connected via 69 representative links that emulate the inter-regional pipeline interconnections. In addition, storage facilities exist in each node in the U.S. and Canada. We use a database of 778 existing projects and 187 new ones provided by the U.S. Energy Information Administration (EIA, 2017) to produce estimates of pipeline investment cost, as well as fixed and marginal cost of transporting natural gas. For the documented pipelines, the database provides the technical characteristics, their cost structure, and whether they are interstate, intrastate or cross-border projects. NANGAM is thus able to account for endogenous flows andinvestment on pipeline capacity. NANGAM runs in 5-year time steps up to 2050, is formulated as a Mixed Complementarity Problem (MCP), and is run using the General Algebraic Modeling System (GAMS) (Figure 4.2).

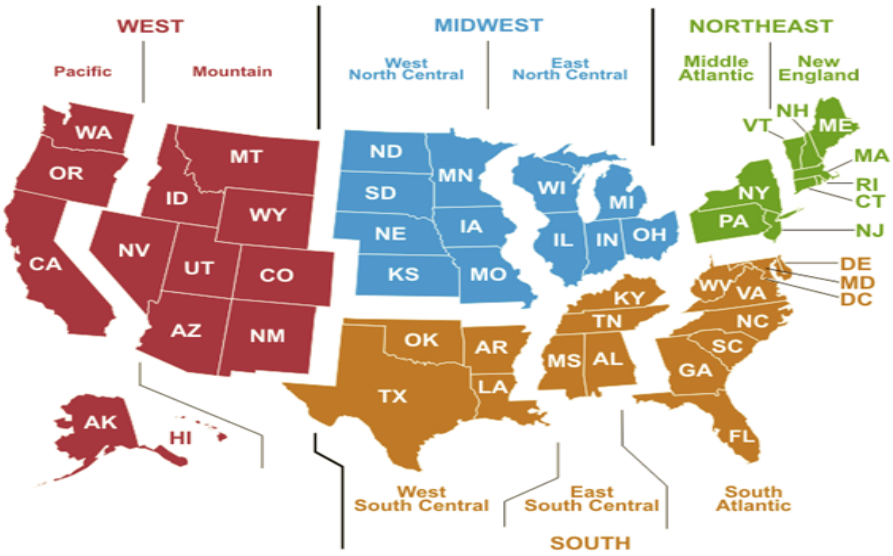

Figure 4.1: Census regions. Source: Energy Information Administration.

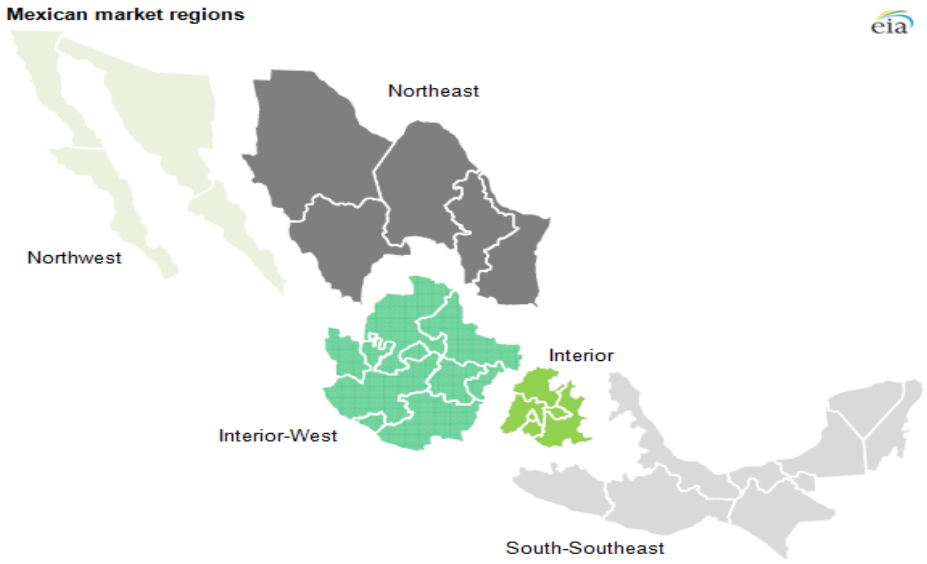

Figure 4.2: Regional disaggregation of Mexico in NANGAM. Source: Energy Information Administration.

The agents in NANGAM include regional suppliers (upstream players) that extract and deliver natural gas to pipeline operators that in turn deliver natural gas to final consumers or storage facilities (midstream). Each agent is assumed to be a profit maximizer and decisions on infrastructure development are endogenously generated based on future profitability. Demand is incorporated via a linear inverse demand function for each region. NANGAM is based on MultiMod (Huppmann and Egging, 2014) from where it inherits all the assumptions regarding the interactions of the market participants. For that, agents compete ala Nash-Cournot and NANGAM computes regional prices and quantities that clear every regional natural gas market. Finally, NANGAM can be used for the analysis of supply or demand-side shocks, policy interventions, and infrastructure investment. The above scenarios can be im-

plemented at a regional, national or international level. NANGAM further inherits all the types of potential regulation that can be applied in MultiMod, such as greenhouse gas emissions constraints and taxes or fuel mandates. Finally, NANGAM, similarly to MultiMod, can be coupled with other energy, climate or economic models.

4.2.2 Reference Scenario

As discussed in Section 4.1.2, production and consumption in the version of NANGAM used in this chapter is consistent with AEO2017 for the U.S. (EIA, 2017), "Canada's Energy Future 2017" for Canada (NEB, 2017), and the "Natural Gas Outlook 2016–2030" of the Mexican Secretary of Energy (Secretaría de Energía) SENER (SENER, 2017) for Mexico. For production and consumption of each region to be consistent with the different databases, we calibrate the linear and quadratic terms of the marginal cost function and the capacity expansion cost of each producer, as well as the pipeline tariffs charged by pipeline operators. Benchmark data on the cost of production (EIA, 2019a) as well as pipeline projects (EIA, 2019b) are extracted from the Energy Information Administration. End-use prices are consequently affected by the calibration of costs across the supply chain, but we do not further calibrate these costs to match end-use prices perfectly (Figure 4.3).

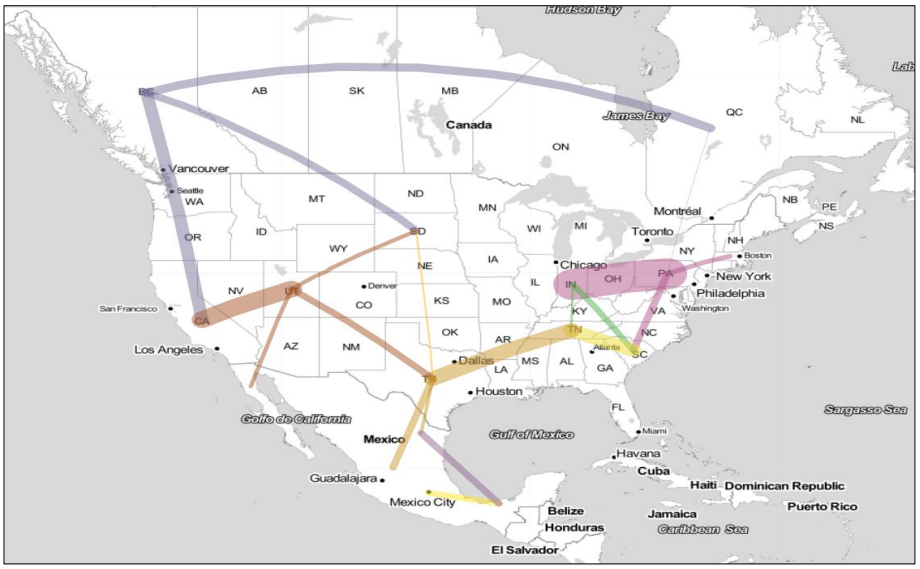

Figure 4.3: Representation of endogenous natural gas flows in NANGAM.

The calibration of the model is an iterative process, with each iteration comprising of two steps. In the first step demand parameters are automatically computed for given demand elasticity. For consistency, costs are manually updated to better match the production in the second step, altering equilibrium demand. The two steps are repeated until equilibrium production and consumption for all regions does not differ from reference data by more than 5% until 2040. For the remaining years we ensure that the deviation of consumption is within 3%, while the deviation of production is within 10% for the major producing regions. Reference production and consumption data for the three regions are shown in Figure 4.4.

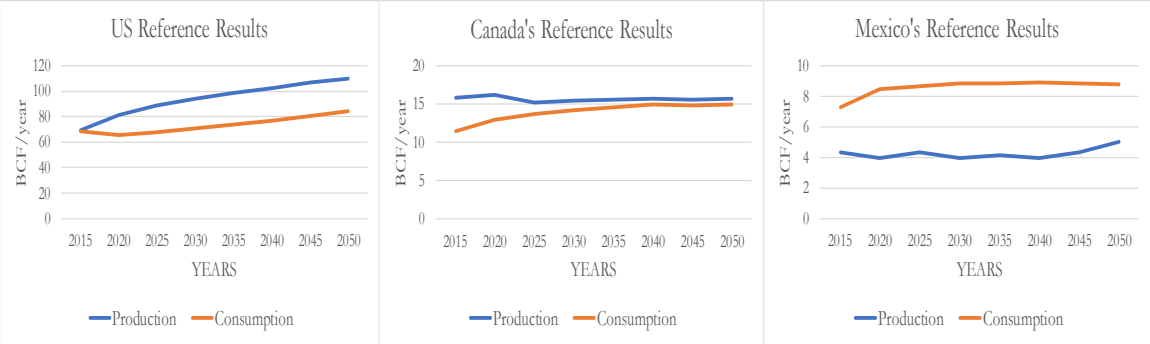

Figure 4.4: Reference production and consumption of the U.S. (left), Canada (center), and Mexico (right).

4.3 Results

4.3.1 Low_Oil_Price Scenario

We implement this scenario by constraining regional natural gas consumption in each country (variable Q^D_{yhnde} in Feijoo et al. (2016)), as explained in Section 4.1.2. We assume that regional natural gas consumption in each region of each country decreases to a new level that differs from the reference value by the percentages shown in Table 4.1 below.

Table 4.1: Percentage change in natural gas consumption per country under the Low_Oil_Price scenario.

	Imposed % change of consumption							
	2015	2020	2025	2030	2035	2040	2045	2050
USA	0.00	-2.21	-2.88	-3.16	-3.86	-4.24	-4.90	-4.16
Canada	0.00	-2.21	-2.88	-3.16	-3.86	-4.24	-4.90	-4.16
Mexico	0.00	-2.21	-2.88	-3.16	-3.86	-4.24	-4.90	-4.16

Except for regional consumption in NANGAM, in the implementation of this scenario we did not alter any other parameter in any agent's decision-making problem. The time-frame of the shock is consistent with the time-frame of NANGAM, *i.e.,* every five years from 2020 to 2050.

The uniform decrease in North American demand implies that production in all three countries readjusts, as shown in Figure 4.5. U.S. production is the one that decreases the most in the mid-term as a result of the projected increasing U.S. exports through 2030. Canada's production decreases by 0.55 BCM (3.7%) in 2050, whereas Mexican production remains largely unaffected in absolute value throughout the time horizon. The decrease in Canada's consumption in 2040 by 6.53 BCM along with a slight adjustment of exports results in Canada decreasing its production by 7.86 BCM or 4.82% compared to reference 2040 natural gas production. Therefore, the percentage change in Canada's natural gas production in 2040, the largest among all countries for all time periods, is attributed to the decrease of domestic natural gas consumption. Moreover, since the U.S. faces the largest absolute change in natural gas consumption, it is the country that drives the change in consumption in North America. North American production decreases from 2015 to its nadir in 2045 and increases in 2050, which is consistent with the change in consumption in Table 4.1.

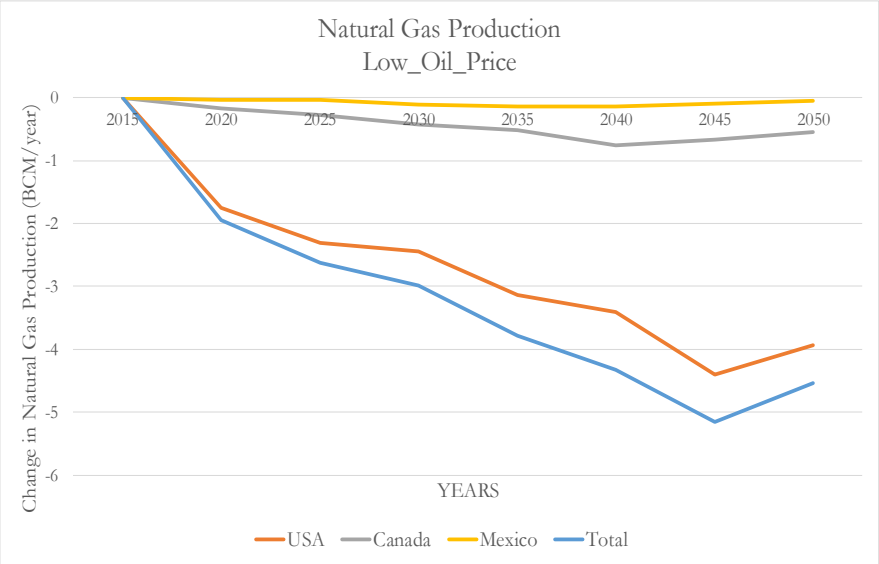

Figure 4.5: Change in natural gas production per country under the Low_Oil_Price scenario. Production in all three countries adjusts according to the applied change in consumption.

Trade between the three countries is also affected, with exports of the U.S. to Mexico decreasing by 4.80%, while imports of the U.S. from Canada also decrease by 12.91%. In Figure 4.6 we can observe how the flows from Middle-Atlantic to East-North-Central decrease by 4.98% and the flows from Mountains to the Pacific region decrease by 5.44% in 2040. Moreover, all flows from West-South-Central decrease, with exports to Mexico decreasing by an aggregate of 4.80% and flows to East-South-Central decreasing by 14.95%. Figure 4.7 illustrates how the adjustment of flows within the U.S. are either comparable or greater than the adjustment of exports to Mexico. Among major inter-regional interconnections, the interconnection between West-South-Central and East-South-Central is the most sensitive.

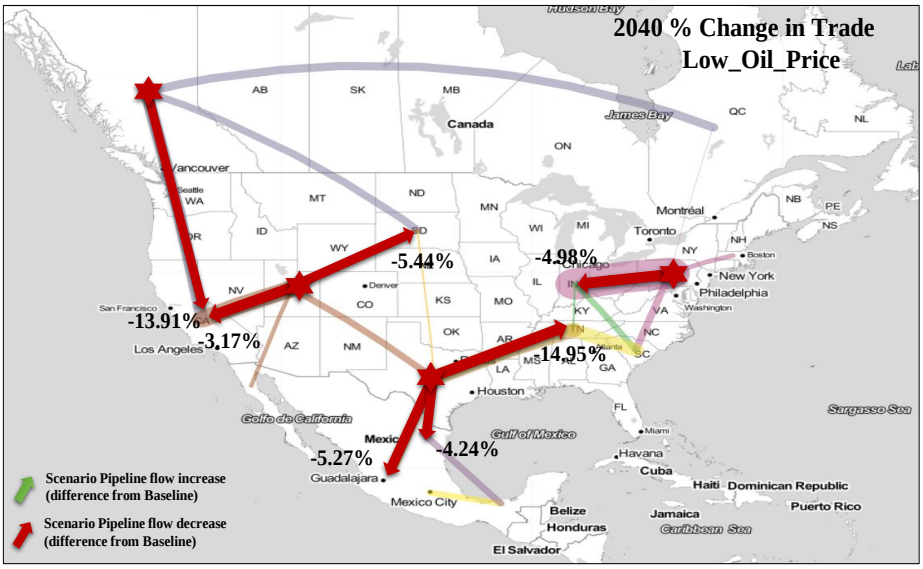

Figure 4.6: Percentage change in natural gas trade between North American regions under the Low_Oil_Price scenario. Trade via major interconnections decreases.

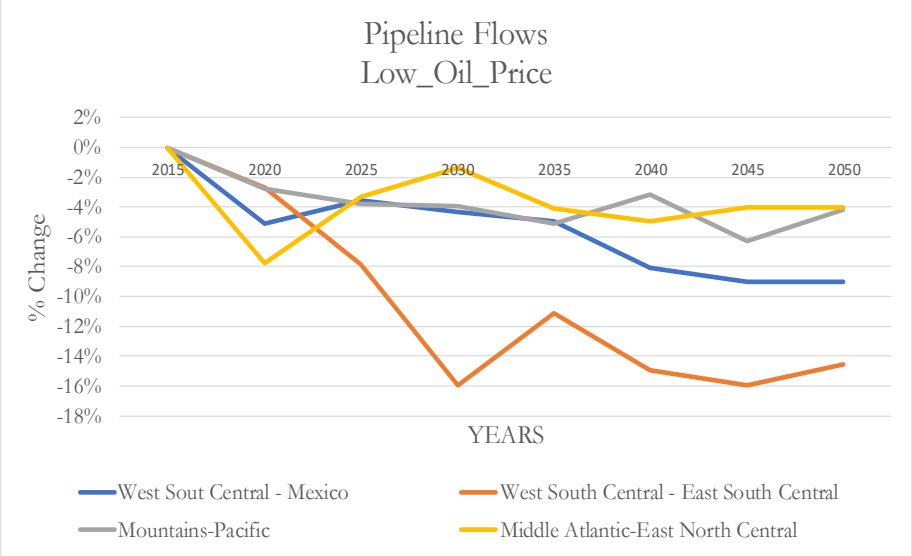

Figure 4.7: Percentage change in natural gas trade between selected North American regions under the Low_Oil_Price scenario. Among major interconnections, the West-South Central – East South Central interconnection is affected the most.

Lower demand in the Low_Oil_Price scenario results in smaller production capacity infrastructure expansion compared to the Reference scenario. Figure 4.8 reveals

that the change in production infrastructure is heterogeneous among regions. The two biggest producing regions in the U.S., Middle Atlantic and West-South Central, decrease their investment in production capacity by 8.51 BCM/year and 16.64 BCM/year respectively. On the other hand, smaller producing regions decrease their investment in new infrastructure only marginally. Figure 4.8 also reveals that the observed decrease in Mexican production is attained by decreasing the utilization rate of available capacity in 2050.

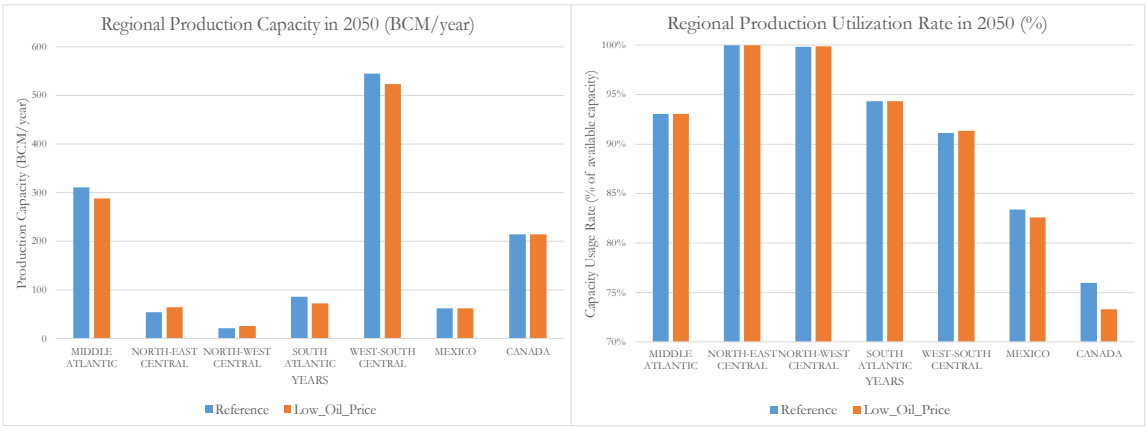

Figure 4.8: Production capacity for selected regions (left) and regional production utilization rate (right) in 2050 in the Reference and Low_Oil_Price scenarios. Producers that do not decrease their investment in new production infrastructure adjust their utilization rate.

In conclusion, the projected increasing exposure of the U.S. to international markets renders the U.S. more vulnerable to shocks in international prices in the mid-term. Investment in new production capacity infrastructure in the North-American system is also smaller. The results highlight the resilience of cross-border trade between the U.S. and Mexico and, consequently, the high sensitivity of neighboring

pipelines. On average, regional decrease in demand leads to further under-utilization of the pipelines connecting major U.S. producers to smaller producing regions with high demand.

4.3.2 High_Gas_Supply Scenario

Enhanced overall productivity in North America results in an increase of production for all three countries. Moreover, the greater availability of low-cost gas results in increased overall consumption. In this scenario, we adjust the linear, quadratic, and Golombek terms of the marginal cost function (parameters lin^{P}_{ysne}, qud^{P}_{ysne}, gol^{P}_{ysne} in Feijoo et al. (2016)) according to the definition of the scenario. That is, by 20% in 2020, by 30% by 2030, with linear ramps between 2020 and 2030 and a 30% change for the remainder of the time horizon after 2030. Figure 4.9 highlights how increased productivity allows Mexico to tap into its unexplored potential and thus grow even more than the U.S. and Canada. In Figure 4.10 we can see that consumption of Mexico grows by 4% in 2050, whereas U.S. and Canada's consumption grow by 5% in 2050.

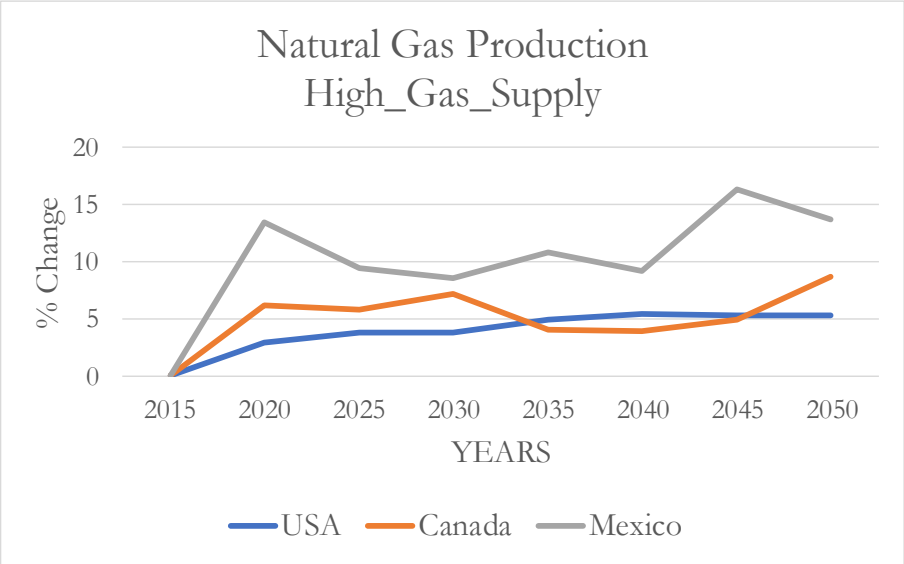

Figure 4.9: Percentage change in natural gas production per country under the High_Gas_Supply scenario. Mexican production increases the most with respect to the Reference scenario.

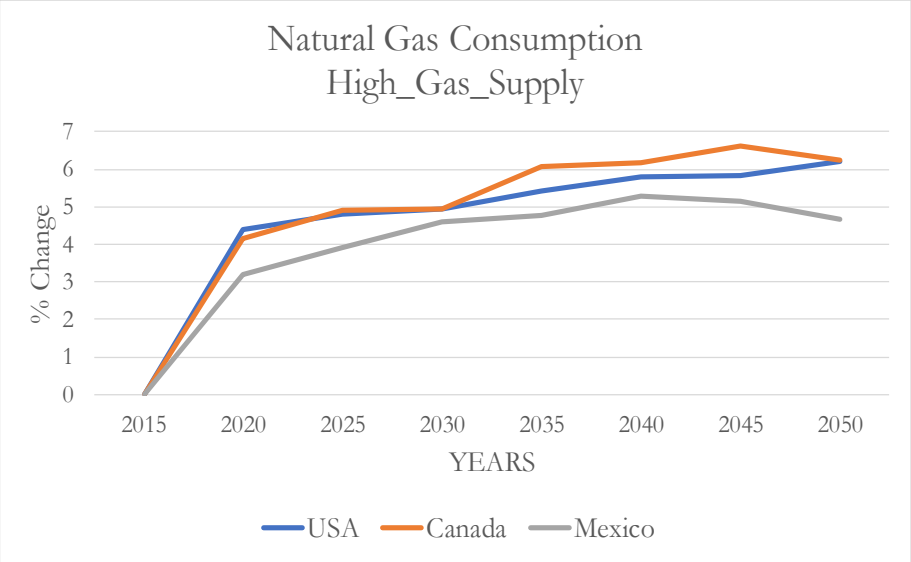

Figure 4.10: Percentage change in natural gas consumption per country under the High_Gas_Supply scenario.

Although Mexico's production grows disproportionately more compared to the Reference scenario than that of the U.S., U.S. exports to Mexico decrease only

marginally. At the same time, Mexican consumption expands as a response to cheaper available natural gas in Mexico. Figure 4.11 shows the intertemporal change of Mexico's natural gas production and consumption. The expansion of Mexico's consumption at a rate similar to the expansion of natural gas production leads to only marginal changes in cross-border trade between the U.S. and Mexico. Figure 4.12 shows the regional disaggregation of net flows between the U.S. and Mexico. Net exports to Mexico-Northeast decrease and net exports to Mexico-Interior-West increase, leading to a 1.97% overall decrease in 2040. The decrease in consumption of both Mexico and the U.S. suggests that the increase of Canada's production stems from the expansion of the domestic market of Canada.

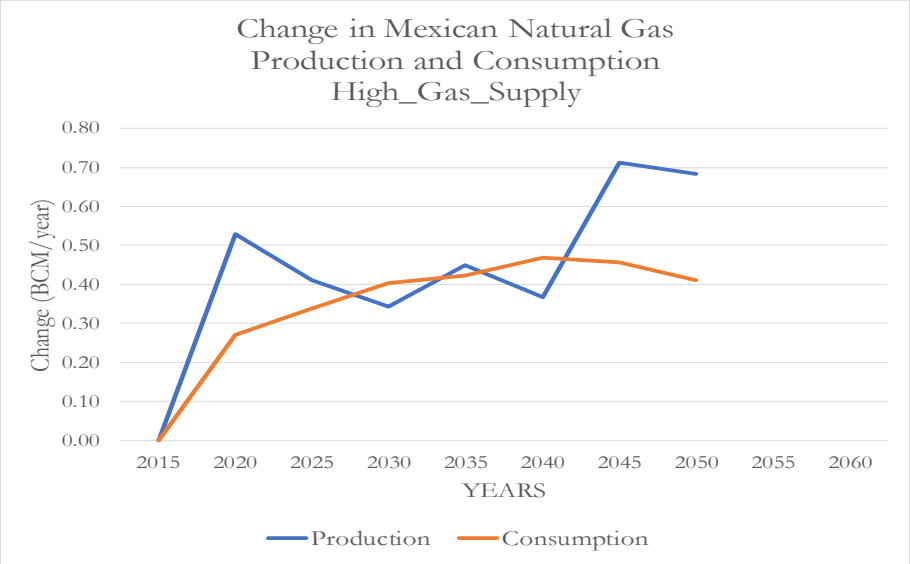

Figure 4.11: Change in Mexican natural gas production and consumption in High_Gas_Supply. Mexican consumption expands due to greater availability of low-cost resources in Mexico. The magnitude of the change in Mexican consumption is comparable to the change in Mexican production intertemporally.

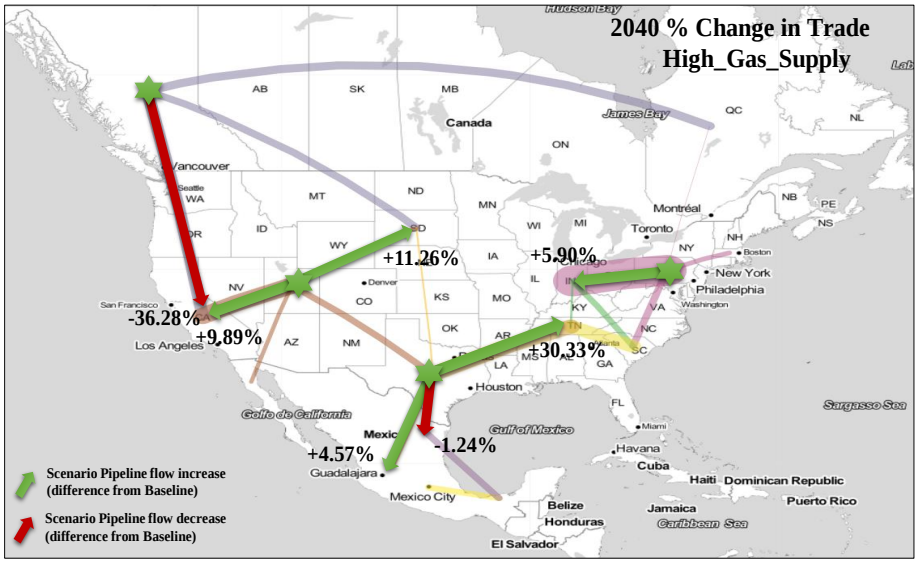

Figure 4.12: Percentage change in natural gas trade between North American regions under the High_Gas_Supply scenario. Trade via most major interconnections increases. Change in trade varies regionally.

Cheaper production capabilities in High_Gas_Supply result in lower overall production capacity infrastructure expansion in the North-American natural gas system. In the Reference scenario, producers often do not deplete their capacity due to the nonlinear marginal cost. From an infrastructure point of view, the lower marginal cost of production allows producers to utilize existing infrastructure more efficiently and subsequently invest in less capacity inter-temporally. Overall investment in North-American natural gas production infrastructure decreases by less than 1% inter-temporally or 3.21 BCM/year. Figure 4.13 reveals that our intuition is true for large producers, the Middle Atlantic and North-West Central regions, but not for small ones, such as North-East Central and North-West Central, that in fact increase their investment in production infrastructure compared to the Reference scenario.

Nevertheless, Fig. 13 also reveals that all regions are able to use all existing and new capacity more efficiently. In fact, the regions that do not expand their production capacity infrastructure compared to the Reference scenario, such as Canada and Mexico, are the ones that are able to tap into the potential of existing available resources.

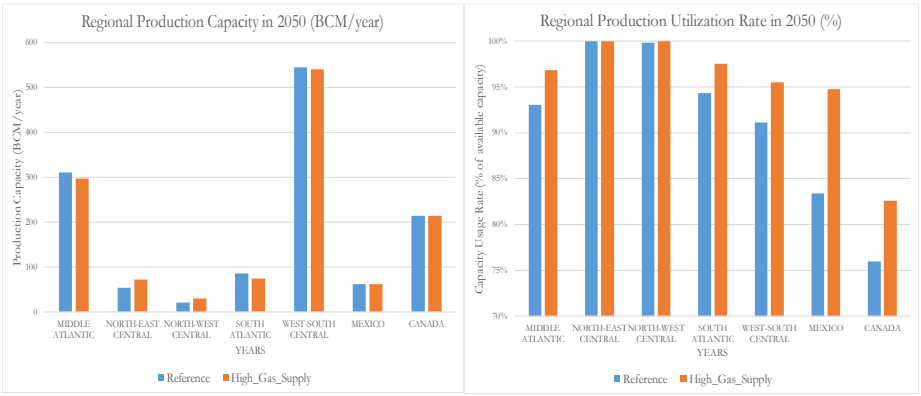

Figure 4.13: Production capacity for selected regions (left) and regional production utilization rate (right) in 2050 in the Reference and High_Gas_Supply scenarios. All producers use their capacity more efficiently.

In conclusion, this scenario highlights the potential of Mexico's production to grow by more than the U.S., given the technological circumstances. This comes as a result of more efficient utilization of existing production infrastructure. Growth of Mexico's production however does not immediately imply that imports from the U.S. are decreased, given the strong trade relations between the two countries. On the other hand, total U.S. exports to Mexico remain unaffected and increase marginally.

4.3.3 Natural Gas Resources Scenarios

The U.S. is the largest natural gas producer and consumer in North America with strong trade relationships with both Canada and Mexico. For that, shocks in the productivity of the U.S. propagate to the rest of North America. Naturally, in the High_NG_Res scenario, the U.S. gains a comparative advantage over the rest of the countries and for that it grows disproportionately more. On the other hand, at the Low_NG_Res scenario the U.S. becomes less competitive with respect to its neighbors, who expand their production at higher rates compared to the Reference scenario. We implement this scenario by constraining all infrastructure decisions by 2030 to their reference level (variables z^P_{ysne}, z^A_{ya} in Feijoo et al. (2016)) and allowing them to adjust thereafter. Moreover, in 2030 and thereafter, we adjust the linear, quadratic, and Golombek terms of the marginal cost function (parameters lin^P_{ysne}, qud^P_{ysne}, gol^P_{ysne} in Feijoo et al. (2016)) according to each scenario's specifications.

In the High_NG_Res scenario, the higher availability of resources in the U.S. results in higher consumption in all countries. Figure 4.14 shows how consumption in the U.S. increases by 6% by 2050 in the High_NG_Res scenario, while consumption of Canada and Mexico increase by 4%. In the Low_NG_Res scenario, U.S. consumption decreases by 3.5% and Mexican and Canada's consumption decrease by more than 2% and 3% respectively. Figure 4.15 shows how the change in availability of U.S. resources affects North American natural gas production.

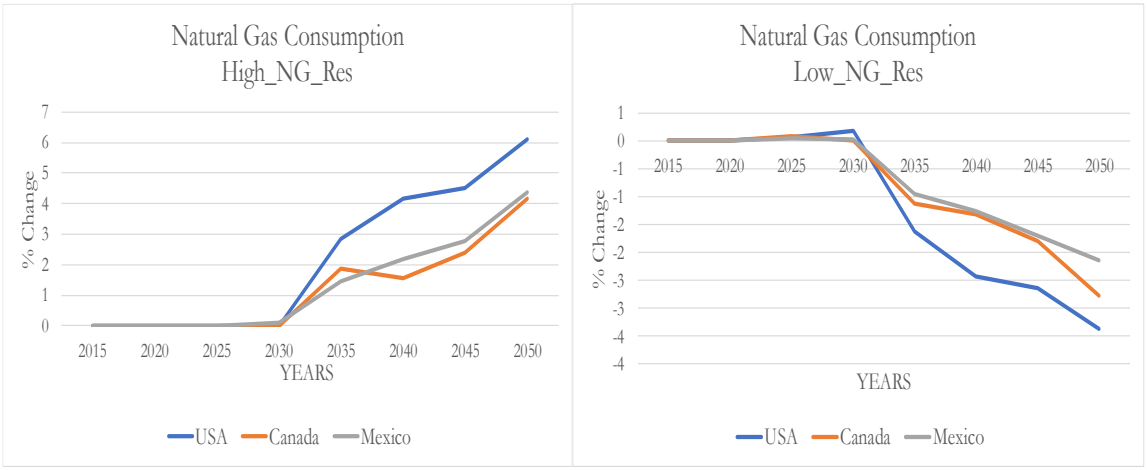

Figure 4.14: Percentage change in natural gas consumption per country under the High (left) and Low (right) Natural Gas Resources scenarios. Greater availability of resources in the U.S. in High_NG_Res drives consumption higher in all three countries. The opposite is true in Low_NG_Res.

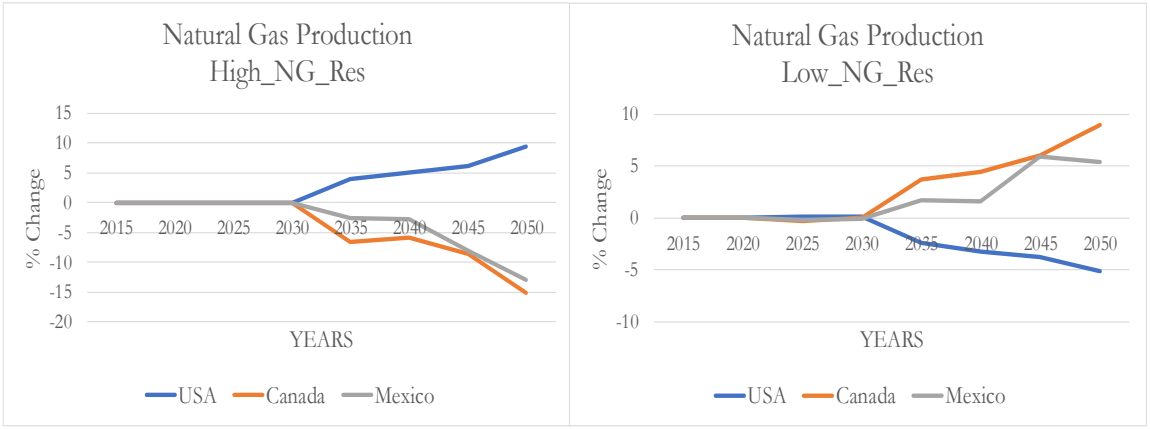

Figure 4.15: Percentage change in natural gas production per country under the High (left) and Low (right) Natural Gas Resources scenarios. Greater availability of resources in the U.S. in High_NG_Res provides U.S. producers with a competitive advantage over Canada's and Mexico's producers. The opposite is true in Low_NG_Res.

Pipeline infrastructure allows Mexico's and Canada's consumers to benefit from low-cost U.S. resources. In addition, in the High_NG_Res scenario, West-South-Central exploits its capabilities as the biggest producing region and at the same time

the major trade partner of Mexico. Total exports from the U.S. to Mexico increase by 6.97%. Trade between other U.S. regions is depicted in Figure 4.16. Notably, Mountains is capable of providing to Pacific all of the demand previously covered by West-Canada. Therefore, trade between West-Canada and the Pacific is eliminated and trade between Mountains and the Pacific region increases by 15.75%. To do so, the Mountains also need to curtail some of their supply to West-North-Central. Finally, Figure 4.17 depicts how the flows from large U.S. producers (West-South-Central and Middle-Atlantic) to regions with limited production (South-Atlantic and North-East-Central respectively) serve as a means for expanding regional markets with limited resources.

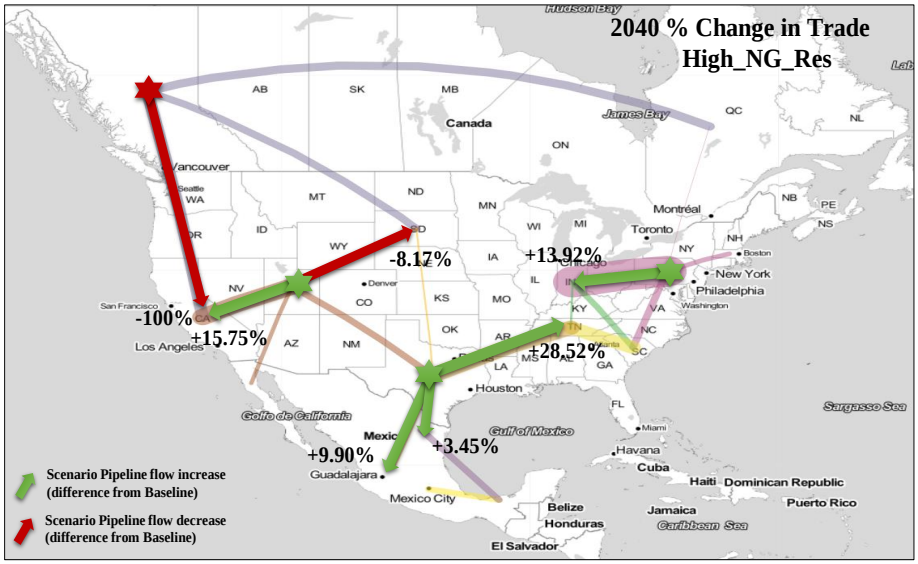

Figure 4.16: Percentage change in natural gas trade between North American regions under the High Natural Gas Resources scenario. Trade via most major interconnections increases.

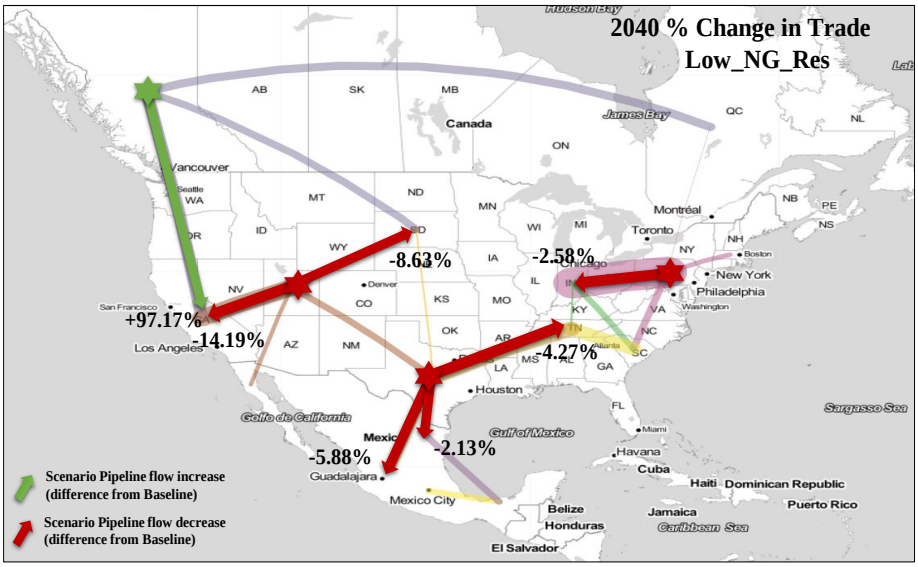

Figure 4.17: Percentage change in natural gas trade between North American regions under the Low Natural Gas Resources scenario. Trade via most major interconnections decreases.

Similarly, in the Low_NG_Res scenario, the scarcity of resources in the U.S. results in a decrease in trade. The reason is the need for producers to cover their regional demand. Therefore, exports from the U.S. to Mexico are reduced by 4.12%. In addition, West-Canada exploits the difficulty of the U.S. to cover their demand and increases both its production and its trade with the Pacific region. Finally, when producers prioritize covering their regional demand then flows to other regions are curtailed, resulting in a decrease in natural gas trade between West-South-Central and East-South-Central.

The changes in natural gas trade do not alter investment decisions in pipeline infrastructure compared to the Reference scenario in the High_NG_Res and Low_NG_Res scenarios respectively. The only pipeline interconnection that is affected is the Middle

Atlantic to North-East Central. In the High_NG_Res scenario its capacity increases by 10.14 BCM/year and in the Low_NG_Res by 2.09 BCM/year by 2050. The reason is that 2015 pipeline infrastructure is sufficient for most interconnections. Figure 4.18 shows that in the Reference scenario, pipeline capacity infrastructure of many major interconnections is underutilized. Therefore, in response to changes in trade, pipeline operators adjust their utilization rate instead of their capacity. The Middle Atlantic to North-East Central interconnection is always at capacity, which is the reason why investment in new infrastructure happens under all scenarios. Finally, the Canada West to Pacific interconnection appears to be very sensitive in these scenarios. The utilization rate becomes zero in 2040 in High_NG_Res but almost doubles in Low_NG_Res.

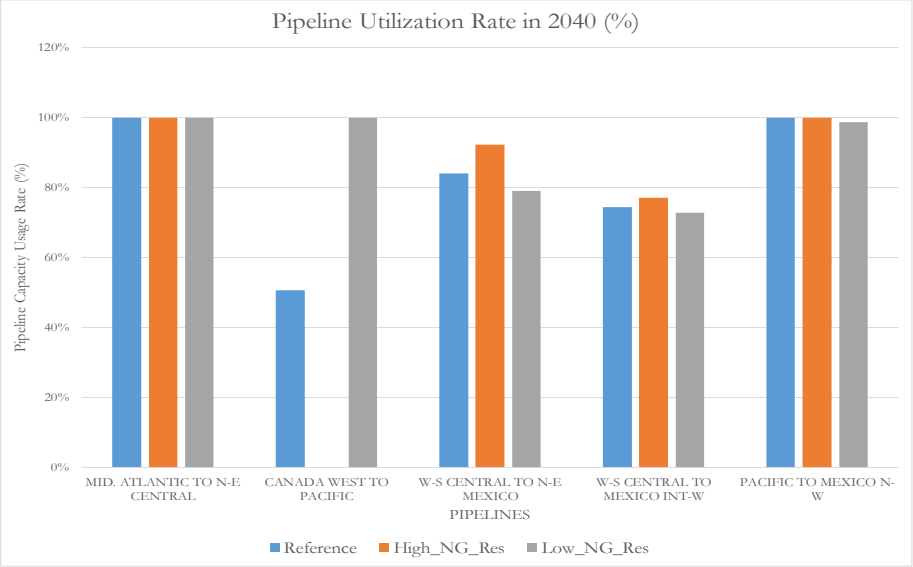

Figure 4.18: Pipeline utilization rate (percentage with respect to pipeline capacity) in 2040 in the Reference, High_NG_Res, Low_NG_Res scenarios for selected pipeline. Pipeline operators respond to a surge in trade by exploiting underutilized capacity instead of expanding their capacity.

In conclusion, the two scenarios highlight that the availability of low-cost resources in the U.S. is exploited primarily by domestic consumers. When more resources are available in the medium and long-term for the U.S., U.S. producers increase their market share in North America. In addition, consumption increases in all three countries as a result of low-cost natural gas in North America overall. Due to the significance of the U.S., the shocks propagate to both Canada and Mexico via the pipeline system, increasing North American demand for natural gas overall. The opposite is true for scarce medium- and long-term resource availability. U.S. production loses a fragment of its market share, while U.S. consumption decreases due to the overall increase in the price of natural gas. However, the impact on production of Canada and Mexico is less severe compared to that on U.S. production, which points to the ability of U.S. natural gas infrastructure to absorb the impact of such shocks before exploiting inter-country trade. The vast majority of pipeline operators respond to changes in trade by adjusting the utilization rate of pipelines, since pipeline infrastructure is underutilized in the Reference scenario.

4.4 Conclusion

The current chapter explores the evolution of North American natural gas infrastructure under a variety of plausible scenarios. For the purpose of this chapter we use NANGAM, a large-scale, bottom-up, equilibrium model of the North American nat-

ural gas system, that allows for the representation of market agents with competing objectives. Our analysis is motivated by the critical role of oil prices, technological progress, and resource availability in the assessment of North American natural gas infrastructure resilience. We run a scenario where the low oil and gas prices observed after 2014 are preserved in the future, a scenario of higher supply due to technological progress, and two scenarios of high and low availability of natural gas resources. The assumptions behind the Reference scenario are based on contemporary knowledge. Therefore, the observed changes under each scenario depend on reference assumptions.

We show that when oil prices remain low, then all three countries' production can decrease by more than 3% by 2040. Total investment in new production capacity infrastructure in the U.S. can also decrease, but the impact varies regionally. Larger U.S. producers decrease their investment in production infrastructure, however certain smaller U.S. producers marginally increase their investment in new infrastructure. Moreover, the exposure of the U.S. to international trade leads to production decreasing faster in the short-term than in the long-term, as a response to the faster short-term decrease in consumption that is imposed in this scenario. Although Canada is not as exposed to international trade as the U.S., the decrease in production between the two is similar through 2050. Mexico on the other hand taps into its potential in the long-term and is able to offset the effects of the shock by 2050. The results suggest that the strong projected link of the U.S. with international mar-

kets renders the U.S. vulnerable to changes in international prices in the mid-term. Decreased demand also leads to decreased flows from major U.S. producing regions to traditional trade partners in mainland U.S. and Mexico.

More aggressive technological progress in North America results in Mexico's production growing by more than the rest of the countries. The disproportional growth of Mexico's natural gas production happens without any investment in new production infrastructure, as the reduced cost allows Mexico to exploit more efficiently its existing resources. However, Mexico continues to rely on the U.S., with U.S. exports to Mexico decreasing only marginally. The result suggests that the Mexican Energy Reform can succeed in exploiting Mexican natural gas resources if it manages to stimulate those market forces that would enhance the productivity of Mexico's natural gas industry by at least as much as the rest of the countries. At the same time, enhancing Mexico's natural gas production does not necessarily mitigate Mexico's dependence on U.S. natural gas.

In the High_NG_Res (Low_NG_Res) scenario where more (less) resources are available in the medium and long-term for the U.S., U.S. producers increase (decrease) their market share in North America. The results suggest that the (un)availability of resources in the U.S. affects primarily U.S. consumption and secondarily U.S. imports and exports. Given that pipeline infrastructure is underutilized in the Reference scenario, pipeline operators respond to changes in trade by adjusting the pipeline utilization rate. From the policy-makers' point of view, the U.S. would bare the

benefits (costs) of resource availability. From a stakeholder's point of view, certain trade infrastructure might not be resilient to changes in its current and projected status.

We identify two modeling assumptions that are critical in our analysis. First, NANGAM agents have perfect foresight through 2050, which implies that agents make operation and investment decisions simultaneously for the whole time horizon. There exist recursive-dynamic energy models, where agents can update their decisions after certain time steps. Although a recursive-dynamic model can be more representative of the actual decision-making process of different agents, its results are more sensitive to the expectations of the individual agents that require special treatment. In natural gas infrastructure planning both approaches are applicable (Babiker et al., 2009). Second, NANGAM has a particular focus on the natural gas sector and does not endogenously account for interactions with other sectors. These interactions are manifested mainly through the demand of natural gas from other sectors. Sankaranarayanan et al. (2018) show that results of certain natural gas infrastructure models are most sensitive to changes in natural gas consumption. A more complete treatment of each shock would require accounting also for the impact of every shock in all other sectors of the economy that affect natural gas consumption. Still, the scenario design in this chapter is consistent with policy reports and published literature.

Future research can assess the impact of a scenario where certain North American regions have higher and other regions have lower long-term resource availability. In

Section 4.3 we highlight the importance of pipeline interconnections between North American regions and countries for the outcome of a shock. Hence, a combination of high and low regional resource availability may not affect natural gas production of certain regions, depending on demand projections of interconnected regions.

Our analysis assumes that all other factors, such as economic growth and energy demand among others, remain unchanged compared to the Reference scenario. More aggressive transition to a low-carbon or net-zero economy can affect natural gas demand and lead to quicker transformation or phase-out of North American natural gas infrastructure. Nevertheless, decreasing international oil prices, technological progress, and resource availability can render natural gas resources less expensive and delay the infrastructure transformation or phase-out process.

Moreover, our analysis assumes the operation of natural gas infrastructure is not disrupted in the long-term by climate change. Global warming can lead to extreme weather events (van Oldenborgh et al., 2017) and compromise the capabilities of natural gas production and pipeline infrastructure. More frequent extreme weather events in the future can incentivize international agents to commit to more aggressive carbon emissions policies, which can affect natural gas demand. Addressing the question of North American natural infrastructure resilience against extreme weather events would require enhancing NANGAM to account for climate change. A treatment of the impact of extreme weather events is possible by coupling NANGAM with climate models.

Our results highlight the spatial distribution of the effects of plausible future development trajectories of the natural gas sector in North America. We stress the importance of using a framework that accounts for the interactions between competing market agents as a means to understand the transformation of the North American natural gas sector and assess its resilience. We study three scenarios that explore the impact of low international oil prices, technological progress in the natural gas sector, and availability of natural gas resources. By using NANGAM, we are able to provide policymakers and stakeholders with an informed outlook on North American regions and pipelines that are most affected both between countries, but also within the U.S. Our analysis focuses on the crucial role of natural gas on the ongoing transformation of the North American energy system towards a low-carbon economy in an attempt to inform future policy design.

Acknowledgements

The author thanks Daniel Chu and Dr. Sauleh Siddiqui, who contributed to the work in this chapter.

Disclaimers

NANGAM is based in part on the multi-fuel energy equilibrium model MultiMod (Feijoo et al., 2016). The MultiMod was developed by Dr. Daniel Huppmann at DIW Berlin as part of the RESOURCES project, in collaboration with Dr. Ruud

Egging (NTNU, Trondheim), Dr. Franziska Holz (DIW Berlin) and others (see `http://diw.de/multimod`). We are grateful to the original developers of MultiMod for sharing their model.

Chapter 5

North American Natural Gas Market Development Under Different Mechanisms of Renewable Policy Coordination

5.1 Introduction

Establishing Renewable Portfolio Standards (RPS) requires renewable technologies to cover a minimum share of retail electricity consumption. Renewable electricity producers — such as wind, solar, or geothermal — generate minimal emissions. Although the capital cost of renewables is high compared to that of fuel generators, its decrease has been a key driver of the growing investment on renewable energy in North America (EIA, 2020). RPS aim to accelerate the introduction and adoption of

non-emitting technologies in the power producing sector. RPS are enforced either at the national, provincial, or regional level and in most states introduce a market for Renewable Energy Certificates (RECs). RECs are financial products that are traded independently of the physical power market. RECs are created when a renewable energy source produces a benchmark amount of energy. Hence, RECs result in additional revenues for renewables. At the same time, emitting technologies need to purchase RECs in order to meet the RPS goal. Therefore, RPS result in emitting technologies subsidizing non-emitting technologies and thus favor the latter over the former (Yin and Powers, 2010).

The idea of RPS was first introduced by (Rader and Norgaard, 1996). Wiser et al. (2007), point out that although the idea was developed by Rader and Norgaard (1996), RPS were already in place in Minnesota and Iowa. These policies were not referred to as RPS until the late '90s. By 2018, more than 29 U.S. states and the District of Columbia had adopted some variation of RPS (Wiser et al., 2019). Moreover, Europe has a similar scheme not just for the electricity sector, but for energy consumption overall. The Renewable Energy Standards (RES) set individual targets for member countries on the percentage of gross energy demand, not just electricity, covered by renewable energy sources (EC, 2009). RES are set centrally from the European Commission, but vary among countries on the basis of their potential to exploit renewable energy resources.

As a result of RPS, production from fossil fuel-fired plants is discouraged. How-

ever, in the case of natural gas, RPS do not necessarily translate into a decrease of production from natural gas-fired plants. Under RPS, gas-fired plants — as any other CO_2 emitting technology — are disadvantaged compared to non-emitting technologies. At the same time, RPS are often coupled with emissions cap or emissions tax policies at the state or federal level. Natural gas-fired plants have benefitted from such schemes in the short term due to their relatively lower emissions factors compared to other fossil fuel-fired plants. In addition, natural gas in North America is becoming cheaper (Feijoo et al., 2016). The combination of RPS, emissions policies, and resource availability in North America has led to an overall increase in natural gas consumption by the electricity sector.

Natural gas is an important source of energy for the residential, commercial, industrial, electricity, and transportation sectors. Shocks in these sectors result in different natural gas infrastructure investment decisions, which in turn affect long-term natural gas prices. The resulting price deviations can be mitigated by developments in the natural gas market. Under integrated natural gas markets, prices between trade partners are more tightly linked, thus more resilient to shocks. Huntington (2009) argues that enhanced integration of the North American natural gas markets leads to more stable long-term natural gas prices and increases energy security of the U.S., Canada, and Mexico. However, the interdependence of electricity and natural gas markets renders the latter vulnerable to changes in the former, regardless of the level of integration of natural gas infrastructure. Moreover, different energy and electric-

ity models are often built using different databases or with different level of detail. Consequently, the models still disagree about the resulting impact of the same policy to the electric and natural gas sectors.

In this chapter we focus on the interplay between RPS and natural gas markets and infrastructure. To do so, we couple four models that provide estimates of natural gas consumption with the North American Natural Gas Model (NANGAM) to simulate the natural gas system in North America. Moreover, the analysis in the current chapter aims to complement the analyses in Chapter 4 and Bistline et al. (2020), conducted within the scope of the Energy Modeling Forum 34 (Huntington et al., 2020). Chapter 4 focuses on the response of North American natural gas markets under different assumptions on key drivers of natural gas production. The current chapter aims to quantify the impact of RPS, as studied in Bistline et al. (2020), on the natural gas system due to the interdependence of the electricity and natural gas sectors. Specifically, we ask:

- What are the implications of different levels of RPS coordination for regional natural gas production and pipeline infrastructure in North America?
- Under the same level of RPS coordination, how sensitive are the results for the natural gas sector to the modeling assumptions regarding mandated renewable shares?
- How do the developments in the natural gas market inform policymaking in the

electricity sector?

5.1.1 Literature Review

RPS are policy tools for reducing CO_2 emissions that explicitly favor renewables, as opposed to technology-neutral policies that do not differentiate between power generation technologies. Young and Bistline (2018) find that the cost of RPS, as measured by the Net Present Value (NPV) through 2050, can be twice that of a technology-neutral portfolio for the same CO_2 emissions target. Upton and Snyder (2017) conclude by using empirical methods that RPS increase electricity prices between 10.9% and 11.4%. Moreover, Palmer and Burtraw (2005) argue that for the same emissions reduction target, a cap-and-trade system is more cost-efficient when compared with RPS, as it forces a greater quantity of coal-fired plants, the highest emitters, out of the system. Their findings are consistent with Fischer and Newell (2008) who identify that a market for CO_2 emissions permits is the most cost-effective policy among six policy alternatives. Weyant (2008) and Schmalensee and Stavins (2017) identify how political concerns can bias the design of emissions reduction policies.

Lack of coordination of climate policies between regions in the electricity sector can lead to increased electricity prices and greater CO_2 emissions. Bistline and Rose (2018) find that in the absence of coordination in the power sector it is more likely for economic activity to shift from more regulated regions to less regulated regions, leading to increased CO_2 emissions and electricity prices. Fullerton and Karney (2018)

highlight the importance of coordinating policies that target different pollutants at different sectors of the economy at the same time. Furthermore, Bistline et al. (2019) conclude that in the absence of RECs, coordinated policies in integrated power markets can decrease the NPV of a RPS scheme in the U.S. by 148 billion dollars. In the presence of RECs, the cost of RPS decreases by 67 billion dollars. Yin and Powers (2010) focus on the treatment of RECs when states set individual renewable energy targets. They find that when states are allowed to trade RECs, then some states may fail to meet their individual emissions targets. In addition, Bowen and Lacombe (2017) argue that there exists strong evidence that states with stringent RPS legislation drive investment in renewables higher in neighboring states with less strict RPS laws.

The majority of the studies that include the natural gas sector when analyzing RPS focus on the impact of natural gas prices on the effectiveness of RPS and vice versa. Shearer et al. (2014) find that under a moderate carbon tax and a strict carbon cap, the availability of cheap natural gas delays the introduction of renewables by a decade. However, under RPS, the introduction of renewables follows the same trajectory for both scarce and abundant natural gas resources. Bistline and Young (2019) study the penetration of wind and solar in the U.S. power generation mix for natural gas prices of 4$, 6$, and 8$ per MMBtu in the presence of RPS. They find that moving from 4$ to 8$ per MMBtu can increase the share of solar and wind by 33%, given transmission expansion costs and CO_2 policies as in their Reference scenario.

Moreover, RPS have been considered in all the Annual Energy Outlooks published by the U.S. Energy Information Administration (EIA) since 1998 (EIA, 1998). In two separate studies by EIA the implementation of a 10% RPS for the U.S. decreases natural gas wellhead prices by 3.67% and 0% respectively (EIA, 2002, 2003). Wiser et al. (2007) collect results of 12 studies published between 1998 and 2003 by EIA, the American Council for an Energy-Efficient Economy (ACEEE), the Tellus Institute, and the Union of Concerned Scientists. The studies quantify the reduction of natural gas wellhead prices due to the introduction of RPS targets of 6.3% in Rhode Island, and 10%, 15%, or 20% in the U.S. (Wiser and Bolinger, 2007).

Studying the impact to one sector of a policy applied to another sector requires understanding the interdependencies between two different sectors. Hence, modelers need to develop tools with the appropriate level of detail in both sectors or link existing bottom-up models. Modelers can choose between a soft-link or a hard-link approach. To the extent that one model's output is used as another model's input, in a soft-link the first model does not account for the response of the agents in the second model. This means that a soft-link, albeit solving faster than a hard-link, may not converge to a point that solves both models (Krook-Riekkola et al., 2017). On the other hand, different models are calibrated using different databases that are often inconsistent for the data at the interdependencies, which is critical for the implementation of a hard-link. Moreover, solving two fully integrated large-scale bottom-up models can prove an arduous task computationally (Böhringer and Rutherford, 2009). Therefore,

the choice of model-coupling method depends both on the models at hand and the research question (Hourcade et al., 2006). Both the soft-link (Hogan and Weyant, 1982; Feijoo et al., 2018) and the hard-link approaches (Tapia-Ahumada et al., 2015) have been used in energy and climate studies. Among the hard-link approaches, Abrell and Weigt (2012) introduce a framework for integrating partial equilibrium models of the electricity and natural gas sectors. The framework is similar to co-optimization (He et al., 2018b) and its variations, namely robust co-optimization (He et al., 2018a) and security-constrained co-optimization (Zhang et al., 2015). Natural gas models have also been integrated with optimal power flow models (Martinez-Mares and Fuerte-Esquivel, 2012).

To the best of our knowledge, little to no emphasis has been given to the impact of RPS on regional natural gas markets. This chapter aims to understand the interplay between RPS and the natural gas market and quantify the regional impact of RPS schemes to natural gas infrastructure. Moreover, it aims to understand how policies in the electricity sector affect the natural gas sector and subsequently influence natural gas trade between the U.S., Canada, and Mexico.

5.1.2 Objectives and Scenarios

Our objective is to quantify the impact of RPS on the natural gas market. RPS result in higher penetration of renewables[1] in the electricity sector. In our formulation,

[1]Following Bistline et al. (2020), the renewable technologies considered are wind, biomass, concentrated solar power (CSP), utility-scale photovoltaic (PV), geothermal, and hydro.

the U.S., Mexico, and Canada[2] mandate that the share of renewables in the power generation mix is greater than or equal to 30% in 2020, 40% in 2030, 50% in 2040, and 60% in 2050, with linear increase between years. These targets are input into the individual electricity or energy models that output natural gas consumption. The resulting change in natural gas consumption is then input into NANGAM to quantify the impact of each policy on natural gas markets and infrastructure. We simulate three different variations that assume different levels of RPS coordination between the U.S., Canada, and Mexico.

a) **International coordination (Scenario 1):** The U.S., Canada, and Mexico are obliged to jointly meet the scenario's renewables penetration targets. International coordination allows for unbundled RECs to be traded between all three countries.

b) **No international coordination (Scenario 2):** Each country is obliged to meet the scenario's renewables penetration targets individually. Lack of coordination implies that unbundled RECs can be traded only among electricity producers of the same country.

c) **No inter-regional coordination (Scenario 3):** Each region within each country is obliged to meet the scenario's renewables penetration targets indi-

[2]Canadian hydropower generation constitutes more than 60% of the energy mix in 2016 (NEB, 2017). Therefore, new renewables would be introduced due to RPS in order for neighboring regions to meet a certain requirement and only to the extent that they are rendered competitive compared to renewables of other regions.

vidually. Lack of coordination implies that unbundled RECs can be traded only between electricity producers of the same region.

The "No inter-regional coordination" scenario can also be modeled with a different combination of coordinating states. We chose an implementation that is consistent with NANGAM's regional disaggregation. However, political strategies or institutional coordination between states could result in a different regional renewable policy coordination scheme.

The impact of different RPS coordination schemes on natural gas consumption is not trivial and is analyzed in detail in Bistline et al. (2020), where the authors show that limiting RPS coordination leads to the displacement of more gas generation in the U.S. This finding builds on existing literature that suggests that RPS increase the displacement of natural gas in the electricity sector (Mai et al., 2018). Moreover, in Scenario 1, regions with little solar and wind potential are able to leverage the potential of their neighbors in order to meet the renewables penetration target. Subsequently, the required renewables capacity needed in North America on aggregate to meet that target is minimized, which in turn allows for more natural gas capacity to be installed. Although natural gas-fired plants are displaced compared to the Reference scenario in all three scenarios, greater RPS coordination among regions results in less installed renewable capacity which leaves more room for investment in natural gas-fired plants. This is particularly the case with Canada that has an already high penetration of hydro. In Scenario 1, Northeastern U.S. leverages the hydro and wind

potential of Canada instead of investing in domestic renewable resources. On the other hand, in Scenario 3, the same regions would have to invest in their own, lower-quality resources to meet their targets. Consequently, a larger part of Northeastern U.S. demand would be covered by renewables in the future, leaving less room for investment in natural gas-fired plants. A more in-depth discussion on the conditions under which this argument suffices to explain the results for gas-fired plants, as well as detailed results for the electricity sector, can be found in Bistline et al. (2020).

5.2 Methods

5.2.1 Multi-Model Integration

For the purpose of our analysis, we used projections of natural gas consumption from four models for the three variations of RPS policies. Moreover, other than the renewables penetration targets, no other features of the models used to provide natural gas consumption projections were altered, including the assumptions on investment and operational costs. The calibration of all models incorporates contemporary knowledge of future trends, *e.g.,* renewable policy mandates and carbon emissions policies. Since the models do not provide forecasts, their foresight deep into the time horizon can be limited. First, we provide an overview of the models.

NANGAM (Feijoo et al., 2016) is a game-theoretic, planning model that simulates

production, consumption, and trade decisions for natural gas in the U.S., Canada, and Mexico. NANGAM comprises 17 regions, including the nine census regions for the U.S., a node for Alaska and Hawaii, five regions for Mexico (Northwest, Northeast, Interior-West, Interior, and South-Southeast), and two regions for Canada (East and West). Representative producers exist in the 13 regions that have natural gas production capacity and regional consumption is approximated using a linear inverse demand curve. Pipeline interconnections between regions are aggregated into 69 arcs, whose investment, fixed, and marginal cost of transporting natural gas is based on a database of 778 existing projects and 187 new ones. In NANGAM every region in the U.S. and Canada is also equipped with a storage facility. At the upstream level, producers compete in a Nash-Cournot style market wherein pipeline operators are assumed to be profit maximizers who ensure that regional natural gas demand is met. Investment decisions on production and pipeline capacity are endogenous and are based on future profitability. NANGAM considers three seasons – peak, high, and low – and runs in five-year time steps up to the year 2050. NANGAM is based on Multimod (Huppmann and Egging, 2014) and therefore can simulate supply-side or demand-side shocks, infrastructure development decisions, and policy interventions.

ReEDS2.0 (Eurek et al., 2016) simulates operation and capacity expansion decisions for the electricity markets of the contiguous U.S., Canada, and Mexico. It comprises 205 Balancing Areas and 454 Resource Supply regions. ReEDS2.0 runs in two-year time steps from 2010 to 2100. Each year is divided into four seasons in

which each season is further divided into four time segments that represent overnight, morning, afternoon, and evening. ReEDS2.0 is a linear program and is suitable for modeling emissions policies such as carbon taxes and emissions caps.

NATEM (Vaillancourt et al., 2018) is based on MARKAL/TIMES, from which it inherits the detailed representation of the entire energy system. As with TIMES, the decisions in NATEM are the result of an intertemporal cost minimization program. NATEM-Canada includes all 13 Canadian provinces and territories. There exist five end-use consumer categories (commercial, residential, industrial, transportation, and agriculture) each of which bases its decision on 70 end-use services. The version of NATEM used in this chapter is intertemporal and produces results in five-year time steps from 2015 to 2050. Each period accounts for four seasons that are further disaggregated into four intra-day periods per season.

NEMS-AEO2019 (EIA, 2009) is a bottom-up model of the U.S. energy system that is maintained by the U.S. Energy Information Administration. NEMS-AEO2019 comprises 16 sub-modules, each with its own technological features as well as regional disaggregation that is based on data availability and practicality for policy analysis. NEMS-AEO2019 yields projections in yearly time steps up to 2050. NEMS-AEO2019 is the version of NEMS used to produce the "Annual Energy Outlook 2019". Compared to previous versions, it includes up-to-date data on taxes, vehicle stock, and updated assumptions for residential and commercial end-use technology, state-specific RPS and the solar Investment Tax Credit.

GENeSYS-MOD (Löffler et al., 2017) is based on the OSeMOSYS model (Open-Source Energy Modeling System) and extends the previous framework in many ways, namely by including a detailed power system, increasing the number of time segments, adding storage technologies, and improving the representation of trade. GENeSYS-MOD is a linear program that minimizes the sum of all the cost components of the energy system subject to constraints that simulate the workings of the energy system. The version used in this chapter divides Mexico into nine regions and includes all main generation technologies, namely utility PV, onshore and offshore wind, geothermal, coal-fired thermal plants and CHP, gas-fired thermal plants and CHP, and oil-fired thermal plants and CHP. Energy demand is disaggregated into demand from the electricity, the transportation, and the industrial heating sectors.

The four models that provide estimates of changes in natural gas consumption have different regional and temporal disaggregation. ReEDS2.0 models the electricity markets of the U.S., Canada, and Mexico in detail; NATEM models the energy system of Canada; NEMSAEO2019 the energy system of the U.S.; and GENeSYS-MOD that of Mexico. Inputs for Scenario 1, which assumes coordination at the international level, were retrieved only from ReEDS2.0 since it includes all three North American countries. All models other than ReEDS2.0 provide percentage changes in country-level total yearly natural gas consumption for the country-specific Scenarios 2 and 3. The country-level percentage change is then applied to every NANGAM region included in each country. ReEDS2.0 has a more granular representation of North

America than NANGAM. For that, ReEDS2.0 yearly output is aggregated to provide percentage changes in natural gas consumption by the electricity sector for every NANGAM region. The change in total natural gas consumption given ReEDS2.0 inputs is derived by the contribution of consumption from the electricity sector in total consumption of natural gas of a region. The derived region-specific change in total natural gas demand is then input into NANGAM for all time periods modeled in NANGAM (2015–2050). Table 5.1 provides an overview of each model's geographical scope and the scenarios each simulates.

The coupling method is a two-step process, as shown in Figure 5.1. In the first step, all models with the exception of NANGAM project natural gas demand. Percentage changes in total natural gas consumption derived by the data provided by each model in each scenario are detailed in Appendix B. The results of each model are compared with respect to their own Reference scenario to compute percentage changes in natural gas consumption in each scenario. Subsequently, we decrease the linear term of the inverse demand curve of regional consumption of NANGAM (parameter int^{D}_{yhnd} in Feijoo et al. (2016)) by the amount provided from the final results.

Due to the scale of the study, we implement a soft-link between NANGAM and the other four models, where NANGAM receives as inputs percentage changes in total natural gas consumption. Had we implemented a hard-link between NANGAM and the individual models, we would have to adjust the calibration of NANGAM to each energy model, which would render the results non-comparable. Moreover, feeding

NANGAM with percentage changes allows us to compare NANGAM results when using inputs from different models, each with different reference calibration.

Table 5.1: Models and scenarios overview.

Model name	Abbr.	Sectors	Countries	Regions	Scenarios	Supporting Organization(s)
North American Natural Gas Model	NANGAM	Natural gas	U.S., Canada, Mexico	17	S1, S2,S3	Johns Hopkins University
Regional Energy Deployment System	ReEDS2.0	Electricity	U.S., Canada, Mexico	73	S1, S2,S3	National Renewable Energy Laboratory
North American TIMES Energy Model	NATEM	Electricity	Canada	13	S2,S3	ESMIA Consultants Inc.
National Energy Modeling System	NEMS-AEO2019	Electricity, end-use	U.S.	22	S2,S3	U.S. Energy Information Administration
Global Energy System Model	GENeSYS-MOD	Electricity	Mexico	9	S2,S3	DIW Berlin

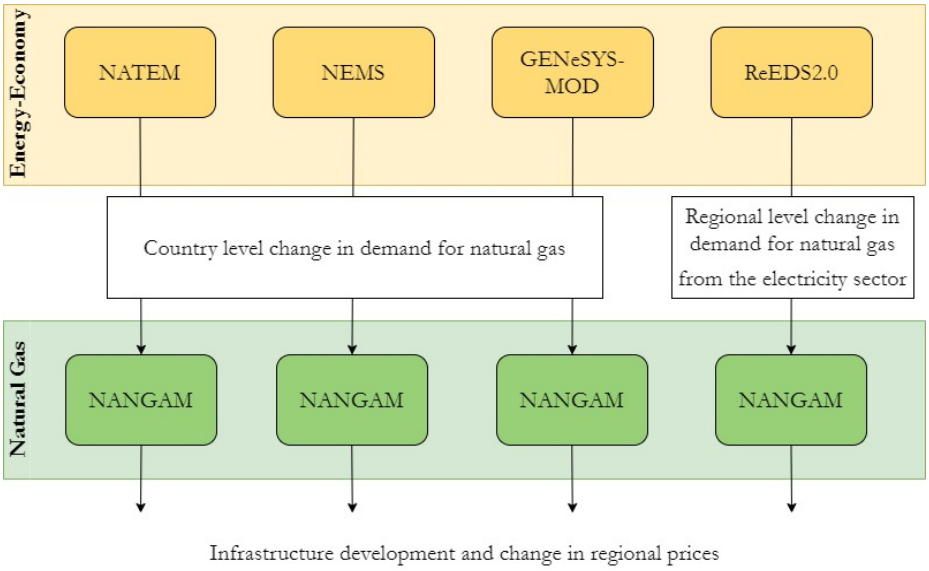

Figure 5.1: Description of linkage between NANGAM and all other models.

5.2.2 Reference Scenario

We calibrate NANGAM in order to match production and consumption projections retrieved from AEO2017 (EIA, 2017) for the U.S., "Canada's Energy Future 2017" for Canada (NEB, 2017), and the "Natural Gas Outlook 2016–2030" published by the Mexican Secretary of Energy (Secretaría de Energía) SENER for Mexico (SENER, 2017). We retrieve reference estimates of regional production costs (EIA, 2019a), and pipeline operating and fixed costs (EIA, 2019b) from the U.S. Energy Information Administration. The calibration process entails adjusting the reference production and transportation costs in order to ensure that regional production, consumption and inter-regional trade in the Reference scenario are consistent with our reference data. Figure 5.2 depicts reference natural gas production and consumption in the

three countries. The size of the U.S. natural gas sector compared to Canada and Mexico implies that changes in the U.S. drive the changes in all of North America. Figure 5.3 highlights the tight connection between the electricity and natural gas sectors in the three countries. The electricity sector constitutes more than 50% of total natural gas demand in Mexico and close to 40% of total natural gas demand in the U.S. intertemporally.

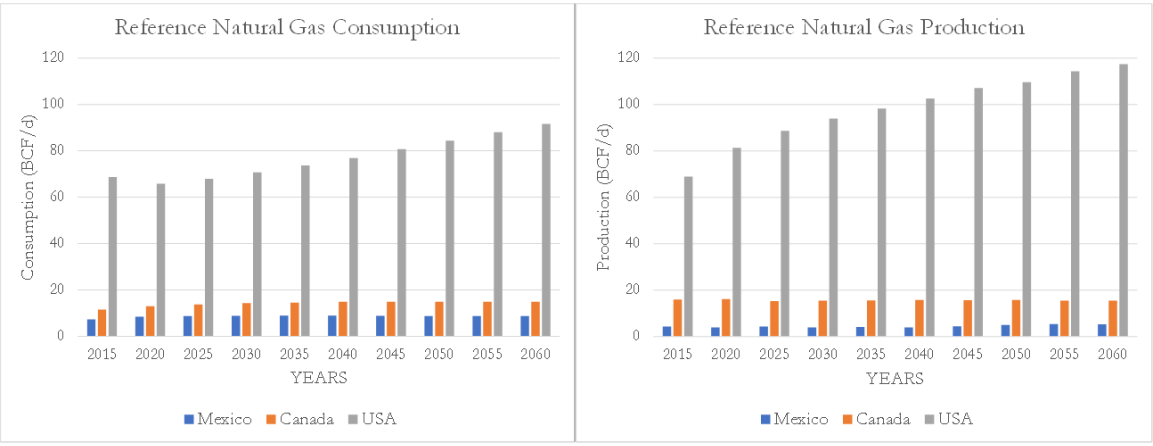

Figure 5.2: Natural gas consumption (left) and production (right) in the Reference scenario for the U.S., Canada, and Mexico.

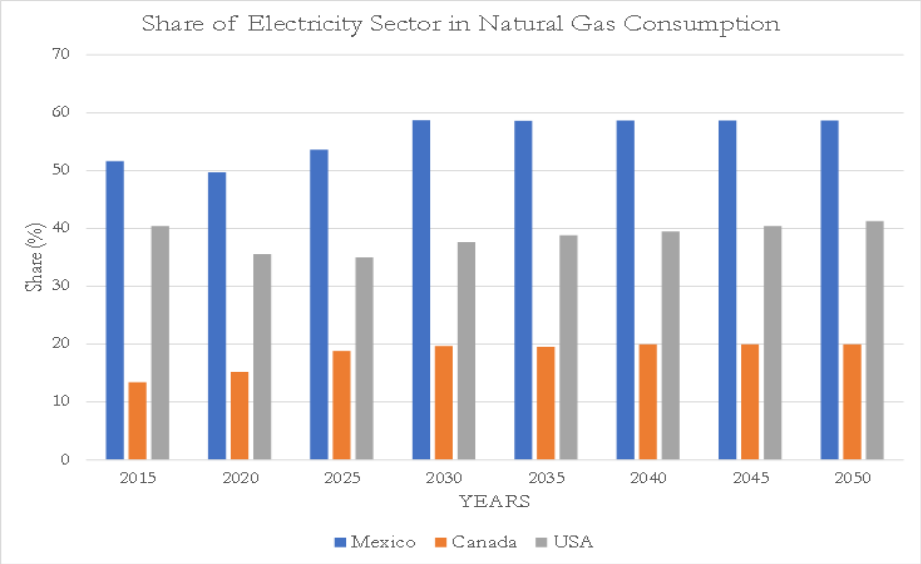

Figure 5.3: Share (%) of consumption of electricity sector with respect to total natural gas consumption in the U.S., Canada, and Mexico, based on EIA (2017), SENER (2017), and NEB (2017).

5.3 Results

5.3.1 Coordination at the Country or Regional Level (Scenarios 2 and 3)

As mentioned in Section 5.2, the four models used to produce estimates of natural gas consumption have different geographical scopes. In this section we compare how results change for each scenario based on inputs from different models. In order to be consistent, we compare country-level results using inputs only from models whose geographical scope includes a particular country. Apart from ReEDS2.0, all other

models simulate the energy system of a single country. For that, they are not able to provide inputs for Scenario 1 which requires joint treatment of all 3 countries.

Fig. 5.4 illustrates how natural gas production in the U.S. changes based on inputs from NEMS-AEO2019 and ReEDS2.0. In Scenario 2, U.S. long-term natural gas production decreases by 11% for both ReEDS2.0 and NEMS-AEO2019 inputs. U.S. natural gas production becomes 100 BCF/d by 2050. When using inputs from NEMS-AEO2019 production starts decreasing later in the time horizon but faster compared to results generated with ReEDS2.0 inputs. Furthermore, between Scenarios 2 and 3, U.S. natural gas production does not change significantly using NEMSAEO2019 inputs, and decreases by 16.74 BCF/d using ReEDS2.0 inputs in 2050. Investment in new production infrastructure adjusts accordingly. In Scenario 2, investment in new production infrastructure capacity decreases by 21% using NEMS-AEO2019 inputs and by 24% using ReEDS2.0 inputs, compared to the Reference scenario. In Scenario 3, investment in new production infrastructure capacity decreases by 23% using NEMS-AEO2019 inputs and by 31% using ReEDS2.0 inputs, compared to the Reference scenario. Figure 5.5 shows that the decrease in investment in new infrastructure is heterogeneous between major producing regions for ReEDS2.0 but not for NEMS-AEO2019 inputs.

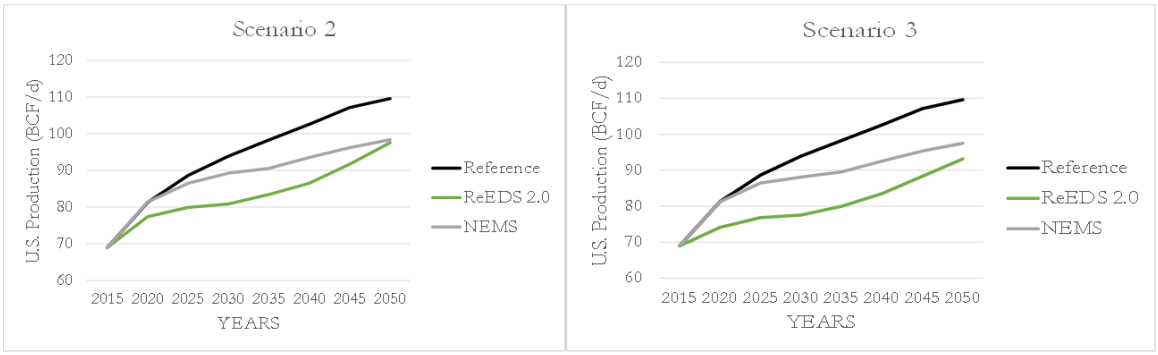

Figure 5.4: NANGAM results. U.S. natural gas production in Scenarios 2 (left) and 3 (right) for inputs from different models.

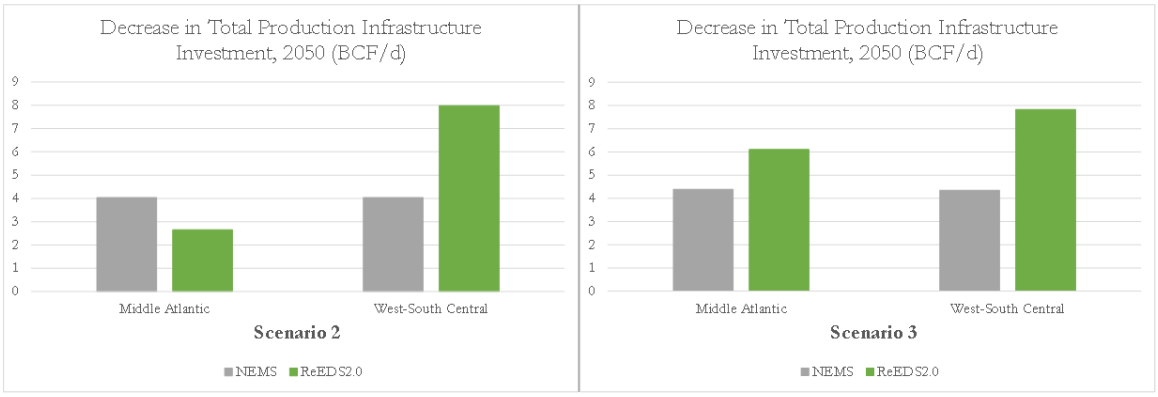

Figure 5.5: NANGAM results. Decrease in regional U.S. natural gas production infrastructure investment by 2050 in Scenarios 2 (left) and 3 (right), compared to the Reference scenario, for inputs from different models.

Mexico's natural gas production decreases the most in 2030 when using inputs from either ReEDS2.0 or GENeSYS-MOD for both Scenarios 2 and 3, as shown in Figure 5.6. Specifically, in Scenario 2 natural gas production decreases by 15% and by 6.5% when using inputs from ReEDS2.0 and GENeSYS-MOD respectively and are equivalent to 0.6 BCF/d and 0.25 BCF/d. Long-term production of Mexico in Scenario 3 is comparable to that of Scenario 2 for both GENeSYS-MOD and ReEDS2.0 inputs. In the case of Mexico, infrastructure investment remains unchanged for Mex-

ico South-Southeast, the major producing region. Figure 5.7 shows that the decreased production is met with a decreased usage rate of existing infrastructure instead.

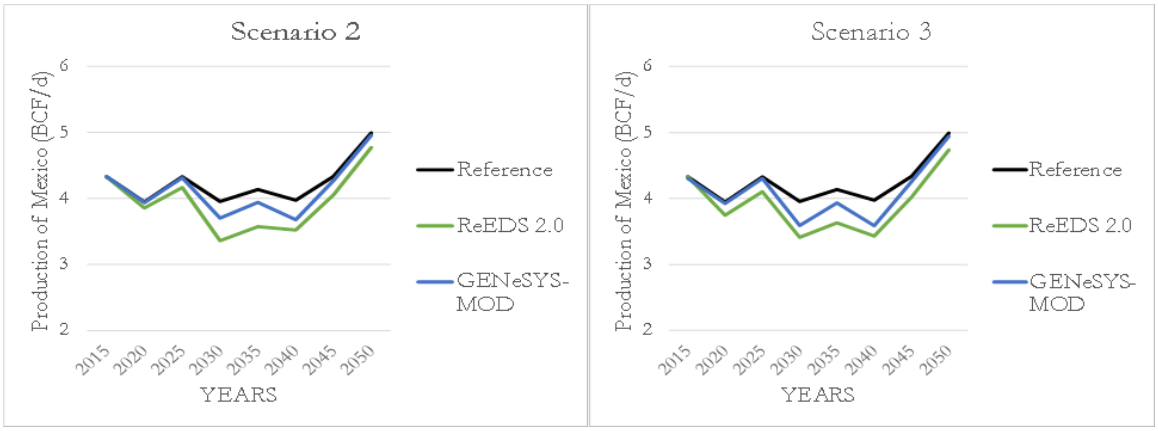

Figure 5.6: NANGAM results. Mexico's natural gas production in Scenarios 2 (left) and 3 (right) for inputs from different models.

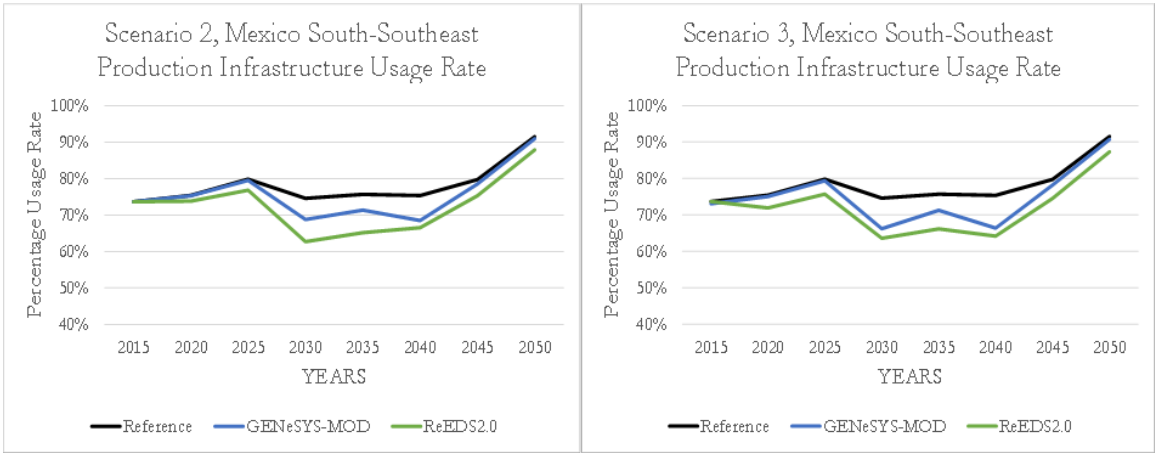

Figure 5.7: NANGAM results. Percentage production infrastructure usage rate for Mexico South-Southeast in Scenarios 2 (left) and 3 (right) for inputs from different models.

Finally, Figure 5.8 summarizes the changes in Canada's natural gas production. Natural gas production using inputs from NATEM barely adjusts for both Scenarios 2 and 3 compared to the Reference scenario. The natural gas production profile of

NATEM follows projections from the National Energy Board (NEB, 2017). NATEM's Reference scenario is based on optimistic assumptions on the access of North American natural gas to markets outside North America. Consequently, the option to export excess natural gas internationally in the form of Liquified Natural Gas (LNG) results in small adjustment of natural gas production when demand from the electricity sector decreases in NATEM. On the other hand, for ReEDS2.0 inputs, Canada's natural gas production decreases by 6.2% in Scenario 2 in 2035 and by 7.2% in Scenario 3 in 2035 before converging to reference production by 2050. The nadir of Canada's consumption is 14.59 BCF/d in Scenario 2 and 14.42 BCF/d in Scenario 3. Similar to Mexico, West Canada, the major natural gas producing region in Canada, meets the decreased production by adjusting the usage rate of existing infrastructure, as shown in Figure 5.9.

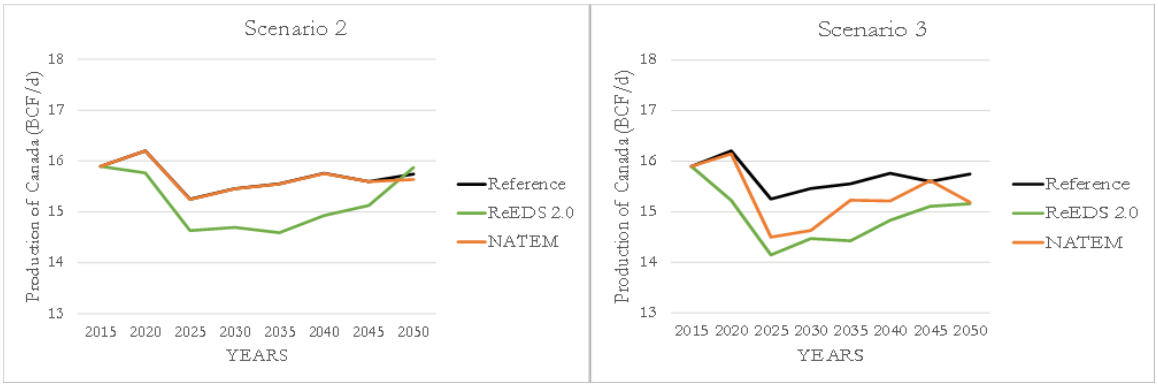

Figure 5.8: NANGAM results. Canada's natural gas production in Scenarios 2 (left) and 3 (right) for inputs from different models.

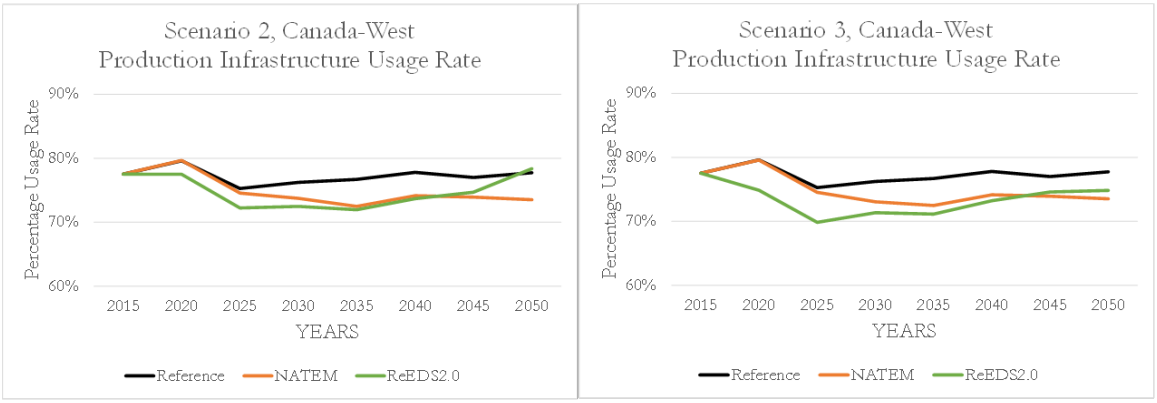

Figure 5.9: NANGAM results. Percentage production infrastructure usage rate for Canada-West in Scenarios 2 (left) and 3 (right) for inputs from different models.

Net exports of natural gas from Canada to the U.S., reported in Figure 5.10**,** adjust downwards as a result of reduced demand for natural gas in the U.S. For NATEM inputs, net exports of Canada to the U.S. in Scenario 2 follow the Reference scenario and even increase by 0.22 BCF/d in 2050, whereas in Scenario 3 net exports decrease more aggressively compared to the Reference scenario. Net exports of natural gas of Canada to the U.S. increase, compared to the Reference scenario, only when using inputs from NATEM, starting from 2020.

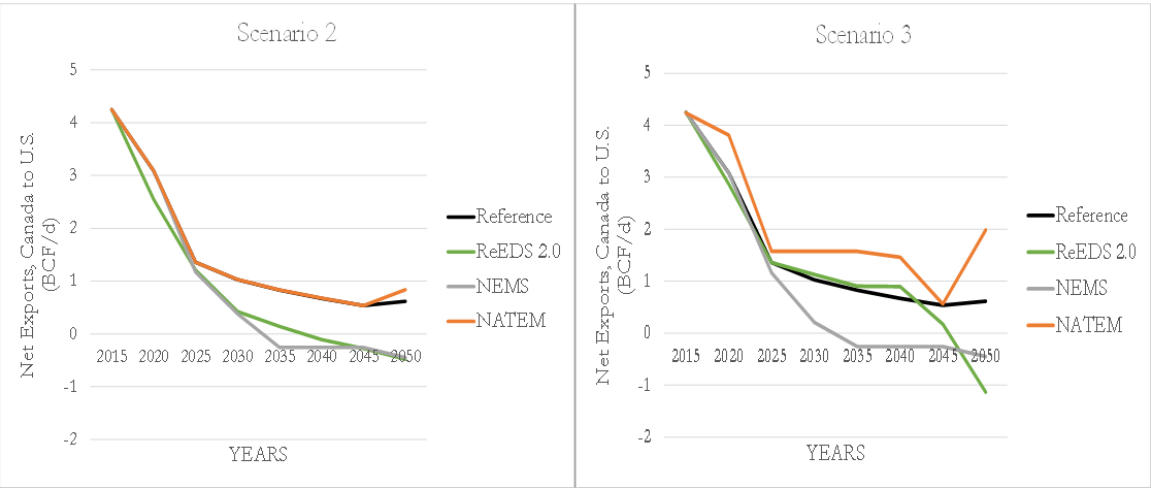

Figure 5.10: NANGAM results. Net Exports of natural gas from Canada to the U.S. in Scenarios 2 (left) and 3 (right) for inputs from different models.

On the other hand, for NEMS-AEO2019 and ReEDS2.0 inputs, Canada becomes a net importer by 2050, importing approximately 0.50 BCF/d in Scenario 2. Moreover, production projections do not change significantly between Scenarios 2 and 3 for NEMS-AEO2019 inputs. However, when using ReEDS2.0 inputs, Canada transforms from a net exporter to a major net importer of U.S. natural gas. In this case, in 2050 Canada imports a net of 1.13 BCF/d from the U.S. We will return to this result in Section 5.3.2.

Figure 5.11 illustrates how net U.S. exports to Mexico are more resilient to changes in coordination of RPS policies. When applying inputs from NEMS-AEO2019, net exports of natural gas from the U.S. to Mexico increase with respect to the Reference scenario in both scenarios by an average of 2.10% in 2050. On the other hand, net U.S. natural gas exports to Mexico decrease when applying inputs from ReEDS2.0

and GENeSYS-MOD. The last two sets of results converge to net exports close to 2.50 BCF/d in 2050 in Scenario 2 but follow different trajectories. When using inputs from GENeSYS-MOD, net exports increase by 2040 before decreasing. Conversely, when using inputs from ReEDS, net exports oscillate around a mean of 3 BCF/d. In Scenario 3 net natural gas exports from the U.S. to Canada reach their nadir in 2050 when they decrease by 42% for GENeSYS-MOD inputs and by 26% for ReEDS2.0 inputs compared to the Reference scenario. Investment in new inter-country pipeline infrastructure remains unchanged. That is because the existing infrastructure suffices to cover trade needs under scenarios where demand decreases. What adjusts instead is the usage rate of certain pipeline infrastructure. Figure 5.12 shows the adjustment of the usage rate of major pipeline interconnections in 2030.

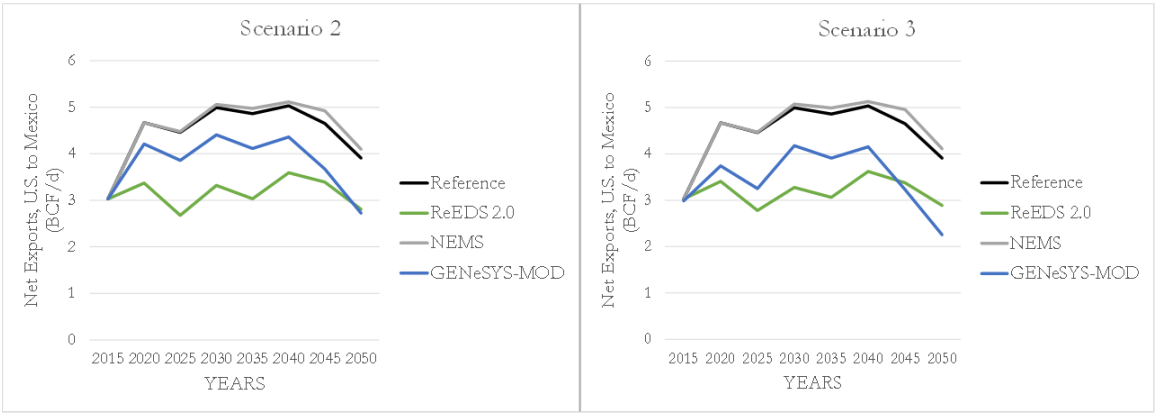

Figure 5.11: NANGAM results. Net Exports of natural gas from the U.S. to Mexico in Scenarios 2 (left) and 3 (right) for inputs from different models.

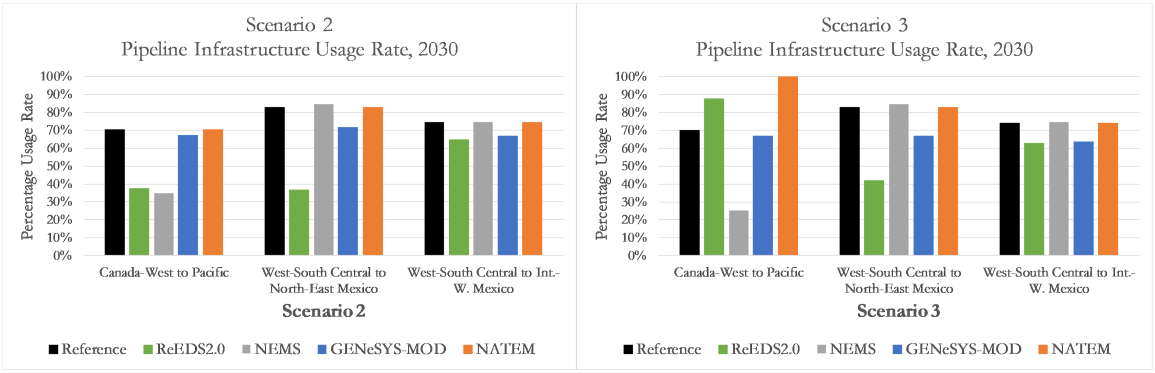

Figure 5.12: NANGAM results. Percentage pipeline infrastructure usage rate for major inter-country pipeline interconnections in Scenario 2 (left) and 3 (right) for inputs from different models in 2030.

In conclusion, we observe that country-level natural gas production and cross-border trade vary significantly depending on the model providing the natural gas consumption projections. Natural gas production of Mexico in Scenario 2 exhibits the highest variation for inputs from all models and can decrease up to 15% compared to the Reference scenario. The decrease in natural gas production results in a decrease in production infrastructure usage rate. Furthermore, we observe that inputs from ReEDS2.0 lead to larger changes in production and trade with respect to results that were generated using inputs from all other models. The last is true for all countries and all scenarios. The reasons are two. First, ReEDS2.0 reports the largest change in demand among all models, which subsequently results in larger adjustment of natural gas production in all three countries. Second, as shown in Figure 5.1, ReEDS2.0 provides regional change in natural gas consumption for all three countries, whereas the rest of the models provide country-level changes for a single country each. This

implies that the change in demand in ReEDS2.0 is regionally more heterogeneous compared to the rest.

5.3.2 Coordination Between All Countries (Scenario 1)

Scenario 1 requires the representation of all three countries within a single model. The only model in this chapter with that level of disaggregation is ReEDS2.0. In this section, we focus on the findings derived by using ReEDS2.0 inputs in order to compare results between scenarios. In Figure 5.13 we can verify that greater coordination among countries in North America mitigates the impact of RPS on natural gas consumption, which is consistent with microeconomic theory. In addition, natural gas infrastructure implications are similar between Scenario 2 and Scenario 3.

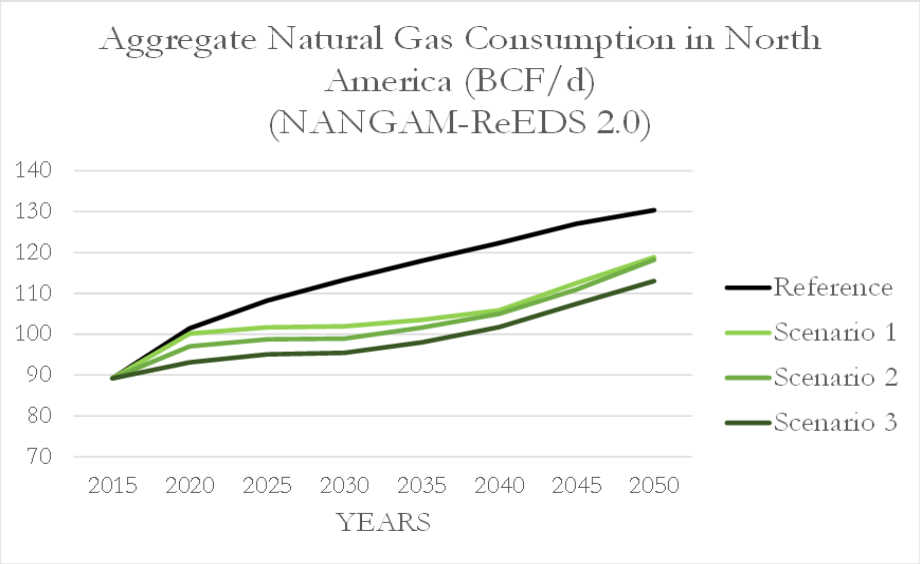

Figure 5.13: NANGAM results using ReEDS2.0 inputs. Aggregate consumption of natural gas in North America for all scenarios.

Country-level consumption follows the same trend for all countries up to 2040, as shown in Figures 5.14–5.16. The only exception is natural gas consumption in Canada for Scenarios 2 and 3, after 2040. Before explaining this finding, we need to clarify that findings deep into the timeline are subject to greater uncertainty. We will first examine the changes in natural gas consumption of each country. In Scenario 3, demand for natural gas in Canada increases in 2050 by 1.18 BCF/d, or 7.94%, compared to the Reference scenario. Canada already meets the RPS requirements given the existing hydro. Constraining trade of RECs to the subnational level means that all North American regions other than Canada cannot tap into the low-cost hydro potential of Canada in the long term. Therefore, in the power sector in Scenario 3, the increased demand for Canada's power supply in the long term is met by increasing

gas-fired capacity and production, which in turn increases demand for natural gas in Canada. Hence, lack of RPS coordination between North American countries and regions increases long-term natural gas consumption in Canada.

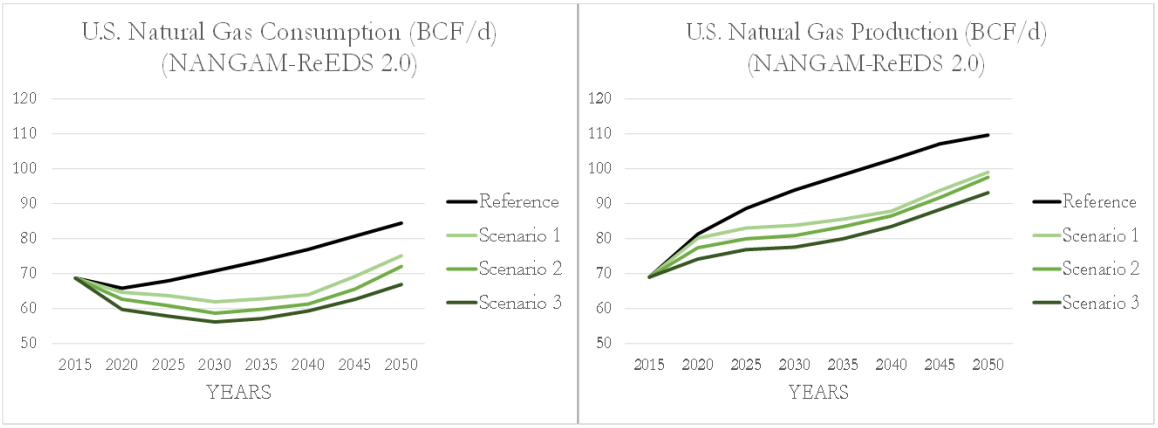

Figure 5.14: NANGAM results using ReEDS2.0 inputs. U.S. natural gas consumption (left) and production (right) under Renewable Portfolio Standards.

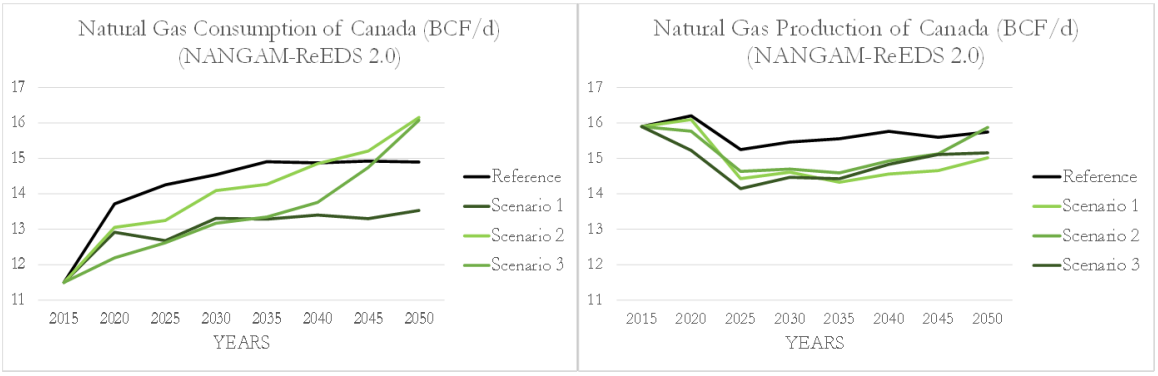

Figure 5.15: NANGAM results using ReEDS2.0 inputs. Canada's natural gas consumption (left) and production (right) under Renewable Portfolio Standards.

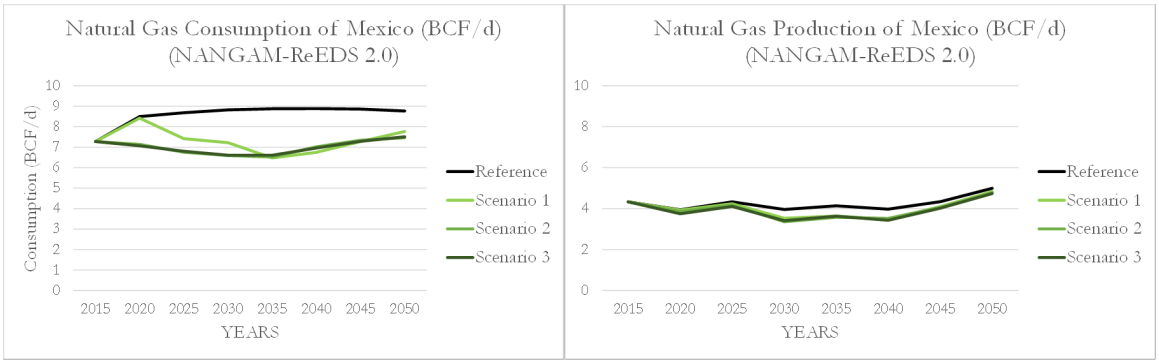

Figure 5.16: NANGAM results using ReEDS2.0 inputs. Mexico's natural gas consumption (left) and production (right) under Renewable Portfolio Standards.

In the U.S., for Scenario 3, consumption decreases by 21% or 17.55 BCF/d in 2050, which drives production to decrease by 15%, or 16.47 BCF/d in 2050 compared to the Reference scenario. The regional heterogeneity of the shock in 2050 implies that low-cost U.S. resources that were exploited in the Reference scenario to satisfy domestic demand are in abundance in this scenario and available to be exported instead. Consequently, Canada's natural gas production remains relatively unchanged. Net exports of the U.S. to Canada in 2050 amount to 1.13 BCF/d. Therefore, part of the increase in natural gas consumption in Canada is supplied by low-cost U.S. natural gas production.

Figure 5.17 highlights that the adjustment of U.S. infrastructure due to RPS is regionally heterogeneous. In all three scenarios, investment in new production infrastructure capacity in Middle Atlantic decreases less than that of West-South Central. Moreover, greater RPS coordination results in milder decrease in new infrastructure investment compared to the Reference scenario. On the other hand, Canada and

Mexico choose to adjust the usage rate of existing production infrastructure. Figures 5.18 and 5.19 show that for both countries, greater RPS coordination results in a higher infrastructure capacity utilization rate for the major producing regions of each country.

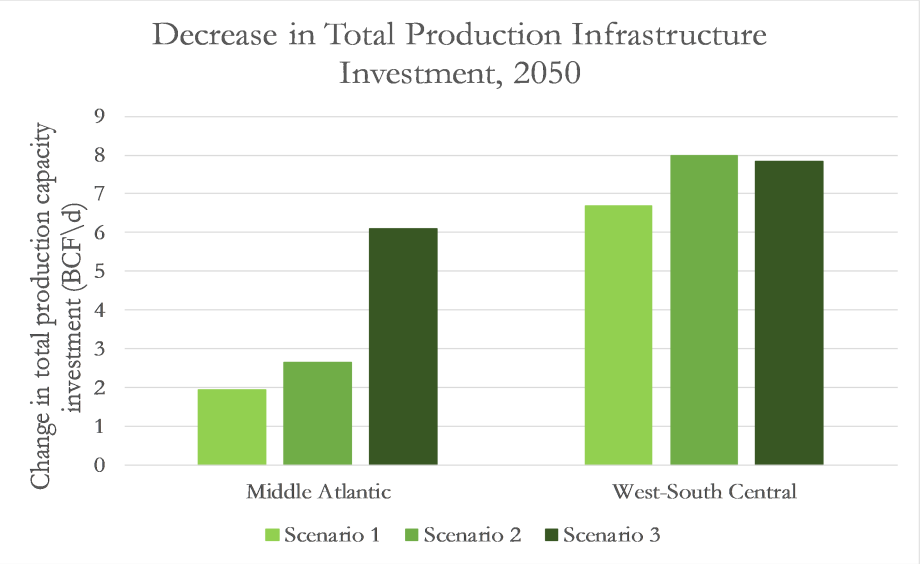

Figure 5.17: NANGAM results using ReEDS2.0 inputs. Decrease in regional natural gas production infrastructure investment by 2050 in the U.S. in all scenarios, compared to the Reference scenario.

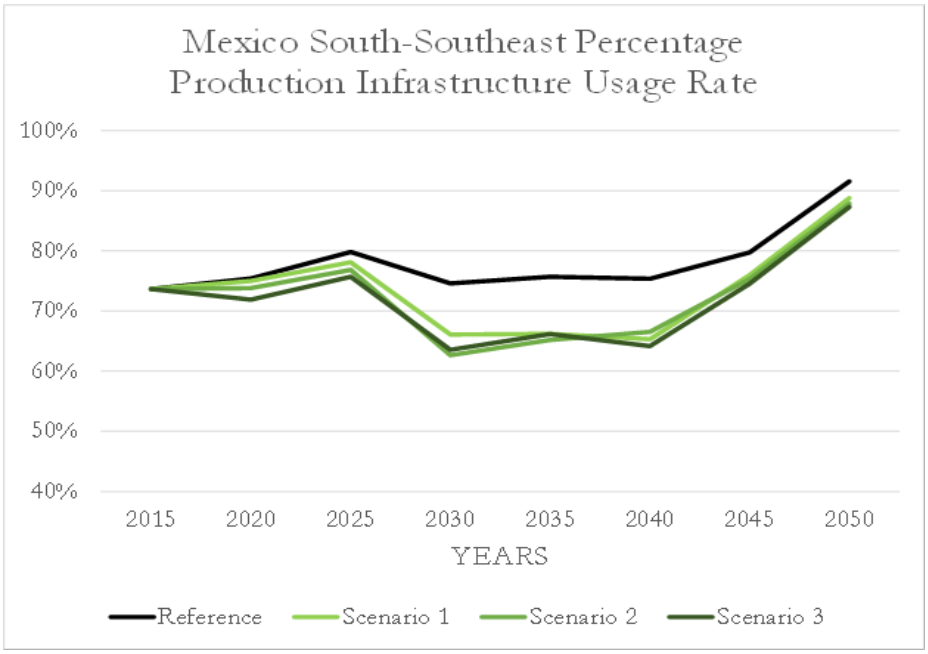

Figure 5.18: NANGAM results using ReEDS2.0 inputs. Mexico South-Southeast production infrastructure usage rate for all scenarios and years.

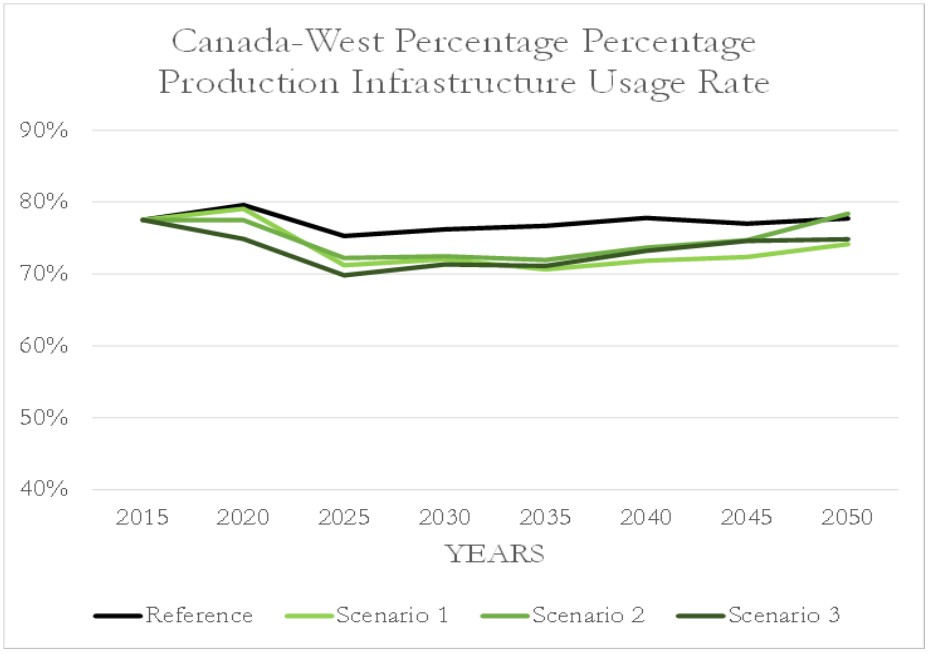

Figure 5.19: NANGAM results using ReEDS2.0 inputs. Canada-West production infrastructure usage rate for all scenarios and years.

Figure 5.20 summarizes all net exports from the U.S. to Mexico and from Canada to the U.S. We observe that net exports from the U.S. to Mexico benefit in the short term from higher coordination of RPS between countries. Net exports in Scenario 1 are greater compared to Scenarios 2 and 3 by approximately 36% in 2020, 20% in 2025, 14% in 2030, and 7.6% in 2050. Between 2035 and 2045, net exports of U.S. to Mexico are approximately 7% lower in Scenario 1 compared to Scenarios 2 and 3. Moreover, net exports of Canada to the U.S. decrease for Scenarios 2 and 3 in the long-term and the U.S. becomes a net exporter of natural gas to Canada in 2050, as explained above.

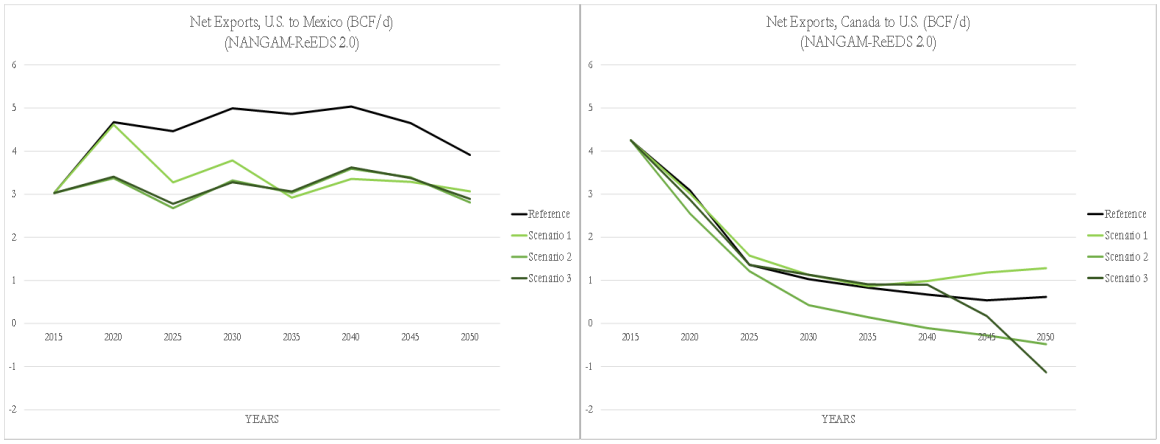

Figure 5.20: NANGAM results using ReEDS2.0 inputs. Net natural gas exports of U.S. to Mexico (left) and Canada to the U.S. (right) for all scenarios and years.

The changes in natural gas trade between the U.S. and Canada highlight that trade between individual regions does not necessarily decrease when natural gas demand in the two regions decreases. What is also important is the regional heterogeneity of the decrease in demand. Specifically, Canada's natural gas consumption decreases

in the short- and medium-term but increases in the long-term in Scenarios 2 and 3 compared to reference consumption. At the same time, the decrease in U.S. demand means that cost-efficient domestic resources are no longer needed for domestic use. The available U.S. natural gas production is more competitive than Canada's natural gas production, leading to an increase in long-term U.S. exports to Canada. Increased Canada's natural gas consumption is met by U.S. natural gas production and the U.S. becomes a net exporter of natural gas in 2050. Net trade, in absolute value, increases by 84% in Scenario 3 compared to the Reference scenario. The different trade level between countries is met by adjusting the usage rate of existing pipeline infrastructure. Figure 5.21 shows that the adjustment of the usage rate of pipeline infrastructure follows the same trend as the adjustment of trade.

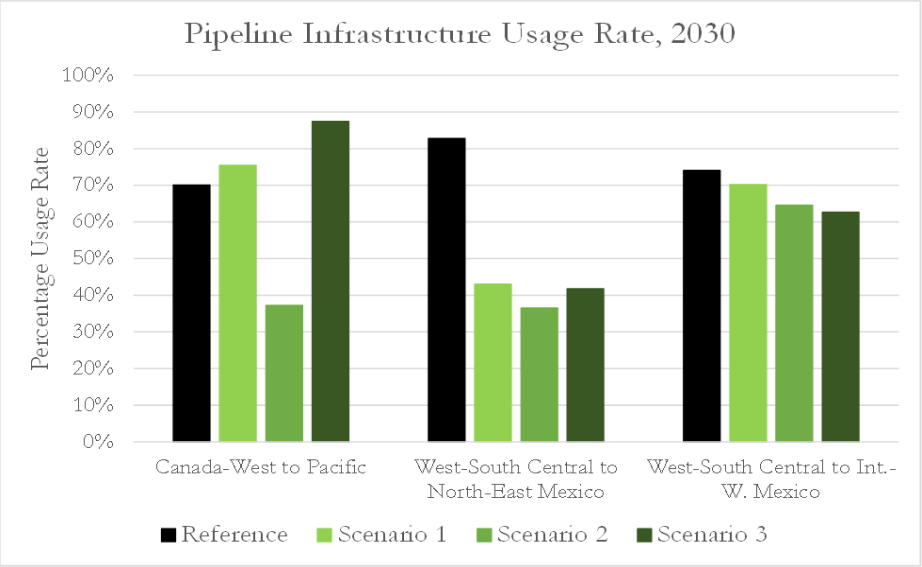

Figure 5.21: NANGAM results using ReEDS2.0 inputs. Infrastructure usage rate for major inter-country pipeline interconnections for all scenarios in 2030.

Finally, RPS coordination at the international level results in smaller discrepan-

cies of U.S. natural gas prices when compared to the Reference scenario, as shown in Figure 5.22. In Scenario 1 all countries experience the highest reduction in consumption prices at 2040. At that year, U.S. natural gas retail prices decrease by 11.88%, Canada's retail prices decrease by 7.29%, and Mexico's retail prices decrease by 9.29% with respect to the Reference scenario. On the other hand, in Scenario 3, the deviation of retail prices is close to the highest for all countries in 2035 compared to the Reference scenario. U.S. natural gas retail prices decrease by 12.7%, Canada's retail prices decrease by 6.6%, and Mexico's retail prices by 9.23%.

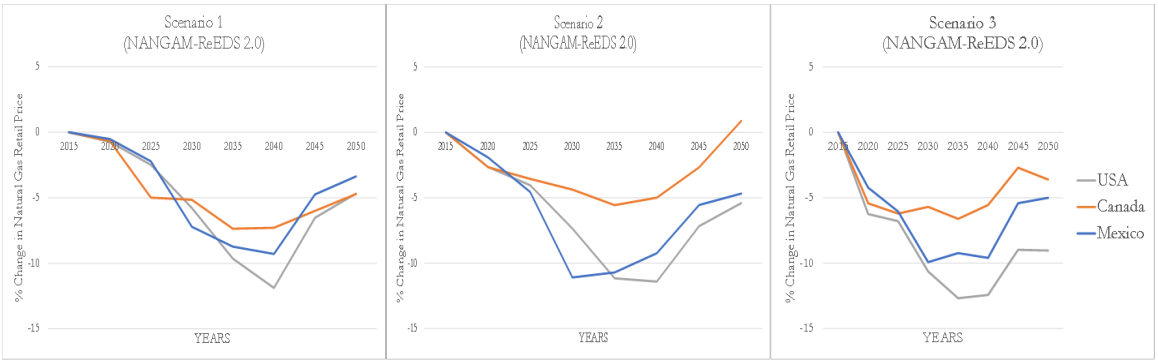

Figure 5.22: NANGAM results using ReEDS2.0 inputs. Percentage change in retail natural gas prices relative to the Reference scenario in the U.S., Canada, and Mexico.

5.4 Conclusion

In this chapter we explore the impact of RPS on natural gas markets under varying regional RPS coordination. We implement a scenario of a joint market for RECs for the U.S., Canada, and Mexico, a scenario of three individual country-level markets, and a scenario in which RECs are traded only by electricity producers within the same

region of a country. RPS generally displace gas-fired producers along with other emitters. However, greater RPS coordination allows regions with low renewables potential to exploit the renewable energy credits of their neighbors, thus allowing for greater investment in gas-fired generation in North America on aggregate. Under the same RPS coordination scheme, projections of natural gas consumption will differ when derived using models that are based on different assumptions. For that, we conduct our analysis using four models with bottom-up representation of the electricity market. We derive the change in natural gas consumption by simulating the effect of RPS targets on the power mix of the U.S., Canada, and Mexico. The change in natural gas consumption of each model with respect to its Reference scenario is then input into NANGAM to generate natural gas infrastructure expansion trajectories for each country.

We find that natural gas infrastructure development is sensitive to model-specific projections of natural gas consumption. Most notably, in Scenarios 2 and 3, the U.S. is projected to become a net exporter to Canada when coupling NANGAM to ReEDS2.0 or NEMS-AEO2019. Moreover, natural gas infrastructure development is also sensitive to renewable policy coordination assumptions. U.S. production infrastructure adjusts heterogeneously, depending on the region. Major producing regions in Canada and Mexico adjust their production infrastructure usage rate instead. In most cases we do not observe significant changes in production and cross-border trade when we switch from a country-level to a regional-level RPS coordination scheme. However,

this is not true when we use inputs from ReEDS2.0; we observe that greater regional participation in a RPS coordination scheme mitigates the impact on natural gas production, trade, and prices.

We also find that no country's natural gas production is higher intertemporally when RPS policies are introduced. On the other hand, lower production with respect to the Reference scenario implies that not all regional cost-efficient natural gas resources are exploited. Among all scenarios, U.S. production infrastructure investment, as well as production infrastructure usage rate of Canada and Mexico, decrease the least in Scenario 1. In the case of cross-border natural gas trade between Canada and the U.S. in Scenario 3, the decrease in natural gas demand in the U.S. is higher than that of Canada. This creates a surplus of competitive available natural gas production in the U.S. that can be exported to Canada. More generally, when the natural gas markets of the three countries are fully integrated but their RPS policies are not coordinated, there is a tradeoff between lower regional demand for natural gas due to RPS but potentially higher trade due to availability of low-cost natural gas production in neighboring regions. Investment in inter-country pipeline infrastructure remains unchanged and pipeline operators choose to respond to the shock by operating at a lower capacity usage rate.

We also find that lack of coordination of RPS schemes results in higher discrepancies in U.S. natural gas prices as compared to the Reference scenario. Consumption of natural gas decreases the most when RECs can-not be traded outside a region, in

contrast to scenarios where RECs can be traded at the country or at the international level. Decrease in short-term consumption results in a decrease of natural gas prices. However, a decrease in natural gas prices renders natural gas competitive for a longer period of time compared to other power generation technologies and thus increases consumption in the long-term. We argue that further research can contribute to the understanding of the impact of RPS coordination on natural gas consumption by studying the natural gas and electricity sectors in an integrated framework.

Our analysis at this point is limited by the one-way link between the electricity and natural gas models. RPS reduce the price of natural gas which would increase investment in natural gas-fired plants and mitigate the impact of RPS on natural gas consumption, if a representative feedback from the natural gas model back to the electricity models existed. For that, our analysis of the natural gas sector is a bounding scenario, as we don't consider feedback from natural gas markets into the electricity sector. Nevertheless, the results reveal the tradeoff between lower consumption but greater U.S.-Canada cross-border trade of natural gas as a result of more stringent RPS targets.

Moreover, in our analysis we treat LNG trade as exogenous. U.S. LNG exports are growing rapidly, with 9.64 BCF/d extra liquefaction capacity being installed by 2020. In addition, net LNG exports are expected to amount to 5.02 BCF/d by 2050 per the 2019 Annual Energy Outlook (EIA, 2019c). Therefore, the treatment of LNG as exogenous implies that natural gas producers are deprived of the option to sell

in the international market when North American demand decreases. The fact that producers would have the option to export natural gas outside North America does imply in a straightforward manner that LNG exports would increase, in the absence of other shocks, as this is a market outcome. Therefore, proper treatment of LNG trade requires modeling of the global market (Moryadee et al., 2014), which is out of the scope of this chapter that focuses on North American production and pipeline infrastructure. Since our modeling assumption constrains the available options of North American producers, the results on production and production capacity can be viewed as a worst-case scenario at the national level. Future research needs to study the sensitivity of the regional results to assumptions regarding LNG infrastructure.

Finally, RPS also contribute in the decrease of CO_2 emissions in the electricity and in the natural gas sector. Therefore, there exists a tradeoff between the cost of RPS that is incurred by different agents in the electricity and natural gas sectors and the social benefit of emissions reduction. As the focus of this chapter has been on infrastructure development, future research can address how the changes in lifecycle emissions for the different RPS coordination schemes impact welfare.

Our results establish the impact of RPS on natural gas markets and natural gas infrastructure. We emphasize the importance of coordinating RPS policies for North American natural gas production. We study three scenarios that assume different levels of coordination of RPS among the U.S., Canada, Mexico, and their regions. By coupling models with detailed representation of the electricity sector with NANGAM

we are able to identify the tradeoff between regional natural gas production and trade. By receiving inputs from four different models we are able to test our findings against different assumption on the electricity sector. We conclude that fine-tuning stringent RPS policies in the electricity sector can prove critical for the timeline of retirement of natural gas infrastructure.

Acknowledgements

The author thanks Dr. John Bistline, Dr. Maxwell Brow, Dr. Kathleen Vaillancourt, and Dr. Sauleh Siddiqui, who contributed to the work in this chapter.

Disclaimers

NANGAM is based in part on the multi-fuel energy equilibrium model MultiMod (Feijoo et al., 2016). The MultiMod was developed by Dr. Daniel Huppmann at DIW Berlin as part of the RESOURCES project, in collaboration with Dr. Ruud Egging (NTNU, Trondheim), Dr. Franziska Holz (DIW Berlin) and others (see `http://diw.de/multimod`). We are grateful to the original developers of MultiMod for sharing their model.

This work was authored in part by the National Renewable Energy Laboratory, operated by Alliance for Sustainable Energy, LLC, for the U.S. Department of Energy (DOE) under Contract No. DE-AC36-08GO28308. Funding provided by U.S. Department of Energy Office of Policy. The views expressed in the article do not necessarily

represent the views of the DOE or the U.S. Government. The U.S. Government retains and the publisher, by accepting the article for publication, acknowledges that the U.S. Government retains a nonexclusive, paid-up, irrevocable, worldwide license to publish or reproduce the published form of this work, or allow others to do so, for U.S. Government purposes.

Chapter 6

Resilient Global Food Systems Against Antimicrobial Resistance

6.1 Introduction

Antimicrobial resistance (AMR) is a threat to global health, accounting for over 700,000 deaths each year (O'Neill, 2014). When a microbial pathogen becomes resistant, antimicrobials are no longer effective against the pathogen. Therefore, the treatment options for a patient who is infected by a resistant microbial pathogen are either unavailable or would require healthcare providers to use less effective treatment methods. Moreover, infection by a resistant microbial pathogen can complicate the recovery of vulnerable patients from complex surgeries (CDC, 2013). This disease burden is predicted to contribute towards 10 million global deaths by 2050 (O'Neill, 2014). AMR and subsequent infection in individuals can result from multiple path-

ways, such as antimicrobial use in the human sector as well as the animal sector. The importance of certain antimicrobials for human medicine, categorized under *"critically important"* antimicrobials, prompted the World Health Organization (WHO) to advise countries to restrict their use in the food animal sector (WHO, 2011). The suggestion is based also on the observation that restriction of antimicrobials for veterinary purposes reduces antimicrobial resistance (WHO, 2002). Antimicrobials are used in livestock husbandry also for disease treatment, prophylaxis (Landers et al., 2012), and for growth promotion (Wegener et al., 1999). Global procurement of antimicrobials in the animal sector related to livestock production is estimated to be 73-100% higher than the purchases for the human health sector (Van Boeckel et al., 2017). Excessive antimicrobial use could reflect unsanitary breeding conditions (Martin et al., 2015) or the use of antimicrobials as a means to increase global livestock production to meet consumer demand.

The use of antimicrobials in animals can lead to resistance and infection in humans through direct and indirect transmission mechanisms, such as exposure to livestock infected with AMR pathogens or through contaminated retail meat (Woolhouse et al., 2015). Many lower and middle income countries (LMICs), such as China, India, and Brazil, are exhibiting drastic increases in their demands and production of livestock for retail meat (Tilman et al., 2011). In tandem, the impacts of the growing AMR burden are also disproportionately felt by LMICs (Van Boeckel et al., 2019).

The inclusion of AMR under Goal 3 of the U.N. Sustainable Development Goals

(SDGs), which aim to "ensure healthy lives and promote well-being for all at all ages" (ECOSOC, 2019), highlights the growing interest of the global community to tackle AMR. Tackling AMR in LMICs is related to at least two Goal 3 targets. Target 3.8. aims to "ensure universal health coverage...for all", while target 3.B. focuses on the "development of vaccines and medicines for the communicable and noncommunicable diseases that primarily affect developing countries" (ECOSOC, 2015). Strong global coordination is needed to monitor and regulate the use of antimicrobials in livestock production to mitigate AMR (Rogers Van Katwyk et al., 2016). Policies can serve as critical tools to initiate coordination efforts and promulgate changes in global norms to support human and animal health.

Given inter-country geopolitical relationships, global livestock trade policies can prove valuable in reducing regional antimicrobial use. Global and national food animal trade policies can mitigate growing AMR burdens by employing mechanisms such as bans, user fees, and restrictions on products raised using antimicrobials. Trade restrictions in particular represent a key policy lever that can reinforce global coordination and commitment to the global reduction of antimicrobial use. However, given that country-specific policies can disproportionately diminish the productivity of one country compared to another, the WHO argues for the need of a global coordination scheme that would ensure the alignment of global incentives (WHO, 2015).

Computational tools can support the design and assessment of global policies targeting antimicrobial use in the livestock sector. Novel food systems models need

to account for the competing objectives of different trade participants, incorporate the use of antimicrobials, and endogenously account for explicit inter-country trade changes (Hanefeld et al., 2017; George, 2018) that will result from global and national AMR policies. Incorporating all three features in a single framework calls for a new modeling paradigm. We categorize the existing models which are used to asses global policies related to antimicrobial use into two broad categories. The first category includes standard partial equilibrium models of the food sector that represent the interactions between a range of agricultural products and are rich in spatial detail, but do not incorporate either the use of antimicrobials in livestock production or the explicit trade links (OECD-FAO, 2015). The second category includes statistical models with detail on the variety and antimicrobial use that do not properly account for the economic and trade interactions between different agents (Van Boeckel et al., 2017).

We identified and assessed potential strategies for governments in LMICs that could reduce the use of antimicrobials in food animal production. We developed a game-theoretic model of global livestock production and trade between 18 countries and aggregate world regions, comprising the largest producing and consuming countries. In our model, each market participant, country-level producer or inter-regional transporter, aims to maximize their individual profit. When considering the economic incentive behind antimicrobial use in livestock production, a game-theoretic model is more suitable compared to a statistical model for the assessment of policy inter-

ventions. We also model the explicit interconnections between countries and the use of antimicrobials in food animal production. We used our model to assess the impact of three different global livestock policies: one scenario driven by a global shift in antimicrobial policy and two scenarios from the trade perspective of Brazil and China. Our analysis revealed potential conflicts of interest between international policy participants and allowed us to provide suggestions to better design similar policy mechanisms to support global health.

6.2 Methods

6.2.1 Integrated Global Antimicrobial Use and Livestock Trade Model (IGAULTM) Description

For the purpose of this chapter, we developed the Integrated Global Antimicrobial Use and Livestock Trade Model (IGAULTM). IGAULTM is a game-theoretic equilibrium model that simulates global livestock production, consumption, and trade between countries and world regions. The model distinguishes between three categories of food animal products: poultry, pork, and beef. Compared to other livestock production models, IGAULTM also incorporates antimicrobial use in livestock production, and country-to-country trade in an integrated framework.

The focus on global policies and trade requires consistent production, consump-

tion, and trade data for all countries and regions included in this chapter. The availability of data from the Food and Agriculture Organization Corporate Statistical Database (FAOSTAT) (FAOSTAT, 2020) led us to model production, consumption, and trade of livestock at the country level. IGAULTM comprises 15 countries and three aggregate geographical regions that include countries not explicitly represented. These countries include all major producers and consumers of pork, beef, and poultry, such as the European Union member countries (EU) except for the Republic of Cyprus[1], the United Kingdom, USA, Russia, China, India, and Brazil, which accounted for 55% of global meat production in 2015. The model also includes major livestock importers, such as the Netherlands, Japan, and the Republic of Korea. Table 6.1 lists all countries considered in the model, either as standalone countries or as parts of a region. Given our focus on the impact of trade, the aggregation of regions for the Rest Of Europe (ROE) and the Rest Of America (ROA) is based on geographic proximity. Finally, the Rest Of World (ROW) region includes all remaining countries for which antimicrobial use data were available. The model runs from 2015 through 2028 with annual time steps.

[1]Data on livestock production (FAOSTAT, 2020) and the use of antimicrobials in the livestock sector (Van Boeckel et al., 2015) were not available for the Republic of Cyprus in the respective databases.

Table 6.1: Regional disaggregation in IGAULTM.

IGAULTM Country/Region	**IGAULTM Acronym**	**Countries included**
Denmark	DNK	Denmark
Germany	DEU	Germany
Spain	SPN	Spain
France	FRA	France
United Kingdom	UK	United Kingdom of Great Britain and Northern Ireland
Netherlands	NLD	Netherlands
Russia	RUS	Russia
Rest Of Europe	ROE	Austria, Belgium, Bosnia and Herzegovina, Bulgaria, Croatia, Czechia, Estonia, Finland, Greece, Hungary, Ireland, Italy, Latvia, Lithuania, Norway, Poland, Portugal, Romania, Serbia, Slovakia, Slovenia, Sweden
United States	USA	United States of America
Canada	CAN	Canada
Mexico	MEX	Mexico
Brazil	BRA	Brazil
Rest Of America	ROA	Argentina, Chile, Colombia, Dominican Republic, Ecuador, French Guyana, Peru, Uruguay, Venezuela
People's Republic of China	CPR	People's Republic of China
Republic of India	IND	Republic of India
Japan	JPN	Japan
Republic of Korea	KOR	Republic of Korea
Rest Of World	ROW	Algeria, Australia, Bangladesh, Egypt, French Polynesia, Indonesia, Jordan, Kazakhstan, Kuwait, Lebanon, Malaysia, Morocco, New Zealand, Pakistan, Philippines, Saudi Arabia, South Africa, Sri Lanka, Thailand, Tunisia, Turkey, United Arab Emirates, Viet Nam, Puerto Rico

6.2.2 Market Agents Representation in IGAULTM

In our framework, production and consumption in each region is decided by an aggregate representative producer and an aggregate representative consumer. A complete listing of model sets, parameters, and variables is provided in Table 6.2. IGAULTM is a game-theoretic model, meaning that every aggregate representative agent optimizes their own objective. Specifically, in the absence of antimicrobials, the representative producer of livestock product *lp* in region r would decide how much to produce in year t by maximizing their inter-temporal profit which comprises total revenues (first term in (6.1)) minus total cost (second term in (6.1)) , *i.e.,*

$$\max_{q^P_{r,t,lp} \geq 0} \sum_{\forall t} \left(\pi_{r,t,lp} \cdot q^P_{r,t,lp} - \int_0^{q^P_{r,t,lp}} \mathrm{mc}_{r,t,lp}\left(s\right) ds \right), \tag{6.1}$$

where $q^P_{r,t,lp}$ is the production of the representative producer of livestock product *lp,* in region *r,* in year t and $\mathrm{mc}_{r,t,lp}(s) = \alpha^P_{r,t,lp} + \beta^P_{r,t,lp} \cdot s$ is the supply curve of the representative producer, when we do not account for the use of antimicrobials in livestock production. Parameters $\alpha^P_{r,t,lp}, \beta^P_{r,t,lp}$ are the interval and the slope of the supply curve of each representative producer and $\pi_{r,t,lp}$ is the market price in region *r,* or livestock product *lp,* in year t. Although the impact of antimicrobials on growth of livestock remains ambiguous (Levy, 2014), antimicrobials are still being used in meat production. Following (NRC, 1999) we assumed that antimicrobials supplement growth, which implies that a decrease in antimicrobial use would increase the marginal

cost of production of livestock. In order to model the impact of antimicrobials on livestock production, we introduced the linear term $\theta^A_{r,t,lp} \cdot q^A_{r,t,lp}$ that is a function of the quantity of antimicrobial used by each producer ($q^A_{r,t,lp}$). Parameter $\theta^A_{r,t,lp} > 0$ represented the effect of antimicrobial use on the marginal cost of production of each representative producer. A greater use of antimicrobials decreases the marginal cost of production, *i.e.*,

$$\mathrm{mc}_{r,t,lp}\left(q^P_{r,t,lp}, q^A_{r,t,lp}\right) = \alpha^P_{r,t,lp} + \beta^P \cdot q^P - \theta^A_{r,t,lp} \cdot q^A_{r,t,lp} \tag{6.2}$$

Whenever $\theta^A_{r,t,lp} > 0$, a smaller quantity of antimicrobials leads to higher marginal cost of production (assuming $q^A_{r,t,lp} > 0$), decreasing production output *ceteris paribus*. Parameter $\theta^A_{r,t,lp}$ is calibrated using data from (NRC, 1999), as explained in Appendix C. In our setting, a smaller value of parameter $\theta^A_{r,t,lp}$ implies smaller impact of antimicrobials on livestock growth.

Antimicrobials have a decreasing rate of benefit, meaning that a higher rate of expenditure doesn't necessarily lead to the same rate of growth. We embed this rationale in the representative producer's decision-making by assuming that producers will use a fixed portion of their income ($\alpha^A_{r,t,lp}$) from sales (right-hand side in (6.3)) to purchase antimicrobials (left-hand side in (6.3)) at a price of $\bar{p}^A_{r,t,lp}$

$$\bar{p}^A_{r,t,lp} \cdot q^A_{r,t,lp} = \alpha^A_{r,t,lp} \cdot \pi_{r,t,lp} \cdot q^P_{r,t,lp} \tag{6.3}$$

When combining (6.1),(6.2),(6.3), the representative producer's optimization problem becomes

$$\max_{q^A_{r,t,lp}, q^P_{r,t,lp} \geq 0} \sum_{\forall t} \left(\pi_{r,t,lp} \cdot q^P_{r,t,lp} - \int_0^{q^P_{r,t,lp}} \mathrm{mc}_{r,t,lp}\left(s, q^A_{r,t,lp}\right) ds \right), \tag{6.4}$$

$$\text{subject to} \quad q^A_{r,t,lp} = \alpha^A_{r,t,lp} \cdot \frac{\pi_{r,t,lp}}{\bar{p}^A_{r,t,lp}} \cdot q^P_{r,t,lp} \quad \perp \quad \mu^A_{r,t,lp}.$$

The price of antimicrobials is exogenous in our model. To account for the price of antimicrobials as an endogenous variable, we would have to model a demand and supply market for antimicrobials, for which there is insufficient data.

Similarly, each trader of food maximizes their profit, comprising their revenues from selling $q^T_{r,rr,t,lp}$ to region rr (at the regional price $\pi_{r,t,lp}$) minus the cost of purchasing an item from region r (at the regional price $\pi_{rr,t,lp}$) and the total cost of transportation ($c^T_{r,rr,t,lp}$)

$$\max_{q^T_{r,rr,t,lp} \in \mathbb{R}_+} \sum_t \left(\left(\pi_{r,t,lp} - \pi_{rr,t,lp} - c^T_{r,rr,t,lp} \right) q^T_{r,rr,t,lp} \right) \tag{6.5}$$

Production in each region, as well as imports and exports need to balance with domestic consumption in each region $q^C_{r,t,lp}$, *i.e.*,

$$q^C_{r,t,lp} = q^P_{r,t,lp} - \underbrace{\sum_{rr} q^T_{rr,r,t,lp}}_{\text{Exports}} + \underbrace{\sum_{rr} q^T_{r,rr,t,lp}}_{\text{Imports}} \tag{6.6}$$

Finally, the market price in each region is computed via the inverse demand function

$$\pi_{r,t,lp} = f^C_{r,t,lp}\left(q^C_{r,t,lp}\right) = \alpha^C_{r,t,lp} + \beta^C_{r,t,lp} \cdot q^C_{r,t,lp}, \tag{6.7}$$

where $\alpha^C_{r,t,lp}, \beta^C_{r,t,lp}$ are the interval and the slope respectively of the inverse demand curve in region r, of livestock product lp, in year t. IGAULTM is used for a

comparative analysis for the years 2015-2028. In the business-as-usual scenario, *i.e.,* the *Reference* scenario, no policy is introduced. When a policy is introduced, we are able to observe how quantities and prices change compared to the Reference scenario for the time horizon using a counterfactual analysis. A description of the model's equations along with their derivation are provided in Appendix C.

Since we focused on trade related to LMICs, we treated trade with the Rest Of World region as exogenous. To ensure model results in the Reference scenario matched historical data and projections, we calibrated certain parameters of our model. In a game-theoretic setting, production and trade quantities maximize producers and traders profit respectively. Therefore, in the calibration process, we ensured that the costs and prices in the individual optimization problems of the agents are such that the reference quantity matched the model output. Based on this principle, we derived the transportation costs $\left(c^{T}_{r,rr,t,lp}\right)$. A detailed description of the calibration process is provided in Appendix C.

Table 6.2: Description of model sets, parameters, variables.

Element	Description
t	**Set:** model running periods (2015-2028)
r	**Set:** exporting region and/or region
rr	**Set:** importing region
lp	**Set:** type of livestock product (beef, poultry, pork)
$f^C_{r,t,lp}$	**Variable:** inverse demand function of region r, in year t, of product lp
$\pi_{r,t,lp}$	**Variable:** food market price of region r, in year t, of product lp
$\text{mc}_{r,t,lp}$	**Variable:** marginal cost of production of region r, in year t, of product lp
$\mu^A_{r,t,lp}$	**Variable:** dual of constraint (6.3) of region r, in year t, of product lp
$q^C_{r,t,lp}$	**Variable:** consumption of region r, in year t, of product lp
$q^P_{r,t,lp}$	**Variable:** production of region r, in year t, of product lp
$q^T_{rr,r,t,lp}$	**Variable:** livestock transported from region r to region rr, in year t, of product lp
$q^A_{r,t,lp}$	**Variable:** quantity of antimicrobial use of region r, in year t, of product lp
$c^T_{r,rr,t,lp}$	**Parameter:** transportation cost from region rr to region r, in year t, of product lp
$\bar{p}^A_{r,t,lp}$	**Parameter:** fixed cost index of antimicrobials in region r, in year t, of product lp
$\alpha^P_{r,t,lp}$	**Parameter:** linear term of supply curve of region r, in year t, of product lp
$\beta^P_{r,t,lp}$	**Parameter:** quadratic term of supply curve of region r, in year t, of product lp
$\alpha^C_{r,t,lp}$	**Parameter:** linear term of inverse demand function of region r, in year t, of product lp
$\beta^C_{r,t,lp}$	**Parameter:** quadratic term of inverse demand function of region r, in year t, of product lp
$\alpha^A_{r,t,lp}$	**Parameter:** Value share of antimicrobial use in production of region r, in year t, of product lp
$\theta^A_{r,t,lp}$	**Parameter:** impact of antimicrobials to the marginal cost of production of region r, in year t, of product lp

6.2.3 Data Sources

Historical data on livestock production, production prices, and trade were retrieved from the Food and Agriculture Organization (FAO) of the United Nations (U.N.) (FAOSTAT, 2020) for 214 countries. Production, consumption, and trade projections were collected from the Organization for Economic Co-operation and Development (OECD) (OECD-FAO, 2019). We retrieve growth rates of production, consumption, and trade from OECD from 2015 through 2028 and apply them to historical production, consumption, and trade of each country. When a country's growth rate was not available in OECD, we used the growth rate of the next larger region available in OECD. Finally, historical and projected regional antimicrobial use data were retrieved from the Center for Disease Dynamics Economics & Policy (CDDEP, 2017) for 70 countries. In the Reference scenario model output, global production between 2015 (Figure 6.1) and 2028 increased by 17%. The projections are not forecasts and serve as a baseline of what will happen in the medium term, given our current knowledge. Having baseline projections allows us to assess changes in meat production, consumption, and trade under a shock. In Appendix C we detailed all data sources and calculations for the Reference scenario.

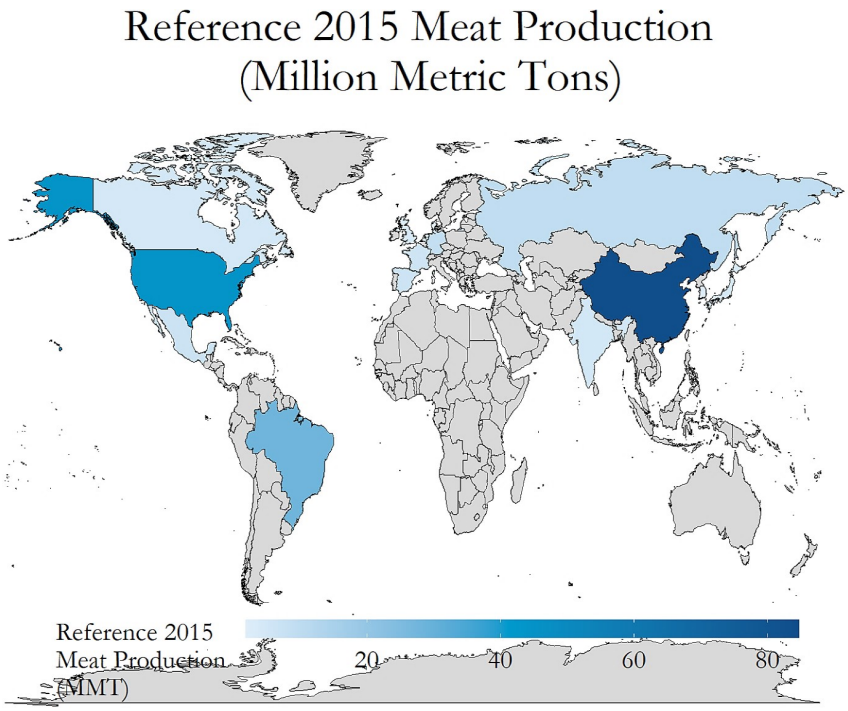

Figure 6.1: Reference regional livestock production for base year (2015).

6.2.4 Scenario Design

For the purpose of this chapter, we formulated three scenarios, in accordance with contemporary AMR-related health concerns in LMICs. The design of the scenarios balanced two main objectives. First, contributed to the ongoing discussion regarding the design of policies against AMR. The scenarios investigated how global coordination policies could curb the use of antimicrobials. Furthermore, the scenarios stressed the importance of the trade network and the interplay between trade and antimicrobial use. We used a global model to assess the impact of the policies on major LMICs, such as India, Brazil, and China. Specifically, we tested a policy targeting

antimicrobial use directly; a shock on the trade side where the leading exporter of meat (Brazil) is denied access to the global market; and a shock in global demand where the leading consumer (China) decreases its livestock consumption.

The first scenario assumed that all countries coordinate and implement a user fee on non-human antimicrobial use. Given their commitment, we assume that the policy is enforced on the producers, meaning that purchasing human antimicrobials and using them in animal food ration instead (Graham et al., 2007) is prohibited. The idea of a user fee on non-human antimicrobial use in order to reduce antimicrobial use in livestock production has been suggested by Hollis and Ahmad (2013). Our implementation is motivated by Van Boeckel et al. (2017) who studied the impact of a 50% user fee on antimicrobial use that aimed to curb the use of antimicrobials in the livestock sector by rendering them more expensive. Following Van Boeckel et al. (2017), we examined the impact of a uniform country-level user fee on antimicrobial used in the livestock sector that would gradually increase the price of antimicrobials by 50% by 2028. The user fee was assumed to increase the price of antimicrobials by 5% yearly, starting in 2019.

The second scenario was motivated by the decision of the U.S., in June 2017, to ban imports of beef from Brazil based on concerns regarding the intensive use of antimicrobials in producing livestock (USDA, 2017a). In addition, the U.S. currently monitors and re-inspects all meat products imported from Brazil since March 2017 due to safety concerns. Almost 11% of meat imports from Brazil have not met the

standards of USDA's Food Safety and Inspection Service, compared to approximately 1% of meat imports from the rest of the world (USDA, 2017b). Similar concerns have been expressed by the EU (EC, 2017), Canada (CFIA, 2020), and China (MALF, 2017). In this scenario, we assessed the case where safety concerns regarding the conditions of meat production in Brazil resulted in Brazil failing to meet international standards, which in turn led all countries to ban imports of meat from Brazil in 2019. Given the importance of exports to Brazil's producers, we assumed that Brazil's meat production will be reformed gradually to address the concerns, similarly to Brazil's commitment in 2017 (USDA, 2017b). For that, we assumed that the ban is relaxed by 11% yearly compared to reference consumption which leads to Brazil gaining full access to international markets by 2028.

The third scenario followed the 2016 announcement of meat consumption guidelines by the Government of China that would curtail the growing consumption of meat by 50% compared to their 2015 consumption by 2030 (NHFPC, 2016). If the goal was to be met starting in 2019, consumption needed to decrease by 5.6% yearly. For this scenario, we constrained annual consumption of China along the time trajectory (variable $q^C_{r,t,lp}$ in equation (C.8)). We applied the same ratio to all three types of meat represented in the model. Livestock consumption in 2028 was decreased by 56% compared to 2015 and 52% compared to projected 2028 reference consumption for the scenario inputs.

In summary, the three scenarios were:

- A user fee that increased the price of antimicrobials uniformly by 50% (parameter $\bar{p}^{A}_{r,t,lp}$ in (C.1)).
  - The first variation assumed a user fee that was adopted by all countries. The fee was introduced in 2019 and increases the price of antimicrobials yearly by 5%.
  - Given the disparate effects of the scenario, we studied a variation of the previous scenario, where user fees increased the price of antimicrobials by 5% each year starting in 2019. In this variation, the policy was adopted by all countries and regions apart from China.
- A global ban of all meat imports from Brazil due to concerns regarding excessive use of antimicrobials in meat production in 2019, which was relaxed gradually in the following years. Imports from Brazil (variable $q^{T}_{r,rr,t,lp}$, where the exporting region rr is Brazil) were constrained to 0 in 2019 and were relaxed by 11% yearly compared to reference exports, recovering to reference levels in 2028.
- A 50% decrease of reference 2015 demand in China for poultry, pork, and beef by 2028. China's consumption (variable $q^{C}_{r,t,lp}$, where r is China) decreased by 5.6% each year, starting in 2019.

6.3 Results

6.3.1 Scenario for Global User Fee on Antimicrobials

The model output showed that a user fee which increased the price of antimicrobials uniformly by 50% and was adopted by all countries led to a 33% decrease in global antimicrobial use in 2028 and a negligible decrease in global production. Our results were consistent with Van Boeckel et al. (2017), who found that a 50% increase of the price of antimicrobials resulted in the U.S. decreasing its antimicrobial use by 31%. The resulting decrease in antimicrobial use in this scenario was fairly uniform, ranging from 31% (Russia) to 40% (India). Studying the competition between Canada and the U.S. for European demand revealed the key role that antimicrobial use played in this scenario. Net exports from the U.S. to all European countries were projected to increase by 0.2 Million Metric Tons (MMT), whereas Canada's net exports to Europe were projected to increase by 0.04 MMT, mostly to Russia. The fact that the U.S. livestock production sector was less dependent on antimicrobials than Canada's (88 mg|PCU versus 119 mg|PCU in 2013), implied that the impact of the policy to the cost of production of Canada was higher compared to the U.S., rendering Canada less competitive in the global market *ceteris paribus*.

The results of the model revealed that the policy increased global trade, since regions traded more, in search of the lowest-cost alternative in the new global market equilibrium. The policy led to a 17% increase in global trade by 2028 in the scenario

output. China had the highest antimicrobial use in our model in 2013 (CDDEP, 2017). For that, China's meat production was projected to decrease the most, by roughly 2.5 MMT in 2028, which was imported instead, leading to a 55% increase in imports compared to the Reference scenario. On the other hand, countries with many trade partners, namely Brazil, the U.S., and Spain, were projected to increase their net exports compared to the Reference scenario regardless of their antimicrobial use[2]. Given their trade network, the three countries had more potential buyers and thus were better positioned to exploit regional discrepancies. Spanish production increased by 8%, the second greatest increase among all countries in 2028. Moreover, net exports of India increased by 0.7 MMT, the highest increase among all countries in 2028. Although India had few trade partners, its production potential and its proximity to China led to a 0.3 MMT increase in net exports to China compared to 2028 reference net exports. Moreover, exports of India to the U.S. also increased by 0.3 MMT, which is roughly 55% of the increase in U.S. total exports in the scenario. The model output suggested that India's low-cost production potential displaced China's meat production, which was heavy in antimicrobial use. Apart from Russia, BRICs (Brazil, Russia, India, China) production and inter-BRICs trade adjusted the most among all regions and regional interconnections in this scenario. Russia's net exports, production, and consumption remained relatively unchanged compared to the Reference scenario. Figure 6.2 shows the change in meat exports of select

[2]Brazil: 53 mg|PCU, USA: 88 mg|PCU, and Spain: 182 mg|PCU in 2013 (CDDEP, 2017)

countries.

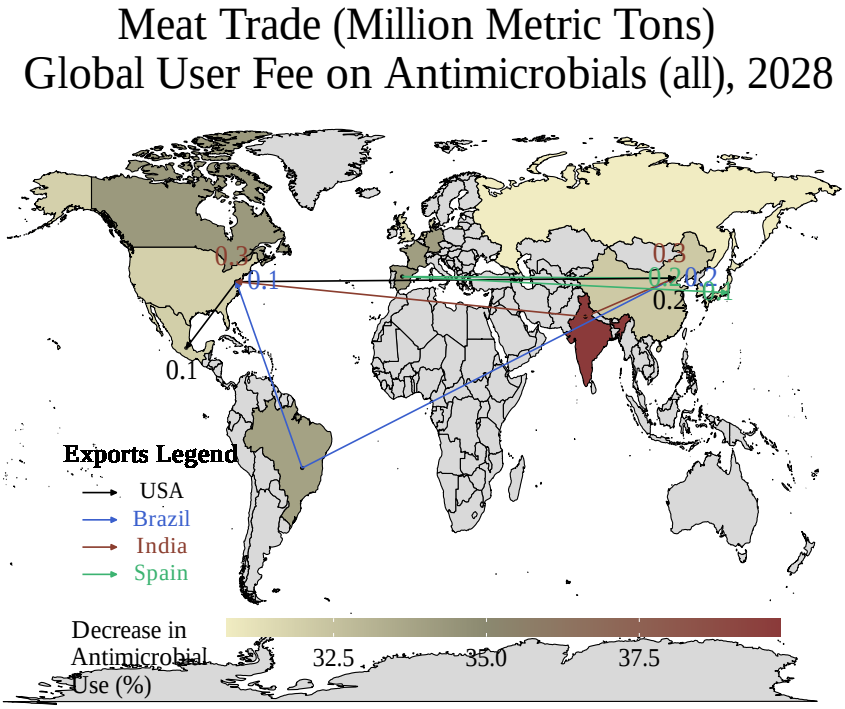

Figure 6.2: Change in meat exports in million metric tons (MMT). Increasing the cost of antimicrobials reduces antimicrobial use world-wide by 33%. Countries with higher connectivity (Brazil and the US) and countries exporting to major exporters (India) are the ones whose exports benefit the most.

The impact of the policy on China, driven by the high antimicrobial use, could prompt China to deviate from the global use fee. Hence, we also studied the case where all countries but China adopt an antimicrobial user fee. In this variation, the model projected that global antimicrobial use was reduced by 12% in 2028 and global production remained relatively unaffected. We noticed that the simulated impact varies regionally, similarly to the previous scenario. On the one hand, our model results showed that all countries adopting the policy reduced their antimicrobial

use by 32% and faced a 2% decrease in production. Spain's and Brazil's livestock production were the least affected. India's livestock production increased by 7% while Spain and Brazil faced a 1% decrease. On the other hand, China was projected to increased its production by 6%. China's productivity was further enhanced by the 1.4% increase in antimicrobial use. China in this scenario opted out of introducing the user fee and was able to increase antimicrobial use without becoming less competitive in the global market. As a result, China's exports increased by 1.2 MMT. The model also revealed that the U.S. faced a 14% decrease in exports in 2028. The result was due to a 70% decrease in U.S. exports to China and a 37% decrease in exports to Japan and Korea. China supplied a greater portion of Asian demand in this scenario, forcing competitors such as the U.S., out of the market. Finally, Japan and the Republic of Korea, who are traditional importers in great proximity to China, were projected to increase their imports by 0.2 MMT and 0.9 MMT respectively. Subsequently, their livestock production decreased by 8% in 2028 which was the largest decrease among all countries. Figure 6.3 illustrates how the change in China's exports affect global trade.

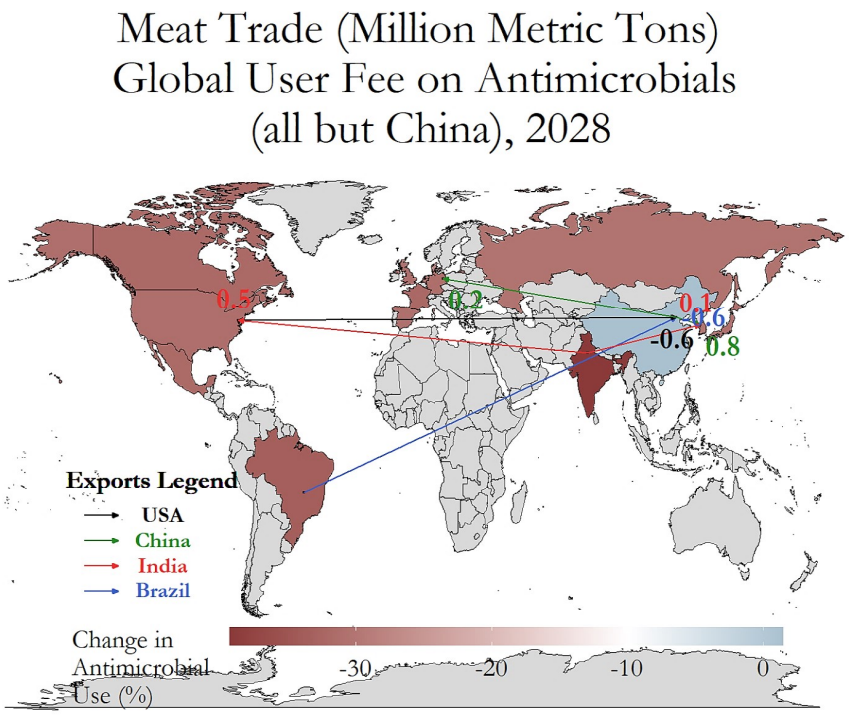

Figure 6.3: Change in meat exports in million metric tons (MMT). Increased antimicrobial user fees reduce antimicrobial use in livestock production world-wide by 12%. When China does not adopt the policy, it gains a competitive advantage in the global market and its meat exports increase.

6.3.2 Global Ban of Imports from Brazil

The model results showed that the trade ban leads to a rearrangement of trade flows, with the U.S. becoming the largest exporter in 2019, surpassing Brazil in this scenario. The U.S. in this scenario covered 25% of international demand, previously covered by Brazil. This led to a 12% increase in U.S. exports in 2019. Although the U.S. had the $6th$ lowest marginal cost of production among all countries in the Reference scenario, it exploited the fact that it retained trade relationships with almost all countries and was projected to supply part of the consumption that was met by

imports from Brazil in the Reference scenario. Specifically, U.S. exports to Europe, China, and Japan increased by 0.4 MMT, 0.1 MMT, and 0.1 MMT respectively. That is 47%, 7%, and 16% of the curtailed exports of Brazil to the respective countries. The other four countries whose exports benefited the most are India, Canada, Spain, and France, whose exports increased by 4% to 5%. Figure 6.4 shows the countries whose exports were affected the most in response to the ban. Brazil's production sector is assumed to gradually adjust in the medium term and is allowed access in the international market. As the restrictions were gradually raised, exports of Brazil recovered gradually as well. Figure 6.5 shows the change in U.S. and Canada's exports in response to the ban in this scenario.

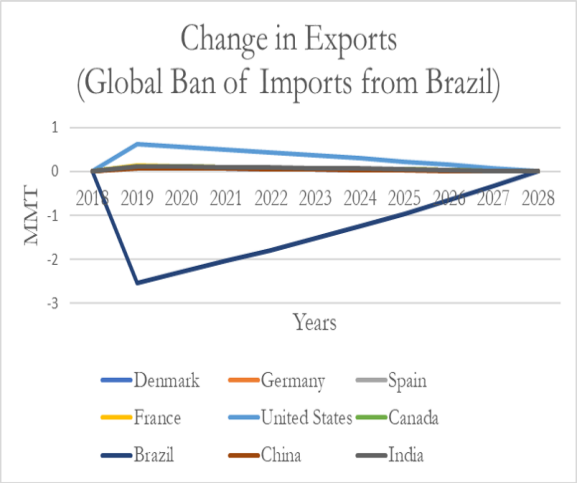

Figure 6.4: Change in meat exports in million metric tons (MMT) of select countries. The U.S. increase its exports the most in response to the ban of imports from Brazil in 2019. As Brazil is gradually allowed access to international markets, Brazil's exports recover and exports of other major exporters gradually decline.

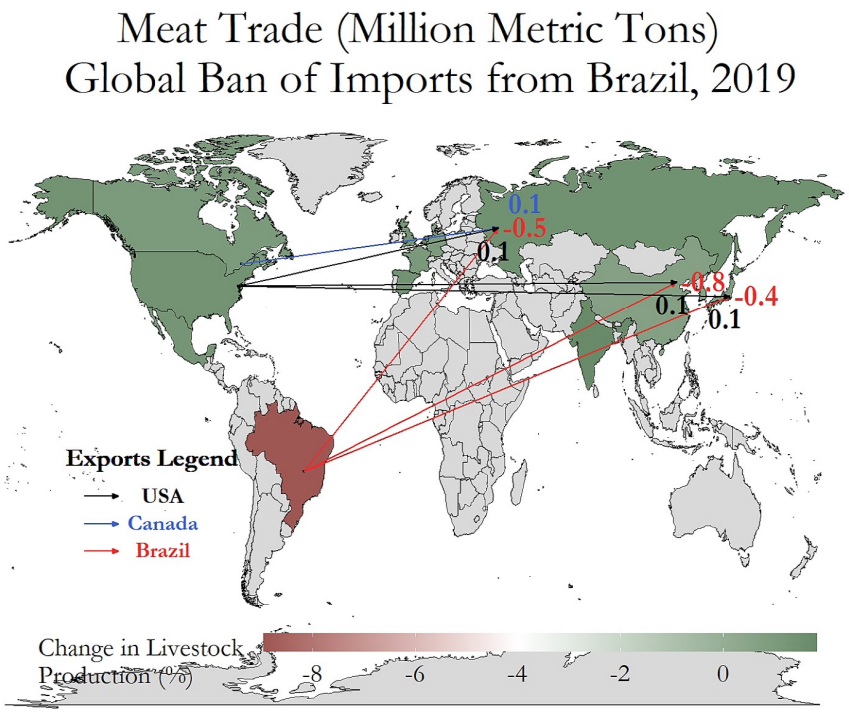

Figure 6.5: Change in meat exports in million metric tons (MMT). The ban decreases Brazil's production by 8.5% in 2019. The U.S. assumes the role of leading exporter, by increasing its exports to all trade partners, including China, Europe, and Japan.

The model projected that antimicrobial use in 2019 decreased by 6% in Brazil and increased by 1% in all other countries, compared to the Reference scenario. In the Reference scenario, Brazil exported 17% of its production each year. In this scenario, in 2019, Brazil's producers did not have the option to export and needed to cover only domestic demand. Hence, Brazil's producers could be competitive in the domestic market by producing at a higher marginal cost of production. Consequently, they were able to reduce their antimicrobial use without losing their share in the domestic market in this scenario. On the other hand, the model projected that producers in all other countries increased their production to cover existing demand. In their attempt

to be more competitive, they also increased their antimicrobial use in order to increase their productivity. The increase of antimicrobial use for all countries other than Brazil is projected to be between 0.2% (India) and 2.6% (Denmark). Figure 6.6 illustrates how Brazil's projected antimicrobial use gradually increased as the restrictions were lifted. In the medium-term, Brazil's producers in the model increased antimicrobial use to compete in the global market.

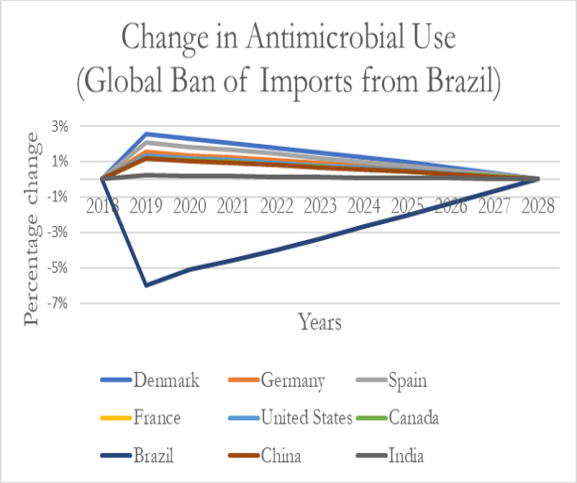

Figure 6.6: Percentage change in antimicrobial use compared to reference antimicrobial use. The ban leads to a decrease in antimicrobial use in Brazil's livestock production sector and an increase of antimicrobial use in the livestock production sectors of the other countries in 2019. Brazil's livestock producers seek to increase their productivity by increasing antimicrobial use when allowed access to the international market.

Finally, the model estimated that domestic demand of all countries remained unchanged. Revenues of Brazil's livestock producers decreased by 9% in 2019 and gradually recovered until 2028, whereas all other countries faced a 1% increase in revenues in 2019.

6.3.3 China's Mid-Term Meat Consumption Target

The model output demonstrated that the severity of the shock, coupled with China's strategic position close to major meat importers, resulted in China –the largest net importer– turning into the leading net exporter. To better understand this result we need to bear in mind that China was the largest livestock producer globally and that in the Reference scenario China's meat production in 2028 was projected to be 9% larger compared to 2015, based on OECD projections (OECD-FAO, 2019). Therefore, given the short- and medium-term production capabilities of China's meat industry, we observed that the curtailment of China's demand resulted in a surplus of supply that can be provided at a lower marginal cost to the international markets, compared to the Reference scenario. China's consumption in our model in 2028 became 49 MMT, a 49% decrease compared to reference 2028 consumption, while China's production in 2028 became 72 MMT, a 23% decrease compared to reference 2028 production. The difference between projected production and consumption was 23 MMT which amounted to 32% of China's production in 2028 in this scenario. Moreover, China's exports in this scenario accounted for 30% of total exports of all countries. The potential of China's meat industry alone though was not sufficient to describe the changes in this scenario. On the one hand, in the Reference scenario, China was the largest net importer of meat in 2015 with a total of 3.7 MMT that

amounted to 17% of global imports in our model. The curtailment of China's demand led to a curtailment of imports into China as well. Moreover, China is situated in proximity to Japan and Korea that were major meat importers, while China retained trade relationships with most European markets. From a total of 23 MMT of total net exports in 2028 in this scenario, 92% was allocated to Europe via Germany and Russia and the rest to Japan and the Republic of Korea.

At a global scale, in 2028, China constituted 30% of global consumption of meat, covering roughly 5% of domestic demand via imports in the Reference scenario. The model results showed that the curtailment of global demand resulted in more available low-cost livestock production in China. In this scenario, our model projected that production of the rest of the countries drops by 12% in 2028 compared to reference 2028 production. Spain experienced a 31% decrease in production and Brazil experienced an 8% decrease in production, the largest and smallest decrease among all countries respectively. Consumption on the other hand was projected to reduce only in China and remained unchanged in most countries. The model output revealed that global income of the livestock sector decreased by 15% in 2028 and by 7% intertemporally compared to the Reference scenario. Figure 6.7 shows how the change in China's exports in this scenario affected global livestock trade of LMICs and major exporting countries.

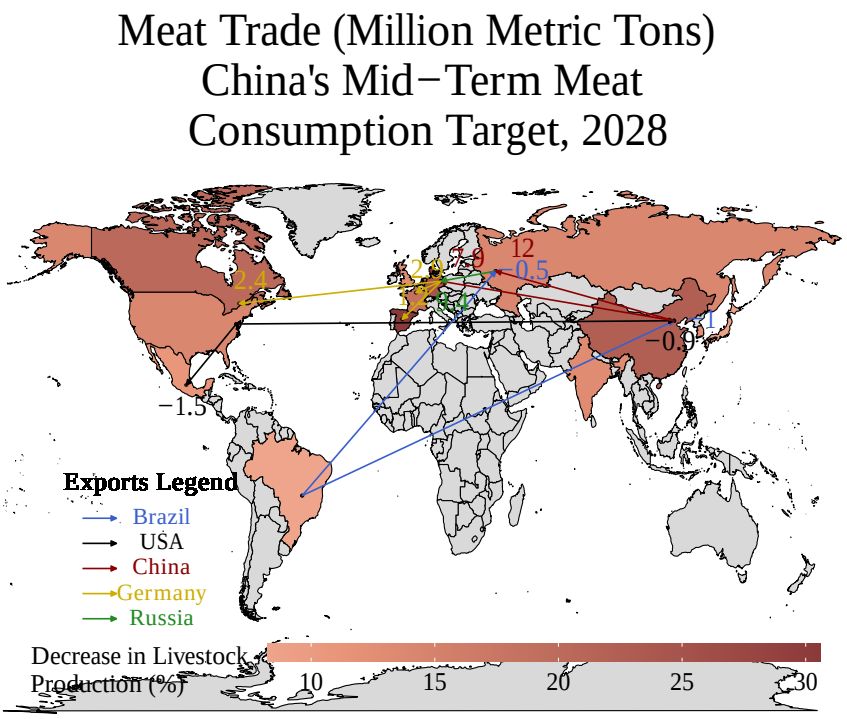

Figure 6.7: Change in meat exports in million metric tons (MMT). Curtailment of China's demand results in China having a surplus of low-cost meat that is sold in the global market. China becomes the leading exporter by increasing its exports to all countries via Germany and Russia.

The model results also revealed that global antimicrobial use remained unchanged in this scenario. However, countries facing greater decrease in production increased their antimicrobial use in the scenario output. China's production decreased by 23% and its antimicrobial use increased by 14% in 2028, compared to the Reference scenario. Similarly, livestock production in Canada, Germany, and Spain decreased by 20%, 25%, and 31% respectively compared to the Reference scenario. The three countries increased their antimicrobial use by 8%, 10%, and 13% respectively in order to increase their productivity, which mitigated the impact of the policy on domestic

livestock production.

6.3.4 Policy Implications

We assessed the impact of global coordination scenarios on LMICs' livestock production and trade that can lead to more sustainable food animal production. We identified the interplay between country-level antimicrobial use and trade as a key driver of the change in country-level livestock production. Our model output showed that in all three scenarios, India and Brazil were among the countries whose livestock production either benefited the most or was least impacted, while China's livestock production did not benefit only when it adopted, along with all other countries, an increased antimicrobial user fee.

We observed that the adoption of a user fee on antimicrobials by all countries in our model in the first scenario decreased the use of antimicrobials without significantly impacting global livestock production. However, the impact on LMICs' production may disincentivize them from adopting the global policy in the future. Using our model, we found that deviating from the policy could provide a country with a competitive advantage over the rest. The deviating country was found to increase antimicrobial use of the deviating country. The model output also showed that livestock production of countries with more trade partners was less affected. We suggested that global *cooperation* could ensure the participation in the policy scheme. This point has both economic and political ramifications. From an economic point of

view, a candidate global policy needs to allocate the burden of the policy in a way that does not favor the prospects of one country over another. From a political point of view, policy-makers run the risk of certain countries backing away from an agreement if the proposed policy fails to address the discomfort of certain country-level producers and consumers.

The second scenario illustrated how trade policies related to a trade ban on meat produced in LMICs can affect global antimicrobial use. The model output showed that there were three fundamental reasons why the U.S. assumed the role of leading exporter. The first was the penetration of U.S. production in almost all major consumers. The U.S. retained trade relationships with Europe, China, and Japan that allowed it to benefit from changes in livestock trade. The second was the ability of the U.S. to increase its production and remain competitive compared to the rest of the countries. Finally, India, Canada, Germany, and Spain also saw a significant increase in their exports. The model output suggested that the policy succeeded in decreasing Brazil's antimicrobial use in the short term. However, the ban created more space for competition among all other countries who increased their antimicrobial use in an effort to increase their productivity and cover a greater portion of global demand in the model scenario.

The third scenario underlined the potential of China's meat sector to transform from a major importer to the leading exporter, assuming a decrease in China's meat consumption. We concluded that this result is possible given the established trade re-

lationships of China with major importers, such as Japan and Europe. Moreover, we were able to isolate the interconnections with the highest potential for China. Finally, this scenario highlighted how changes in China's meat consumption can severely affect, via trade, global production, resulting in losses for producers worldwide. China's livestock producers in our model increased antimicrobial use in the livestock sector in this scenario in order to increase their productivity and cover a larger portion of the international market.

6.3.5 Limitations

The limitations of our analysis arose from the unavailability of sub-national production, consumption, and trade data for all countries and the uncertainty regarding the impact of antimicrobial use on livestock growth. IGAULTM was designed to account for the impact of antimicrobials on livestock production (parameter $\theta^{A}_{r,t,lp}$). However, there is evidence that antimicrobials may not contribute to growth promotion (Levy, 2014), or increase profitability (Graham et al., 2007). In this chapter, following (NRC, 1999), we assumed that antimicrobials had a positive impact on breeding productivity. Finally, country-level antimicrobial expenditures by livestock producers were not available and were computed using data from (NRC, 1999). These are critical parameters in our analysis. Hence, the provided quantitative results served to illustrate the underlying economic rationale behind antimicrobial use in the global livestock market and were conditional on available data at the time this work was conducted.

The antimicrobial use of each country was inferred using data from (CDDEP, 2017) which did not distinguish between antimicrobials for therapeutic and non-therapeutic purposes. To the best of our knowledge, the purpose of antimicrobial use at the country level is not publicly available, which impacted scenario design and implementation. With such data, we would have been able to formulate more informed scenarios that targeted growth-promoting antimicrobial use. In the case where only growth-promoting antimicrobials were either banned or taxed, the producers' decision-making process would need to account for purchase and use of human antimicrobials instead. Moreover, antimicrobials for therapeutic purposes in some cases reflect poor sanitary breeding conditions. Our model did not account for the substitution between sanitary conditions and antimicrobial use in every country, since such data were not available.

As described in the Methods section, historical data on production, consumption, and trade were retrieved from FAOSTAT. The FAOSTAT dataset comprised consistent data up to 2015 and reference production, trade, and consumption projections were computed by applying the growth rates of OECD data to the respective quantities. In some cases OECD's outlook did not report the growth rate of a particular country, but of a region. In that case we used the growth rate of the next largest region to project country-level production, consumption, and trade to 2028. Modeling of the supply side was driven by the available data and the question at hand, which required the representation of a range of countries at the global level. We dis-

tinguished between three types of livestock, namely beef, pork, and poultry. We did not explicitly model endogenous investment decisions. This simplification was based on the time horizon of our analysis, which was short- and medium-term, and the unavailability of livestock farm capacity data at the level of regional detail required in this chapter. Finally, demand elasticity estimates were collected from various sources and were not available at the country level for most countries. When country-level demand elasticities were not available, the regional demand elasticity is applied to the countries of each region. Therefore, our analysis may fail to grasp the variance in demand patterns of countries in the same region. We provided a detailed list of data sources in Appendix C.

6.4 Conclusion

The use of antimicrobials in the livestock sector is based on the assumption that antimicrobials enhance livestock growth. Even when veterinary medicinal products are regulated, countries may not have the resources to enforce the regulations. In resource-limited LMICs, taxing or banning antimicrobial use in livestock production could result in producers purchasing antimicrobials from other providers (Barroga et al., 2020). Consequently, enhanced AMR monitoring systems and surveillance of antimicrobials consumption (Cheng et al., 2014) are necessary complements to global policies against AMR.

Moreover, there is evidence in the case of poultry in Denmark that the savings from restricting antimicrobial use in livestock production almost completely offset the losses in animal growth (WHO, 2002). Hence, future research needs to quantify under what conditions it is economically beneficial for livestock producers to use antimicrobials. Under certain conditions, the boost in livestock productivity may not justify the purchase of antimicrobials. Identifying these conditions can inform animal breeding practices and future AMR policy design.

AMR limits the therapeutic and prophylactic effects of existing antimicrobials on humans and animals (Collignon et al., 2016). For that, even when it is economically beneficial for livestock producers to use antimicrobials, the WHO suggests that countries restrict the use of antimicrobials which are *"critically important"* for human medicine in the livestock sector. In this chapter we showed that LMICs' livestock production can be affected by policies against AMR. The disparity of the impact between countries in our scenarios suggest the need for more detailed data on antimicrobial use and regional production costs. Specifically, there is a need for more data on the use of different classes of antimicrobials, the purpose of the use of each antimicrobial, and the contribution of each to livestock producers' profitability. Incorporating the different uses of different classes of antimicrobials into the producers' decision-making problem would allow us to study scenarios that target only the particular subset of growth-promoting antimicrobials.

From a societal perspective, limiting AMR can reduce second-line treatment and

hospitalization costs. Moreover, addressing AMR by restricting the use of antimicrobials in food animal production contributes towards meeting Goal 3 of the United Nation's Sustainable Development Goals that emphasizes health and well-being. To the extent that restricting antimicrobials in food animal production contributes to sustainable agricultural production, tackling AMR contributes also to Goals 2 and 12 of the United Nation's Sustainable Development Goals (IACG, 2018). In this chapter we emphasized the interplay between the underlying economic incentive of antimicrobial use and livestock trade as key aspects in the design of global policies. Our framework allowed us to represent the decision-making process of different agents in global livestock supply chains. In the case of a tax on antimicrobial use in livestock production, the framework can be enhanced to represent country-level or international agencies that decide on the optimal tax on antimicrobial use in livestock production by taking into account also the healthcare costs associated with AMR. This kind of analysis would require robust, country-level estimates of all direct and indirect costs related to AMR. Given the complexity of AMR, which spans more dimensions than the ones emphasized in this chapter, informed policy design calls for more data on livestock production and antimicrobial use.

Acknowledgements

The author thanks Dr. Anastasia Lambrou, Dr. Wei Jiang, and Dr. Sauleh Siddiqui, who contributed to the work in this chapter.

Chapter 7

Conclusion and Future Work

7.1 Concluding Remarks

This dissertation addresses challenges of critical interdependent infrastructures due to technological progress, climate change, and shifts in national and global policies toward more resilient energy and food supply chains. Localized failures in a single infrastructure, such as blackouts, can propagate through network interconnections to multiple regions, affecting millions of people, at different time scales. At the same time, disruptions propagate to other infrastructures through their interdependencies. This was the case in the 2003 Northeastern Blackout and the more recent 2021 Texas Blackout. In this dissertation, we focus on three trends that reshape energy and food infrastructures. First, the transformation of power systems into smart grids through mechanisms that allow more efficient power system operations. Second,

climate change and the implications for the energy sectors of environmental and renewable policies. Third, the transformation of food supply chains toward more resilient, less antibiotic-intensive production and consumption. The United Nations identify all three challenges under the United Nations Sustainable Development Goals (ECOSOC, 2015).

Motivated by inefficient use of transmission resources under extreme loading in a power system, we consider a single cause of blackouts, voltage collapse, which evolves at the seconds scale. For the special case of a star direct current network, we design a distribution-level controller that addresses a failure in the transmission system. The implementation of a voltage collapse stabilization controller depends on the ability of modern power electronics to track the fast system dynamics at the point of voltage collapse. Nevertheless, we argue that voltage collapse is primarily a demand-side problem, and thus a demand-side controller can, in critical conditions, provide the system operator with more time to navigate the situation, commit more generation capacity, and activate response mechanisms without disrupting supply for extended periods of time.

The response to climate change spans multiple decades and initially benefited natural gas, whose emissions factor is smaller compared to most fossil fuels (Feijoo et al., 2016). However, more aggressive renewable policies and emissions reduction targets (UN, 2015) introduce greater uncertainty to the long-term natural gas outlook. In this dissertation, we focus on a single world region, North America, comprising

Canada, Mexico, and the U.S., and evaluate long-term changes in their natural gas infrastructure through 2050. We assess long-term transformation of regional natural gas production and transportation infrastructure in the presence of technological progress, resource availability, market shocks, and changes in renewable policies in the electricity sector. We find that the impact of any single shock can vary regionally, and show that changes in renewable policies can greatly affect regional natural gas infrastructure development and prices. Therefore, a more detailed representation of the natural gas sector can contribute to a more comprehensive assessment of the impact of renewable policies during the transition to a low-carbon or net-zero economy.

At the international scale, animal husbandry practices can contribute to antimicrobial resistance and indirectly impact human livelihoods. However, there exists a tradeoff between the use of antimicrobials for growth promotion in livestock production and the social costs of AMR, including research and development for new antimicrobials, longer hospitalization periods, and increased danger of surgery complications. We focus on three medium term policies and find that trade relationships with more countries can play an important role in the response to a global policy. We also find that decreasing antimicrobial use requires careful design of international coordination policies that accounts for the disparate effects on Low and Middle Income Countries to ensure participation in the policy scheme.

The analyses in Chapters 4 through 6 are sensitive to future consumption and resource availability assumptions. The agents in the respective applications have

perfect foresight, which is consistent with the published literature. Even though a recursive-dynamic approach can be more realistic, it would require a more diligent treatment of each agent's future expectations and would remain sensitive to reference assumptions. Nevertheless, our analysis reveals critical tradeoffs under each shock that can inform policy design. In the natural gas and food sectors, an equilibrium is computed within minutes, rendering the respective models easier to integrate to large-scale models.

Resilient infrastructure design involves deciding the optimal allocation of finite resources between the disaster prevention, damage propagation, and recovery phases. Assessment of failures requires leveraging the comparative advantages of different models. At the interdependencies of any two models, differences in variables between models or the unavailability of data can constrain the model integration process and limit the interpretability of model results. In this dissertation we also provide a bilevel optimization framework that can generate data at the interdependencies of critical infrastructures and reconcile inconsistencies between exchanging variables of different models.

We contribute to the published literature on resilience of modern infrastructures by proposing methodologies to address resilience challenges; and assess supply chain vulnerabilities to inform infrastructure design. The data generation framework in Chapter 2 allows systems modelers to fill data gaps within and across modern infrastructures. Moreover, the framework allows for the calibration of all unknown

parameters of large-scale equilibrium models to a reference scenario in a systematic way, which is an advancement over the current practice of arbitrary adjustment of a subset of model parameters (Huppmann and Egging, 2014). In the electricity sector, countermeasures against voltage collapse predominantly focus on reinforcing the capabilities of the generation and transmission systems. Our methodology in Chapter 3 introduces a distribution-level mechanism and offers an additional way to address excess demand in a node. The transition to a low-carbon or net-zero economy will transform the natural gas sector, which can be vulnerable to market shocks, technological progress, and policy shifts in interdependent infrastructures. Our analysis contributes to existing resilience assessment studies of energy infrastructures by looking at how potential future technological and market assumptions can affect natural gas prices and thus accelerate or delay the phase out of natural gas use. We also quantify the impact of renewable policies on regional North American natural gas infrastructure. In the food sector, we go beyond existing statistical models by proposing an equilibrium model that accounts for market interactions between international agents in meat supply chains. The methodology accounts for intercountry meat trade, which allows us to identify the tradeoff between global coordination policies and trade for meat production and consumption of Low and Middle Income Countries.

Our analysis is generalizable to shocks in modern infrastructures that have similar characteristics to the shocks in the sectors modeled in this dissertation. Chapter 3 shows that in a sector with scarce resources, agents can decide based only on their

individual needs if resources are not depleted. When a resource is depleted, selfish behavior of agents can compromise the operation of the whole sector and some level of coordination needs to be in place. This is the case in a transportation network under a rapidly evolving extreme weather event. Agents utilize the capacity of the transportation network to evacuate an area. However, lack of coordination can cause traffic and disrupt the evacuation. A centralized signal to all agents can communicate that the traffic network is at capacity and agents can be prioritized based on their proximity to the event. In this way, a central planner can achieve the evacuation of an area and maintain maximum flow of people out of the area through the network. In the food sector, increasing the cost of antimicrobial use worldwide increases the livestock production cost. Livestock producers face an additional cost that is related to the social cost of antimicrobial resistance. A similar strategy can be employed to reduce carbon emissions in the livestock sector if livestock production is taxed based on the social cost of emission. The analysis in Chapter 6 reveals the importance of the trade network for the outcome of global coordination policies and can also inform the design of global food policies toward carbon emissions reduction. In addition, the proposed framework incorporates the reaction of different agents in international food supply chains, which allows us to study a broader range of policies compared to statistical models.

Modern infrastructures interact with most sectors in an economy, rendering the success of national environmental policies contingent on their response. There exist

a range of policies against climate change, including carbon emissions reduction in the electricity and commercial air travel sectors, more aggressive renewables penetration, electricity consumption reduction, and enhancement of operational efficiencies in all sectors. Natural gas is the primary source of carbon emissions in the U.S. (EIA, 2019c), hence climate change mitigation strategies need to account for the response of agents in the natural gas sector. The interdependence of carbon emissions, environmental policies, and natural gas production implies that our conclusions in Chapters 4 and 5 go beyond assessing the vulnerabilities of regional natural gas infrastructures. Our findings suggest that the success of a national plan that introduces environmental policies to different sectors depends also on intersectoral interdependencies. An environmental policy in one sector can potentially undermine the effect of another environmental policy at an interdependent sector. Therefore, our analysis can inform climate studies and environmental policy design in North America to ensure that natural gas stakeholders are incentivized to adopt a national climate change mitigation plan.

The mathematical frameworks in Chapters 2, 3, and 6 were developed to study a specific challenge, however they are applicable to more fields and topics. The bilevel data-generation framework in Chapter 2 can fill data gaps between any collection of interacting systems and across spatial and temporal scales. The systems can represent agents at the national level, *e.g.,* any combination of interacting sectors of the economy, or agents at the community level, *e.g.,* all interacting energy demand-response

devices in a smart city. In Chapter 3 we show that we can transform the type of bifurcation of a nonlinear dynamical system through the appropriate control strategy, even when the transition equations are highly nonlinear. In Chapter 6 we model additional global coordination policies through equilibrium models that account for inequality constraints, an advancement over statistical models.

We conclude that challenges within modern infrastructures can arise from the lack of coordination between individual agents within infrastructures and the propagation of technological and market disruptions through network interconnections. We argue that the coordination of agents with individual objectives can mitigate the impact of an extreme event on an infrastructure, while intersectoral policy coordination can minimize the impact of a policy change or disruption in one sector to interdependent sectors. In the next section we discuss potential future model enhancements and research areas that can deepen our understanding of the challenges of networked interdependent energy and food infrastructures.

7.2 Future Research

7.2.1 Voltage Collapse Stabilization in Alternating Current Networks

In Chapter 3 we discuss how the analysis of system dynamics around the bifurcation point are highly nonlinear and for that, stability analysis is hard, even for the very specific case of a star direct current network. The design of a voltage collapse stabilization controller is based on the response of individual loads to an outside signal that conveys information about the state of the system without revealing information about the state of specific loads. There are three natural extensions of this work, along with an open question.

The first extension is the generalization of our controller to a star Alternating Current (AC) network. Modern power systems are AC systems. Voltage collapse in an AC system is associated with a shortage of reactive power in a single node. Introducing reactive power in our analysis implies that we also need to account for the voltage angle in a bus. Our controller would need to ensure that both voltage and frequency at the consumption node are within acceptable limits from their nominal values. The second extension is the generalization of our controller to a general network, which is also a non-trivial extension. The voltage at one bus may collapse due to load changes

at another bus of the network, so a controller would need to account for the network effects in an interconnected system with different production and consumption buses. Third, the controller could be adjusted to account for the ability of certain loads in the future to also provide resources to the network. For example, an electric vehicle could not only decrease its consumption under extreme loading conditions, but also provide power to the network and participate in emergency response. The question of characterizing the dynamical behavior at the bifurcation point remains open. Understanding the higher order dynamics could shed more light into how we can improve the voltage collapse stabilization controller.

7.2.2 Cyber-Physical Security of Critical Infrastructures

Cyberattacks on electricity Mieth et al. (2021), natural gas USDHS (2021), and water infrastructures AWWA (2019) warrant revisiting resilience and security of critical infrastructures. In Chapters 4 and 5 we focus on the resilience of regional North American natural gas infrastructure to sector-specific disruptions and policy changes. More efficient design and operation of energy infrastructures implies moving toward a smart grid in the power sector, greater and faster information sharing in any infrastructure network and the substitution of manual decisions from machine learning and other decision algorithms. If any of the additional communication or decision layers are

not carefully designed, they could allow cyberattacks and compromise cyber-physical security. The recent cyberattack against the Colonial Pipeline on May 2021 USWH (2021) urged the U.S. Department of Homeland Security to release new cybersecurity requirements for critical pipeline owners and operators (USDHS, 2021). Cyberattacks have been reported also for the power system (Mieth et al., 2021) and water infrastructure (AWWA, 2019). Therefore, beyond natural hazards, consumer-induced stresses, and technological and policy changes, it is also important to incorporate the cyber-physical layer in resilience analysis. An informed cyberattack could exploit infrastructure-specific intricacies along with infrastructure interdependencies, such as the networked structure, the state of the system, and the physical laws governing an infrastructure, to maximize the impact of a disruption. Cyberattacks could stress the system toward failures that seem *"highly unlikely"* by standard resilience metrics.

7.2.3 Rethinking Resilience: Equity-Driven Design of Critical Infrastructures

The analysis in this dissertation is rooted in the assumption of allocating resources efficiently among agents with conflicting objectives. The modeling assumption is in part consistent with the scale of our analysis, which is for most topics national or international. However, infrastructure design and operation are not neutral in their impact on local livelihoods (Hellegers et al., 2008). In the case of optimization-based

Food, Energy, Water (FEW) systems models, researchers often emphasize efficient resource allocation within–and between–the three sectors but do not incorporate in their analysis other critical political economy drivers, such as entitlements and the power relationships between groups (Spiegelberg et al., 2017). In addition, failures in critical infrastructures disproportionally affect vulnerable populations. This was the case for the elderly population and those assisted by medical devices in the 2019 California power shutoffs (Fuller, 2019).

The disparate impact of environmental catastrophes and public health disruptions on communities of diverse racial and social background (Klinenberg, 1999) imply that there is room to enhance resilience of urban infrastructures in order to allow for equitable allocation of resources among different groups. For example, the rise of Distributed Energy Resources (DERs) does not necessarily imply access to these resources for everyone. Costs or the geographical location of consumers may prevent them from tapping into the potential of DERs. Under extreme weather conditions or following natural hazards access to DERs can greatly impact consumers access to energy and subsequently heating, communication, and other essential operations. Finally, there is growing interest of local government bodies on social justice and environmental justice tensions. To understand the social implications of infrastructure design we would need to downscale our analysis to the urban and community level. At the same time, we would have to revisit our tools and incorporate equitable access to energy and food resources in resilience studies. Therefore, resilience studies can

benefit from accounting for social and socio-ecological outcomes toward an equity-driven design of urban energy infrastructures.

Appendix A

Proofs of Lemmas in Chapter 3

Lemma 2.

Proof. An eigenvalue-eigenvector pair $(\rho, x) \in \mathbb{C} \times \mathbb{C}^n$ of B needs to satisfy

$$Bx = \rho x \tag{A.1}$$

Since $w\mathbf{1}_n^T$ is a rank one matrix, it has $n-1$ eigenvalues $\lambda_i\left(w\mathbf{1}_n^T\right) = 0$, $i = 1, \ldots, n-1$, and one non-zero eigenvalue $\lambda_1\left(w\mathbf{1}^T\right) = \mathbf{1}_n^T w$. Moreover, $q\mathbb{I}$ is a scaled identity matrix and thus shifts the eigenvalues of $w\mathbf{1}_n^T$ by q, i.e., $\rho_i(B) = \lambda_i\left(w\mathbf{1}_n^T\right) + q$. Finally, we can check that $\{e_1 - e_2, e_1 - e_3, \ldots, e_1 - e_n, w\}$ spans $\mathbb{C}^n$ and every pair of (3.16) satisfies (A.1). □

Lemma 3.

Proof. If $(\lambda, u) \in \mathbb{C}\times\mathbb{C}^{n+1+n_F}$ an eigenvalue-eigenvector pair of $J_{SC}(g)$, then $J_{SC}(g)u = \lambda u$ with $u = \begin{bmatrix} u_F & u_I & u_\phi & \hat{u} \end{bmatrix}^T \in \mathbb{R}^{n_F} \times \mathbb{R}^{n_I} \times \mathbb{R} \times \mathbb{R}^{n_F}$, which further leads to

$$\frac{2v^2}{\bar{g}_{\mathrm{N}} + g_l} g_i \bar{u}_N - \left(v^2 + \lambda + b\right) u_{F_i} + b\hat{u}_i = \kappa_i u_\phi, \qquad \forall i \in F \tag{A.2a}$$

$$\frac{2v^2}{\bar{g}_{\mathrm{N}} + g_l} g_i \bar{u}_N - \left(v^2 + \lambda\right) u_{I_i} = 0, \qquad \forall i \in I \tag{A.2b}$$

$$c \cdot \bar{u}_N = \lambda u_\phi \tag{A.2c}$$

$$a u_F - a\hat{u} = \lambda \hat{u} \tag{A.2d}$$

with

$$\bar{u}_F = \sum_{i\in F} u_{F_i}, \quad \bar{u}_I = \sum_{i\in I} u_{I_i}, \quad \bar{u}_N = \bar{u}_F + \bar{u}_I. \tag{A.3}$$

First we will prove that $-a$ is an eigenvalue of $J_{SC}(g)$ only when

$$a = v^2 - \frac{2v^2}{\bar{g}_{\mathrm{N}} + g_l} \sum_{i\in I} g_i. \tag{A.4}$$

If $\lambda = -a$, by (A.2d) $u_F = \mathbf{0}_{n_F}$ and by (A.3), $\bar{u}_N = \sum_{i\in I} u_i$. Summing (A.2b) yields

$$\left(\frac{2v^2}{\bar{g}_{\mathrm{N}} + g_l} \sum_{i\in I} g_i - v^2 + a \right) \bar{u}_N = 0.$$

If (A.4) is true for some $g \in \mathbb{R}^n_{\geq 0}$, then for any $\bar{u}_N \neq 0$, by (A.2c), we get

$$\text{(A.2c)} \Rightarrow u_\phi = \frac{c \cdot \bar{u}_N}{\lambda} = -\frac{c \cdot \bar{u}_N}{a};$$

$$\text{(A.2b)} \overset{\text{(A.4)}}{\Rightarrow} u_i = \frac{g_i}{\bar{g}_{\mathrm{I}}} \bar{u}_N, \quad \forall i \in I;$$

$$\text{(A.2a)} \Rightarrow \hat{u}_i = -\frac{1}{b}\left(\frac{2v^2 g_i}{\bar{g}_{\mathrm{N}} + g_l} + \frac{\kappa_i c}{a}\right)\bar{u}_N,\ \forall i \in F.$$

The respective eigenvector is

$$\left[\begin{array}{cccc} \mathbf{0}_{n_F} & \frac{1}{\bar{g}_{\mathrm{I}}} g_I & -\frac{c}{a} & -\frac{1}{b}\left(\frac{2v^2}{\bar{g}_{\mathrm{N}}+g_l} g_F + \frac{c}{a}\kappa\right) \end{array}\right]^T \bar{u}_N,$$

for some $\bar{u}_N \neq 0$ and corresponding eigenvalue $-a$.

If (A.4) does not hold, then $-a$ is an eigenvalue if $\bar{u}_N = 0$. By contradiction, substituting $\bar{u}_N = 0$ and $\lambda = -a \neq 0$ into (A.2c) yields $u_\phi = 0$. Substituting $u_\phi = \bar{u}_N = u_{F_i} = 0$ for all $i \in N$ into (A.2a) yields $\hat{u} = \mathbf{0}_{n_F}$. Substituting $\bar{u}_N = 0$ into (A.2b) yields

$$\left(v^2 - a\right) u_{I_i} = 0 \overset{(3.28)}{\Rightarrow} u_{I_i} = 0 \quad \forall i \in I.$$

Therefore, $u = \mathbf{0}_{n+1+n_F}$ and $-a$ cannot be an eigenvalue of $J_{SC}(g)$.

When $\lambda \neq -a$, then by (A.2d)

$$\hat{u} = \frac{a}{\lambda + a} u_F. \tag{A.5}$$

By (3.28), $g_i > 0\ \forall i \in I$, therefore $\bar{g}_{\mathrm{I}} = \sum_{i \in I} g_i > 0$. Summing (A.2b) over all $i \in I$ gives

$$\frac{2v^2}{\bar{g}_{\mathrm{N}} + g_l}\bar{g}_{\mathrm{I}}\bar{u}_F + \left(\frac{2v^2}{\bar{g}_{\mathrm{N}} + g_l}\bar{g}_{\mathrm{I}} - v^2 - \lambda\right)\bar{u}_I = 0$$

$$\begin{aligned} \overset{(\bar{g}_{\mathrm{I}} > 0)}{\Rightarrow} \bar{u}_F &= \left(\frac{\bar{g}_{\mathrm{N}} + g_l}{2v^2 \bar{g}_{\mathrm{I}}}\left(v^2 + \lambda\right) - 1\right)\bar{u}_I \\ &= f_{\bar{u}_F}(\lambda)\,\bar{u}_I. \end{aligned} \tag{A.6}$$

Substituting (A.5) into (A.2a) and summing over all $i \in F$ gives

$$\left(\frac{2v^2\bar{g}_{\mathrm{F}}}{\bar{g}_{\mathrm{N}}+g_l}-v^2-\lambda-b+\frac{ab}{\lambda+a}\right)\bar{u}_F+\frac{2v^2\bar{g}_{\mathrm{F}}}{\bar{g}_{\mathrm{N}}+g_l}\bar{u}_I$$

$$\begin{aligned}\overset{(A.6)}{=}&\left[\left(\frac{2v^2\bar{g}_{\mathrm{F}}}{\bar{g}_{\mathrm{N}}+g_l}-v^2-\lambda-b+\frac{ab}{\lambda+a}\right)f_{\bar{u}_F}(\lambda)\right.\\&\left.+\frac{2v^2\bar{g}_{\mathrm{F}}}{\bar{g}_{\mathrm{N}}+g_l}\right]\bar{u}_I \qquad (A.7)\\=&f_{\bar{u}_I}(\lambda)\,\bar{u}_I=\bar{\kappa}u_\phi.\end{aligned}$$

Multiplying (A.2c) by $\bar{\kappa}$ yields

$$\lambda\bar{\kappa}u_\phi=\bar{\kappa}c\left(\bar{u}_F+\bar{u}_I\right)\overset{(A.6)}{=}\frac{\bar{\kappa}c\left(\bar{g}_{\mathrm{N}}+g_l\right)}{2v^2\bar{g}_{\mathrm{I}}}\left(v^2+\lambda\right)\bar{u}_I.$$

Plugging (A.7) above yields

$$\left[\lambda f_{\bar{u}_I}(\lambda)-\bar{\kappa}c\frac{\bar{g}_{\mathrm{N}}+g_l}{2v^2\bar{g}_{\mathrm{I}}}\left(v^2+\lambda\right)\right]\bar{u}_I=0. \qquad (A.8)$$

Equation (A.8) implies that either the first term or $\bar{u}_I$ is zero. We will distinguish between the two cases:

- Let $\bar{u}_I=0$. Substituting $\bar{u}_I=0$ into (A.6) yields $\bar{u}_F=0$ and thus $\bar{u}_N=\bar{u}_I+\bar{u}_F=0$. By substituting (A.5) and $\bar{u}_F=\bar{u}_N=0$ into (A.2a) and summing over all $i\in F$ we get $u_\phi=0$. Moreover, substituting $\bar{u}_I=\bar{u}_F=0$ into (A.2b) results in

$$\mathbf{0}_{n_I}=-\left(v^2+\lambda\right)u_I \qquad (A.9)$$

  Equation (A.9) can be satisfied either when $u_I=\mathbf{0}_{n_I}$ or $\lambda=-v^2$. If $u_I=\mathbf{0}_{n_I}$ in

(A.9), by substituting $u_\phi = 0$ and (A.5) into (A.2a) we get

$$\left(v^2 + \lambda + b - \frac{ab}{\lambda + a}\right) u_F = \mathbf{0}_{n_F}. \tag{A.10}$$

If $u_F = \mathbf{0}_{n_F}$ then by (A.2d) $\hat{u} = \mathbf{0}_{n_F}$ and $u = \mathbf{0}_{n+1+n_F}$ cannot be an eigenvector of (3.27). Therefore, $u_F \neq \mathbf{0}_{n_F}$ which means that the first term in (A.10) is zero. Multiplying the first term in (A.10) by $\lambda + a$ and rearranging the terms results in (3.29). Equation (3.29) is a second order polynomial with respect to λ whose discriminant is

$$\begin{aligned}\Delta &= \left(a + b + v^2\right)^2 - 4av^2 \\ &= \left(a - v^2\right)^2 + b^2 + 2ab + 2bv^2 > 0.\end{aligned}$$

Therefore, it has two distinct solutions λ_1, λ_2. We can check that there exist $2n_F - 2$ eigenvalue-eigenvector pairs of $J_{SC}(g)$ of the form

$$\left(\lambda_1, \begin{bmatrix} e_1 - e_i & \mathbf{0}_{n_I} & 0 & \frac{a(e_1 - e_i)}{\lambda_1 + a} \end{bmatrix}^T\right), \qquad i = 2, \ldots n_F;$$
$$\left(\lambda_2, \begin{bmatrix} e_1 - e_i & \mathbf{0}_{n_I} & 0 & \frac{a(e_1 - e_i)}{\lambda_2 + a} \end{bmatrix}^T\right), \qquad i = 2, \ldots n_F;$$

that satisfy (A.2). In fact, there exist *exactly* $2n_F - 2$ eigenvalues of this form. By (A.2a)

$$\underbrace{\left(\frac{2v^2}{\bar{g}_{\mathrm{N}} + g_l} g_F \mathbf{1}_{n_F}^T - v^2 \mathbb{I}_{n_F}\right)}_{J_F(g)} u_F = \left(b - \frac{ab}{\lambda + a} + \lambda\right) u_F,$$

i.e., $\left(\left(b - \frac{ab}{\lambda + a} + \lambda\right), u_F\right)$ is an eigenvalue-eigenvector pair of $J_F(g)$. Matrix $J_F(g)$

is a $n_F \times n_F$ RPSI matrix. By Lemma 2, there exist exactly $n_F - 1$ eigenvalue-eigenvector pairs for each λ_i, $i \in \{1, 2\}$, that satisfy $\bar{u}_F = 0$. Therefore, $2\,(n_F - 1)$ in total.

If $\lambda = -v^2$ in (A.9), then by substituting $u_\phi = 0$ and (A.5) into (A.2a) gives

$$\left(b + \frac{ab}{-v^2 + a}\right) u_F = \mathbf{0}_{n_F} \overset{(\lambda \neq -a)}{\Rightarrow} u_F = \mathbf{0}_{n_F}.$$

When $u_F = \mathbf{0}_{n_F}$, by (A.2d) $\hat{u} = \mathbf{0}_{n_F}$. Since $\bar{u}_F = 0$, we can rewrite (A.9) as

$$\underbrace{\left(\frac{2v^2}{\bar{g}_\mathrm{N} + g_l} g_I \mathbf{1}_{n_I}^T - v^2 \mathbb{I}_{n_I}\right)}_{J_I(g)} u_I = \lambda u_I,$$

i.e., (λ, u_I) is an eigenvalue-eigenvector pair of $J_I(g)$ that satisfies $\bar{u}_N = 0$. Matrix $J_I(g)$ is a $n_I \times n_I$ RPSI matrix. By Lemma 2 there exist exactly $n_I - 1$ eigenvalue-eigenvector pairs that satisfy $\bar{u}_I = 0$ and these are

$$\left(-v^2, \begin{bmatrix} \mathbf{0}_{n_I} & e_1 - e_i & 0 & \mathbf{0}_{n_F} \end{bmatrix}\right), \quad i = 1, \ldots, n_I - 1.$$

- If $\bar{u}_I \neq 0$, then by (A.8)

$$\begin{aligned} & \lambda f_{\bar{u}_I}(\lambda) - \bar{\kappa} c \frac{\bar{g}_\mathrm{N} + g_l}{2v^2 \bar{g}_\mathrm{I}} \left(v^2 + \lambda\right) = 0 \\ \Rightarrow & -\lambda^3 + \lambda^2 \left(-\tilde{\lambda}\left(\bar{g}_\mathrm{N}\right) - v^2 - b\right) + \\ & + \lambda \left(-v^2 \left(\tilde{\lambda}\left(\bar{g}_\mathrm{N}\right) + b\right) - \bar{\kappa} c + \frac{2bv^2 \bar{g}_\mathrm{I}}{\bar{g}_\mathrm{N} + g_l}\right) - \bar{\kappa} c v^2 \\ & + \frac{ab\lambda}{\lambda + a} \left(v^2 + \lambda - \frac{2v^2 \bar{g}_\mathrm{I}}{\bar{g}_\mathrm{N} + g_l}\right) = 0. \end{aligned}$$

We multiply both sides with $-(\lambda + a)$ and group terms together to obtain (3.30).

Finally, the computation of (3.30a) is based on the assumption $\lambda \neq -a$, which we have shown is true for all $g \in \mathbb{R}^n$ such that $a \neq v^2 - \frac{2v^2\bar{g}_{\mathrm{N}}}{\bar{g}_{\mathrm{N}}+g_l}$. When $a = v^2 - \frac{2v^2\bar{g}_{\mathrm{N}}}{\bar{g}_{\mathrm{N}}+g_l}$, then $\lambda = -a$ is an eigenvalue of $J_{SC}(g)$. However, if we substitute $\lambda = -a$ into (3.29) we find that

$$(-a)^2 + (a + b + v^2)(-a) + av^2 = ab \neq 0,$$

i.e., $\lambda = -a$ is not a root of (3.29). Therefore, when $a = v^2 - \frac{2v^2\bar{g}_{\mathrm{N}}}{\bar{g}_{\mathrm{N}}+g_l}$, the statement of Lemma 3 is consistent only if $\lambda = -a$ is a root of (3.30a).

$$\begin{aligned}
&\bar{\kappa}acv^2 - a\left(av^2\tilde{\lambda} + \bar{\kappa}c\left(a + v^2\right)\right) + \\
&+ a^2\left(\bar{\kappa}c + v^2(a + b) - \frac{2bv^2\bar{g}_{\mathrm{I}}}{\bar{g}_{\mathrm{N}} + g_l} + \tilde{\lambda}\left(a + v^2\right)\right) - \\
&- a^3\left(b + a + v^2 + \tilde{\lambda}\right) + a^4 \\
=&a^2b\underbrace{\left(v^2 - \frac{2v^2\bar{g}_{\mathrm{I}}}{\bar{g}_{\mathrm{N}} + g_l}\right)}_{a} - a^3b = 0,
\end{aligned}$$

In the special case where $g \in \mathbb{R}^n$ is such that $a = v^2 - \frac{2v^2\bar{g}_{\mathrm{N}}}{\bar{g}_{\mathrm{N}}+g_l}$, then the derivation of (3.30a) discards the root $\lambda = -a = -v^2 + \frac{2v^2\bar{g}_{\mathrm{N}}}{\bar{g}_{\mathrm{N}}+g_l}$. Therefore, the statement of the lemma is consistent for all $g \in \mathbb{R}^n$. □

Lemma 4.

Proof. (1) We start by observing that the only term in the first column of the Ruth-Hurwitz table that is affected by $b > 0$ is b_1. Taking $a \to 0^+$ in (3.34) yields

$$\lim_{a\to 0^+} b_1\left(g^*\right) = \left(b + \tilde{\lambda}^*\right)\left(v^{*2} + \frac{\bar{\kappa}c^*}{b + \tilde{\lambda}^* + v^{*2}}\right) - \tag{A.11}$$

$$- \frac{2bv^{*2}\bar{g}_{\mathrm{I}}^*}{\bar{g}_{\mathrm{N}}^* + g_l} \tag{A.12}$$

$$= f(\bar{g}_{\mathrm{N}}^*) - \frac{2bv^{*2}\bar{g}_{\mathrm{I}}^*}{\bar{g}_{\mathrm{N}}^* + g_l}. \tag{A.13}$$

We will study the sign of all terms of b_1 in (A.13) for $\{(g^*,\ \phi^*,\ \hat{g}^*) \in \mathcal{E}_s : \bar{g}_{\mathrm{N}}^* \geq g_l\}$ and for different values of $b > 0$.

Notice that $\bar{g}_{\mathrm{N}}^* > g_l \overset{(3.31)}{\Rightarrow} \tilde{\lambda}^* < 0$ and

$$\frac{d\tilde{\lambda}^*}{d\bar{g}_{\mathrm{N}}^*} = \frac{2{v^*}^2}{\left(\bar{g}_{\mathrm{N}}^* + g_l\right)^2}\left(\bar{g}_{\mathrm{N}}^* - 2g_l\right),$$

which is negative in $[g_l, 2g_l)$, positive in $(2g_l, +\infty)$, and zero for $\bar{g}_{\mathrm{N}}^* = 2g_l$. Therefore, $\tilde{\lambda}^*$ is strictly decreasing in $[g_l, 2g_l)$, strictly increasing in $(2g_l, +\infty)$, and

$$\min_{\bar{g}_{\mathrm{N}}^* \in [g_l, +\infty)} \tilde{\lambda}^* = \tilde{\lambda}(2g_l) = -\frac{E^2}{27}.$$

Let $h(\bar{g}_{\mathrm{N}}^*) = \lambda(\bar{g}_{\mathrm{N}}^*) + b$ and $b \in \left(0, \frac{E^2}{27}\right)$

$$h(g_l) = \tilde{\lambda}(g_l) + b = b > 0, \quad h(2g_l) = \tilde{\lambda}(2g_l) + b < 0.$$

Since $h(\bar{g}_{\mathrm{N}}^*)$ is continuous on $\bar{g}_{\mathrm{N}}^*$, by the IVT there exists $\xi_b \in (g_l, 2g_l)$ such that $h(\xi_b) = 0$, or, equivalently, $h(g_l + m_b) = 0$ for $m_b = \xi_b - g_l$. Since h is strictly decreasing

on $(g_l, 2g_l)$, ξ_b is the unique intersection of h with the zero axis and $h(\bar{g}_{\mathrm{N}}^*) > 0$ for $\bar{g}_{\mathrm{N}}^* \in (g_l, g_l + m_b)$.

Similarly, for $\bar{g}_{\mathrm{N}}^* \in (2g_l, +\infty)$,

$$h(2g_l) = \tilde{\lambda}(2g_l) + b < 0, \quad \lim_{\bar{g}_{\mathrm{N}}^* \to +\infty} \tilde{\lambda}(\bar{g}_{\mathrm{N}}^*) + b = b > 0.$$

Since $h(\bar{g}_{\mathrm{N}}^*)$ is continuous, strictly increasing in $(2g_l, +\infty)$, there exists unique $\Xi_b \in (2g_l, +\infty)$ that $h(\Xi_b) = 0$, or, equivalently, $h(g_l + M_b) = 0$ for $M_b = \Xi_b - g_l$. When $b \in \left(0, \frac{E^2}{27}\right)$, combining the two results leads to

$$h(\bar{g}_{\mathrm{N}}^*) = \lambda(\bar{g}_{\mathrm{N}}^*) + b : \begin{cases} \geq 0, & \forall \bar{g}_{\mathrm{N}}^* \in [g_l, g_l + m_b) \\ \leq 0, & \forall \bar{g}_{\mathrm{N}}^* \in [g_l + m_b, g_l + M_b) \\ \geq 0, & \forall \bar{g}_{\mathrm{N}}^* \in [g_l + M_b, +\infty) \end{cases} \tag{A.14}$$

Moreover,

$$(3.32) \Rightarrow c^* = \left(\frac{v^{*2}}{\bar{g}_{\mathrm{N}} + g_l} (g_l - \bar{g}_{\mathrm{N}}^*) \right)^2 > 0,$$
$$(3.31) \Rightarrow \tilde{\lambda}^* + v^{*^2} + b = 2v^{*^2} \left(1 - \frac{\bar{g}_{\mathrm{N}}^*}{\bar{g}_{\mathrm{N}}^* + g_l} \right) + b > 0.$$

By substituting the above into (A.13) leads to $f(\bar{g}_{\mathrm{N}}^*) < 0$ for $g_l + m_b \leq \bar{g}_{\mathrm{N}}^* \leq g_l + M_b$ and subsequently $b_1(g^*) < 0$. By the Ruth-Hurwitz criterion, when $b \in \left(0, \frac{E^2}{27}\right)$, then $\{(g^*,\ \phi^*,\ \hat{g}^*) \in \mathcal{E}_s : g_l + m_b \leq \bar{g}_{\mathrm{N}}^* \leq g_l + M_b\}$ is unstable.

(2) Let $b_1, b_2 \in \left(0, \frac{E^2}{27}\right)$, $b_1 < b_2$. By applying the IVT on $(g_l, 2g_l)$ we have shown

that there exist unique $0 < m_{b_1}, m_{b_2} \leq g_l$ such that

$$\begin{aligned}
&\tilde{\lambda}(g_l + m_{b_1}) + b_1 = \tilde{\lambda}(g_l + m_{b_2}) + b_2 = 0 \\
\Rightarrow &\tilde{\lambda}(g_l + m_{b_1}) - \tilde{\lambda}(g_l + m_{b_2}) = b_2 - b_1 > 0 \\
\Rightarrow &\tilde{\lambda}(g_l + m_{b_1}) > \tilde{\lambda}(g_l + m_{b_2}).
\end{aligned}$$

Since $\tilde{\lambda}$ is strictly decreasing in $(g_l, 2g_l)$, then

$$g_l + m_{b_1} < g_l + m_{b_2} \Rightarrow m_{b_1} < m_{b_2}. \tag{A.15}$$

Moreover, by applying the IVT on $(2g_l, +\infty)$ we have shown that there exist $g_l < M_{b_1}, M_{b_2} < +\infty$ such that

$$\begin{aligned}
&\tilde{\lambda}(g_l + M_{b_1}) + b_1 = \tilde{\lambda}(g_l + M_{b_2}) + b_2 = 0 \\
\Rightarrow &\tilde{\lambda}(g_l + M_{b_1}) - \tilde{\lambda}(g_l + M_{b_2}) = b_2 - b_1 > 0 \\
\Rightarrow &\tilde{\lambda}(g_l + M_{b_1}) > \tilde{\lambda}(g_l + M_{b_2})
\end{aligned}$$

Since $\tilde{\lambda}$ is strictly increasing in $(2g_l, +\infty)$, then

$$g_l + M_{b_1} > g_l + M_{b_2} \Rightarrow M_{b_1} > M_{b_2}. \tag{A.16}$$

□

Appendix B

Implemented percentage change in total natural gas consumption in Chapter 5

The following appendix provides The percentage change in total natural gas consumption used as input to NANGAM from every model and for each country and scenario in Chapter 5.

Table B.1: Percentage change in total natural gas consumption of Mexico in NANGAM for inputs from GENeSYS-MOD.

	Mexico, GENeSYS-MOD							
	2015	2020	2025	2030	2035	2040	2045	2050
Scenario 2	0.00	-4.10	-5.47	-7.74	-8.57	-9.04	-9.08	-10.60
Scenario 3	0.00	-8.36	-10.92	-11.08	-10.44	-11.78	-13.13	-14.78

Table B.2: Percentage change in total natural gas consumption of Mexico in NANGAM for inputs from ReEDS2.0.

	Mexico, ReEDS2.0							
	2015	2020	2025	2030	2035	2040	2045	2050
Scenario 1	0.00	-0.82	-11.62	-15.49	-22.61	-20.49	-14.72	-9.39
Scenario 2	0.00	-12.65	-17.76	-21.72	-22.43	-18.05	-14.31	-12.22
Scenario 3	0.00	-13.89	-17.69	-21.39	-21.48	-18.74	-14.84	-12.12

Table B.3: Percentage change in total natural gas consumption of Canada in NANGAM for inputs from NATEM.

	Canada, NATEM							
	2015	2020	2025	2030	2035	2040	2045	2050
Scenario 1	0.00	-0.39	-6.97	-6.28	-8.34	-9.47	-9.57	-8.32
Scenario 2	0.00	-0.05	-3.49	-1.97	- 2.80	-1.40	1.07	6.63
Scenario 3	0.00	-5.89	-7.68	-7.22	-7.89	-7.24	-1.39	5.20

Table B.4: Percentage change in total natural gas consumption of Canada in NANGAM for inputs from ReEDS2.0.

	Canada, ReEDS2.0							
	2015	2020	2025	2030	2035	2040	2045	2050
Scenario 1	0.00	-0.39	-6.97	-6.28	-8.34	-9.47	-9.57	-8.32
Scenario 2	0.00	-0.05	-3.49	-1.97	-2.80	-1.40	1.07	6.63
Scenario 3	0.00	-5.89	-7.68	-7.22	-7.89	-7.24	-1.39	5.20

Table B.5: Percentage change in total natural gas consumption of U.S. in NANGAM for inputs from NEMS-AEO2019.

	U.S., NEMS-AEO2019							
	2015	2020	2025	2030	2035	2040	2045	2050
Scenario 2	0.00	-0.17	-2.75	-6.35	-10.50	-11.34	-12.73	-12.86
Scenario 3	0.00	-0.07	-2.80	-8.01	-11.81	-12.54	-13.72	-13.78

Table B.6: Percentage change in total natural gas consumption of U.S. in NANGAM for inputs from ReEDS2.0.

	U.S., ReEDS2.0							
	2015	2020	2025	2030	2035	2040	2045	2050
Scenario 1	0.00	-1.51	-5.63	-10.73	-13.51	-15.71	-12.61	-9.84
Scenario 2	0.00	-4.80	-9.68	-15.01	-17.17	-18.64	-16.63	-13.11
Scenario 3	0.00	-8.37	-12.99	-18.04	-20.23	-20.62	-19.66	-18.61

APPENDIX B. IMPLEMENTED PERCENTAGE CHANGE IN TOTAL NATURAL GAS CONSUMPTION IN CHAPTER 5

Appendix C

IGAULTM Model Formulation, Data Collection, and Calibration Process

C.1 Problem Formulation and Solution Method

The optimization problem of the representative producer of livestock product lp in region r is written as

$$\min_{q^P_{r,t,lp}, q^A_{r,t,lp} \geq 0} \quad \sum_t \left(\pi_{r,t,lp} \cdot q^P_{r,t,lp} - \int_0^{q^P_{r,t,lp}} \left(\alpha^P_{r,t,lp} + \beta^P_{r,t,lp} \cdot s - \theta^A_{r,t,lp} q^A_{r,t,lp} \right) ds \right)$$

$$\text{subject to} \quad q^A_{r,t,lp} = \alpha^A_{r,t,lp} \cdot \frac{\pi_{r,t,lp}}{\bar{p}^A_{r,t,lp}} \cdot q^P \quad \perp \quad \mu^A_{r,t,lp} \tag{C.1}$$

The simplified Karush-Kuhn Tacker (KKT) conditions of (C.1) for all livestock

products lp and in all regions r are written as

$$\begin{aligned}
&q^P_{r,t,lp} \geq 0, \quad \alpha^P_{r,t,lp} + \beta^P_{r,t,lp} q^P_{r,t,lp} - \theta^A_{r,t,lp} q^A_{r,t,lp} - \alpha^A_{r,t,lp} \frac{\pi_{r,t,lp}}{\bar{p}^A_{r,t,lp}} \mu^A_{r,t,lp} - \pi_{r,t,lp} \geq 0, \\
&q^P_{r,t,lp} \cdot \left(\alpha^P_{r,t,lp} + \beta^P_{r,t,lp} q^P_{r,t,lp} - \theta^A_{r,t,lp} q^A_{r,t,lp} - \alpha^A_{r,t,lp} \frac{\pi_{r,t,lp}}{\bar{p}^A_{r,t,lp}} \mu^A_{r,t,lp} - \pi_{r,t,lp} \right) = 0, \quad \forall t; \\
&q^A_{r,t,lp} \geq 0, \quad -\theta^A_{r,t,lp} q^P_{r,t,lp} + \mu^A_{r,t,lp} \geq 0, \quad q^A_{r,t,lp} \cdot \left(-\theta^A_{r,t,lp} q^P_{r,t,lp} + \mu^A_{r,t,lp} \right) = 0, \quad \forall t; \\
&\mu^A_{r,t,lp} : \text{free}, \quad q^A_{r,t,lp} - \alpha^A \frac{\pi_{r,t,lp}}{\bar{p}^A_{r,t,lp}} q^P = 0, \quad \mu^A_{r,t,lp} \cdot \left(q^A_{r,t,lp} - \alpha^A \frac{\pi_{r,t,lp}}{\bar{p}^A_{r,t,lp}} q^P \right) = 0, \quad \forall t.
\end{aligned} \tag{C.2}$$

The first three conditions in (C.2) are written compactly for all regions r, years t, and livestock products lp, as

$$0 \leq q^P_{r,t,lp} \quad \perp \quad \alpha^P_{r,t,lp} + \beta^P_{r,t,lp} q^P_{r,t,lp} - \theta^A_{r,t,lp} q^A_{r,t,lp} - \alpha^A_{r,t,lp} \frac{\pi_{r,t,lp}}{\bar{p}^A_{r,t,lp}} \mu^A_{r,t,lp} - \pi_{r,t,lp} \geq 0 \tag{C.3}$$

The symbol $\perp$ is used to represent that either the left-hand side, or the right-hand side (or both) are zero. The two sides are thus complementary and (C.3) is called a complementarity condition. Equation (C.3) encapsulates the micro-economic principle of perfect competition, where production is positive when the marginal cost $\left(\alpha^P_{r,t,lp} + \beta^P_{r,t,lp} q^P_{r,t,lp}\right)$ adjusted for the marginal increase in productivity due to antimicrobials $\left(\theta^A_{r,t,lp} q^A_{r,t,lp}\right)$ and the marginal payment for antimicrobials $\left(\alpha^A_{r,t,lp} \frac{\pi_{r,t,lp}}{\bar{p}^A_{r,t,lp}} \mu^A_{r,t,lp}\right)$ needs to clear with the market price $(\pi_{r,t,lp})$. When the adjusted marginal cost is higher than the market price, *i.e.,*

$$\alpha^P_{r,t,lp} + \beta^P_{r,t,lp} \cdot q^P_{r,t,lp} - \theta^A_{r,t,lp} q^P_{r,t,lp} - \alpha^A_{r,t,lp} \frac{\pi_{r,t,lp}}{\bar{p}^A_{r,t,lp}} \mu^A_{r,t,lp} - \pi_{r,t,lp} > 0,$$

the complemetarity condition implies that production is zero. Under perfect competition the adjusted marginal cost can-not be smaller than the market price, as that would mean that producers accrue a rent, therefore the right-hand side of (C.3) is always greater or equal than zero and (C.3) is consistent with our assumption.

The next three conditions in (C.2) are written as

$$0 \leq \quad q^A_{r,t,lp} \quad \perp \quad \mu^A_{r,t,lp} - \theta^A_{r,t,lp} q^P_{r,t,lp} \quad \geq 0, \qquad \forall r,t,lp. \tag{C.4}$$

The right-hand condition in (C.4) implies that producers decide on the use of antimicrobials by comparing the marginal benefit from increased productivity $\left(\theta^A_{r,t,lp} q^P_{r,t,lp}\right)$ to the payment for antimicrobials $\left(\mu^A_{r,t,lp}\right)$.

The last three conditions in (C.2) are written as

$$\text{free} \quad : \mu^A_{r,t,lp} \quad \perp \quad q^A_{r,t,lp} - \alpha^A \frac{\pi_{r,t,lp}}{\bar{p}^A_{r,t,lp}} q^P_{r,t,lp} \qquad = 0, \qquad \forall r,t,lp. \tag{C.5}$$

Each livestock trader decides the transported quantity that maximizes their profit, *i.e.*,

$$\max_{q^T_{r,t,lp} \geq 0} \sum_t \left(\left(\pi_{r,t,lp} - \pi_{rr,t,lp} - c^T_{r,rr,t,lp} \right) \cdot q^T_{r,rr,t,lp} \right) \tag{C.6}$$

The respective KKT conditions are

$$0 \leq \quad q^T_{r,rr,t,lp} \quad \perp \quad c^T_{r,rr,t,lp} + \pi_{rr,t,lp} - \pi_{r,t,lp} \quad \geq 0, \qquad \forall r,t,lp. \tag{C.7}$$

The regional meat balance constraints are

$$q^C_{r,t,lp} = q^P_{r,t,lp} - \underbrace{\sum_{rr} q^T_{rr,r,t,lp}}_{\text{Exports}} + \underbrace{\sum_{rr} q^T_{r,rr,t,lp}}_{\text{Imports}} \tag{C.8}$$

The market price in each region is computed via the inverse demand function

$$\pi_{r,t,lp} = f^C_{r,t,lp}\left(q^C_{r,t,lp}\right) = \alpha^C_{r,t,lp} + \beta^C_{r,t,lp} \cdot q^C_{r,t,lp} \tag{C.9}$$

A point $\left(\pi^*_{r,t,lp}, q^{P*}_{r,t,lp}, q^{C*}_{r,t,lp}, q^{T*}_{rr,r,t,lp}, q^{A*}_{r,t,lp}\right)$ that satisfies the best-responses of all agents in the market, *i.e.,* all KKT conditions, and the regional balance constraints is a Nash Equilibrium (NE) of the market. Conditions (C.3), (C.4), (C.5), (C.7), along with (C.8), (C.9) compute a NE and can be rewritten as complementarity conditions in an integrated framework.

$$0 \leq q^P_{r,t,lp} \quad \perp \quad \begin{array}{r} \alpha^P_{r,t,lp} + \beta^P_{r,t,lp} q^P_{r,t,lp} - \theta^A_{r,t,lp} q^A_{r,t,lp} \\ -\alpha^A_{r,t,lp} \frac{\pi_{r,t,lp}}{\bar{p}^A_{r,t,lp}} \mu^A_{r,t,lp} - \pi_{r,t,lp} \end{array} \geq 0, \quad \forall r,t,lp; \tag{C.10}$$

$$0 \leq q^A_{r,t,lp} \quad \perp \quad \mu^A_{r,t,lp} - \theta^A_{r,t,lp} q^P_{r,t,lp} \geq 0, \quad \forall r,t,lp; \tag{C.11}$$

$$\text{free} : \mu^A_{r,t,lp} \quad \perp \quad q^A_{r,t,lp} - \alpha^A_{r,t,lp} \frac{\pi_{r,t,lp}}{\bar{p}^A_{r,t,lp}} q^P = 0, \quad \forall r,t,lp; \tag{C.12}$$

$$0 \leq q^T_{r,rr,t,lp} \quad \perp \quad c^T_{r,rr,t,lp} + \pi_{rr,t,lp} - \pi_{r,t,lp} \geq 0, \quad \forall r,t,lp; \tag{C.13}$$

$$\text{free} : \pi_{r,t,lp} \quad \perp \quad q^C_{r,t,lp} - q^P_{r,t,lp} + \sum_{rr} \bar{q}^T_{rr,r,t,lp} - \sum_{rr} \bar{q}^T_{r,rr,t,lp} = 0, \quad \forall r,t,lp; \tag{C.14}$$

$$\text{free} : q^C_{r,t,lp} \quad \perp \quad \pi_{r,t,lp} - \alpha^C - \beta^C \cdot q^C_{r,t,lp} = 0, \quad \forall r,t,lp. \tag{C.15}$$

The problem defined by (C.10), (C.11), (C.12), (C.13), (C.14), (C.15) is a Mixed Complementarity Problem (MCP). Finding a NE of the market is equivalent to finding

a solution to the MCP. We formulate the MCP in the General Algebraic Modeling System (GAMS) and solve it using the PATH solver (Ferris and Munson, 2000).

C.2 Data Collection

We collect historical production and trade data for poultry, beef, and pork of all 214 countries and areas available in FAOSTAT (FAOSTAT, 2020) for the period 2000-2018. The FAOSTAT database for quantities and values in 2015 is the most complete in the last five years and for that we pick 2015 as our base year. We aggregate FAOSTAT meat products into beef, pork, and poultry, as shown in Table C.2. We project all production quantities from 2015 through 2028 using growth rates retrieved from OECD's projections. When a country's growth rate was not available in OECD, we used the growth rate of the next larger region available in OECD. The mapping between OECD countries and E-GLT countries and regions is detailed in Table C.1. We project livestock trade between regions using the growth rate of the exports from the exporting country. For aggregate regions, we first project country-level production and trade through 2028 and then aggregate the respective quantities. In Table C.1 we illustrate which OECD region's growth rate was used for each country.

Moreover, we also retrieve the 2015 gross production value for all countries. We compute production prices by dividing the production value with the produced quantity of each country. For aggregate regions, we divide the weighted mean production

value with the sum of the production of all regions. The production values of the Republic of Korea and the United Kingdom were not available for 2015. For these two countries, we compute the production prices for 2010 and project them from 2010 using FAO's production price index. Indian 2015 production prices were also not available and were retrieved from (WB, 2011).

Given production and trade from 2015 to 2028, Reference consumption for the periods 2015-2028 is computed such that the regional balance of quantities is met, *i.e.,*

$$\bar{q}^{C}_{r,t,lp} = \bar{q}^{P}_{r,t,lp} - \underbrace{\sum_{rr} \bar{q}^{T}_{rr,r,t,lp}}_{\text{Exports}} + \underbrace{\sum_{rr} \bar{q}^{T}_{r,rr,t,lp}}_{\text{Imports}} \qquad \forall r, t, lp,$$

where $\bar{q}^{C}_{r,t,lp}$ is the reference consumption, $\bar{q}^{P}_{r,t,lp}$ is the reference production, of region r, in year t, of livestock product lp, between 2015-2028 and of livestock product lp. Moreover, $\bar{q}^{T}_{r,rr,t,lp}$ denotes the reference exports quantity from region rr to region r.

Our method of computing regional consumption is a variation of the method used by FAOSTAT (FAOSTAT, 2020) since we account for both human consumption and consumption from the processing sector. This is due to our focus on production changes.

We collect the antimicrobial use per population correction unit (PCU) in 2013 ($au^{A}_{r,lp}$) as well as the projected percentage change in antimicrobial use ($\beta^{A}_{r,lp}$) in 2030 with respect to 2013 for all 70 countries and livestock products reported in the

database of The Center for Disease Dynamics Economics & Policy (CDDEP, 2017). Using the country specific meat production and antimicrobial intensity in 2013, as well as the value for the population correction unit $\left(au_{lp}^{\mathrm{PCU}}\right)$ of each livestock product (FDA, 2017), we compute the use of antimicrobials for each livestock product lp in each country r as

$$\bar{q}_{0r,lp}^{A}\left(\mathrm{mg}\right)=\bar{q}_{0r,lp}^{P}\left(\mathrm{tons}\right)\cdot au_{r,lp}^{A}\left(\frac{\mathrm{mg}}{\mathrm{PCU}}\right)\cdot\alpha_{lp}^{pcu}\left(\frac{\mathrm{PCU}}{\mathrm{ton}}\right)$$

where $\bar{q}_{0,r,lp}^{A}$ is the reference consumption of antimicrobials, $\bar{q}_{0,r,lp}^{P}$ is the reference production of region r and livestock product lp in 2013. Assuming that yearly antimicrobial use at each region r and for every livestock product lp changes between 2013 and 2030 with a growth rate, then yearly antimicrobial use for all years between 2013 and 2028 are computed as

$$\bar{q}_{r,t,lp}^{A}=\bar{q}_{0r,lp}^{A}\left[\left(\beta_{r,lp}^{A}\right)^{\frac{1}{17}}-1\right]^{(t-2013)},\qquad\forall r,t,lp.$$

Following (NRC, 1999), we assume that antimicrobial use enhances livestock productivity, which in turn results in a decrease in the marginal cost of production. Table C.3 reports by how much the marginal cost of production would increase in the absence of antimicrobials, as found in (NRC, 1999).

The own-price demand elasticity of each livestock product for all European, Asian and North American countries are retrieved from (A. Gallet, 2012). For the aggregate

regions Rest Of World and Rest Of Americas and for each livestock product we use the total own-price demand elasticity reported in (Liu, 2016). For the two remaining countries, Rusia and Brazil, we use for all three products the own-price elasticities reported for meat in (Seale Jr et al., 2003).

Producers spend 3.75% of their ration cost for antimicrobials (NRC, 1999). Table C.4 reports feed ration cost as a percentage of total livestock production cost. We compute the share of the cost of antimicrobials as a percentage in the gross production cost to be

$$\alpha^{A}_{r,t,lp} = \frac{3.75}{100} \cdot \frac{frc_{r,t,lp}}{100}.$$

C.3 Calibration Process

In Section C.2 of the current Appendix we collect data on reference 2015 variables and project them to compute reference variables through 2028. Calibration is the process of adjusting model parameters, such that the results in the business-as-usual scenario match the collected data for all years between 2015 and 2028.

In Section C.1 of the current Appendix we formulate the model as a MCP. Therefore, by calibrating our model, we calculate unknown model parameters and prices such that the collected and projected Reference quantities for 2015 through 2028 $\left(\bar{q}^{P}_{r,t,lp}, \bar{q}^{C}_{r,t,lp}, \bar{q}^{A}_{r,t,lp}, \bar{q}^{T}_{r,t,lp},\right)$ and costs ($\bar{\text{mc}}_{r,t,lp}$) satisfy the KKT conditions (C.10), (C.11),(C.13), (C.14), (C.15).

First, we compute the production price which we use as a proxy of the marginal cost of production:

$$\bar{\text{mc}}_{r,lp} = \text{Production Price}\left(\frac{\$}{kg}\right) = \frac{\text{2015 Production Value (Million \$)}}{\text{2015 Quantity (kilo-tons)}}$$

Parameter $\theta^A_{r,t,lp}$ grasps the impact of the use of antimicrobials on the marginal cost of production. Its value is calibrated such that reference antimicrobial use $\bar{q}^A_{r,t,lp}$ decreases the marginal cost of production by $\gamma^A_{r,t,lp}$, *i.e.*,

$$\theta^A \bar{q}^A_{r,t,lp} = \gamma^A_{r,t,lp} \bar{\text{mc}}_{r,t,lp} \Rightarrow \theta^A_{r,t,lp} = \gamma^A_{r,t,lp} \frac{\bar{\text{mc}}_{r,t,lp}}{\bar{q}^A_{r,t,lp}}$$

Since $\bar{q}^A_{r,t,lp} > 0$ for all regions r, livestock products lp, in all years t, the complementarity condition (C.11) is satisfied when the right-hand side is zero, *i.e.*,

$$\text{(C.11)} \Rightarrow \bar{\mu}^A_{r,t,lp} = \theta^A_{r,t,lp} \cdot \bar{q}^P_{r,t,lp}, \qquad \forall r, t, lp. \tag{C.16}$$

Moreover, the country-level marginal cost of production is often assumed to be constant (Van Boeckel et al., 2015), which would imply that

$$\alpha^P_{r,t,lp} = \bar{\text{mc}}_{r,lp}, \qquad \beta^P_{r,t,lp} \to 0.$$

For computational reasons, we introduce a slope in the production function, such that $\beta^P_{r,t,lp} \neq 0$. Moreover, the marginal cost is further affected by the existence of antimicrobials. In the absence of antimicrobials, the marginal cost increases by $\gamma^A_{r,t,lp}$,

i.e.,

$$\alpha^P_{r,t,lp} = 0.85 \cdot \left(1 + \gamma^A_{r,t,lp}\right) \cdot \bar{\text{mc}}_{r,lp}, \quad \beta^P_{r,t,lp} = 0.15 \cdot \left(1 + \gamma^A_{r,t,lp}\right) \cdot \frac{\bar{\text{mc}}_{r,lp}}{\bar{q}^P_{r,t,lp}}. \tag{C.17}$$

Notice that with the above computations we retrieve the reference marginal cost, since

$$\theta^A_{r,t,lp}\bar{q}^A_{r,t,lp} = \gamma^A_{r,t,lp}\bar{\text{mc}}_{r,lp}, \quad \alpha^P_{r,t,lp} + \beta^P_{r,t,lp} \cdot \bar{q}^P_{r,t,lp} = \left(1 + \gamma^A_{r,t,lp}\right)\bar{\text{mc}}_{r,lp}$$

$$\Rightarrow \alpha^P_{r,t,lp} + \beta^P_{r,t,lp} \cdot \bar{q}^P_{r,t,lp} - \theta^A_{r,t,lp}\bar{q}^A_{r,t,lp} = \bar{\text{mc}}_{r,lp}.$$

By rearranging the right-hand side of (C.12), we find

$$\text{(C.12)} \Rightarrow \alpha^A \frac{\bar{\pi}_{r,t,lp}}{\bar{p}^A_{r,t,lp}} = \frac{\bar{q}^A_{r,t,lp}}{\bar{q}^P_{r,t,lp}} \tag{C.18}$$

Since $\bar{q}^P_{r,t,lp} > 0$ for all regions r, livestock products lp, in all years t, the complementarity condition (C.10) is satisfied when the right-hand side is zero. By substituting (C.16), (C.17), (C.18) into (C.10) we get

$$\alpha^P_{r,t,lp} + \beta^P_{r,t,lp}\bar{q}^P_{r,t,lp} - \theta^A_{r,t,lp}\bar{q}^A_{r,t,lp} - \alpha^A_{r,t,lp}\frac{\bar{\pi}_{r,t,lp}}{\bar{p}^A_{r,t,lp}}\bar{\mu}^A_{r,t,lp} - \bar{\pi}_{r,t,lp} = 0$$

$$\Rightarrow \bar{\pi}_{r,t,lp} = \alpha^P_{r,t,lp} + \beta^P_{r,t,lp}\bar{q}^P_{r,t,lp} - \theta^A_{r,t,lp}\bar{q}^A_{r,t,lp} - \frac{\bar{q}^A_{r,t,lp}}{\bar{q}^P_{r,t,lp}}\bar{\mu}^A_{r,t,lp} \tag{C.19}$$

The complementarity condition (C.13) of livestock traders implies that for connections where $\Delta\bar{q}^T_{r,rr,t,lp} = q^T_{r,rr,t,lp} - \bar{q}^T_{rr,r,t,lp} > 0$, the right-hand side of (C.13) is zero. The transportation costs $c^T_{r,rr,t,lp}$ are calibrated by substituting (C.19) into (C.13) to ensure that the right-hand side of (C.13) is zero for interconnections where $\Delta\bar{q}^T_{r,rr,t,lp} > 0$,

i.e.,

$$\bar{\pi_{rr,t,lp}} + c^T_{r,rr,t,lp} - \bar{\pi_{r,t,lp}} = 0 \Rightarrow c^T_{r,rr,t,lp} = \bar{\pi_{r,t,lp}} - \bar{\pi_{rr,t,lp}}.$$

By construction, our model computes net exports from region rr to region r. Notice that when $\bar{\pi}_{r,t,lp} < \bar{\pi}_{rr,t,lp}$ and net trade between two countries $\Delta\bar{q}^T_{r,rr,t,lp} > 0$, then $c^T_{r,rr,t,lp} < 0$. The negative sign implies that the production of region rr that is exported is heavily subsidised, to the extend that producers of the less competitive region rr can compete with producers in region r.

Whenever a trade partnership between region r and rr exists, we assume that trade can also happen in the opposite direction. If $c^T_{r,rr,t,lp} > 0$, we assume that $c^T_{rr,r,t,lp} = c^T_{r,rr,t,lp}$, meaning that the transportation cost from one region to another would be the same for the opposite route too. If $c^T_{r,rr,t,lp} \leq 0$ then we assign a transportation cost $c^T_{rr,r,t,lp} = 1.2 \cdot (\bar{\pi}_{rr,t,lp} - \bar{\pi}_{r,t,lp})$, meaning that the transportation cost is greater than the difference of the livestock prices of the two trading regions. Both computations force the right-hand side of (C.13) to be positive, which in turn leads to $q^T_{rr,r,t,lp} = 0$ as needed. The transportation cost in the latter case needs to be strictly greater than the price difference between the two regions. Due to lack of transportation cost data, we multiply the price difference by 1.2. The arbitrary assignment of the transportation costs of routes where $\Delta q^T_{rr,r,t,lp} = 0$ implies that our model allows for a change in the direction of net trade between two countries, but is biased against such change. Hence, solutions where $\Delta q^T_{r,rr,t,lp}$ is very close to zero could be biased and need to be further examined.

Reference regional consumption of each livestock product is calculated in Section C.2 of the current Appendix such that the regional production, consumption, and trade balance is met

$$\bar{q}^C_{r,t,lp} = \bar{q}^P_{r,t,lp} - \sum_{rr} \bar{q}^T_{rr,r,t,lp} + \sum_{rr} \bar{q}^T_{r,rr,t,lp},$$

and so (C.14) is trivially satisfied.

For the calibration of the parameters $\alpha^C_{r,t,lp}, \beta^C_{r,t,lp}$ of the inverse demand function (C.9) we use the retrieved own-price demand elasticities $\epsilon^C_{r,t,lp}$, reference consumption $\bar{q}^C_{r,t,lp}$, and the calculated price $\bar{\pi}_{r,t,lp}$ in (C.19). We compute $\alpha^C_{r,t,lp}, \beta^C_{r,t,lp}$ by solving a system of two equations for each region r, livestock product lp, and each year t,

$$\begin{cases} \bar{\pi}_{r,t,lp} = \alpha^C + \beta^C_{r,t,lp} \cdot \bar{q}^C_{r,t,lp} \\ \beta^C_{r,t,lp} \cdot \epsilon^C_{r,t,lp} = \frac{q^C_{r,t,lp}}{\bar{\pi}_{r,t,lp}} \end{cases}, \qquad \forall r, t, lp.$$

with respect to $\alpha^C_{r,t,lp}$, $\beta^C_{r,t,lp}$. The first equation is the definition of the inverse demand function and the second is derived from the definition of the the own-price demand elasticity, assuming $f^C\left(q^C_{r,t,lp}\right)$ to be linear.

C.4 Supplementary Tables

Table C.1: OECD – E-GLT regions mapping.

OECD region	**E-GLT countries**	**E-GLT Region**
Argentina	Argentina	ROA
EUROPE	Austria, Belgium, Bosnia and Herzegovina, Bulgaria, Croatia, Czechia, Estonia, Finland, Greece, Hungary, Ireland, Italy, Latvia, Lithuania, Norway, Romania, Poland, Portugal, Serbia, Slovakia, Slovenia, Sweeden	ROE
	Denmark	DNK
	France	FRA
	Germany	DEU
	Netherlands	NLD
	Spain	ESP
United Kingdom of Great Britain and Northern Ireland	United Kingdom	GBR

Table C.1: OECD – E-GLT regions mapping, continued.

OECD region	**E-GLT countries**	**E-GLT Region**
Russian Federation	Russia	RUS
United States of America	USA	USA
Canada	Canada	CAN
Mexico	Mexico	MEX
Brazil	Brazil	BRA
Developing Countries	Algeria, Kuwait, Lebanon, Morocco,	ROW
	Sri Lanka	
	Dominican Republic	ROA
Developed Countries	Australia, Kuwait, United Arab Emirates	ROW
Asia	Bangladesh, Tunisia	ROW
	Puerto Rico	ROA
China	People's Republic of China	CHN
India	India	IND
Japan	Japan	JPN
Republic of Korea	Republic of Korea	KOR
Australia	Australia	ROW
Colombia	Colombia	ROA
Chile	Chile	ROA
Egypt	Egypt	ROW
Indonesia	Indonesia	ROW
Kzakhstan	Kazakhstan	ROW
Malaysia	Malaysia	ROW
Pakistan	Pakistan	ROW
Peru	Peru	ROA
Philippines	Philippines	ROW
Saudi Arabia	Saudi Arabia	ROW
South Africa	South Africa	ROW
Thailand	Thailand	ROW
Turkey	Turkey	ROW
Viet Nam	Viet Nam	ROW

Table C.2: FAOSTAT – E-GLT items mapping.

FAOSTAT Item Code	FAOSTAT Item	E-GLT Item
867	Meat, cattle	beef
868	Offals, edible, cattle	beef
870	Meat, cattle, boneless (beef and veal)	beef
1061	Meat, chicken, canned	chicken
1036	Offals, pigs, edible	pork
1058	Meat, chicken	poultry
1059	Offals, liver chicken	chicken
1035	Meat, pig	pork
1038	Meat, pork	pork
1074	Offals, liver geese	poultry
1075	Offals, liver duck	poultry
1080	Meat, turkey	poultry
1069	Meat, duck	poultry
1073	Meat, goose and guinea fowl	poultry

Table C.3: Percentage change in production cost in the absence of antimicrobials, parameter γ_{lp}^{A}.

chicken	1.76	retrieved from (NRC, 1999)
turkey	2.94	retrieved from (NRC, 1999)
poultry	1.82	chicken constitutes 95% of poultry production and turkey constitutes 5% of poultry production in our dataset. The change in the marginal cost is computed as a weighted average of the above two items, *i.e.*, $0.95 \cdot 1.76 + 0.05 \cdot 2.94 = 1.82$.
pork	2.5	retrieved from (NRC, 1999)
beef	2.1	retrieved from (NRC, 1999)

Table C.4: Ration cost as a percentage of total production cost, parameter frc_{lp}.

Food Product	Ration cost to total cost (%)	Comment
chicken	65	retrieved from (NRC, 1999)
turkey	70	retrieved from (NRC, 1999)
poultry	65.25	chicken constitutes 95% of poultry production and turkey constitutes 5% of poultry production in our dataset. The change in the marginal cost is computed as a weighted average of the above two items, *i.e.*, $0.95 \cdot 65 + 0.05 \cdot 70 = 65.25$.
pork	70	retrieved from (NRC, 1999)
beef	51.3	We divide the total feed cost with the total production cost in Table 4 of (Shaudys and Sitterley, 1963).

APPENDIX C. IGAULTM MODEL FORMULATION, DATA COLLECTION, AND CALIBRATION PROCESS

Appendix D

Publications

10. C. Avraam, A. S. Lambrou, W. Jiang, and S. Siddiqui. Antimicrobial resistance and livestock trade for low and middle income countries: Regional analysis of global coordination policies. *Frontiers in Sustainable Food Systems*, 5:79, 2021b.

9. C. Avraam, Y. Zhang, S. Sankaranarayanan, B. Zaitchik, E. Moynihan, P. Juturu, R. Neff, and S. Siddiqui. Optimization-based systems modeling for the food-energy-water nexus. *Current Sustainable/Renewable Energy Reports*, 8:4–16, 2021c.

8. L. Sarmiento, A. Molar-Cruz, C. Avraam, M. Brown, J. Rosellón, S. Siddiqui, and B. Solano Rodrígez. Mexico and U.S. power systems under variations in natural gas prices. *Energy Policy*, xx:xxxx, 2021. Accepted.

7. C. Avraam, J. E. Bistline, M. Brown, K. Vaillancourt, and S. Siddiqui. North American natural gas market and infrastructure developments under different

mechanisms of renewable policy coordination. *Energy Policy*, 148:111855, 2021a.

6. M. Brown, S. Siddiqui, C. Avraam, J. Bistline, J. Decarolis, H. Eshraghi, S. Giarola, M. Hansen, P. Johnston, S. Khanal, and A. Molar-Cruz. North American energy system responses to natural gas price shocks. *Energy Policy*, 149:112046, 2021.

5. C. Avraam, D. Chu, and S. Siddiqui. Natural gas infrastructure development in North America under integrated markets. *Energy Policy*, 147:111757, 2020.

4. S. Siddiqui, K. Vaillancourt, O. Bahn, N. Victor, C. Nichols, C. Avraam, and M. Brown. Integrated North American energy markets under different futures of cross-border energy infrastructure. *Energy Policy*, 144:111658, 2020.

3. H. G. Huntington, A. Bhargava, D. Daniels, J. P. Weyant, C. Avraam, J. Bistline, J. A. Edmonds, S. Giarola, A. Hawkes, M. Hansen, P. Johnston, A. Molar-Cruz, M. Nadew, S. Siddiqui, K. Vaillancourt, and N. Victor. Key findings from the core North American scenarios in the EMF34 intermodel comparison. *Energy Policy*, 144:111599, 2020.

2. C. Avraam, J. Rines, A. Sarker, E. Mallada, and F. Paganini. Voltage collapse stabilization in star DC networks. In *2019 American Control Conference (ACC)*, pages 1957–1964, 2019.

1. F. Feijoo, G. C. Iyer, C. Avraam, S. A. Siddiqui, L. E. Clarke, S. Sankara-

narayanan, M. T. Binsted, P. L. Patel, N. C. Prates, E. Torres-Alfaro, and M. A. Wise. The future of natural gas infrastructure development in the United States. *Applied Energy*, 228:149–166, 2018.

Bibliography

C. A. Gallet. A meta-analysis of the price elasticity of meat: Evidence of regional differences. *Business and Economic Research*, 2, 2012.

I. Abada, S. Gabriel, V. Briat, and O. Massol. A generalized Nash–Cournot model for the Northwestern European natural gas markets with a fuel substitution demand function: The GaMMES model. *Networks and Spatial Economics*, 13:1–42, 2013.

J. Abrell and H. Weigt. Combining energy networks. *Networks and Spatial Economics*, 12(3):377–401, 2012.

G. S. Alemán-Nava, V. H. Casiano-Flores, D. L. Cárdenas-Chávez, R. Díaz-Chavez, N. Scarlat, J. Mahlknecht, J.-F. Dallemand, and R. Parra. Renewable energy research progress in Mexico: A review. *Renewable and Sustainable Energy Reviews*, 32:140–153, 2014.

F. Alvarado, I. Dobson, and Y. Hu. Computation of closest bifurcation in power systems. *IEEE Transactions on Power Systems*, 9(2):918 – 928, 1994.

J. J. Anagnost and C. A. Desoer. An elementary proof of the Routh-Hurwitz stability criterion. *Circuits Systems Signal Process*, 10(1):101–114, 1991.

F. R. Aune, K. E. Rosendahl, and E. L. Sagen. Globalisation of natural gas markets – effects on prices and trade patterns. *The Energy Journal*, 30:39–53, 2009.

H. Avetisyan, S. Gabriel, S. Siddiqui, and S. Moryadee. Analyzing the effects of CO2 pricing and U.S. shale gas availability on global natural gas market. In *Changing Roles of Industry, Government and Research, 30th USAEE/IAEE North American Conference*. International Association of Energy Economics, 2011.

C. Avraam and E. Mallada. Voltage collapse stabilization in star DC networks, 2021.

C. Avraam, J. Rines, A. Sarker, E. Mallada, and F. Paganini. Voltage collapse stabilization in star DC networks. In *2019 American Control Conference (ACC)*, pages 1957–1964, 2019.

C. Avraam, D. Chu, and S. Siddiqui. Natural gas infrastructure development in North America under integrated markets. *Energy Policy*, 147:111757, 2020.

C. Avraam, J. E. Bistline, M. Brown, K. Vaillancourt, and S. Siddiqui. North American natural gas market and infrastructure developments under different mechanisms of renewable policy coordination. *Energy Policy*, 148:111855, 2021a.

C. Avraam, A. S. Lambrou, W. Jiang, and S. Siddiqui. Antimicrobial resistance and livestock trade for low and middle income countries: Regional analysis of global coordination policies. *Frontiers in Sustainable Food Systems*, 5:79, 2021b.

C. Avraam, Y. Zhang, S. Sankaranarayanan, B. Zaitchik, E. Moynihan, P. Juturu, R. Neff, and S. Siddiqui. Optimization-based systems modeling for the food-energy-water nexus. *Current Sustainable/Renewable Energy Reports*, 8:4–16, 2021c.

AWWA. Cybersecurity risk & responsibility in the water sector, 2019. URL `https://www.awwa.org/Resources-Tools/Resource-Topics/Risk-Resilience/Cybersecurity-Guidance`. American Water Works Association. Prepared by Judith H. Germano.

M. Babiker, A. Gurgel, S. Paltsev, and J. Reilly. Forward-looking versus recursive-dynamic modeling in climate policy analysis: A comparison. *Economic Modelling*, 26(6):1341–1354, 2009.

T. Barroga, R. Morales, C. Benigno, S. Castro, M. Caniban, M. Cabullo, A. Agunos, K. de Balogh, and A. Dorado-Garcia. Antimicrobials used in backyard and commercial poultry and swine farms in the philippines: A qualitative pilot study. *Frontiers in Veterinary Science*, 7:329, 2020.

E. H. E. Bayoumi. Power electronics in smart grid power transmission systems: a review. *International Journal of Industrial Electronics and Drives*, 2:98–115, 2015.

M. A. Beltramo, A. S. Manne, and J. P. Weyant. A North American gas trade model (GTM). *The Energy Journal*, 7(3):15–32, 1986.

C. Böhringer and T. F. Rutherford. Integrated assessment of energy policies: Decomposing top-down and bottom-up. *Journal of Economic Dynamics and Control*, 33 (9):1648–1661, 2009.

J. Bistline and S. Rose. Social cost of carbon pricing of power sector CO2: accounting for leakage and other social implications from subnational policies. *Environmental Research Letters*, 13:014027, 2018.

J. Bistline, N. Santen, and D. Young. The economic geography of variable renewable energy and impacts of trade formulations for renewable mandates. *Renewable and Sustainable Energy Reviews*, 106:79–96, 2019.

J. E. Bistline, M. Brown, S. A. Siddiqui, and K. Vaillancourt. Electric sector impacts of renewable policy coordination: A multi-model study of the North American energy system. *Energy Policy*, 145:111707, 2020.

J. E. T. Bistline and D. T. Young. Economic drivers of wind and solar penetration in the US. *Environmental Research Letters*, 14(12):124001, 2019.

E. Bompard, E. Carpaneto, G. Chicco, and R. Napoli. A dynamic interpretation of the load-flow Jacobian singularity for voltage stability analysis. *International Journal of Electrical Power & Energy Systems*, 18(6):385 – 395, 1996.

E. Bowen and D. J. Lacombe. Spatial dependence in state renewable policy: effects of renewable portfolio standards on renewable generation within NERC regions. *The Energy Journal*, 38:1–8, 2017.

S. Boyd and L. Vandenberghe. *Convex Optimization*. Cambridge University Press, USA, 2004.

M. Brown, S. Siddiqui, C. Avraam, J. Bistline, J. Decarolis, H. Eshraghi, S. Giarola, M. Hansen, P. Johnston, S. Khanal, and A. Molar-Cruz. North American energy system responses to natural gas price shocks. *Energy Policy*, 149:112046, 2021.

K. Bruninx, K. Van den Bergh, E. Delarue, and W. D'haeseleer. Optimization and allocation of spinning reserves in a low-carbon framework. *IEEE Transactions on Power Systems*, 31(2):872–882, 2016.

CDC. Antibiotic resistance threats in the united states, 2013. Technical report, Centers for Disease Control and Prevention. U.S. Department of Health and Human Services, 2013. URL `https://www.cdc.gov/drugresistance/pdf/ar-threats-2013-508.pdf`.

CDDEP. The Center for Disease Dynamics Economics & Policy. Resistance Map: Antibiotic resistance, 2017. URL `https://resistancemap.cddep.org/CountryPageSub.php?country=UnitedStates`. Date accessed: June 11, 2020.

CFIA. Final report of an audit of the meat inspection systems and animal health controls of Brazil – October 15 to 26, 2018. Technical report, Canadian Food Inspection Agency, 2020. URL `https://www.inspection.gc.ca/importing-food-plants-or-animals/food-imports/foreign-systems/audits/final-report-october-15-to-26-2018/eng/1580241764471/1580241855561`.

T. C. Y. Chan, T. Lee, and D. Terekhov. Inverse optimization: Closed-form solutions, geometry, and goodness of fit. *Management Science*, 65:955–1453, 2018.

G. Cheng, H. Hao, S. Xie, X. Wang, M. Dai, L. Huang, and Z. Yuan. Antibiotic alternatives: the substitution of antibiotics in animal husbandry? *Frontiers in Microbiology*, 5:217, 2014.

CISA. Critical infrastructure sectors, 2021. URL `https://www.cisa.gov/critical-infrastructure-sectors`.

CNN. Most lights back on in Cleveland, 2003. URL `https://www.cnn.com/2003/US/08/15/blackout.cleveland/index.html`. Friday, August 15, 2003 Posted: 8:43 PM EDT (0043 GMT).

P. Collignon, J. Conly, T. Dang Ninh, P. Donado-Godoy, P. Fedorka-Cray, H. Fernandez, M. Galas, R. Irwin, B. Karp, G. Matar, P. McDermott, S. McEwen, E. Mitema, R. Reid-Smith, H. M. Scott, R. Singh, C. S. DeWaal, J. Stelling, M. Toleman, H. Watanabe, and G.-J. Woo. World Health Organization ranking of antimicrobials according to their importance in human medicine: A critical step for developing risk management strategies to control antimicrobial resistance from food animal production. *Clinical Infectious Diseases*, 63(8):1087–1093, 2016.

T. V. Cutsem. A method to compute reactive power margins with respect to voltage collapse. *IEEE Transactions on Power Systems*, 6(1):145–156, 1991.

A. S. De Vany and W. D. Walls. *The emerging new order in natural gas: markets versus regulation*. Quorum Books Westport, Conn, 1995.

A. J. DeBlasio, T. J. Regan, M. E. Zirker, K. Lovejoy, and K. Fichter. Learning from the 2003 blackout. *Public Roads*, 68(2), 2004.

I. Dobson. Observations on the geometry of saddle node bifurcation and voltage collapse in electrical power systems. *IEEE Transactions on Circuits and Systems-I: Fundamental Theory and Applications*, 39:240–243, 1992.

EC. EUR-lex. Directive 2009/28/EC., 2009. URL `https://eur-lex.europa.eu/`. Accessed: February 7, 2019.

EC. EU reference scenario 2016. energy, transport, and ghg emissions trends to 2050., 2016. URL `http://pure.iiasa.ac.at/id/eprint/13656/1/REF2016_report_FINAL-web.pdf`.

EC. Final report of an audit carried out in Brazil from 02 May 2017 to 12 May 2017 in order to evaluate the operation of controls over the production of beef, horse and poultry meat, and products derived therefrom intended for export to the European Union. Technical report, European Commission, 2017. URL `https://ec.europa.eu/food/audits-analysis/act_getPDF.cfm?PDF_ID=13322`.

EC. A clean planet for all. a European long-term strategic vision for a prosperous, modern, competitive and climate neutral economy, 2018.

ECOSOC. Transforming our world: The 2030 agenda for sustainable development. Technical report, United Nations Economic and Social Council. United Nations, 2015. URL https://sdgs.un.org/2030agenda.

ECOSOC. Special edition: progress towards the sustainable development goals. report of the Secretary-General. Technical report, United Nations Economic and Social Council. United Nations, 2019. URL https://sustainabledevelopment.un.org/content/documents/24978Report_of_the_SG_on_SDG_Progress_2019.pdf.

R. Egging. Benders decomposition for multi-stage stochastic mixed complementarity problems – applied to a global natural gas market model. *European Journal of Operational Research*, 226(2):341–353, 2013.

R. Egging, F. Holz, and S. A. Gabriel. The world gas model: A multi-period mixed complementarity model for the global natural gas market. *Energy*, 35(10):4016–4029, 2010.

EIA. Natural gas policy Act of 1978, 1978. URL https://www.eia.gov/oil_gas/natural_gas/analysis_publications/ngmajorleg/ngact1978.html. Accessed: September 20, 2019.

EIA. Annual energy outlook, 1998.

EIA. Impacts of a 10-percent renewable portfolio standard (SR/OIAF/2002-03), 2002.

EIA. Impacts of a 10-percent renewable portfolio standard (SR/OIAF/2003-01), 2003.

EIA. NEMS - national energy modeling system: an overview - EIA, 2009. URL https://www.eia.gov/analysis/pdfpages/0581(2009)index.php.

EIA. Annual energy outlook 2017 with projections to 2050, 2017.

EIA. Natural gas market module of the national energy modeling system: model documentation 2018, 2018. URL https://www.eia.gov/outlooks/aeo/nems/documentation/ngmm/pdf/ngmm(2018).pdf.

EIA. Open data, 2019a. URL https://www.gob.mx/cms/uploads/attachment/file/236863/NG_Outlook_2016-2030_P.compressed.pdf. U.S. Energy Information Administration. Accessed: December 9, 2019.

EIA. Natural gas pipeline projects, 2019b. URL https://www.eia.gov/naturalgas/data.php. Accessed: September 12, 2019.

EIA. Annual energy outlook 2019 with projections to 2050, 2019c.

EIA. International Energy Statistics., 2019d. URL https://www.eia.gov/international/data/world. Accessed: September 12, 2019.

EIA. Ieo2019 issues in focus: Effects of renewable technology capital costs on electricity capacity and generation in two illustrative regions, 2020.

K. Eurek, W. Cole, D. Bielen, N. Blair, S. Cohen, B. Frew, J. Ho, V. Krishnan, T. Mai, B. Sigrin, and D. Steinberg. Regional energy deployment system (ReEDS) model documentation: Version 2016. Technical report, U.S. Department of Energy, Office of Scientific and Technical Information, 2016.

F. Facchinei and J. S. Pang. *Finite-Dimensional Variational Inequalities and Complementarity Problems*. Springer Series in Operations Research. Springer, 2003.

FAOSTAT. Food and Agriculture Organization Statistical Database, 2020. United Nations. Retrieved June 11, 2020 from http://www.fao.org/faostat/en/.

N. Faysse. Coping with the tragedy of the commons: Game structure and design of rules. *Journal of Economic Surveys*, 19:239–261, 2005.

FDA. FDA's proposed method for adjusting data on antimicrobials sold or distributed for use in food-producing animals, using a biomass denominator. Technical report, United States Food and Drug Administration, 2017.

F. Feijoo, D. Huppmann, L. Sakiyama, and S. Siddiqui. North American natural gas model: Impact of cross-border trade with Mexico. *Energy*, 112:1084–1095, 2016.

F. Feijoo, G. C. Iyer, C. Avraam, S. A. Siddiqui, L. E. Clarke, S. Sankaranarayanan, M. T. Binsted, P. L. Patel, N. C. Prates, E. Torres-Alfaro, and M. A. Wise. The future of natural gas infrastructure development in the United States. *Applied Energy*, 228:149–166, 2018.

FERC. Natural gas wellhead decontrol act of 1989, 1989. URL https://www.ferc.gov/legal/fed-sta/natural-gas-wellhead-decontrol-1989.pdf. Accessed: September 20, 2019.

M. C. Ferris and T. S. Munson. Complementarity problems in gams and the PATH solver. *Journal of Economic Dynamics and Control*, 24(2):165–188, 2000.

C. Fertel, O. Bahn, K. Vaillancourt, and J.-P. Waaub. Canadian energy and climate policies: A SWOT analysis in search of federal/provincial coherence. *Energy Policy*, 63:1139–1150, 2013.

C. Fischer and R. G. Newell. Environmental and technology policies for climate mitigation. *Journal of Environmental Economics and Management*, 55(2):142–162, 2008.

D. Fudenberg and J. Tirole. *Game Theory*. MIT Press, 1991.

T. Fuller. For the most vulnerable, California blackouts can be life or death, 2019. URL `https://www.nytimes.com/2019/10/10/us/california-power-outage.html?smid=tw-share`. October 10th, 2019.

D. Fullerton and D. H. Karney. Multiple pollutants, co-benefits, and suboptimal environmental policies. *Journal of Environmental Economics and Management*, 87:52–71, 2018.

S. A. Gabriel, J. Zhuang, and S. Kiet. A large-scale linear complementarity model of the North American natural gas market. *Energy Economics*, 27(4):639–665, 2005.

S. A. Gabriel, A. J. Conejo, C. Ruiz, and S. Siddiqui. Solving discretely constrained, mixed linear complementarity problems with applications in energy. *Computers & Operations Research*, 40(5):1339–1350, 2013.

D. A. Gantz. The United States-Mexico-Canada Agreement: Energy production and policies, 2019. Accessed: September 17, 2019.

A. George. Antimicrobial resistance, trade, food safety and security. *One Health*, 5: 6–8, 2018.

A. Gilbert and M. Bazilian. The Texas electricity crisis and the energy transition, 2021. URL `https://www.utilitydive.com/news/the-texas-electricity-crisis-and-the-energy-transition/595315/`. Published Feb. 19, 2021.

R. Golombek, E. Gjelsvik, and K. E. Rosendahl. Effects of liberalizing the natural gas markets in Western Europe. *The Energy Journal*, 16:85–112, 1995.

L. H. Goulder, M. A. Hafstead, and M. Dworsky. Impacts of alternative emissions allowance allocation methods under a federal cap-and-trade program. *Journal of Environmental Economics and Management*, 60(3):161–181, 2010.

D. Graham. Mexico's López Obrador suspends oil auctions for 3 years, 2018. URL `https://www.ft.com/content/6cec89fa-f899-11e8-af46-2022a0b02a6c`. Accessed: August, 2019.

J. P. Graham, J. J. Boland, and E. Silbergeld. Growth promoting antibiotics in food animal production: an economic analysis. *Public Health Reports*, 122(1):79–87, 2007.

J. Hanefeld, M. Khan, G. Tomson, and R. Smith. Trade is central to achieving the sustainable development goals: a case study of antimicrobial resistance. *British Medical Journal*, 358:j3505, 2017.

C. He, L. Wu, T. Liu, and Z. Bie. Robust co-optimization planning of interdependent electricity and natural gas systems with a joint n-1 and probabilistic reliability criterion. *IEEE Transactions on Power Systems*, 33(2):2140–2154, 2018a.

C. He, L. Wu, T. Liu, W. Wei, and C. Wang. Co-optimization scheduling of interdependent power and gas systems with electricity and gas uncertainties. *Energy*, 159:1003–1015, 2018b.

P. Hellegers, D. Zilberman, P. Steduto, and P. McCornick. Interactions between water, energy, food and environment: evolving perspectives and policy issues. *Water Policy*, 10(1):1–10, 2008.

J. E. Hobbs. Food supply chains during the covid-19 pandemic. *Canadian Journal of Agricultural Economics/Revue canadienne d'agroeconomie*, 68(2):171–176, 2020.

W. W. Hogan and J. P. Weyant. Combined energy models. Technical report, U.S. Department of Energy, Office of Scientific and Technical Information, 1982.

A. Hollis and Z. Ahmad. Preserving antibiotics, rationally. *The New England Journal of Medicine*, 369(26):2474–2476, 2013.

F. Holz, C. von Hirschhausen, and C. Kemfert. A strategic model of European gas supply (gasmod). *Energy Economics*, 30(3):766–788, 2008.

J.-C. Hourcade, M. Jaccard, C. Bataille, and F. Ghersi. Hybrid modeling: New answers to old challenges introduction to the special issue of The Energy Journal. *The Energy Journal*, 27:1–11, 2006.

H. G. Huntington. Natural gas across county borders: an introduction and overview. *The Energy Journal*, 30:1–8, 2009.

H. G. Huntington, A. Bhargava, D. Daniels, J. P. Weyant, C. Avraam, J. Bistline, J. A. Edmonds, S. Giarola, A. Hawkes, M. Hansen, P. Johnston, A. Molar-Cruz, M. Nadew, S. Siddiqui, K. Vaillancourt, and N. Victor. Key findings from the core North American scenarios in the EMF34 intermodel comparison. *Energy Policy*, 144:111599, 2020.

D. Huppmann and R. Egging. Market power, fuel substitution and infrastructure – a large-scale equilibrium model of global energy markets. *Energy*, 75:483–500, 2014.

IACG. AMR Indicators and their relevance to the global indicator framework for the SDGs and targets for the 2030 Agenda for Sustainable Development. Technical report, Analytic support provided by McKinsey & Company, funded by the Wellcome Trust, to inform the United Nations Inter-Agency Coordination Group (IACG) on Antimicrobial Resistance, 2018. URL `https://www.who.`

int/antimicrobial-resistance/interagency-coordination-group/AMR_SDG_indicators_analysis_slides.pdf.

G. D. Irisarri, X. Wang, J. Tong, and S. Mokhtari. Maximum loadability of power systems using interior point nonlinear optimization method. *IEEE Transactions on Power Systems*, 12(1):162–172, 1997.

F. B. John W. Simpson-Porco, Florian Dorfler. Voltage collapse in complex power grids. *Nature Communications*, 7:10790, 2016.

L. Karp and J. Livernois. Using automatic tax changes to control pollution emissions. *Journal of Environmental Economics and Management*, 27(1):38–48, 1994.

H. K. Khalil. *Nonlinear Systems*. Prentice Hall, 3rd edition, 2002.

E. Klinenberg. Denaturalizing disaster: A social autopsy of the 1995 chicago heat wave. *Theory and Society*, 28(2):239–295, 1999.

A. Krook-Riekkola, C. Berg, E. O. Ahlgren, and P. Söderholm. Challenges in top-down and bottom-up soft-linking: Lessons from linking a Swedish energy system model with a CGE model. *Energy*, 141:803–817, 2017.

P. Kundur, N. Balu, and M. Lauby. *Power System Stability and Control*. Discussion Paper Series. McGraw-Hill Education, 1994.

P. Kundur, J. Pasebra, V. Ajjarapu, G. Andersson, A. Bose, C. Canizares, N. Hatziargyriou, D. Hill, A. Stankovic, C. Taylor, T. V. Cutsem, and V. Vittal. Definition and classification of power system stability IEEE/CIGRE joint task force on stability terms and definitions. *IEEE Transactions on Power Systems*, 19:1387 – 1401, 2004.

T. F. Landers, B. Cohen, E. Wittum, Thomas, and E. L. Larson. A review of antibiotic use in food animals: Perspective, policy, and potential. *Public Health Reports*, 127: 4–22, 2012.

S. Levy. Reduced antibiotic use in livestock: How Denmark tackled resistance. *Environmental Health Perspectives*, 122(6):A160–A165, 2014.

K. Löffler, K. Hainsch, T. Burandt, P.-Y. Oei, C. Kemfert, and C. Von Hirschhausen. Designing a model for the global energy system—GENeSYS-MOD: An application of the open-source energy modeling system (OSeMOSYS). *Energies*, 10(10), 2017.

J. Li and M. Colombier. Managing carbon emissions in China through building energy efficiency. *Journal of Environmental Management*, 90(8):2436–2447, 2009.

J. Linn and L. Muehlenbachs. The heterogeneous impacts of low natural gas prices on consumers and the environment. *Journal of Environmental Economics and Management*, 89:1–28, 2018.

H. Liu. The income and price sensitivity of diets globally. Economics Discussion / Working Papers 16-22, The University of Western Australia, Department of Economics, 2016. URL `https://ideas.repec.org/p/uwa/wpaper/16-22.html`.

Z.-Q. Luo, J.-S. Pang, and D. Ralph. *Mathematical Programs with Equilibrium Constraints*. Cambridge University Press, 1996.

T. Mai, J. Bistline, Y. Sun, W. Cole, C. Marcy, C. Namovicz, and D. Young. The role of input assumptions and model structures in projections of variable renewable energy: A multi-model perspective of the U.S. electricity system. *Energy Economics*, 76:313–324, 2018.

MALF. Statement by the Brazilian Ministry of Agriculture, Livestock and Food Supply, 2017. URL `http://www.brazil.gov.br/about-brazil/news/2017/03/china-announces-full-reopening-of-its-market-to-brazilian-meat`. Ministry of Agriculture, Livestock and Food Supply of Brazil. Mar 25, 2017. Press Release: Brazília.

M. J. Martin, S. E. Thottathil, and T. B. Newman. Antibiotics overuse in animal agriculture: A call to action for health care providers. *American Journal of Public Health*, 105:2409–2410, 2015.

A. Martinez-Mares and C. R. Fuerte-Esquivel. A unified gas and power flow analysis in natural gas and electricity coupled networks. *IEEE Transactions on Power Systems*, 27(4):2156–2166, 2012.

L. Mathiesen. Computational experience in solving equilibrium models by a sequence of linear complementarity problems. *Operations Research*, 33(6):1225–1250, 1985.

D. Maxwell and Z. Zhu. Natural gas prices, LNG transport costs, and the dynamics of LNG imports. *Energy Economics*, 33(2):217–226, 2011.

R. Mieth, S. Acharya, A. Hassan, and Y. Dvorkin. Learning-enabled residential demand response: Automation and security of cyberphysical demand response systems. *IEEE Electrification Magazine*, 9(1):36–44, 2021.

S. Moryadee, S. A. Gabriel, and H. G. Avetisyan. Investigating the potential effects of U.S. lng exports on global natural gas markets. *Energy Strategy Reviews*, 2(3): 273–288, 2014.

NEB. Canada's energy future 2017, 2017.

NHFPC. *Statement: Regarding the official version of "The Pagoda of Balanced Diet for Chinese Residents (2016)"*, 2016. URL `http://dg.cnsoc.org/article/04/8a2389fd54b964c80154c1d781d90197.html`. National Health and Family Planning Commission of China. May 18, 2016. Press Release: Beijing.

NRC. *The Use of Drugs in Food Animals: Benefits and Risks.* The National Academies Press, Washington, DC, 1999.

NWS. Valentine's week winter outbreak 2021: Snow, ice, & record cold, 2021. URL `https://www.weather.gov/hgx/2021ValentineStorm`.

O. O. Obadina and G. J. Berg. Determination of voltage stability limit in multimachine power systems. *IEEE Transactions on Power Systems*, 3(4):1545–1554, 1988.

OECD-FAO. *Aglink-Cosimo Model Documentation. A partial equilibrium model of world agricultural markets.* Organisation for Economic Co-operation and Development and Food and Agriculture Organization of the United Nations (OECD-FAO), 2015. URL `http://www.agri-outlook.org/documents/Aglink-Cosimo-model-documentation-2015.pdf`.

OECD-FAO. OECD-FAO Agricultural Outlook 2019-2028, 2019. Organisation for Economic Co-operation and Development and Food and Agriculture Organization of the United Nations. Retrieved June 11, 2020 from `http://www.fao.org/faostat/en/`.

J. O'Neill. Antimicrobial resistance: Tackling a crisis for the health and wealth of nations. Technical report, The UK Prime Minister commissioned the Review on Antimicrobial Resistance to address the growing global problem of drug-resistant infections. It is Chaired by Jim O'Neill and supported by the Wellcome Trust and the UK Government, but operates and speaks with full independence from both, 2014.

D. Ore, D. B. Solomon, and S. Navaratnam. Mexico's Pemex announces discovery of 'giant' crude oil deposit, 2019. URL `reut.rs/2qtrkOp`. Published: December 7. Accessed: March 5, 2020.

M. Ouyang, L. Dueñas-Osorio, and X. Min. A three-stage resilience analysis framework for urban infrastructure systems. *Structural Safety*, 36-37:23–31, 2012.

K. Palmer and D. Burtraw. Cost-effectiveness of renewable electricity policies. *Energy Economics*, 27(6):873–894, 2005.

N. A. Rader and R. B. Norgaard. Efficiency and sustainability in restructured electricity markets: the renewables portfolio standard. *The Electricity Journal*, 9(6): 37–49, 1996.

D. Ralph. Mathematical programs with complementarity constraints in traffic and telecommunications networks. *Philosophical Transactions of the Royal Society A: Mathematical, Physical and Engineering Sciences*, 366:1973–1987, 2008.

L. Reiley. Texas freeze killed winter produce, with some food prices expected to spike, 2021. URL `https://www.washingtonpost.com/business/2021/02/26/texas-storm-produce-shortage/`. Posted Feb. 26, 2021 at 5:51 p.m. EST.

R. T. Rockafellar. *Convex Analysis*. Princeton University Press, 2015.

S. Rogers Van Katwyk, M. Danik, I. Pantis, R. Smith, J.-A. Røttingen, and S. J. Hoffman. Developing an approach to assessing the political feasibility of global collective action and an international agreement on antimicrobial resistance. *Global Health Research and Policy*, 1(20):20, 2016.

W. Rudin. *Principles of Mathematical Analysis*. Mc-Graw Hill, 3rd edition, 1976.

S. Sankaranarayanan, F. Feijoo, and S. Siddiqui. Sensitivity and covariance in stochastic complementarity problems with an application to North American natural gas markets. *European Journal of Operational Research*, 268(1):25–36, 2018.

L. Sarmiento, A. Molar-Cruz, C. Avraam, M. Brown, J. Rosellón, S. Siddiqui, and B. Solano Rodrígez. Mexico and U.S. power systems under variations in natural gas prices. *Energy Policy*, xx:xxxx, 2021. Accepted.

R. Schmalensee and R. N. Stavins. The design of environmental markets: What have we learned from experience with cap and trade? *Oxford Review of Economic Policy*, 33(4):572–588, 2017.

J. Seale Jr, A. Regmi, and J. A. Bernstein. International evidence on food consumption patterns. Technical report, United States Department of Agriculture, 2003. USDA Technical Bulletin TB-1929.

SENER. Natural gas outlook 2016-2030, 2017. URL `https://www.gob.mx/cms/uploads/attachment/file/236863/NG_Outlook_2016-2030_P.compressed.pdf`.

A. Serletis. Is there an East-West split in North-American natural gas markets? MPRA Paper 1746, University Library of Munich, Germany, 1997.

A. Serletis and J. Herbert. The message in North American energy prices. *Energy Economics*, 21(5):471–483, 1999.

E. Shaudys and J. Sitterley. Costs, returns, and profitability of the beef cow calf enterprise in Southeastern Ohio by systems of management. Technical report, Ohio Agricultural Experiment Station, Wooster, Ohio, 1963.

C. Shearer, J. Bistline, M. Inman, and S. J. Davis. The effect of natural gas supply on US renewable energy and CO2 emissions. *Environmental Research Letters*, 9 (9):094008, 2014.

S. Siddiqui and S. A. Gabriel. An SOS1-based approach for solving MPECs with a natural gas market application. *Networks and Spatial Economics*, 13:205–227, 2013.

S. Siddiqui, K. Vaillancourt, O. Bahn, N. Victor, C. Nichols, C. Avraam, and M. Brown. Integrated North American energy markets under different futures of cross-border energy infrastructure. *Energy Policy*, 144:111658, 2020.

B. Siliverstovs, G. L'Hégaret, A. Neumann, and C. von Hirschhausen. International market integration for natural gas? A cointegration analysis of prices in Europe, North America and Japan. *Energy Economics*, 27(4):603–615, 2005.

M. Spiegelberg, D. E. Baltazar, M. P. E. Sarigumba, P. M. Orencio, S. Hoshino, S. Hashimoto, M. Taniguchi, and A. Endo. Unfolding livelihood aspects of the water–energy–food nexus in the Dampalit Watershed, Philippines. *Journal of Hydrology: Regional Studies*, 11:53–68, 2017.

A. Stilman. Mexico's AMLO sees $4.5 billion in savings in pipeline pacts, 2019. URL `https://www.bloomberg.com/news/articles/2019-08-27/mexico-s-amlo-says-a-deal-is-reached-with-pipeline-companies`. Accessed: December 20, 2018.

J. Stock and M. Watson. *Introduction to Econometrics (3rd edition)*. Addison Wesley Longman, 2011.

G. Strbac. Demand side management: Benefits and challenges. *Energy Policy*, 36: 1096–1102, 2008.

G. Strbac, S. Ahmed, D. Kirschen, and R. N. Allan. A method for computing the value of corrective security. *IEEE Transactions on Power Systems*, 13:1096–1102, 1998.

S. H. Strogatz. *Nonlinear Dynamics and Chaos: With Applications to Physics, Biology, Chemistry and Engineering*. Westview Press, 2015.

K. Tapia-Ahumada, C. Octaviano, S. Rausch, and I. Pérez-Arriaga. Modeling intermittent renewable electricity technologies in general equilibrium models. *Economic Modelling*, 51:242–262, 2015.

TDSHS. Winter storm-related deaths – April 28, 2021, 2021. URL `https://dshs.texas.gov/news/updates.shtm`. Texas Department of State Health Services is

tracking deaths related to the February winter storms that affected Texas and posting data that is preliminary and subject to change. Accessed: June 1, 2021.

D. Tilman, C. Balzer, J. Hill, and B. L. Befort. Global food demand and the sustainable intensification of agriculture. *Proceedings of the National Academy of Sciences*, 108(50):20260–20264, 2011.

C.-C. Tsao, J. Campbell, and Y. Chen. When renewable portfolio standards meet cap-and-trade regulations in the electricity sector: Market interactions, profits implications, and policy redundancy. *Energy Policy*, 39(7):3966–3974, 2011.

A. Ulbig, T. S. Borsche, and G. Andersson. Impact of low rotational inertia on power system stability and operation. *IFAC Proceedings Volumes*, 47(3):7290–7297, 2014. 19th IFAC World Congress.

UN. Paris Agreement to the United Nations Framework Convention on climate change, 2015. URL `https://treaties.un.org/Pages/showDetails.aspx?objid=0800000280458f37`. December 12, 2015.

G. B. Upton and B. F. Snyder. Funding renewable energy: An analysis of renewable portfolio standards. *Energy Economics*, 66:205–216, 2017.

U.S.-Canada-Power-System-Outage-Task-Force. Interim report: Causes of the August 14th blackout in the United States and Canada. Technical report, U.S.-Canada Power System Outage Task Force, 2003. URL `https://www.ferc.gov/sites/default/files/2020-05/blackout-report.pdf`.

U.S.-Canada-Power-System-Outage-Task-Force. Final report on the implementation of task force recommendations. Technical report, U.S.-Canada Power System Outage Task Force, 2006. URL `https://www.dhs.gov/news`.

USDA. *USDA on Tainted Brazilian Meat: None Has Entered U.S., 100 Percent Re-Inspection Instituted*, 2017a. URL `https://www.usda.gov/media/press-releases/2017/03/22/usda-tainted-brazilian-meat-none-has-entered-us-100-percent-re`. U.S. Department Of Agriculture. March 22, 2017. Press Release: Washington, DC.

USDA. *Perdue: USDA Halting Import of Fresh Brazilian Beef*, 2017b. URL `https://www.usda.gov/media/press-releases/2017/06/22/perdue-usda-halting-import-fresh-brazilian-beef`. U.S. Department Of Agriculture. June 22, 2017. Press Release: Washington, DC.

USDHS. DHS announces new cybersecurity requirements for critical pipeline owners and operators, 2021. URL `https://www.dhs.gov/news`. Release Date: May 27, 2021.

USWH. Fact sheet: The Biden-Harris administration has launched an all-of-government effort to address Colonial pipeline incident, 2021. URL `https://www.whitehouse.gov/briefing-room/`. Briefing Room. Statements and Releases. May 11, 2021.

K. Vaillancourt, O. Bahn, P.-O. Roy, and V. Patreau. Is there a future for new hydrocarbon projects in a decarbonizing energy system? A case study for Quebec (Canada). *Applied Energy*, 218:114–130, 2018.

T. P. Van Boeckel, C. Brower, M. Gilbert, B. T. Grenfell, S. A. Levin, T. P. Robinson, A. Teillant, and R. Laxminarayan. Global trends in antimicrobial use in food animals. *Proceedings of the National Academy of Sciences*, 112(18):5649–5654, 2015.

T. P. Van Boeckel, E. E. Glennon, D. Chen, M. Gilbert, T. P. Robinson, B. T. Grenfell, S. A. Levin, S. Bonhoeffer, and R. Laxminarayan. Reducing antimicrobial use in food animals. *Science*, 357(6358):1350–1352, 2017.

T. P. Van Boeckel, J. Pires, R. Silvester, C. Zhao, J. Song, N. G. Criscuolo, M. Gilbert, S. Bonhoeffer, and R. Laxminarayan. Global trends in antimicrobial resistance in animals in low- and middle-income countries. *Science*, 365:eaaw1944, 2019.

T. Van Cutsem and C. Vournas. *Voltage Stability of Electric Power Systems*. Kluwer international series in engineering and computer science. Springer, 1998.

G. J. van Oldenborgh, K. van der Wiel, A. Sebastian, R. Singh, J. Arrighi, F. Otto, K. Haustein, S. Li, G. Vecchi, and H. Cullen. Attribution of extreme rainfall from hurricane Harvey, august 2017. *Environmental Research Letters*, 12(12):124009, 2017.

C. D. Vournas and N. G. Sakellaridis. Problems and solutions for local identification of voltage instability and emergency control. In *2008 IEEE Power and Energy Society General Meeting - Conversion and Delivery of Electrical Energy in the 21st Century*, pages 1–7, 2008.

C. D. Vournas, C. Lambrou, and M. Kanatas. Application of local autonomous protection against voltage instability to IEEE test system. *IEEE Transactions on Power Systems*, 31(4):3300–3308, 2016.

WB. Demand-led transformation of the livestock sector in india. achievements, challenges, and opportunities. Technical report, World Bank, 2011.

H. C. Wegener, F. Aarestrup, L. Jensen, A. Hammerum, and F. Bager. Use of antimicrobial growth promoters in food animals and enterococcus faecium resistance to therapeutic antimicrobial drugs in Europe. *Emerging Infectious Diseases*, 5(3): 329–35, 1999.

J. P. Weyant. A critique of the Stern Review's mitigation cost analyses and integrated assessment. *Review of Environmental Economics and Policy*, 2(1):77–93, 2008.

WHO. Impacts of antimicrobial growth promoter termination in denmark. Technical report, World Health Organization, 2002. URL `https://apps.who.int/iris/bitstream/handle/10665/68357/WHO_CDS_CPE_ZFK_2003.1.pdf?sequence=1`.

WHO. Critically important antimicrobials for human medicine, 3rd revision. Technical report, World Health Organization, 2011. URL `https://apps.who.int/iris/bitstream/handle/10665/77376/9789241504485_eng.pdf?sequence=1`.

WHO. Global action plan on antimicrobial resistance. Technical report, World Health Organization, 2015. URL `https://apps.who.int/iris/bitstream/handle/10665/193736/9789241509763_eng.pdf?sequence=1`.

J. H. Williams, A. DeBenedictis, R. Ghanadan, A. Mahone, J. Moore, W. R. Morrow, S. Price, and M. S. Torn. The technology path to deep greenhouse gas emissions cuts by 2050: The pivotal role of electricity. *Science*, 335(6064):53–59, 2012.

R. Wiser and M. Bolinger. Can deployment of renewable energy put downward pressure on natural gas prices? *Energy Policy*, 35(1):295–306, 2007.

R. Wiser, C. Namovicz, M. Gielecki, and R. Smith. Renewables portfolio standards: A factual introduction to experience from the United States, 2007. URL `https://escholarship.org/content/qt9wr9062r/qt9wr9062r.pdf`.

R. Wiser, C. Namovicz, M. Gielecki, and R. Smith. Updated renewable portfolio standards will lead to more renewable electricity generation, 2019. URL `https://www.eia.gov/todayinenergy/detail.php?id=38492`. Accessed: February 7, 2019.

M. Woolhouse, M. Ward, B. van Bunnik, and J. Farrar. Antimicrobial resistance in humans, livestock and the wider environment. *Philosophical Transactions of the Royal Society B*, 370:20140083, 2015.

H. Yin and N. Powers. Do state renewable portfolio standards promote in-state renewable generation? *Energy Policy*, 38(2):1140–1149, 2010.

P. You and E. Mallada. Saddle flow dynamics: Observable certificates and separable regularization, 2020.

D. Young and J. Bistline. The costs and value of renewable portfolio standards in meeting decarbonization goals. *Energy Economics*, 73:337–351, 2018.

X. Zhang, M. Shahidehpour, A. S. Alabdulwahab, and A. Abusorrah. Security-constrained co-optimization planning of electricity and natural gas transportation infrastructures. *IEEE Transactions on Power Systems*, 30(6):2984–2993, 2015.

Vita

Charalampos Avraam was born in Athens, Greece and grew up in Nea Smyrni, Athens, Greece. He attended the National Technical University of Athens and graduated with a diploma in Electrical and Computer Engineering in 2015. He completed his Master of Philosophy in Management Science and Operations at Hughes Hall, Cambridge Judge Business School of the University of Cambridge. In 2016, he moved to Baltimore to join the doctoral program of the Department of Civil and Systems Engineering of the Johns Hopkins University. During the 2017-2020 academic years he was an A.G. Leventis Foundation graduate scholar. In 2020, he completed his Master of Science in Applied Mathematics and Statistics at the Johns Hopkins University. During his time at Johns Hopkins University, Charalampos co-organized the Civil and Systems Engineering graduate seminar, served as the representative of the Civil and Systems Engineering Department to the Graduate Representative Organization, and was an advocate in movements aiming to repeal university policies with potentially negative impact on the surrounding community.